UNIVERSITY OF VALENCIA
PHYSIOLOGY DEPARTMENT
PHYSIOLOGY PhD PROGRAM

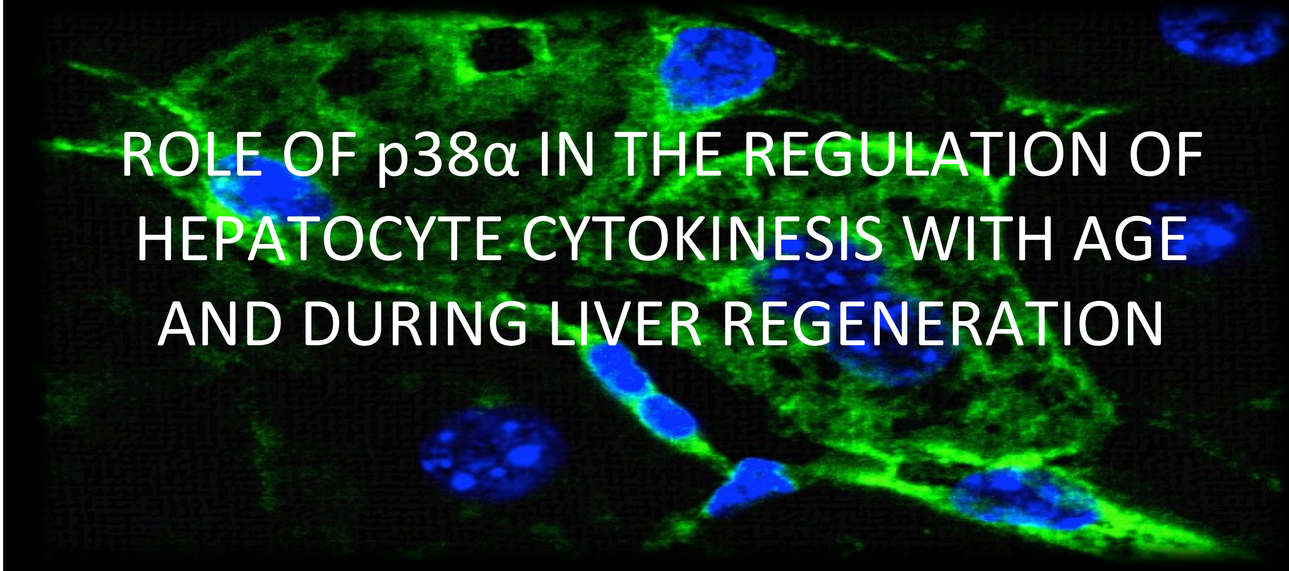

ROLE OF p38α IN THE REGULATION OF HEPATOCYTE CYTOKINESIS WITH AGE AND DURING LIVER REGENERATION

PhD THESIS PRESENTED BY:

Ana María Martínez Tormos

DIRECTED BY:

Juan Sastre Belloch, PhD

Raquel Taléns Visconti, PhD

VALENCIA, 2015

UNIVERSITY OF VALENCIA

PHYSIOLOGY DEPARTMENT

PHYSIOLOGY PhD PROGRAM

ROLE OF p38α IN THE REGULATION OF HEPATOCYTE CYTOKINESIS WITH AGE AND DURING LIVER REGENERATION

PhD THESIS PRESENTED BY:

Ana María Martínez Tormos

DIRECTED BY:

Juan Sastre Belloch, PhD

Raquel Taléns Visconti, PhD

Valencia, 2015

Departamento de Fisiología

El Prof. Dr. Juan José Sastre Belloch, Catedrático del Departamento de Fisiología de la Universidad de Valencia y la Prof. Dra. Raquel Taléns Visconti, Ayudante Doctor del Departamento de Farmacia y Tecnología Farmacéutica de la Universidad de Valencia.

CERTIFICAN:

Que Ana María Martínez Tormos, Licenciada en Farmacia en la Universidad de Valencia, ha realizado bajo nuestra dirección la presente Tesis Doctoral titulada:

“Role of p38α in the regulation of hepatocyte cytokinesis with age and during liver regeneration”

para la obtención del título de Doctor.

Y para que conste a los efectos oportunos, firmamos la presente en Burjassot (Valencia), a 10 de Julio de 2015.

Fdo. Juan Sastre Belloch Fdo. Raquel Taléns Visconti

La presente Tesis Doctoral se ha podido realizar gracias a la financiación de los siguientes proyectos:

- Ministerio de Educación y Ciencia (Consolider CSD-2007-0020)
- Ministerio de Ciencia y Tecnología (SAF 2009-07605)
- Ministerio de Economía y Competitividad (SAF 2012-39694)

A mis padres, por su apoyo sincero e incondicional.

A Miguelito, porque lo compartes conmigo.

AGRADECIMIENTOS

A Juan, que confió en mí y me dio esta gran oportunidad. Gracias por enseñarme a no "tirar la toalla". Espero que esta Tesis sea el inicio de una gran carrera científica.

A Raquel, que llegaste cuando más te necesitaba. Gracias por ayudarme a madurar en esta etapa de mi vida. Gracias por tu dedicación, por tu valioso tiempo. Has sido y serás un gran apoyo: personal y profesional. Nunca olvidaré lo que has hecho por mi.

A Alessandro Arduini, que es un auténtico genio. Alex, fuiste mi guía en mis primeros y más decisivos pasos.

A Ana Bonora, porque me encantó aprender contigo. Anita, eres fenomenal.

Gracias a mis estupendísimos compañeros de Departamento: Miguel, María, Tere, Jose, Joan, Antonio… A Javier Miranda, porque me sacaste una sonrisa cuando más lo necesitaba. A Pilar, porque me lo hiciste todo fácil. A Miriam, por ser tan "auténtica". A Salva Banacloche, que tanto me ha ayudado. A Mari Blanch, que no se cuantos bolsos le debo. A Chelo Burguete, que es un encanto. A mis compañeros de juergas y dudas técnicas, por esas noches "detox" inolvidables: Chabeli, Inés, María, Juanlu, Toni, Dan, Miguel, Javi Pereda, Mariam, Isabella, Pablo, Julián y Ángel; y es que "no sólo de ciencia vive el hombre". A Salva Pérez, porque conseguimos ser un buen equipo. A Sergio, porque ha sido un placer enseñarte. A María Gamón, por nuestra "química". A Juan Pablo y a Carmen, que siempre me apoyaron y me hicieron sentir tan querida.

A todo el personal de los Servicios Universidad de Valencia que ha hecho que este trabajo funcione: a Inmaculada Noguera y su fantástico equipo del estabulario, a Jelena Markovich y Guadalupe Calvo por su ayuda en citometría, al Servicio de Microscopía (en especial a MariTere, la eficiencia personificada) y al Servicio de Cultivos Celulares.

Al Dr. Rahman y todo su equipo: Tanveer, Janice, Chad, Isaac y Yao. Y a todos aquellos que estuvieron a mi alrededor: Fleur, Laurie, Chris, Ibone, Ellen, Prasoon y la superfamilia Silvestre, que me acogió como si fuera una mas. Mi estancia en Rochester fue una experiencia inolvidable, tanto en lo personal como en lo profesional.

A todas las personas ajenas al "labo" que me han apoyado en momentos "científicamente difíciles". A mi maravillosa familia: Papá, Mamá, Miguelito, Tica, Carlos, Nuria… El gusto con el que mis padres me han educado es la base de todo este trabajo. Me haceis sentir muy afortunada. A mi tia Pili, que siempre está pendiente y se preocupa de todos los detalles. A mis abuelos, que desgraciadamente no han podido acompañarme. A mis amigos: Liou, Ire, Juls, David, Marta, Pi, Stela, Rafa, Lau, Berta. A Javi y Laura Perea, fotógrafos ratunos. A Cris, mi " bessona" y cómplice cientifica.

Y mis últimas y más especiales gracias son para Bruno, que me acompaña durante tantos años y ha "entendido la ciencia" en innumerables ocasiones. Has demostrado ser mi perfecto compañero. Me haces la persona más feliz de este planeta y esa felicidad es la que me hace levantarme todas las mañanas con ganas de aprender. Bru, esta Tesis es tuya. Te quiero.

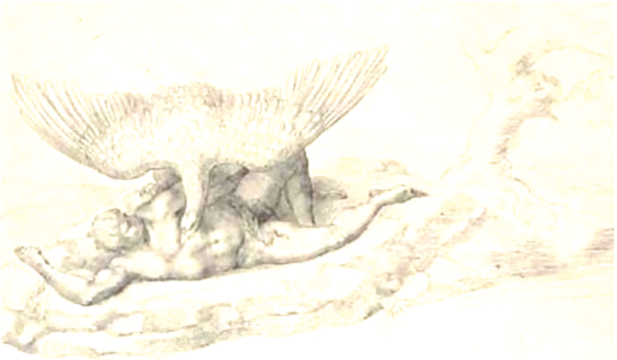

'The punishment of Tityus'

by Michelangelo Buonarroti

Tityus enraged his father Zeus by attempting the virtue of Leto. As punishment, Zeus condemned Tityus to Hades, where for all eternity two vultures devoured his liver, which continually growed back again to prolong the agony.

INDEX

INDEX

INDEX I

INDEX OF FIGURES IX

INDEX OF TABLES XV

ABBREVIATIONS XIX

ABSTRACT/RESUMEN/RESUM XXVII

I. INTRODUCTION 1

1. The liver 3
  1.1. Anatomical location and features 3
  1.2. Histology 5
  1.3. Liver function 9
  1.4. Liver regeneration 9
    1.4.1. Partial hepatectomy as a model of liver regeneration 10
  1.5. Liver disease 12
    1.5.1. Cholestatic disorders 13
    1.5.2. Bile duct ligation as a model of cholestasis 14
  1.6. New alternatives to liver transplantation: partial liver transplantation and hepatocyte transplantation 15

2. Liver ploidy 17
  2.1. Cell cycle and cytokinesis 17
  2.2. Poliploidy 19
  2.3. Binucleation 20
    2.3.1. Binucleation in liver development 21
    2.3.2. Binucleation in aging liver 22
    2.3.3. Ploidy reversal in hepatocytes 23
    2.3.4. Binucleation and liver regeneration 24
      2.3.4.1. Binucleation in partial hepatectomy 25
      2.3.4.2. Binucleation in biliary cirrhosis 25
    2.3.5. Binucleation, liver cancer and chemotherapy 26
    2.3.6. Binucleation and oxidative stress 26

3. Mitogen-activated protein kinases (MAPKs) 28
  3.1. p38 MAPK family 30

3.1.1. p38 MAPK activation 31
3.1.2. p38 MAPK inactivation by phosphatases 33
3.1.3. p38 and JNK crosstalk 35
3.1.4. Scaffolds or adaptor proteins 36
3.2. Substrates of p38α 37
3.2.1. Protein kinases 37
3.2.1.1. Mitogen- and stress-activated kinases 1 and 2 (MSK1/2) 38
3.2.1.2. Mitogen kinases 2, 3 and 5 (MK2/3/5) 39
3.2.1.3. MAP kinase-activated protein kinase 1 and 2 (MNK1/2) 40
3.2.2. Cytoplasmic substrates 40
3.2.3. Transcription factors 40
3.3. p38α signaling 40
3.3.1. p38α in development 41
3.3.2. p38α in aging 42
3.3.3. p38α and cell differentiation 42
3.3.4. p38α and cytokine expression 43
3.3.5. p38α in survival and apoptosis 44
3.3.6. p38α and cell migration 45
3.3.7. p38α and cell cycle 45
3.3.8. p38α in cancer 47
3.4. p38α and oxidative stress 48
3.4.1. p38α, oxidative stress and cell cycle 48
3.4.2. p38α and antioxidant defense 49

II. OBJECTIVES 51

III. MÉTODOS 55

1. Aparatos 57

2. Reactivos 60

3. Animales de experimentación y cirugía 63
3.1. Técnicas quirúrgicas 66
3.1.1. Laparotomía y extracción del hígado en ratones viejos 66
3.1.2. Ligadura del ducto biliar (BDL) 66
3.1.3. Hepatectomía parcial 68
3.1.4. Aislamiento de hepatocitos primarios murinos 70

4. Técnicas de laboratorio 73
4.1. Medida de la masa hepática 73
4.2. Técnicas de bioquímica hemática 73
4.2.1. Obtención del suero 73

4.2.2. Determinación de bilirrubina total 74
4.2.3. Determinación de actividad alanina aminotransferasa (ALT) 75
4.2.4. Determinación de actividad γ-glutamil transpeptidasa (γ-GT) 77
4.3. Técnicas de análisis histológico 78
4.3.1. Preparación del tejido para histología 78
4.3.2. Estudio de la inflamación hepática por tinción con hematoxilina-eosina 81
4.3.3. Estudio de la fibrosis hepática mediante tinción rojo Sirio 81
4.3.4. Inmunohistoquímica 82
4.3.5. Detección de apoptosis por método TUNEL 84
4.4. Técnicas de *Western blot* 85
4.4.1. Extracción de proteínas tisulares 85
4.4.2. Aislamiento de núcleos 86
4.4.3. Determinación de proteínas con método BCA. 87
4.4.4. Determinación de proteínas específicas mediante *Western blot* 88
4.4.4.1. Electroforesis de proteínas 88
4.4.4.2. Transferencia de proteínas a membrana 89
4.4.4.3. Detección de proteínas con tinción Ponceau 90
4.4.4.4. Reconocimiento de la proteína de estudio con anticuerpos específicos 90
4.4.4.5. Captura de imagen digital 94
4.4.5. Estudio de la polimerización de la actina 94
4.5. Técnica de *Real Time Polymerase Chain Reaction* (RT- PCR) 96
4.5.1. Extracción de ácido ribonucleico (ARN) 96
4.5.2. Diseño de *primers* 97
4.5.3. Retrotranscripción del ARN a ADN complementario 98
4.5.4. Puesta a punto de *primers* 98
4.5.5. Eficiencia de la reacción de PCR 99
4.5.6. Amplificacion del ADNc por PCR cuantitativa a tiempo real 101
4.6. Citometría de flujo 103
4.6.1. Estudio del ciclo celular con Sytox green® 104
4.6.2. Cuantificación de la producción de radicales libres del oxígeno con Cell Rox® 104
4.7. Determinación de GSH y GSSG por espectrofotometría de masas 104

5. Análisis estadístico 106

IV. RESULTS 107

1. p38α regulates cytokinesis in hepatocytes upon aging 109
1.1. p38α deficiency caused a decrease in liver mass in old mice 109
1.2. Hepatocyte size in wild type and p38α knock out mice 111
1.3. Increase in binucleation rate in p38α knock out mouse liver 112
1.4. Apoptosis in p38α knock out mice 113

1.5. Hepatocyte proliferation in old p38α knock out livers 115
1.6. The absence of p38α blocked pathways required for hepatocyte cytokinesis completion: MNK1 116
1.7. Actin polymerization was abrogated by p38α deficiency in old hepatocytes 118
1.8. Progressive impairment of actin polymerization in p38α knock out liver with age 120
1.9. Blockade of actin polymerization pathways in p38α knock out livers: Role of HSP27 122
1.10. p38α regulated the RhoA pathway in old livers 125
1.11. p38α deficiency led to a decrease in GSH levels in adulthood 127
1.12. p38α induced the liver antioxidant defense in adulthood but not in old livers 128
1.13. NF-κB nuclear traslocation and activation correlated with the REDOX oscilations 129

2. p38α in hepatocyte proliferation after partial hepatectomy 131
2.1. p38α deficiency reduced liver mass recovery after partial hepatectomy ... 131
2.2. Binucleation after partial hepatectomy 132
2.3. Effect of p38α deletion on cell cycle transitions after partial hepatectomy 133
✓ G_1/S transition 133
✓ S phase progression 134
✓ G_2/M transition 135
✓ Mitotic progression 136
2.4. p38α downstream pathways involved in cytokinesis completion 139
2.5. Consequences of p38α deletion on the REDOX status after partial hepatectomy 141

3. p38α in hepatocyte proliferation in liver disease induced by chronic cholestasis 142
3.1. Liver damage in wild type and p38α knock out mice after BDL 142
3.2. p38α knock out BDL mice exhibited reduced survival after BDL. 142
3.3. p38α knock out BDL mice did not exhibit enhanced inflammatory response 144
3.4. p38α knock out BDL mice developed the same degree of profibrotic response as wild type BDL 146
3.5. p38α ablation did not cause an increase in apoptosis after BDL................ 147
3.6. p38α downstream pathways after BDL. Role of Akt 148
3.7. HSP27 phosphorylation after BDL 151
3.8. p38α deficiency in liver abrogates compensatory hepatomegaly after BDL 152
3.9. Deficiency of p38α in liver induced hepatocyte binucleation that was enhanced after BDL 153
3.10. Increased hepatocyte binucleation rate was associated with restrained cell proliferation after BDL 154
3.11. Increased cyclin B1 and p21 in p38α knock out mice 157

3.12. p38α deficiency decreased the hepatic proliferative response after BDL. 158
3.13. Oxidative stress after BDL 159

4. Cytokinesis failure upon hepatocyte isolation 160
4.1. Hepatocyte isolation triggers an increase in binucleation in primary hepatocytes, which can be inhibited by NAC addition to the perfusion media . 160
4.2. Hepatocyte isolation leads to an increase in ROS and promotes oxidative stress in primary hepatocytes, prevented by NAC 161
4.3. Hepatocyte isolation promotes cell cycle entry, palliated by NAC............. 163

V. DISCUSSION 165

1. p38α and cytokinesis regulation in aging liver: proper actin polymerization maintains physiological binucleation rates and liver mass 168
1.1. p38α regulates hepatocyte cytokinesis during physiological liver development maintaining liver size 169
1.2. MNK1 and liver binucleation 169
1.3. p38α controls actin polymerization in aging liver: Role of the MK2/HSP27 axis 170
1.4. p38α controls actin polymerization in aging liver: Role of the RhoA pathway.. 171
1.5. Oxidative stress is not the cause of liver binucleation in p38α knock out mice 173
1.6. Oxidative stress may be the activator of RhoA in wild type old hepatocytes.. 174
1.7. p38α, alternatively with NF-κB, regulates the antioxidant defense in the liver with age...174

2. p38α and partial hepactectomy: binucleation, ploidy reversal and oxidative stress 176
2.1. p38α deficiency increases binucleation rate in after weaning hepatocytes 176
2.2. p38α deficiency reduces liver growth after partial hepatectomy 177
2.3. p38α is not needed for ploidy reversal in hepatocytes 177
2.4. p38α deficiency blocks mitotic progression during hepatocyte cell cycle after partial hepatectomy 179
2.5. Oxidative stress after partial hepatectomy in p38α knock out mice 180

3. p38α in chronic liver injury: binucleation and survival during chronic cholestasis 182
3.1. p38α knock out adult mice exhibited decreased survival after chronic cholestasis ……………………………………………………………………………………………..182
3.2. The absence of p38α did not affect inflammation, neither fibrosis nor apoptosis after chronic cholestasis 183
3.3. p38α pathways after chronic cholestasis 183

3.4. p38α knock out mice maintained their high binucleation levels after chronic cholestasis 184
3.5. p38α knock out mice did not develop compensatory hepatomegaly after BDL 185
3.6. Delayed mitotic transition in p38α knock out mice after chronic cholestasis 185
3.7. p38α deficiency enhances oxidative stress after chronic cholestasis 186

4. Hepatocyte isolation: when oxidative stress orchestrates binucleation 188
4.1. Collagenase digestion triggers oxidative stress 188
4.2. Oxidative stress promotes hepatocyte cell cycle entry but blocks cytokinesis upon hepatocyte isolation 189

VI. CONCLUSIONS 191

VII. REFERENCES 195

INDEX OF FIGURES

INDEX OF FIGURES

Figure 1. Classical liver lobe 3

Figure 2. Liver parenchyma representation 4

Figure 3. Schematic representation of liver histology 7

Figure 4. Cell cycle representation with its different phases and checkpoints 17

Figure 5. Conformational changes prior to cytokinesis 18

Figure 6. Representation of MAPK phosphorylation cascade 28

Figure 7. Mammalian MAPK pathways: the conventional MAPK pathways 29

Figure 8. Canonical (A) and non-canonical (B) activation of p38α 33

Figure 9. Summary of p38α protein kinases targets 38

Figura 10. Descripción esquemática del transgén Alfp Cre 64

Figura 11. Descripción esquemática de la estrategia LoxP para obtener el ratón *knock out* de p38α 64

Figura 12. Técnica quirúrgica: ligadura del ducto biliar común 67

Figura 13. Representación esquemática de los segmentos hepáticos en ratón 68

Figura 14. Técnica quirúrgica: hepatectomía parcial 69

Figura 15. Aislamiento de hepatocitos murinos 71

Figure 16. p38 in liver homogenates with age 110

Figure 17. Liver mass ratio (%) with age 110

Figure 18. Count of hepatocytes per field from old wild type and p38α knock out mouse liver immunohistochemistry 111

Figure 19. Binucleation in old liver 112

Figure 20. Apoptosis mediators in old liver 113

Figure 21. Apoptosis quantification by TUNEL in old liver 114

Figure 22. Real-time PCR analysis of the expressions of mRNA for *Gas2* 115

Figure 23. Cell cycle study in old liver 116

Figure 24. MNK1 activation 117

Figure 25. MNK1 activation in old liver 118

Figure 26. Actin polymerization in aging 119

Figure 27. F-actin staining in old liver slides 120

Figure 28. F-actin staining in after weaning and adult liver slides 121
Figure 29. F-actin distribution in adult liver slides 122
Figure 30. p38α downstream pathway in aging: MK2 123
Figure 31. HSP27 phosphorylation within age 124
Figure 32. RhoA pathway regulation by p38α in aging liver 126
Figure 33. REDOX variations in liver with age 127
Figure 34. Real-time PCR analysis of antioxidant enzymes 128
Figure 35. Transcription factors mediating antioxidant defense in adult liver 129
Figure 36. Transcription factors mediating antioxidant defense in old liver 130
Figure 37. Liver mass ratio (%) in SHAM and after 24 and 72h of partial hepatectomy 131
Figure 38. Binucleation rate (%) in SHAM and after 72h of partial hepatectomy 132
Figure 39. Real-time PCR analysis of the expressions of mRNA for *CyclinD1* after 72 hours partial hepactectomy 133
Figure 40. Cyclin D1 protein levels after partial hepatectomy 134
Figure 41. Real-time PCR analysis of the expressions of mRNA for *CyclinA1* after 72 hours partial hepactectomy 134
Figure 42. Real-time PCR analysis of the expressions of mRNA for G_2/M regulators after 72 h partial hepatectomy 135
Figure 43. Cyclin B1 protein levels after partial hepatectomy 136
Figure 44. Real-time PCR analysis of the expressions of mRNA for *Cyclin F* 72 hours after partial hepatectomy 137
Figure 45. Mitotic index quantification after hepatectomy by Western blot 137
Figure 46. Mitotic index quantification after hepatectomy by immunohistochemistry 138
Figure 47. p38α downstream pathway after partial hepatectomy: MK2 and HSP27 140
Figure 48. Phosphorylation of MNK1 after partial hepatectomy 140
Figure 49. REDOX status variations 72 hours after partial hepatectomy 141
Figure 50. Survival curve after cholestasis induction in wild type and p38α knock out mice 143

Figure 51. Real-time PCR analysis of the expressions of mRNA for pro-inflammatory cytokines 144

Figure 52. Real-time PCR analysis of the expressions of mRNA for *Il10* after BDL 145

Figure 53. Representative liver sections of haematoxylin and eosin staining in BDL mice, after 28 days BDL 145

Figure 54. Real-time PCR analysis of the expressions of mRNA for pro-fibrotic factors 146

Figure 55. Representative liver sections of Sirius Red staining in BDL mice, after 28 days BDL 147

Figure 56. Cleavage of caspase 3 after BDL 147

Figure 57. Real-time PCR analysis of the expressions of mRNA of pro-apoptotic factors 148

Figure 58. p38α downstream pathway after BDL: MK2 149

Figure 59. p38α downstream pathway after BDL: AKT and mTOR 150

Figure 60. p38α downstream pathway after BDL: GSK3β and βcatenin 151

Figure 61. HSP27 phosphorylation after BDL 152

Figure 62. Evolution of liver weight after 28 days of cholestasis induction 152

Figure 63. Liver mass ratio after 28 days BDL 153

Figure 64. Binucleation rate (%) in SHAM and after 12 and 28 days BDL 154

Figure 65. Quantification of mitotic index in BDL mice by Western blot 155

Figure 66. Mitotic index in 12 days BDL mice by immunohistochemistry 156

Figure 67. Cell cycle study in BDL nuclear extracts by Western blot 158

Figure 68. Hepatic proliferative response to liver injury after BDL 159

Figure 69. GSSG/GSH ratio quantification in wild type and p38α knock out SHAM and 28 days BDL mice 159

Figure 70. Hepatocyte binucleation during culture 160

Figure 71. Isolated hepatocyte ploidy analysis by flow cytometry 161

Figure 72. Oxidative stress upon hepatocyte isolation 162

Figure 73. Cell cycle study in isolated hepatocytes 163

Figure 74. p38α regulation of cytokinesis: is there a role for oxidative stress? 167

Figure 75. SNAPSHOT: F-actin polymerization pathways in wild type old hepatocytes 175

Figure 76. Ploidy reversal upon p38α deficiency 178

Figure 77. SNAPSHOT: after weaning liver wild type and p38α knock out upon 72 hours partial hepatectomy 181

Figure 78. SNAPSHOT: adult hepatocytes from wild type and p38α knock out mice after BDL 187

Figure 79. ROS generation upon hepatocyte isolation and their effects on hepatocyte cell cycle 190

INDEX OF TABLES

INDEX OF TABLES

Table 1. Cyclins and phase regulation 19
Tabla 2. Distribución de grupos para los experimentos de citoquinesis y p38α 65
Tabla 3. Anticuerpos primarios utilizados en inmunohistoquímica................................83
Tabla 4. Anticuerpos secundarios utilizados en inmunohistoquímica............................83
Tabla 5. Anticuerpos primarios utilizados para *Western Blot*.................................. 92-93
Tabla 6. Anticuerpos secundarios utilizados para el *Western Blot*.................................94
Tabla 7. Primers para la cuantificación de ARNm por RT-PCR............................... 100-101
Table 8. Serum biochemistry in SHAM and BDL mice..142

ABBREVIATIONS

ABBREVIATIONS

ABB	**DEFINITION**
ADNc	ADN complementario
AKT	Protein kinase B
AP1	Activator protein 1
ASK1	Apoptosis signal-regulating kinase 1
ATF	Activating transcription factor
BAD	Bcl-2-associated death promoter
BAX	Bcl-2-associated X protein
BCA	Bicinchoninic acid
Bcl-2	B-cell lymphoma 2
Bcl-XL	B-cell lymphoma-extra large
BDL	Bile duct ligation
BEC	Biliary epithelial cell (cholangiocyte)
Birc2	Baculoviral IAP repeat-containing protein 2
BSA	Bovine serum albumin
c-fos	Human cellular homolog of the oncogene Finkel-Biskis-Jinkis murine osteosarcoma virus
C/EBPß	CCAAT / enhancer binding protein β
CBDL	Common bile duct ligation
Ccr5	C-C chemokine receptor type 5
Cdc14	Cell division cycle 14
Cdc25	Cell division cycle 25
Cdc42	Cell division cycle 42
Cdc7	Cell division cycle 7
CDK	Cyclin dependent kinase
CHOP	C/EBP homologous protein
Col1	Collagen 1
CREB	cAMP response element binding
CSBP	Cycling sequence binding protein

Ct	Threshold cycle
DDIT3	DNA damage-inducible transcript 3
DLK	Dual leucine zipper-bearing kinase
DUSP	Dual specific phosphatases
EBA	Extrahepatic biliary atresia
EGF	Epidermal growing factor
eIF4E	Eukaryotic translation initiation factor 4E
ELK1	Ets LiKe gene1
ERK	Extracellular signal-regulated kinase
Gly	Glycine
Gas2	Growth arrest-specific protein
GSK3β	Glycogen synthase kinase 3 β
GTPase	Guanosin triphosphatase
H3	Histone 3
HBP1	HMG-box transcription factor 1
HCC	Hepatocellular carcinoma
HePTP	Haemopoietic tyrosine phosphatase
HGF	Hepatocyte growing factor
hog	Hyperosmolarity activated gene
HPx	Partial hepatectomy
HSC	Hepatic stellate cell
HSP27	Heat shock protein 27
HVB	Hepatitis virus B
HVC	Hepatitis virus C
IGF1	Insulin growing factor 1
IL	Interleukin
IRS-1	Insulin receptor substrate 1
JLP	JNK-associated leucine zipper protein.
JNK	c-jun N-terminal kinase
Keap 1	Kelch-like ECH-associated protein 1

Ki67	Cellular marker for proliferation 67 discovered in Kiel
LSP1	Lymphocyte-specific protein 1
MAPK	Mitogen activated protein kinase
MAPKK	MAPK kinase
MAPKKK	MAPKK kinase
MEF	Mouse embryonic fibroblasts
MEF2A/C	Myocyte-specific enhancer factor 2A/2C
mHOG1	Mammalian product of the budding yeast hog1 gene
MITF1	Microphthalmia transcription factor 1
MK	MAPK-activated protein kinase
MKP	Mitogen-activated protein kinase phosphatases
MLK	Mixed-lineage kinase
MMPs	Matrix metalloproteases
MNK	MAPK- interacting kinase
MSK	Mitogen-and-stress-activated kinase
mTOR	Mechanistic target of rapamycin
NAFLD	Nonalcoholic fatty acid liver disease
NEM	N-etilmaleimida
NFAT	Nuclear factor of activated T cells
NFκB	Kappa-light-chain-enhancer of activated B cells
Nrf-2	Nuclear factor (erythroid-derived-2)-like 2
OLT	Orthotopic liver transplantation
OSM	Osmosensing scaffold for MEKK3
p56lck	p56 lymphocyte-specific protein tyrosine kinase
PBC	Primary biliary cirrhosis
PBS	Phosphate buffered saline
PCA	Perchloric acid
PCNA	Proliferating cell nuclear antigen
PCR	Polymerase Reaction Chain
PI3K	Phosphatidylinositide 3-kinase

PP2A	Protein phosphatase 2A
PP2C	Protein phosphatase 2C
PRL	Phosphatase of regenerating liver
PSC	Primary sclerosing cholangitis
PTEN	Phosphatase and tensin homologues deleted on chromosome 10
PTK	Protein tyrosine kinase
PTP	Protein tyrosine phosphatases
PTP-SL	Protein tyrosine phosphatase SL
PVDF	Polivinilidene fluorure
Rac1	Ras-related C3 botulinum toxin substrate 1
Raf-1	Rapidly Accelerated Fibrosarcoma
RhoA	Ras homolog gene family, member A
ROS	Reactive oxygen species
rpm	Revolutions per minute
RSK	Ribosomal S6 kinase
Sap1	Switching activating protein 1
SAPK2	Stress-activated protein kinase kinase 2
SASP	Senescene-associated secretory phenotype
SD	Standard deviation
SEC	Sinusoid epithelial cell
Ser	Serine
SFSS	Small-for-size syndrome
SHPC	Small hepatocyte-like progenitors
STAT1	Signal transducer and activator of transcription 3
STAT3	Signal transducer and activator of transcription 3
STEP	Striatal enriched tyrosine phosphatase
TAB1	TGFβ activated protein 1 binding protein 1
TAK1	TGFβ activated kinase 1
TAO 1/2	Thousand-and-one amino acid kinase
TBS-T	Tris Buffered Saline - Tween

TGFβ	Transforming growth factor beta
Thr	Threonine
Timp1	Metallopeptidase inhibitor 1
TNFα	Tumor necrosis factor alpha
TPL2	Tumor progression locus 2
Tyr	Tyrosine
WHO	World health organization
ZAK1	Zaphod kinase
ZAP70	ζ –chainassociated protein kinase of 70 kDa

ABSTRACT / RESUMEN / RESUM

ABSTRACT

The p38 MAPK family is an environmental stress transducer group of kinases that respond to hyperosmolarity, UV irradiation, heat shock, inhibition of protein synthesis, oxidative stress and numerous mediators of inflammation. The role of the p38 MAPK pathway in apoptosis, cell growth inhibition, cell differentiation, and inflammatory response is well established and has been broadly reviewed. However, the regulation of the last stage of the cell cycle, cytokinesis, by p38 MAPKs is not characterized yet.

Polyploid cells contain more than two sets of homologous chromosomes. Among all the different mechanisms that may lead to polyploid cells (mononuclear or polynuclear shapes), cytokinesis failure is the one that generally occurs in hepatocytes. We observe that the absence of p38α in mouse liver induces

hepatocyte binucleation. In fact, a significant increase in hepatocyte binucleation has been shown under basal conditions, after partial hepatectomy and during biliary cirrhosis in p38α knock out mice. However, binucleation reversal, also known as ploidy reversal, seems not to be essentially regulated by p38α. Moreover, induction of hepatocyte binucleation is associated with the reduction in relative liver mass (liver weight/body weight) upon age, after partial hepatectomy and during biliary cirrhosis. Indeed, p38α knock out hepatocytes exhibit numerous markers of mitotic delay. Thus, in this Thesis we propose a role for p38α in the regulation of the hepatocyte mitosis progression and cytokinesis upon age and during liver regeneration.

On the one hand, our results suggest a p38α-mediated regulation of cyclins expression that seems necessary to accomplish the mitotic checkpoints during

hepatocytes's replication and, on the other hand, they highlight the key role of MNK1, required for cell abcission and activated by p38α, in the regulation of hepatocyte cytokinesis. Interestingly, actin polymerization deficiencies in old p38α knock out hepatocytes could also enhance cytokinesis failure *via* HSP27 inhibition and Rho pathway inactivation.

Furthermore, since two of the main functions of the liver are metabolism and detoxification -involving reactive oxygen species generation-, and considering the significant link between binucleation and oxidative stress generation, we have determined the REDOX status upon p38α deficiency. As an approach, we have studied the role of reactive oxygen species during binucleation induction in the isolation of murine primary hepatocyte. We demonstrate that oxidative stress contributes to hepatocyte binucleation in hepatocyte isolation and may play a role in the induction of binucleation under p38α absence in liver regeneration.

In conclusion, the cell cycle control in hepatocytes and the induction of binucleation are regulated by p38α, establishing a better understanding of liver polyploidization, which is definitively needed for clinical research and provides more clues for the mystery of liver regeneration.

RESUMEN

La familia p38 MAPK está constituida por un grupo de quinasas trasductoras de señales que responden a la hiperosmolaridad, la radiación ultravioleta, el choque térmico, la inhibición de la sínteis de proteínas, el estrés oxidativo y los mediadores de la inflamación. El papel de la ruta p38 MAPK durante la apoptosis, la respuesta inflamatoria y la inhibición del crecimiento y diferenciación celular es muy conocido, y ha sido objeto de revisión en numerosas ocasiones. Sin embargo, la función que desempeñan las p38 MAPKs en la regulación de la última etapa de la mitosis, es decir, la citoquinesis, es todavía desconocido.

Las células poliploides son las que contienen más de dos comjuntos de cromosomas homólogos. Entre los diferentes mecanismos que desencadenan la aparición de células poliploides (tanto mononucleares como polinucleares), el fallo en la citoquinesis es el que habitualmente genera la poliploidía en los hepatocitos. En relación a ello, hemos observado que la ausencia de p38α en el hígado murino induce binucleación en los hepatocitos. De hecho, el incremento significativo en la binucleación hepática aparece tanto en condiciones basales, como tras la hepatectomía parcial y durante la cirrosis biliar en los ratones deficientes de p38α. Sin embargo, la reversión de la binucleación, conocida como reversión de la ploidía, no es una función que dependa exclusivamente de p38α. Además, la inducción de la binucleación en los hepatocitos mediada por la deficiencia de p38α está asociada con la disminución de la masa hepática relativa (peso del hígado/ peso del ratón) según los ratones son más viejos, y tras la hepatectomía parcial y la indución de la colestasis. Incluso los hepatocitos deficientes de p38α presentan numerosos marcadores de enlentecimiento mitótico. Todo ello nos conduce a proponer el papel de p38α

en la regulación de la progresión mitótica y la citoquinesis durante el envejecimiento y la regeneración hepática.

Por un lado, nuestros resultados sugieren la regulación, mediada por p38α, de la expresión de ciclinas, las cuales son necesarias para completar los diferentes puntos de control de la mitosis en los hepatocitos. Por otro lado, proponemos que la activación de MNK1 –necesaria para la división celular- durante la citoquinesis está mediada por p38α. Además, nuestros hallazgos muestran el efecto de la ablación de p38α sobre la polimerización de la actina con la edad, en los hepatocitos: las deficiencias que aparecen en la polimeración de la actina tras la deficiencia de p38α también potencian el fallo de la citoquinesis debido a la inhibición de HSP27 y la inactivación de la vía de las Rho GTPasas.

Igualmente, dado que dos de las principales funciones del hígado son el metabolismo y la detoxificación, las cuales generan especies reactivas del oxígeno; y considerando la relación que existe entre el estrés oxidativo y la inducción de la binucleación, en esta Tesis hemos querido determinar el estado REDOX tras la ablación de p38α. Como una aproximación inicial, y para demostrar que el estrés oxidativo puede ser causa de la binucleación, hemos estudiado el papel de las especies reactivas del oxígeno en la generación de hepatocitos binucleados durante el aislamiento de hepatocitos primarios murinos. Asimismo, hemos demostrado que el estrés oxidativo contribuye a la inducción de la binucleación en los hepatocitos durante su aislamiento. Por ello, el estado pro-oxidante que exhiben los hígados deficientes de p38α podría estar influyendo en las altas tasas de binucleación hepática que presentan estos ratones.

En conclusión, tanto la regulación del ciclo celular como la inducción de la binucleación son procesos mediados por p38α en los hepatocitos murinos. De este modo, los resultados de esta Tesis contribuyen al conocimiento más detallado de la poliploidización hepática, proporcionando información de gran interés en la clínica y en la investigación básica, aportando más datos que nos permitirán, en un futuro, aclarar los misterios de la regeneración hepática.

RESUM

La família p38 MAPK està constituïda per un grup de quinases transductores de senyals que responen a la hiperosmolaritat, la radiació ultraviolada, el xoc tèrmic, la inhibició de la síntesi proteica, l'estrès oxidatiu i els intermediaris de la inflamació. La funció de les p38 MAPKs durant l'apoptosi, la resposta inflamatòria i la inhibició del creixement i diferenciació cel·lular és molt sabuda i ha sigut àmpliament revisada. Tanmateix, el paper que exerceix p38 MAPK sobre la regulació de l'última etapa de la mitosi, és a dir, la citocinesi, és encara prou desconeguda.

Las cèl.lules poliploides sòn les que contienen més de dos conjunts de cromosomes homòlegs. Entre els diferents mecanismes que desencadenen l'aparició de cèl·lules poliploides (tant mononuclears como polinuclears), l'error en la citocinesi és el que sovint genera la poliploïdia als hepatòcits. En referència a aquesta descoberta, hem observat que l'absència de p38α al fetge de ratolí genera binucleació en els hepatòcits. De fet, l'increment significatiu en la binucleació hepàtica apareix tant en condicions basals, com després de l'hepatectomia parcial i durant la cirrosi biliar als ratolins deficients de p38α. Tanmateix, la reversió de la binucleació, coneguda como reversió de la ploïdia, no és una funció que depenga exclusivament de p38α. A més, la inducció de la binucleació als hepatòcits mitjançada per la deficiència de p38α està associada amb la disminució de la massa hepàtica relativa (pes del fetge/ pes del ratolí) segons els ratolins són mes vells, i després de l'hepatectomia parcial i la inducció de la colèstasi. Fins i tot, els hepatòcits deficients de p38α presenten nombrosos marcadors d'alentiment mitòtic, cosa que ens condueix a proposar, el paper de p38α en la regulació de la progressió mitòtica i la citocinesi durant l'envelliment i la regeneració hepàtica.

Per una banda, els nostres resultats sugereixen la regulació, arbitrada per p38α, de l'expressió de les ciclines, les quals són necessàries per a completar els diferents punts de control de la mitosi als hepatòcits. Per l'altra, proposem l'activació de MNK1 -necessària per a la divisió cel.lular- mitjançada per p38α durant la citocinesi. Endemés, les nostres troballes mostren l'efecte de la manca de p38α sobre la polimerització de l'actina als hepatòcits senescents: les deficiències que apareixen en la polimerització de l'actina a causa d'absència de p38α també potencien la fallada de la citocinesi per la inhibició de HSP27 i la inactivació de la via de les Rho GTPases.

Igualment, considerant que les principals funcions del fetge són el metabolisme i la destoxificació, les quals impliquen la generació d'espècies reactives de l'oxigen relacionades amb la generació de binucleació, en aquesta Tesi hem volgut determinar l'estat REDOX després de la delecció de p38α. Per demostrar que l'estrès oxidatiu pot ser causa de la binucleació hepàtica, hem estudiat l'efecte de les espècies reactives de l'oxigen en la generació de hepatòcits binucleats durant l'aïllament de hepatòcits primaris de ratolí. Així mateix, hem demostrat que l'estrès oxidatiu contribueix a la inducció de la binucleació dels hepatòcits durant l'aïllament. Per tant, l'estat prooxidant que mostren els fetges deficients de p38α podria estar influint en les altes taxes de binucleació hepàtica que presenten aquests ratolins.

En conclusió, tant la regulació del cicle cel·lular como la inducció de la binucleació són processos regulats per p38α. De manera que els resultats d'aquesta Tesi contribueixen al coneixement més detallat de la poliploidització hepàtica, procuren informació de gran interès en la clínica i en la investigació bàsica, i proporcionen més dades que ens permetran, en un futur, descobrir les claus més misterioses de la regeneració hepàtica.

INTRODUCTION

Chapter 1

I. INTRODUCTION

1. The liver

1.1. Anatomical location and features

The liver is the largest organ in the body. In humans, adult male liver weighs from 1,4 to 1,6 kg and in adult females from 1,2 to 1,4 kg. In fact, the liver is about one thirty-sixth of the entire body weight. It presents the appearance of a wedge, the base of which is directed to the right and the thin edge towards the left. It is located in the upper and right part of the abdominal cavity, occupying almost the whole of the right hypochondrium, the greater part of the epigastrium, and it usually extends into the left hypochondrium and the mammary line [Standring S. 2008].

The liver is composed of lobes, held together by loose connective tissue, in which blood vessels (portal vein, hepatic artery, and hepatic veins), lymphatic vessels, hepatic ducts and nerves ramify. The entire structure is covered by a serous and a fibrous coat [Gebhardt R. and Ueberham E. 2006] (Figure 1).

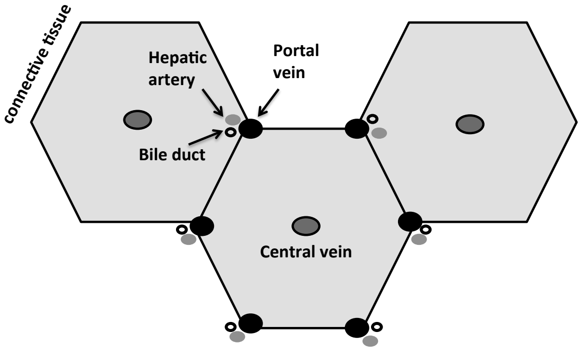

Figure 1. Classical liver lobe. The functional microscopic unit of the liver is referred to as the liver lobule: It is a six-sided prism that has in its center the central vein and in its corners the portal triads (portal vein, hepatic artery and bile duct).

The mouse liver has 6 lobes: median, left, anterior right, posterior right, right median, and caudate lobe [Hori T. *et al.,* 2012]. Each lobe is filled by cords of hepatic parenchymal cells, the hepatocytes, which radiate from the central vein and are separated by vascular sinusoids (blood channels) and bile ducts (Figure 2). Blood enters the liver and flows along sinusoids towards the central veins [Spear B.T. *et al.,* 2006].

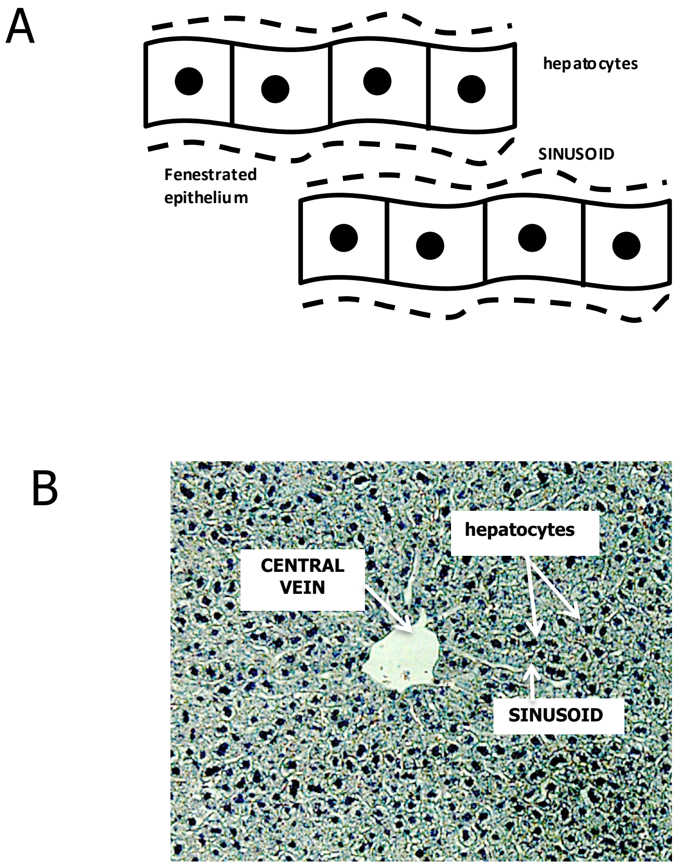
A
hepatocytes
SINUSOID
Fenestrated epithelium
B
hepatocytes
CENTRAL VEIN
SINUSOID

Figure 2. Liver parenchyma representation. It consists of hepatocyte cords arranged around the central vein: schematic representation (A), and representative hematoxylin and eosin image (B).

The hepatic artery supplies oxygen-rich blood while the portal vein supplies blood low in oxygen, but rich in nutrients and metabolic subproducts from the gastrointestinal tract. Bile flows in the opposite direction of blood flow, towards the portal triad where it is transported *via* bile ducts to the gall bladder for storage before being released into the small intestine [Everson G.T. *et al.*, 1983].

There are other ways of dividing the liver parenchyma into units: the acini. They are functional units formed by the vessels of the portal triad but not the portal triad itself. The acinus is a smaller unit than liver lobe and is oriented around the afferent vascular supply of the liver lobes and thus, it represents a unit of relevance to liver function.

1.2. Histology

The liver consists of a wide variety of cells, being hepatocytes the main cell type (Figure 3). Hepatocytes are around 70% of the liver mass and the majority of the liver function can be attributed to them. Hepatocytes are polyhedral polarized epithelial cells and measure from 12 to 25 μm in diameter. Polarization implies that the apical portion of the hepatocyte is exposed to the canalicular lining where bile flow and secretion occurs and, that the basolateral sides are involved in exchange of nutrients, toxins, and metabolic products [Spear, B.T. *et al.,* 2006].

Hepatocytes contain a high percentage of endoplasmic reticulum and are rich in mitochondria. Mitochondria provide them with great synthetic potential [Malarkey D.E. *et al.,* 2005]. Hepatocytes are usually granular. Granules can have glycogen, fat or iron. Moreover, hepatocytes have one or two distinct nuclei, with different ploidy [Gentric G. *et al.,* 2012]. The nucleus also exhibits refractile nucleoli [Campo-Ruiz V. *et al.,* 2005].

Sinusoid epithelial cells (SECs) or liver sinusoids are the second most common cell type in the liver and they represent 20% of the cellular content [Malarkey D.E. *et al.,* 2005]. They are fenestrated cells that lack of a basal membrane, keeping hepatocytes in direct contact with blood. SECs form the blood hepatocyte barrier and thus, they are necessary for the exchange of materials with blood. Thus, next to the sinusoids, there are cells involved in the immune response: Kupffer cells and Pit cells.

Kupffer cells are resident macrophages of the liver that are primarily located in the sinusoids, often in the ones that are nearer to the portal vein. They present antigens, produce a variety of cytokines and chemokines and have phagocytic capacity for bacteria, damaged and aged red blood cells, as well as for macromolecules from the circulation [Crofton R.W. *et al.,* 1978; Wisse E. *et al.,* 1996; Spear B.T. *et al.,* 2006].

Pit cells are resident natural killer cells of the liver, anchored to the sinusoidal endothelium by pseudopodia [Bouwens L. and Wisse E. 1992].

Fenestrations in SECs permit blood plasma to flow freely over the exposed surfaces of the hepatocytes through the space of Disse, made up of connective tissue, where liver fibroblasts reside [Braet F. and Wisse E. 2002]. In addition, hepatic stellate cells (HSCs) are also located at intervals within the space of Disse, being the major sites of vitamin A storage in adults and good producers of extracellular matrix. The activation of HSCs is a critical event in liver fibrosis and regeneration [Friedman S.L. 2008].

Other less abundant cellular groups are biliary epithelial cells (BECs) or cholangiocytes, which represent 5% of total cells in the liver. They are ciliated epithelial cells that share a common lineage with hepatocytes [Spear, B.T. *et al.,* 2006]. Cholangiocytes that recover the major ducts are predominantly involved in secretory functions. They contribute to bile secretion *via* the release of bicarbonate and water [Tietz P.S. and Larusso N.F 2006]. Cholangiocytes that are located in smaller ducts have roles in inflammatory and proliferative responses [Alpini G. *et al.,* 1996; Alpini G. *et al.,* 1997].

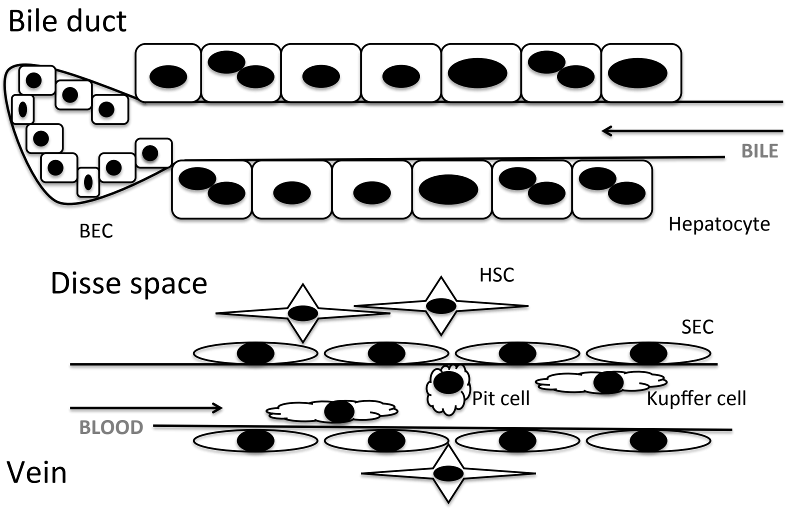

Figure 3. Schematic representation of liver histology. Main cellular types are: hepatocytes, biliary epithelial cells (BECs), hepatic stellate cells (HSCs), sinusoid epithelial cells (SECs), Pit cells and Kupffer cells.

Stem cells can also be found in the liver. They are classified into two categories: liver stem cells and hematopoietic stem cells.

(a) Liver stem cells or hepatocyte precursor cells, also called oval cells owing to its morphological aspect: scarce cytoplasm and ovoid nucleus [Oh S.H. *et al.,* 2002]. Oval cells are also referred as small hepatocyte-like progenitors (SHPCs) in rodents [Gordon G.J. *et al.,* 2000; Roskams T. *et al.,* 2004] and intermediate cells in humans [Roskams T. *et al.,* 2004;

Roskams T. 2006]. They were first described by Kinosita in 1937 [Kinosita R. *et al.,* 1937] and are considered as an undifferentiated cell group that is able to reestablish the liver tissue, intestinal epithelium, and pancreas. Oval cells have the ability for self-renovation, proliferation, and differentiation [Thorgeirsson S.S. 1996]. Oval cells express morphological and immunophenotypic features typical of both hepatic and biliary epithelial cells, known as bipotential characteristics [Grompe M. 2003].

(b) Hematopoietic stem cells or progenitors of hematopoietic cells can also be found in liver tissue. These cells derived from the bone marrow may have the role of progenitor cells in tissues under aggression. Cells originated from the bone marrow are distinct from oval cells, although they share some functions [Crosby H.A. *et al.,* 2002; Sell S. 2001]. In fact, oval cells may be considered another specific progenitor of liver stem cells, and not a progeny from hematopoietic stem cells [Sell S. 2001; Tarla M.R. *et al.,* 2006].

Regarding regeneration after liver damage, three lines of defense are considered. First line of defense is provided by hepatoblasts (hepatocyte and cholangiocyte precursors) and hepatocytes that are thought to be functional stem cells by themselves [Shafritz D.A. and Dabeva M.D. 2002]. Then, if more severe liver damage occurs, oval cells are activated. In fact, their capacity to regenerate tissues after injury takes place when hepatocytes are unable to proliferate [Theise N.D. *et al.,* 1999]. Hematopoietic stem cells may contribute to the renewal of hepatocytes, but only at lower rate in the case of extensive damage and under very strong positive selective pressure [Dakalas E. *et al.,* 2005; Thorgeirsson S.S. and Grisham J.W. 2006].

1.3. Liver function

The liver is a vital organ with highly diversified functions. It is involved in over 150 different vital functions including: metabolism, detoxification, storage, and maintenance of homeostasis in the body. The liver possesses endocrine functions: the production or removal of glucose, the processing of fatty acids and triglycerides, the maintenance of cholesterol homeostasis *via* its synthesis or catabolism, the synthesis and interconversion of non-essential amino acids, secretion of large amounts of bile into the digestive tract. It also produces serum proteins, including clotting factors and transport proteins, such as albumin and transferrin [Lemaigre F. and Zaret K.S. 2004], and removes serum proteins, red blood cells, microorganisms and toxic endogenous compounds such as ammonia [Spear B.T. *et al.,* 2005].

Interestingly, the liver performs these wide range of functions meanwhile has the extraordinary capacity of efficient regeneration. Thus, appropriate liver functions are fundamental to human health and the loss of these functions can be severely compromising.

1.4. Liver regeneration

Regeneration of the liver consists on a compensatory hyperplasia that tries to meet the functional needs of the body. Liver regeneration can be divided into three phases: priming (1), proliferation (2), and cessation of proliferation (3) [Diehl A.M. 2000; Fausto N. 2000; Taub R. 2004].

(1) The first stage begins with the secretion of pro-infammatory cytokines such as interleukin 6 (IL-6) and tumor necrosis factor alpha (TNFα), and the following activation of nuclear factor kappa-light-chain-enhancer of activated B cells (NF-κB), activator protein 1 (AP1) and signal transducer and activator of transcription 3 (STAT3). The activation of these transcription factors is responsible for the G_0/G_1 transition [Diehl A.M. 2000; Fausto N. 2000; Taub R. 2004] (Figure 4). IL-6 is responsible for activating approximately 40% of these genes. Studies in liver-specific STAT3 null mice demonstrated a significant contribution of the IL-6-induced STAT3 pathway to the priming stage [Streetz K.L. *et al.,* 2000].

(2) Priming is continued by hepatocyte proliferation, which is directed by the release of several mitogens: hepatocyte growth factor (HGF), ligands of the epidermal growth factor (EGF), fibroblast growth factor receptors [Borowiak M. *et al.,* 2004; Huh C.G. *et al.,* 2004; Mitchell C. *et al.,* 2005], insulin-like growth factor 1 (IGF-1) and its receptor [Pennisi P.A. *et al.,* 2004; Desbois-Mouthon C. *et al,* 2006]. These growth factors go over the G_1 restriction point, allowing hepatocytes to pass into the S phase (Figure 4). DNA synthesis starts in the hepatocytes near the portal vein and progress to the cells adjacent to the central vein [Grisham J.W. 1962]. Moreover, a recent work by Song [Song G. *et al.,* 2010] has demonstrated the importance of micro RNAs (miRNAs) in regulating hepatocyte proliferation during liver regeneration.

(3) When the initial liver mass is restored, transforming growth factor β (TGFβ) and activin signaling [Oe S. *et al.,* 2004] gives back hepatocytes to a quiescent status.

1.4.1. Partial hepatectomy as a model of liver regeneration

Liver regeneration induced by the resection of two-thirds of the liver (partial hepatectomy or 70% hepatectomy) is an excellent model to study compensatory hepatic hypertrophy. It was firstly proposed by Higgins and Anderson in 1931 [Higgins G.M. and Anderson R.M. 1931]. During this regenerative process hepatocytes and cholangiocytes start DNA synthesis in order to multiplicate and recover the loss of liver mass in a few days. In fact, most of the hepatocytes undergo around three rounds of DNA synthesis until liver is restored [Gupta S. 2000].

Although mouse partial hepatectomy has been used extensively in studies of liver regeneration, it does not require progenitor cell proliferation [Mao S.A. *et al.*, 2014]. It exclusively involves hepatocyte and cholangiocytes proliferation. Liver regeneration after partial hepatectomy is different from other chemical-induced "true" liver regeneration, as for example it happens in D-galactosamine toxicity, where replication of progenitor cells does occur [Lemire J.M. *et al.,* 1991]. In humans, liver regeneration usually occurs after injury from an ischemic or toxic insult (drug overdose, alcohol consumtion) [Koniaris L.G. *et al.,* 2003]. Thus, new models that involve regenerating pathways where progenitor cells play a major role would be required.

Furthermore, one interesting detail after this surgery is the increase in ploidy of liver that occurs in the long term after partial resection [Sigal S.H. *et al.,* 1999]. The increase in mature/senesced cells with polyploidy DNA content was described some decades ago [Alison M.R. and Wright N.A. 1985; Sigal S.H. *et al.,* 1999].

Although it was also postulated that polyploid hepatocytes loss their mitotic potential after a second injury -and the consequent regenerative process [Sigal S.H. *et al.,* 1999]- the hepatocyte ability for performing reductive mitosis [Duncan A.W. *et al.,* 2010] would explain the capacity of the liver to regenerate after repeated partial hepatectomies [Simpson G.E. and Finckh E.S. 1963; Solopaev B.P. and Bobyleva N.A. 1972].

1.5. Liver disease

Due to the fact that the liver carries so many functions, it is not surprising that liver disease is a considerable health problem worldwide [Cave M. *et al.,* 2007; Corey K.E. and Kaplan L.M. et al., 2014]. Liver disease is also highly prevalent worldwide. Each year, it is estimated that 2 million people die of liver disease [Rozga J. 2006]. The World Health Organization (WHO) reported in 2012 that liver cirrhosis stood on the 12th position of the 20 leading causes of death and it was the first cause of death of no communicable digestive disease. Liver cirrhosis represented 1,8% of deaths in the world in 2012 and is getting higher each year. Moreover, liver cirrhosis was the 17th global cause of years of life lost reported in WHO's World Health Statics 2012 [cited from WHO website (1)].

Fibrosis and cirrhosis are the consequences of a sustained wound healing response to chronic liver injury from viral, autoimmune, drug induced, cholestatic –impairment of bile flow and accumulation of bile acids in the liver- or metabolic diseases. Liver cirrhosis is the result of sustained liver injury and the last stage of fibrosis [Friedman S.L. 2003; Mahli H. and Gores G.J. 2008]. Although progression of fibrosis depends on age, gender, environmental factors, and genetic factors [Hillebrandt S. *et al.,* 2005], hepatic fibrosis and cirrhosis are among the most common digestive diseases [Hillebrandt S., *et al.,* 2002].

Indeed, liver cirrhosis can lead to hepatocellular carcinoma (HCC) [Halilbasic E. *et al.,* 2013]. Liver cancer appeared on the 17th position of the 20 leading causes of death in 2012. HCC is the most common primary malignancy of the liver [Lahousse S.A. *et al.,* 2011] and the third most common cause of cancer death globally. It carries a terrible prognosis because it usually becomes metastatic before being diagnosed [Hoenerhoff M.J. *et al.,* 2011]. In 2012, HCC represented 1,3% of deaths in the world [cited from WHO website (1)] and its incidence is increasing in developed countries, such as the United States of America and European countries [Zhu A.X. 2010].

The main factors that nowadays contribute to the development of liver disease are: Hepatitis B and Hepatitis C virus (HBV and HCV) - WHO's data for 2013 established that 240 million people suffer from HBV and 150 million for HCV [cited fromWHO website (2)], autoimmune and metabolic disorders, and alcohol. In addition, the increasing prevalence of obesity and insulin resistance lead to non-alcoholic fatty liver disease (NAFLD) and establishment of steatosis (or accumulation of triacylglycerol in hepatocytes), steatohepatitis, fibrosis, cirrhosis [Burt A.D. *et al.,* 1998], HCC [Siegel A.B. and Zhu A.X. 2009], portal hypertension, and liver failure [Burt A.D. *et al.,* 1998].

1.5.1. Cholestatic disorders

Cholestatic disorders result from a failure in the secretory transport in the hepatocytes or in the ductular cells (intrahepatic cholestasis), or from the blockade of the excretory pathways outside the liver (extrahepatic cholestasis) [Trauner M. 1997, Trauner M. and Boyer J.L. 1999].

Cholestatic disorders comprise familial cholestatic disorders, obstructive cholestasis, extrahepatic biliary atresia (EBA), primary sclerosing cholangitis (PSC), cholestasis of pregnancy, sepsis-induced cholestasis, drug-induced cholestasis, and primary biliary cirrhosis (PBC) [Rodriguez-Garay E.A. 2003;

Trauner M. and Boyer J.L. 2003; Kouroumalis E. and Notas G. 2006]. They all have common clinical manifestations and pathogenic features that include the response of hepatocytes and colangiocytes to injury [Hirschfield G.M. *et al.,* 2010].

Primary biliary cirrhosis is a disease of unknown etiology characterized by the progressive destruction of the small intrahepatic ducts that finally develops liver cirrhosis and hepatic failure. Due to the frequent presence of autoantibodies, it is considered to be an autoimmune disease [Kouroumalis E. and Notas G. 2006].

1.5.2. Bile duct ligation as a model of cholestasis

Bile duct ligation (BDL) or common bile duct ligation (CBDL) is an *in vivo* model of obstructive cholestasis that is based on the impairment of the biliary excretion system at the level of the extrahepatic bile ducts [Rodriguez-Garay E.A. 2003]. Under this condition, the excretion of the bile is blocked and it severely affects the liver, causing increased permeability of the hepatocyte membrane that leads to a loss of osmotic driving forces [Boyer J.L. 1983]. The lack of required excretion promotes the multiplication and elongation of the bile ductules (ductular reaction) that appear after cholestasis induction [Desmet V.J. 1995]. The sustained parenchymal cell damage leads to liver cirrhosis, ascites, and portal hypertension [Bataller R. and Brenner D.A. 2005]. Obstructive jaundice is developed during this procedure and causes depletion of the antioxidant vitamin E, and overproduction of reactive oxygen species (ROS) [Tsai L.Y. *et al.*, 1993; Karageorgos N. *et al.,* 2006].

1.6. New alternatives to liver transplantation: partial liver transplantation and hepatocyte transplantation

As it has been described, liver cells (hepatocytes, and progenitor cells) are quiescent cells that can go through the cell cycle when an injury affects liver function. However, the severity of some conditions limits the self-renewal capacity of the liver and risks to liver failure. The only curative mode of management for liver failure when intrinsic proliferative potential is limited is liver transplantation [Dutkowski P. *et al.,* 2014].

Orthotopic liver transplantation (OLT) is an invasive technique that carries higher morbidity and mortality, requires immunosupresive therapy, and it is limited by the number of donors [Jorns C. *et al*., 2012]. In addition to this, it is not always necessary to replace the whole organ if only hepatocytes are affected. Considering the limitations of OLT, improvements in the approach of hepatocyte transplantation are very welcomed.

Novel alternatives, such as partial liver transplantation and hepatocyte transplantation, are used until an organ is available for transplantation or when the patient is not suitable for liver transplantation.

Partial liver transplantation from a living donor is being performed with increasing frequency. In this surgical approach, the objective is that the new implanted draft undergoes proliferation and can potentially restore the host liver mass. Small for-size-syndrome (SFSS) results from an inability of a small graft to regenerate, and it is the main limiting factor in expanding partial liver transplantation [Serenari M. *et al.,* 2013]. SFSS progresses to acidosis, hypoglycemia, septic shock, renal and pulmonary failure, and death without retransplantation [Dahm F. *et al*., 2005]. Moreover, little evidence exists so far to explain how altered liver pathology may affect the process of liver regeneration.

Hepatocyte transplantation has grown over the last decade in clinics, and nowadays it is considered the less aggressive clinical approach for patients with life-based metabolic disorders or with acute/chronic liver failure [Bonavita A.G. *et al.,* 2010; Dhawan A. *et al.,* 2010]. Primary hepatocytes are isolated from organs that would be rejected for transplantation, which are still suitable for digestion. In general, they come from steatotic or non-heart beating donors [Mitry R.R. *et al.,* 2004; Hughes R.D. *et al.,* 2006]. Considering that the cell quality obtained from these livers is really poor, upgrades during the isolation and the transplantation procedure are needed in order to improve the engraftment, survival and function of transplanted hepatocytes.

Although novel techniques have appeared in the last decade, understanding the regenerative process in order to recover from injury is essential for the treatment of liver failure.

2. Liver ploidy

2.1. Cell cycle and cytokinesis

Cell cycle is composed by five phases, called as follows: G_0, G_1, S, G_2 and M (Figure 4).

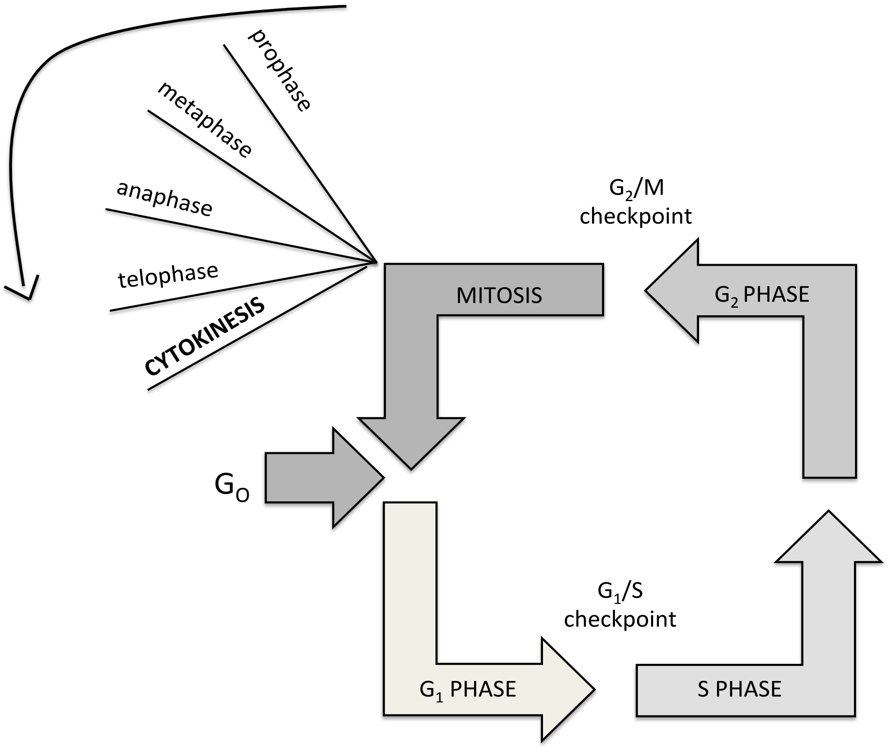
prophase
metaphase
anaphase
telophase
CYTOKINESIS
MITOSIS
G_2/M checkpoint
G_2 PHASE
G_O
G_1/S checkpoint
G_1 PHASE
S PHASE

Figure 4. Cell cycle representation with its different phases and checkpoints. Mitotic phase is composed by four stages: prophase (chromatids compact tightly, the nuclear envelope disappears, centrioles separate and radiating fibers appear), metaphase (chromosomes gather at the equatorial plane), anaphase (the two chromatids of each chromosome separate), and telophase (daughter nuclei is formed).

Upon stimulation, cells abandon their quiescent state G_0 in order to enter into G_1 phase and then progress to S phase, where DNA replication takes place. After DNA replication, the G_2 phase lets the cell grow and be ready for mitosis

(M phase) and cytokinesis. Cytokinesis or cytoplasmatic division is the last stage of mitosis. During this process, the mother cells gives two daughter cells by physical separation. Cytokinesis begins after the creation of the mitotic spindle that signals: the contraction of the actomyosin ring (1), the ingression of the cleavage furrow -invagination of the cell's surface that begins cleavage- (2) and the formation of the intracellular bridge whose degradation would lead to the cell abscission (3) [Schiel J.A. and Prekeris R. 2010]. Cytokinesis relies on complex and coordinated cell shape changes associated with membrane and cytoskeleton rearrangements [Piekny A. *et al.,* 2005; Barr F.A and Gruneberg U. 2007; Schiel J.A. and Prekeris R. 2010] (Figure 5).

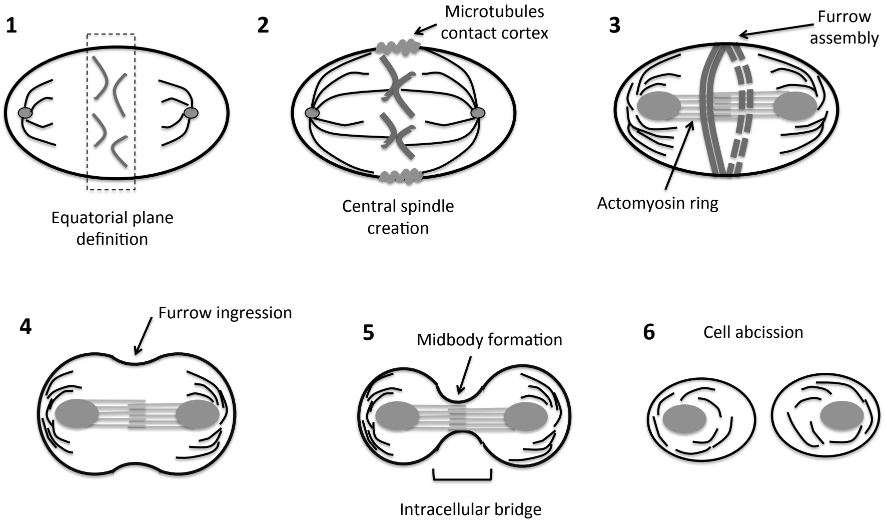
1
Equatorial plane definition
2
Microtubules contact cortex
Central spindle creation
3
Furrow assembly
Actomyosin ring
4
Furrow ingression
5
Midbody formation
Intracellular bridge
6
Cell abcission

Figure 5. Conformational changes prior to cytokinesis. During metaphase chromosomes align on the equatorial plane (1). Anaphase involves the microtubules' contact with the cell cortex (2). In early telophase, the formation and contraction of the actomyosin ring, and assembly and ingression of the cleavage furrow take place (3,4). Midbody formation and definition of the intracellular bridge occur during late telophase (5) and it is followed by cell abscission (6).

In mammals, regulation of cell cycle progression is mainly controlled by a group of protein kinases named cyclin dependent kinases (CDKs). CDKs bind to various cyclins to form CDKCs (CDK cyclin complexes). The increase in these complexes controls progression throughout the cycle [Vermeulen K. 2003; Malumbres M. and Barbacid M. 2009] (Table 1).

Table 1. Cyclins and phase regulation.

cyclin	CDKs	phase
D	CDK4 CDK6	G_1 phase
E	CDK2 CDK3	G_1/S
A	CDK1 CDK2	S phase, G_2/M, early M phase
F	No CDK partner	G_2/M, early M phase
B	CDK1	G_2/M, early M phase

[Vermeulen L. *et al.,* 2003; Satyanarayana A. and Kaldis P. 2009].

2.2. Poliploidy

Polyploidy is the heritable condition of possessing more than two complete sets of chromosomes [Comai L. 2005]. Gene duplication can provide new genetic material for mutation and, as a result, specialization or new gene functions. Without gene duplication the plasticity of a genome or species would be severely limited in adapting to changing environments [Magadum S. 2013]. Polyploid organisms are tolerated in animals –such as fish and amphibians [Stöck M. and Lamatsch D.K. 2013]- and it is completely viable in only two mammals: the red and the golden viscacha rats (*Tympanoctomys barrerae* and *Pipanacoctomys aureus,* repectively) [Gallardo M.H. *et al.,* 2006].

In humans, polyploidy is only found in certain tissues and not in the whole body [Coe S.J. *et al.,* 1993; Malan V. *et al.,* 2006]. In general, eukaryotic cells are generally prevented from becoming polyploid, due in part to the mitotic spindle checkpoint, and do not exit from mitosis until the mitotic cyclin, cyclin B, is successfully degraded [Hixon M.L. *et al,* 2000; Hixon M.L. *et al,* 2000]. In hepatocytes, the frequency of polyploidy varies with age and species, being up to 90% in mouse hepatocytes and to 50% in human hepatocytes [Duncan A.W. and Soto-Gutierrez A. 2013].

2.3. Binucleation

Among all the mechanisms that may lead to polyploid cells, cytokinesis failure is the one that generally occurs in hepatocytes [Guidotti J.E. *et al.,* 2003; Margall-Ducos G. *et al.,* 2007]. As liver is a mitotically quiescent organ but has the unique capacity to regulate its growth and mass, it is a fascinating model for understanding controlled cytokinesis failure. The defects that can trigger cytokinesis failure occur when: (a) the establishment of the division/equatorial plane; (b) the furrow ingression through contraction of an actomyosin ring; and (c) the cell abscission.

2.3.1. Binucleation in liver development

Hepatocyte binucleation is considered as an age-dependent process, though it appears in late fetal development and postnatal maturation [Overturf K. *et al.*, 1996]. As it happens in other tissues, hepatocytes synthesize DNA at highest rate during liver fetal development [Gupta S. 2000]. After birth, and during the first 3 weeks that correspond with the suckling period, DNA synthesis keeps going, associated with hepatocellular growth. These mitotic rates are lower comparing to the ones shown during fetal development and thus, postnatal liver growth is accomplished primarily with hepatic hypertrophy [Gupta S. 2000]. It is during postnatal liver growth when polyploidization is stablished, accompanied with the decreasing hepatocyte ability to proliferate [Celton-Morizur S. *et al.,* 2010; Celton-Morizur S. and Desdouets C. 2010].

Controlled failure of cytokinesis in the liver occurs as a result of the absence of actin cytoskeleton organization at the cleavage plane. They do not form a contractile ring and thus cleavage-plane specification is never established. Consequently, active Ras homolog gene family member A (RhoA) does not concentrate in the furrow formation leading to an absence of activation of its downstream signals targets involved in cytokinesis dynamics [Guidotti J.E. *et al.,* 2003; Margall-Ducos G. *et al.*, 2007]. RhoA co-localizes with F-actin during cytokinesis and concentrates at the equatorial cell cortex at the site of the nascent cleavage furrow. In fact, RhoA is a key regulator for the proper assembly and contraction of the actomyosin ring [Piekny A.J. and Glotzer M. 2008; Miller A.L. and Bement W.M. 2009].

Cytokinesis failure and thus, binucleation is clearly associated with the end of the weaning. Liver of fetal and suckling animals only contains mononuclear diploid hepatocytes and after the weaning, they become polyploid (4N and binucleated) due to mitotic performances that end up with failed cytokinesis.

Nutritional and hormonal changes appearing around the weaning period greatly modify glucose and fatty acid metabolism [Girard J. *et al*., 1992]. In fact, the increase in the circulating insulin concentration is sufficient to induce the appearance of binucleated progeny. Physiological cytokinesis failure in hepatocytes during the weaning is regulated by insulin signaling that may act *via* the phosphatidylinositide 3-kinase/ protein kinase B/ mechanistic target of rapamycin (PI3K/AKT/mTOR)–cytoskeleton regulation pathway [Celton-Morizur S. *et al.,* 2010]. The orchestration of PI3K pathway has been already established in cell cycle progression [Liang J. and Slingerland J.M. 2003] and mTOR has been proposed as an effector involved in the control of the cytoskeleton regulation [Sarbassov D.D. *et al.,* 2004; Enomoto A*. et al.,* 2005; Buttrick G.J. and Wakefield J.G. 2008; Kakinuma N. *et al.,* 2008].

2.3.2. Binucleation in aging liver

The progressive polyploidization and binucleation observed in mouse liver during senescence, by formation of nuclei up to 32N in DNA content is a feature of the liver aging process [Nuñez F*. et al.,* 2000]. Binucleation in aging liver could be a tissue-specific adaptation to cellular loss [Lu P. *et al.,* 2007] or may be a protective response to the accumulation of damaged DNA [Nuñez F*. et al.,* 2000]. Unrepaired DNA lesions can give rise to genome instability, carcinogenesis, or cell death [Nuñez F*. et al.,* 2000] and the fact of having multiple copies of one gene seems to be an advantage when DNA damage occurs [Celton-Morizur S. and Desdouets C. 2010].

However, the reduction in the regenerative potential with hepatocyte aging [Bucher N.L., *et al.,* 1964; Stocker E. and Heine W.D. 1971; Wang X. *et al.,* 2002; Krupczak-Hollis K. *et al.*, 2003] might be attributed to the difficulties to go through mitosis of binucleated and polyploid hepatocytes [Schmucker D.L. 1990; Beyer H. S. *et al.*, 1991; Kudryavtsev B.N. *et al.,* 1993; Hoare M. *et al.,* 2010]. For instance, orthotopic liver transplantation from older donors has been associated with worse results [Marino I.R. *et al.,* 1995].

2.3.3. Ploidy reversal in hepatocytes

Although under physiological conditions, after weaning hepatocytes are unable to complete cytokinesis, it has been shown that hepatocytes are able to change from polyploid to diploid, and from binucleated to mononucleated by a phenomenon called somatic reductive mitoses, thanks to multipolar mitotic spindles.

Multipolar mitotic spindles are formed frequently in polyploid hepatocytes, associated with numerous centrosomes that can lead to their ploidy reversal. Multipolar spindles affect the fidelity of nuclear segregation [Duncan A.W. *et al.,* 2010] and the existence of multiple poles make chromosomes distribute unevenly during mitosis. Indeed, multipolar spindles may resolve into a bipolar orientation, in which chromosomes are unable to take part in the daughter nuclei. Although it was thought that most of hepatocytes had balanced DNA content [Guidotti J.E. *et al.,* 2003], these reductive mitoses produce genetic heterogeneity. In fact, aneuploidy seems to be in approximately 70% of adult mouse hepatocytes [Duncan A.W. *et al.,* 2010; Faggioli F. *et al.,* 2011] and 30–

90% of adult human hepatocytes [Duncan A.W. *et al.,* 2012]. Liver is the tissue with higher levels of aneuploidy, although this feature has been observed in oocytes, blood, skin, brain, and placenta [Weier J.F. *et al.,* 2005; Weier J.F. *et al.,* 2005; Westra J.W. *et al.,* 2008; Conlin L.K. *et al.,* 2010].

Aneuploidy is relevant in cells that are continuously challenged by stress, a condition that could predispose to genomic instability [Faggioli F. *et al.,* 2011]. Thus, ploidy reversal could be considered as an adaptation mechanism, as plants do [Weiss-Schneeweiss H. *et al.,* 2013], giving cells the opportunity of being polyploid, aneuploid and having genetic diversity.

Exceptionally, binucleated hepatocytes that have a discordant chromosome number between the two nuclei may indicate a possible fusion of two cells with different DNA content or the asynchronic division of the two hepatocyte nuclei [Faggioli F. *et al.,* 2011].

2.3.4. Binucleation and liver regeneration

Considering that polyploid hepatocytes were thought to have limited mitotic capacity [Hoare M. *et al.,* 2010] and diploid hepatocytes do easily undergo several cell cycles, it seems to be an advantage to keep or change hepatocytes into diploid shapes for a better performance.

2.3.4.1. Binucleation in partial hepatectomy

Ploidy conveyor was described at the same time that it became apparent that polyploid hepatocytes were able to proliferate [Duncan A.W. *et al.,* 2010]. During regenerative growth of the liver, after two-thirds resection (liver partial hepatectomy), diploid hepatocytes have a proliferative advantage above the polyploid ones. For instance, in rat liver, the rate of binucleation decreased from 27% (before hepactectomy) to 5% (at 45 h after hepactectomy) as pre-existing binuclear cells replicated and formed mononuclear daughter cells [Gerlyng P. *et al.,* 1993]. However, days after partial hepatectomy, hepatocytes shifted to higher ploidy rates [Sigal S.H. *et al.,* 1999]. Thus, ploidy reversal is only needed for the first stage after partial hepatectomy when liver needs to grow as fast as possible. Indeed, the ploidy reversal potential would help to understand previous studies showing the capacity of the liver to regenerate after repeated partial hepatectomies [Simpson G.E. and Finckh E.S. 1963; Solopaev B.P. and Bobyleva N.A. 1980].

2.3.4.2. Binucleation in biliary cirrhosis

Liver cirrhosis is a pathological condition of the liver that finally implies loss of liver function [Delhaye M. *et al.,* 1999]. The loss of liver function during cirrhosis is recovered by a compensatory hypertrophy of the tissue and binucleation seems to be a great disadvantage when liver tries to compensate its mass [Hoare M. *et al.,* 2010]. In fact, the hepatocyte ploidy in rat livers who successfully dealt with thioacetamide chronic cirrhosis presented a significant increase in diploid hepatocytes and a decrease in the binucleation rate [Gandillet A. *et al.*, 2003].

2.3.5. Binucleation, liver cancer and chemotherapy

A negative correlation between growth capacity and ploidy can also be demonstrated in neoplastic nodules, and HCCs, suggesting that suppression of binucleation and polyploidization may be a growth advantage [Seglen P.O. 1997]. In general, liver tumor promoters tend to induce a non-binucleating hepatocellular growth pattern, and may be similar to the one observed during liver regeneration. In fact, HCC's hepatocytes proliferate as diploid cells [Saeter G. *et al*., 1988, Celton-Morizur S. and Desdouets C. 2010]. In addition to this, a diploid cell is less protected against mutagenic change than a polyploid genome, and thus, diploid tumor cells may undergo more easily mutated than polyploid cells, increasing malignancy [Seglen P.O. 1997].

On the other hand, liver carcinogens have shown their ability to suppress binucleation in hepatocytes. Moreover, toxicological studies have demonstrated that mononuclear cells are more sensitive to them. 2-acetylaminofluorene, cyproterone acetate, alpha-hexachlorocyclohexane, methylclofenapate suppressed binucleation and induced an increase in proliferative activity and in the fraction of diploid hepatocytes relative to control animals [Gerlyng P. *et al.,* 1994]. Interestingly, etoposide resistance in HCC is mediated by multinucleation dependent on the catalytic activity of AKT [Mukherjee A. *et al.,* 2013].

2.3.6. Binucleation and oxidative stress

Considering that one of the main functions of the liver is metabolism and detoxification, chemical exposure and generation of ROS is a highly frequent situation. Following toxic injury, the increase in binucleation could be linked to hepatic recovery as a result of oxidative stress generation [Nakatani T. *et al.*, 1997; Gorla G.R. *et al.,* 2001]. Confirming the hypothesis that postulate a role of oxidative stress in liver binucleation, it has been already published that vitamin C deficiency induces an increase of cytochrome p450 2E1 (CYP2E1) expression and elevates ROS production, which causes oxidative liver injury and the elevation of hepatocyte binucleation in senescence marker protein-30 (SMP-30) knock out mice [Park J.K. *et al*., 2010].

Gold nanoparticles, lead chronic exposure, vanadium inhalation and microcystins intoxication induced rat liver binucleation as a consequence of liver injury, followed by inflammation, apoptosis or necrosis. These particles interacted with the antioxidant defense and lead to ROS generation and binucleation -considered as a regenerating hepatocytes marker- [Abdelhalim M.A. and Jarrar B.M. 2012; Mattos L.J. *et al.,* 2014]. Besides this, liver steatosis and hepatocyte binucleation seem to be associated [Nascimento F.A. *et al.,* 2010].

In all these situations, hepatocyte binucleation may be a protective mechanism against oxidative stress occurring by controlling gene copy number and expression [Lu P. *et al.,* 2007].

3. Mitogen-activated protein kinases (MAPKs)

MAPKs are a family of protein Serine/Threonine kinases that transform extracellular stimuli into a wide range of cellular responses. Eukaryotic cells have multiple MAPK pathways, which are in charge of multiple processes such as gene expression, mitosis, metabolism, motility, survival, apoptosis, and differentiation [Nebreda A.R. and Porras A. 2000; Ambrosino C. and Nebreda A.R. 2001; Cuadrado A. and Nebreda A.R. 2010]. In fact, they are one of the most ancient signaling transduction pathways evolutionarily conserved, and they have played an extraordinary role during the evolution of many physiological processes [Li M. *et al.,* 2011].

Each MAPK cascade consists of a set of 3 sequentially acting kinases. Starting from the most upstream kinase, they are as follows: MAPKK kinase (MAPKKK/MEKK), MAPK kinase (MAPKK/MKK), and a MAPK. The MAPKKKs, the first ones of the pathway, may be activated through phosphorylation and/or as a result of their interaction with a small GTP-binding protein of the Ras/Rho family in response to extracellular stimuli. MAPKKK activation is followed by phosphorylation and activation of a MAPKK that will lead to MAPK activity (Figure 6) [Seger R. and Krebs E.G. 1995; Schaeffer H.J. and Weber M.J. 1999].

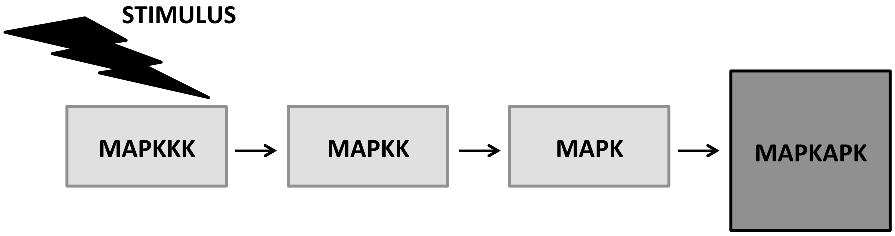

Figure 6. Representation of MAPK phosphorylation cascade.

In mammals, typical MAPKs family is composed by the c-jun amino (N)-terminal kinases 1/2/3 (JNK1/2/3), p38 isoforms (α, β, γ and δ), the extracellular signal-regulated kinases 1/2 (ERK1/2), and ERK5, "the big MAPK" [Cheng Z. *et al.,* 2001; Kyriakis J.M. and Avruch J. 2001; Pearson G. *et al.,* 2001] (Figure 7).

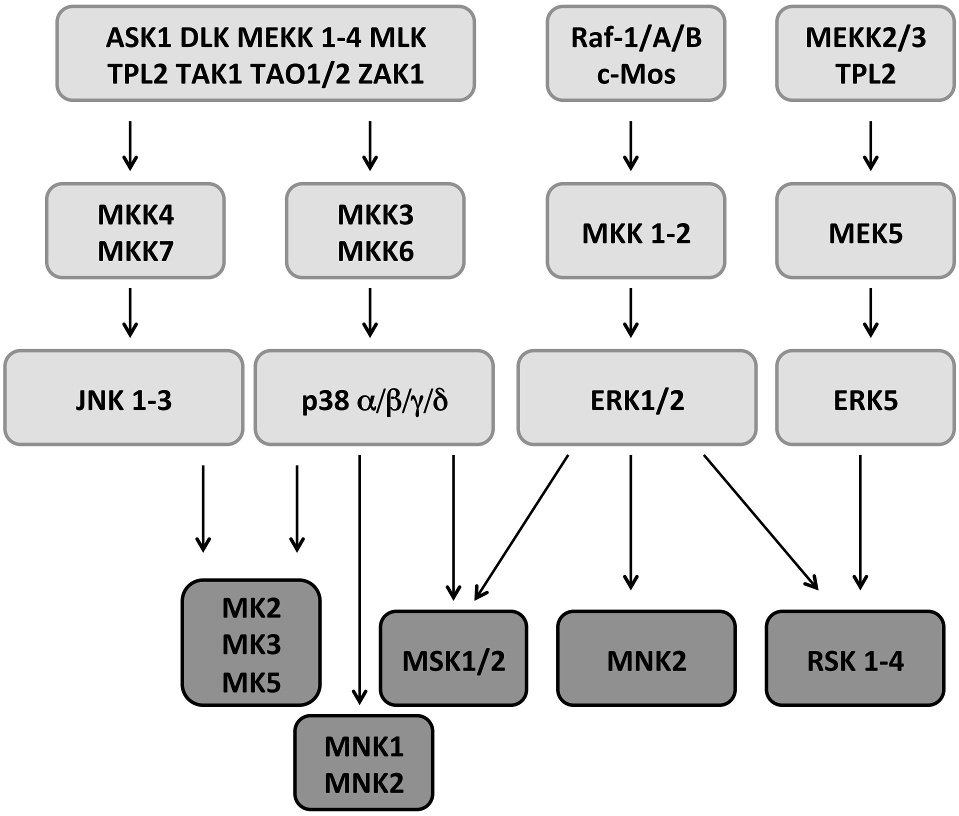
ASK1 DLK MEKK 1-4 MLK
TPL2 TAK1 TAO1/2 ZAK1
Raf-1/A/B
c-Mos
MEKK2/3
TPL2
MKK4
MKK7
MKK3
MKK6
MKK 1-2
MEK5
JNK 1-3
p38 α/β/γ/δ
ERK1/2
ERK5
MK2
MK3
MK5
MSK1/2
MNK2
RSK 1-4
MNK1
MNK2

Figure 7. Mammalian MAPK pathways: the conventional MAPK pathways. All targets are activated by phosphorylation. Apoptosis signal-regulating kinase 1 (ASK1), dual leucine zipper-bearing kinase (DLK), MAPK kinase kinase (MEKK), MAPK-activated protein kinase (MK), MAPK kinase (MKK), MAPK-interacting kinase (MNK), mitogen-and-stress-activated kinase (MSK), ribosomal-S6-kinase (RSK), rapidly accelerated fibrosarcoma 1/A/B (Raf-1/A/B), transforming growth factor β-activated kinase 1 (TAK1), thousand-and-one amino acid kinase 1/2 (TAO1/2), tumor progression locus 2 (TPL2) and Zaphod kinase (ZAK1). The interaction of ERK5 with RSK1-4 remains controversial *in vivo.*

Atypical or unconventional MAPKs, which are not organized in the conventional tripartite module, have been also described and are ERK3/4, ERK7/8, and Nemo-like kinase (NLK) [Cargnello M. and Roux P.P. 2011]. Like typical MAPKs, they phosphorylate non-protein kinase substrates or MAPK activated protein kinases (MAPKAPKs).

3.1. p38 MAPK family

The p38 family is an environmental stress transducer, and responds to hyperosmolarity, UV irradiation, heat shock, inhibition of protein synthesis, and numerous mediators of inflammation, including chemoattractants, cytokines, chemokines, and bacterial lipopolysaccharide (LPS) [Han J. *et al.,* 1994; Raingeaud J. *et al.,* 1995; Zarubin T. and Han J. 2005].

In general, activation of p38 MAPKs by mediators of inflammation or cellular stress generally promotes inhibition of cell growth and induces apoptosis [Kyriakis J.M. and Avruch J. 1996; Guo, J. H. *et al.,* 1998; Kyriakis, J. M. and Avruch, J. 2001]. The role of the p38 MAPK pathway in apoptosis, growth inhibition, inflammatory response, and cell differentiation is well established and has been broadly reviewed [Zarubin T and Han J. 2005; Han J and Sun P. 2007; Hui L. *et al.,* 2007]. However, the regulation of the last stage of cell cycle (cytokinesis) by p38 MAPKs is less characterized.

The p38 family of MAPKs has four members: $\alpha, \beta, \gamma, \delta$ [Cuenda A. and Rousseau S. 2007]. Although they are 60% identical in their amino acid sequence, these 4 isoforms can be divided into two subgroups according to their expression pattern, substrate specificity and sensitivity to pharmacological inhibitors, such as SB203580.

- **p38α and p38β** are universally expressed. Only p38α and β are sensitive to the anti-inflammatory agents SB203580 and SB202190 [Kumar S. *et al.,* 1997], which inhibit both isoforms by acting as competitive inhibitors of ATP binding site [Kumar S. *et al.,* 1999; Davies S.P. *et al.,* 2000]. Substrates for p38α and p38β include other protein kinases, as well as several transcription factors and metabolic enzymes [Kuma Y. et al.2004; Roux P.P. and Blenis J. 2004].

p38α is the archetypal member of the group. p38α is also known as cycling sequence binding protein (CSBP), product of the budding yeast hog1 gene (mHOG1), and stress-activated protein kinase 2 (SAPK2). It is ubiquitously expressed and the most abundant p38 isoform. It shares a significant homology with the product of the budding yeast hyperosmolarity activated gene (hog) and is 50% identical to ERK2.

- **p38δ and p38γ** have more tissue-specific expression patterns. They are not inhibited by SB203580 [Cuenda A. *et al.,* 1995; Davies S.P. *et al.*, 2000]. P38γ and δ can phosphorylate atypical transcription factors and do not phosphorylate common targets, such as MK2 and MK3 [Goedert M. *et al.*, 1997, Kuma Y. *et al.,* 2005].

There is a more potent inhibitor of p38 kinase activity by indirectly competing with the binding of ATP: BIRB0796. All MAPK family members are inhibited by BIRB0796, but p38γ and δ are inhibited at higher concentrations [Pargellis G. *et al.,* 2002; Regan J. *et al.,* 2002; Kuma Y. *et al.,* 2005].

3.1.1. p38 MAPK activation

The canonical p38 MAPK activation pathway involves the upstream MAPK kinases MKK3 and MKK6 (Figure 7). Despite 80% homology between MKK3 and

MKK6, MKK6 activates all p38 isoforms, whereas MKK3 is more selective, as it preferentially phosphorylates the α, γ and δ isoforms [Parker C.G. *et al*., 1998]. In addition, MKK4 has also been shown to possess some activity toward p38α and β in specific cell types [Meier R. *et al.,* 1996, Jiang Y. *et al.,* 1997].

Upstream MKKKs responsible for activating the p38MAPK pathway are cell type and stimulus specific and include ASK1, DLK1, MEKK3, MEKK4, MLK3, TAK1, TAO1, TAO2, TPL2 and ZAK1 (Figure 7) [Trempolec N. *et al.,* 2013].

Final dual phosphorylation of p38 in its Thr-X-Tyr motif (where X is any amino acid) is the fact that leads to activation of the kinase. Phosphorylation of threonine and tyrosine residues in the activation loop induces conformational changes that allow binding to substrates and the catalytic activity of p38 MAPKs.

On the other hand, p38α can also be regulated by a MAPK kinase independent mechanism named non-canonical activation of p38α. These mechanisms are likely to happen in p38α activation under the following conditions [Cuadrado A. and Nebreda A.R. 2010; Beenstock J. *et al.,* 2014]. (Figure 8):

(a) Phosphorylation of p38*α* on Tyr323 –noncanonical activating residue- by the T-cell receptor proximal tyrosine kinases *ζ* –chain associated protein kinase of 70 kDa (ZAP70) and p56 lymphocyte-specific protein tyrosine kinase (p56lck), which activate p38α by causing changes in its structural conformation that leads to p38*α* autophosphorylation on the activation loop –Thr-Gly-Tyr- [Salvador J.M. *et al.,* 2005; Salvador J.M. *et al.,* 2005]. This p38α activation mechanism might be necessary for normal lymphocyte T helper 1 function [Jirmanova L. *et al.,* 2009].

(b) p38α autophosphorylation by TAB1 (transforming growth factor β activated protein 1 binding protein 1). TAB1 induces p38 to autophosphorylate Thr180 and Tyr182 [Ge B. *et al.,* 2002]. This mechanism may contribute to p38*α* regulation during myocardial ischemia [Tanno, M. *et al.,* 2003; Li J. *et al.,* 2005] and some immunological processes [Matsuyama W. *et al*., 2003; Kim L. *et al.,* 2005].

(c) p38α activation can be promoted upon down-regulation of the protein kinase Cdc7 (cell division cycle 7), which induces an abortive S-phase leading to p38*α* activation. The activation of p38α by down-regulation of Cdc7 mediates apoptosis in HeLa cells [Im J. S. and Lee J. K. 2008].

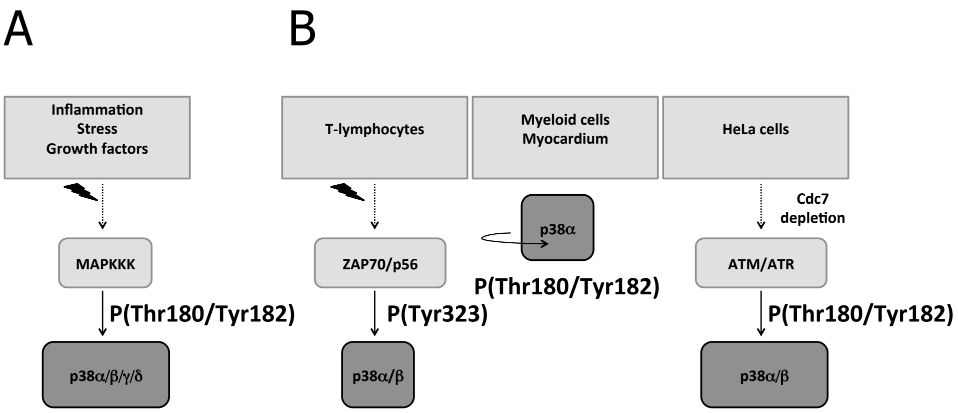
A
B
Inflammation
Stress
Growth factors
MAPKKK
P(Thr180/Tyr182)
p38α/β/γ/δ
T-lymphocytes
ZAP70/p56
P(Tyr323)
p38α/β
Myeloid cells
Myocardium
p38α
P(Thr180/Tyr182)
HeLa cells
Cdc7
depletion
ATM/ATR
P(Thr180/Tyr182)
p38α/β

Figure 8. Canonical (A) and non-canonical (B) activation of p38α.

3.1.2. p38 MAPK inactivation by phosphatases

p38 MAPKs can be reversible dephosphorylated by protein tyrosine phosphatases (PTPs). This crosstalk regulates a broad spectrum of fundamental signaling pathways and physiological processes [Pearson G. *et al.,* 2001; Alonso A., *et al* 2004; Stocker A. W. 2005].

In general, MAPKs are dephosphorylated by the dual-specificity phosphatases (DUSP) family, a subgroup of the type-I cysteine-based PTP superfamily. DUSPs can be divided into six subgroups on the basis of sequence: slingshots, PRLs (phosphatases of regenerating liver), Cdc14 phosphatases, PTENs (phosphatase and tensin homologues deleted on chromosome 10), myotubularins, MKPs (mitogen-activated protein kinase phosphatases), and atypical DUSPs [Patterson K.I. *et al.,* 2009]. The exclusive feature that characterizes DUSPs is their ability to dephosphorylate both tyrosine and serine/threonine residues in one substrate [Denu J. M. and Dixon J. E. 1998].

Although MAPKs are dephosphorylated by broad specificity DUSPs, they are specific targets of MKPs, which are able to dephosphorylate MAPK isoforms with different specificity, as well as cellular and tissue localization. Their specificity for MAPKs depends on sequences in the NH_2-terminal domain of MKPs: the kinase interaction motif. Dual-specificity MKPs comprise a subfamily of 10 catalytically active proteins but there are only 7 isoforms of MKPs-DUSPs that dephosphorylate p38 MAPKs [Jeffrey K.L. *et al.,* 2007; Bermudez O*. et al.,* 2010].

- The inducible nuclear MKPs: DUSP1/MKP-1, DUSP2/PAC-1, DUSP4/MKP-2 and DUSP5
- Cytoplasmic and nuclear MKPs: DUSP8, DUSP10/MKP-5 and DUSP16/MKP-7

Individual MKPs show different preference for one MAPK isoform, although the MAPK substrate preference for individual MKPs *in vitro* does not always reflect the preference *in vivo* [Cuadrado A. and Nebreda A.R. 2010].

The MKPs form part of a complex negative regulatory network that acts to control MAPK activities [Owens D.M. and Keyse S.M. 2007]. In fact, certain MKPs are encoded by genes that are transcriptionally up-regulated by stimuli that activate MAP kinase signaling at the same time. Dysregulation of MAPK activation cascades has been implicated in various diseases and is the focus of extensive research [Chang L. and Karin M. 2001; Johnson G.L. and Lapadat R. 2002; Dickinson R.J. and Keyse S.M. 2006].

On the other hand, there are other specific phosphatases that do not belong to DUSPs but can dephosphorylate p38 MAPKs: Serine/Threonin phosphatases, such as protein phosphatases 2A and 2C (PP2A/C), and PTPs such as protein tyrosine phosphatase SL (PTP-SL), striatal enriched tyrosine phosphatase (STEP), and haemopoietic tyrosine phosphatase (HePTP) [Takekawa M. *et al.,* 1998; Takekawa M. *et al.,* 2000; Sundaresan P. and Farndale R.W. 2002; Budziszewska B. *et al.,* 2010].

3.1.3. p38 and JNK crosstalk

p38 and JNK share stimuli and upstream activators. Most of the stimuli that activate p38 MAPKs also stimulate JNK isoforms, and many MAPKKKs in the p38 module are shared with the JNK module [Cuevas B.D. *et al.,* 2007]. Nevertheless, this two MAPK signaling pathways have opposite effects: the activation of p38 and the JNK/c-jun pathways may regulate each other through a negative feedback loop.

On the one hand, the JNK/c-jun pathway was found to be increased in *in vitro* models treated with a p38 chemical inhibitor [Cheung P.C. *et al.,* 2003]. Moreover, the activation of JNK pathway was found in p38α deficient mice models: fetal liver cells, erythroblasts, mouse embryonic fibroblasts (MEFs), myoblasts, liver tumor cells, and in adult lung tissues [Hui L. *et al.,* 2007; Perdiguero E. *et al.,* 2007; Ventura J.J. *et al.,* 2007; Heinrichsdorff J. *et al.,* 2008, Wagner E.F. and Nebreda A.R. 2009].

On the other hand, hyperactivation of p38 has also been described in primary hepatocytes lacking c-jun [Hochedlinger K. *et al.,* 2002; Eferl R. *et al.,* 2003], in regenerating livers of mice lacking c-jun [Stepniak E. *et al.,* 2006; Wada T. *et al.,* 2008], and in MEFs lacking the JNK activator MKK7 [Wada T. *et al.,* 2008].

3.1.4. Scaffolds or adaptor proteins

MAPK signaling modules may interact with scaffold proteins in order to create a functional complex. Scaffold proteins not only help by mediating interaction between proteins, but also regulating their targets allosterically.

Not many scaffold proteins are found in the p38 MAPK pathway [Cuenda A. and Rousseau S. 2007]. The main ones are: the osmosensing scaffold for MEKK3 (OSM) [Uhlik M.T. *et al.,* 2003] and JLP-Cdc42 [Morrison D.K. and Davis R.J. 2003; Kang J.S. *et al.*, 2008]. TAB1 can also be considered as a scaffold when it interacts with TAK1 and TAB2/TAB3 in response to inflammatory stimuli [Cheung P.C. et al., 2003].

3.2. Substrates of p38α

p38 isoforms are present in the nuclei and cytoplasm of quiescent cells and have been shown to accumulate in the nuclei of cells subjected to certain stresses [Chen R. H. *et al.,*1992; Raingeaud J. *et al.,* 1995; Ben-Levy R. *et al.,* 1998; Wood C.D. 2009]. p38 MAPK traslocation to the cytosol is due to MK2/3, which act as a cytoplasmic anchors for p38α [Ben-Levy R. *et al.,* 1998; Gaestel M. 2006; Ronkina N. *et al.,* 2008]. This translocation seems to require both phophorylation and subsequent dimerization of MAPK, but the molecular details of the transport process and its dynamics remain unclear [Seternes O.M. *et al.,* 2002]. There is also evidence that p38α accumulates in the cytosol in response to specific stimuli [Ben-Levy R. *et al.,* 1998].

p38α phosphorylates a large number of substrates in many cellular compartments, including the cytoplasm and the nucleus [Cuadrado A. and Nebreda A.R. 2010].

However, p38α also has kinase-independent functions by binding other proteins and modifying their conformational structure, promoting a change in their location or by competing with other substrates, i.e, regulating the activating transcription factor/cAMP response element binding (ATF/CREB) [Gao Y. *et al.,* 2006], in HeLa cells proliferation [Fan L. *et al.,* 2005] and in the regulation of O-GlcNAc transferase during brain isquemia-reperfusion [Cheung W.D. and Hart G.W. 2008].

3.2.1. Protein kinases

p38α activates different subgroups of protein kinases that belong to the MAPK-activated protein kinase (MAPKAPK) family. This family contains 11 members (RSK1-4, MNK1-2, MSK 1-2, MK2/3/5). They share similar activation loop sequences that are targeted for phosphorylation by the upstream MAPK (Figure 9).

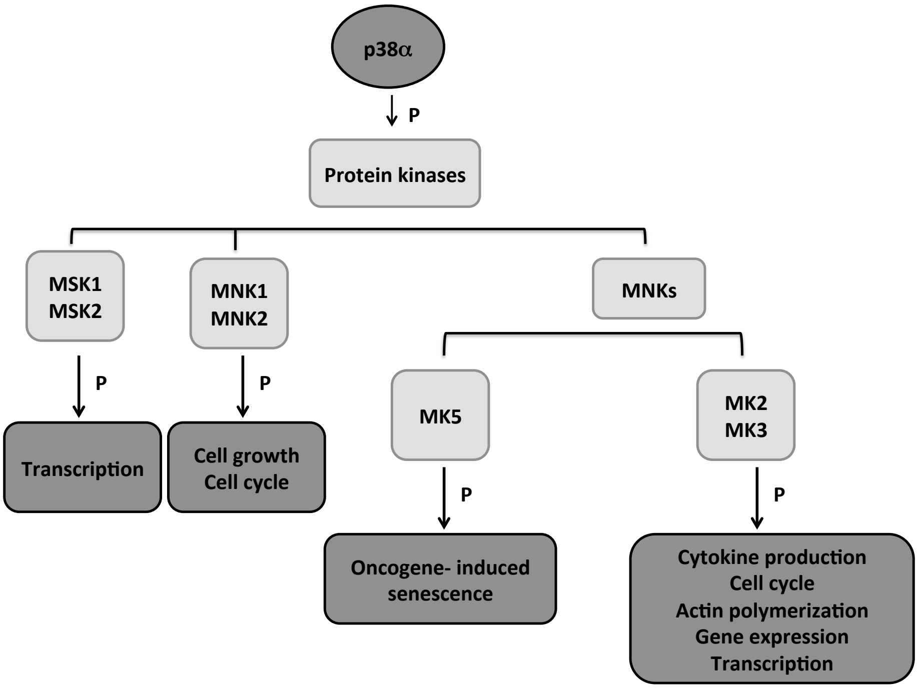
p38α
P
Protein kinases
MSK1
MSK2
MNK1
MNK2
MNKs
P
P
Transcription
Cell growth
Cell cycle
MK5
MK2
MK3
P
P
Oncogene- induced senescence
Cytokine production
Cell cycle
Actin polymerization
Gene expression
Transcription

Figure 9. Summary of p38α protein kinases targets.

3.2.1.1. Mitogen- and stress-activated kinases 1 and 2 (MSK1/2)

MSK1/2 mainly regulate nuclear events. They phosphorylate transcription factors such as the human cellular homolog of the oncogene Finkel-Biskis-Jinkis murine osteosarcoma virus (c-Fos), JunB, CREB, ATF1, NF-κB (p65), STAT1, STAT3), histone 3 (H3) and high mobility group protein 14 (HMG-14) [Wiggin G.R. *et al.,* 2002; Vermeulen L. *et al.,* 2003; Arthur J.S. 2008; Vermeulen L. *et al.,* 2009].

These MSKs are key regulators of the stress response, inducing the recruitment of transcription machinery or promoting actin remodeling by nucleosomal regulation [Thompson S. *et al.,* 1999]. Importantly, MSK2 inhibits p53 in basal conditions [Llanos S. *et al.,* 2009].

3.2.1.2. Mitogen kinases 2, 3 and 5 (MK2/3/5)

MK2 was the first identified substrate for p38α. However, MKs were first discovered as activators of heat shock protein 27 (HSP27) [Stokoe D. *et al.,* 1992]. HSP27 phosphorylation by MK2/3 is necessary for the regulation of actin dynamics in several cellular processes [Shi Y. and Gaestel M. 2002] and it supports the role of p38α in cell migration [Hedges J.C. *et al*., 1999; Rousseau S. *et al.,* 2006; Chang E. *et al.,* 2011], proliferation and differentiation [Salinthone S. *et al.,* 2007; Boivin B. *et al.,* 2012] by mediating actin remodeling [Benndorf R. *et al.,* 1994]. Moreover, MK2/3 is a key player in p38 mediated cytokine production [Gaestel M. 2006; Ronkina N. *et al.,* 2008], cell cycle regulation [Ambrosino C. and Nebreda A.R. 2001] and control of gene expression [de Nadal, E. and Posas F. 2010]. MK2 is also able to phosphorylate tristetraprolin (TTP) and thus regulate mRNA stability [Mahtani K.R. *et al.,* 2001]. MK2 phosphorylates multiple transcription [Cuadrado A. and Nebreda A.R. 2010] and other proteins such as tirosine hydroxylase and lymphocyte-specific protein 1 (LSP1) [Zarubin T. and Han J. 2005].

MK5 only displays 38% homology to MK2/3 [Shiryaev A. and Moens U. 2010; Cargnello M. and Roux P.P. 2011] and shares some substrate preferences [Shi Y. *et al.,* 2003] but recent findings suggest that MK5 mainly regulates oncogene-induced senescence [Sun P. *et al.,* 2007] and actin dynamics [Gerits N. *et al.,* 2007].

3.2.1.3. MAP kinase-activated protein kinase 1 and 2 (MNK1/2)

MNK1/2 regulates the initiation of transduction by phosphorylating eukaryotic translation initiation factor 4E (eIF4E) and thus controlling cell growth and proliferation [Richter J.D. and Sonenberg N. 2005]. MNK1 kinase activity is also required for cell abcission. Centriolin localization at the midbody during cell division is essential for a properly cytokinesis completion and the separation of the two daughter cells [Rannou Y. *et al.,* 2012].

3.2.2. Cytoplasmic substrates

Phospholipase A2, microtubule associated protein tau, *Na-H exchanger* (NHE-1), cyclin D1, CDK inhibitors, B-cell lymphoma 2 (Bcl-2) family, growth factors receptors, and keratins [Ono K. and Han J. 2000; Shi Y. and Gaestel M. 2002; Cuenda A. and Rousseau S. 2007].

By regulating cytoplasmic substrates, p38α also exerts its action in protein turnover [Khurana A. *et al.*, 2006], autophagy [Webber JL and Tooze S.A. 2010], and endocytosis [Cavalli V.*et al*., 2001].

3.2.3. Transcription factors

p38 MAPKs are key regulators of the gene transcription. Although some transcription factors have previously been reviewed, other p38 targets are named as follows: ATF2, ATF6, C/EBP homologous protein (CHOP), switching activating protein 1 (Sap1), p53, myocyte-specific enhancer factor 2C (MEF2C), MEF2A, DNA damage-inducible transcript 3 (DDIT3), Ets LiKe gene1 (ELK1), nuclear factor of activated T cells (NFAT), HMG-box transcription factor 1 (HBP1), CCAAT / enhancer binding protein β (C/EBPß), microphthalmia transcription factor 1 (MITF1), and AP1 [Cuadrado A. and Nebreda A.R. 2010].

3.3. p38α signaling

The biological consequences of p38α activation are described as follows:

3.3.1. p38α in development

p38α is highly expressed in specific tissues during embryogenesis, such as the somites, brachial arches, limb buds, heart, and placenta [Adams R.H. *et al.,* 2000].

Functions of p38α in embryonic development were first analyzed using constitutive knock out mice [Adams R.H. *et al.,* 2000; Allen M. *et al.,* 2000; Mudgett J.S. *et al.,* 2000; Tamura K. *et al.,* 2000]. Loss of p38α caused embryonic lethality between embryonic day 10.5 and 16.5 due to insufficient vascularization and impaired erithropoyetin expression in placental development [Tamura K. *et al.,* 2000]. In contrast, mice with a conditional deletion of p38α specifically in the embryo, but not in the placenta, developed to term and were born, but died within one week after birth due to the indispensable p38α effect on fetal hematopoietic development. They also exhibited severe structural lung defects, disrupted vessels in the alveolar interstitial, and hematopoietical infiltration [Adams R.H. *et al.,* 2000].

A more recent study tested the role of p38 signaling in mice embryos and confirmed that treatment with SB203580 blocked the accumulation of filamentous actin [Natale D.R. *et al.,* 2004] and affected cell shape in granulosa cells and embryonic cleavage stages. In fact, these embryos displayed a reduction in F-actin fluorescence [Natale D.R. *et al.,* 2004]. Moreover, p38α was required for axial specification in *Drosophila* embryos [Suzanne M. *et al*., 1999], sea urchin [Bradham C.A. *et al.,* 2006], *Xenopus*, and zebrafish [Roth S. *et al.,* 1989; Rushlow C.A. *et al,* 1989; Steward R. 1989; Schneider S. *et al.,* 1996]. In mice embryos, p38α inhibition always resulted in a functional asymmetry during embryo development by depolymerization of filamentous actin [Natale

D.R. *et al.,* 2004] and formation of unstable adherens junctions [Paliga A.J. *et al.*, 2005].

3.3.2. p38α in aging

p38α activity can induce senescence-associated secretory phenotype (SASP) in human fibroblasts *via* the transcriptional activation of NF-κB signaling [Freund A. *et al.,* 2011]. Accordingly, p38MAPK/MSK signaling induced changes in chromatin structure during cellular senescence at the same time that promoted the expression of pro-inflammatory genes that enhances SASP [Funayama R. and Ishikawa F. 2007].

Oxidative stress activates the MKK3/6-p38 pathway and induces cellular senescence. In agreement with that, SB203580 could revert the morphology of senescent Werner syndrome fibroblasts and increased their replication capacity to the normal rate [Davies T. *et al.,* 2013].

3.3.3. p38α and cell differentiation

p38α is involved in the differentiation of myocytes, 3T3-L1 cells, neurons and keratinocytes [Jones N.C. *et al.,* 2005; Aouadi M. *et al.,* 2006]. In myogenesis, mice myoblasts lacking p38α do not differenciate into multinucleated myotubes [Perdiguero E. *et al.,* 2007]. 3T3-L1 cells are unable to differenciate into adipocytes when p38α inhibitor is present [Engelman J.A. *et al.,* 1998]. In keratinocytes, p38α induces upregulation of involucrin, which is a protein expressed during differentiation [Jans R. *et al.,* 2004].

3.3.4. p38α and cytokine expression

The best-known role of p38α in disease is related to its function in cytokine signaling and promotion of inflammation. p38α regulates cytokine expression by regulating transcription factors, such as NF-κB [Karin M. 2006], or at the mRNA level by modulating their stability and translation through MNK1 [Buxade M. *et al*., 2008] and MK2/3 [Kotlyarov A. *et al.,* 1999].

p38α appears to be the main p38 isoform involved in the inflammatory response, as its deletion in epithelial cells was found to reduce proinflammatory gene expression [Kim C. *et al.,* 2008]. TNFα, IL-1β and IL-6 are inflammatory mediators mainly regulated by p38α [Cuenda A. and Rosseau S. 2007; Schieven G.L. 2005]. They are key players in rheumathoid arthritis, Chron's disease, inflammatory bowel disease, psoriasis, and ankylosing spondylitis [Cuenda A. and Rousseau S. 2007; Coulthard L.R. *et al.,* 2009]; and they exhacerbate other illnesses, such as cardiovascular disease and stroke [MacGowan G.A. *et al.,* 1997; Dinarello C.A. and Pomerantz B.J. 2001], ischemic retinopaties [Gardiner T.A. *et al*., 2005], and insulin resistance [Takeda R. *et al.,* 2005]. Furthemore, p38 MAPK is emerging as a regulator of a number of pulmonary diseases, such as asthma, cystic fibrosis, idiopathic pulmonary fibrosis, and chronic obstructive pulmonary disease [Chopra P. *et al.,* 2008]. Therefore, inhibition of p38α is an interesting therapeutic strategy and hence, selective p38α inhibitors are presently considered for the treatment of chronic inflammatory disorders [Goldstein D.M. *et al*., 2009].

Numerous extracellular mediators of inflammation also activate p38: chemokines, cytokines, bacterial lipopolysaccharide (LPS) and chemoatractants [Cuadrado A. and Nebreda A.R. 2010] creating a primitive feedback mechanism that would amplify the inflammatory cascade.

3.3.5. p38α in survival and apoptosis

Although some studies have reported pro-survival functions for p38α [Phong M.S. *et al.,* 2010] many more have associated p38α activity with the induction of apoptosis by cellular stress [Kummer J.L. *et al.,* 1997; Cuadrado A. *et al.,* 2007; Svensson C. *et al.,* 2011; Ferrari G. *et al.,* 2012]. These effects can be mediated by transcriptional and posttranscriptional mechanisms, which affect death receptors, survival pathways, or pro- and antiapoptotic Bcl-2 family proteins [Cuenda A. and Rousseau S. 2007]. p38-induced pro-apoptotic stimuli are commonly triggered by ROS [Dolado I. *et al.,* 2007].

Survival effects mediated by p38α may be due to up-regulation of IL-6 expression [Dolado I. and Nebreda A.R. 2008; Yang H.T. *et al.,* 2008], its role in autophagy [Comes F. *et al.,* 2007], and by the phosphorylative inactivation of glycogen synthase kinase 3 β (GSK3β) that might be regulated by the AKT pathway [Thornton T.M. *et al*., 2008]. The role of p38α in DNA cell cycle control after DNA damage can also be considered as a pro-survival regulatory mechanism [Thornton T.M. and Rincon M. 2009].

3.3.6. p38α and cell migration

p38α has been shown to have a role in regulating chemotactil signals in neutrophils [Cara D.C. *et al.,* 2001; Liu X. *et al.,* 2012], vascular smooth muscle cells [Pichon S. *et al.,* 2004], lymphocytes [Hu P. *et al.,* 2012], and epithelial cells [Shahabuddin S. *et al*., 2006].

p38α dependent phosphorylation of caldesmon and paxillin [Goncharova E.A. *et al.,* 2002; Huang C. *et al.,* 2004] and regulation of matrix metalloproteases (MMPs) [Simon C. *et al.,* 1998] justify its role in cell motility and migration. In addition, inhibition of p38α impairs the activation of MK2 and actin capping protein HSP27, which blocks cytoskeleton reorganization [Guay J. *et al.,* 1997; Hedges J.C. *et al.,* 1999; Pichon S. *et al.,* 2004]. Actin-based motility p38 MAPK-HSP27 dynamic response pathway was required in contractility [Chaudhuri S. and Smith P.G. 2008], membrane receptor exocytosis [Okamoto C.T. 1999], stress response [Guay J. *et al.,* 1997; Koshikawa M. *et al*., 2005], and membrane blebbing [Huot J. *et al.,* 1998].

p38α also regulates the release of vascular endotelial growth factor (VEGF) promoting angiogenesis [Pagès E. *et al*., 2000; Rousseau S. *et al.,* 2000].

3.3.7. p38α and cell cycle

Although the major function of MAPKs in response to stress is to modulate cell cycle progression [Duch A. *et al.,* 2012], under physiological conditions p38α negatively regulates cell cycle progression at both the G_1/S and G_2/M transitions by a number of mechanisms, including downregulation of cyclins and upregulation of CDK inhibitors [Thornton T.M. and Rincon M. 2009]. p38α can promote growth arrest by downregulating cyclin D1 [Lavoie J.N *et al.,* 1996] and by activating the p53/p21 and/or p16/Retinoblastoma (Rb) pathways [Bulavin D.V. *et al.,* 2002, Bulavin D.V. *et al.,* 2004], among others [Takenaka K. *et al.,* 1998]. p38α arrested proliferation in muscle cells [Perdiguero E. *et al.,* 2007; Perdiguero E. *et al.,* 2007], cardiomyocytes [Engel F.B. *et al.,* 2005], MEFs and hepatocytes [Stepniak E. *et al.,* 2006].

Contrarely, it seems that p38α may play a role in the positive regulation of cell cycle [Recio J.A. and Merlino G. 2002; Platanias L.C. 2003; Halawani D. *et al.,* 2004; Fan L. *et al.,* 2005; Ricote M. *et al.,* 2006] and promotes cytokinesis completion [Fujii R. *et al.,* 2000; Song L. *et al.,* 2010]. Previous studies have confirmed that p38α mediated regulation of cytokinesis could be related with the fact that this kinase is involved in actin polymerization. Inhibition of p38α impaired mice embryonic compactation due to abnormal cell cleavage [Natale D.R. *et al.*, 2004] and dysregulation of filamentous actin [Paliga A.J. *et al.*, 2005].

In addition, p38α acts as a downstream target of guanosin triphosphatases (GTPases), such as Ras-related C3 botulinum toxin substrate 1 (Rac1) and cdc42 *via* MLKs [Schwartz M. 2004]. p38 activation is likely to contribute to the biological effects of Rac and cdc42 on actin cytoskeleton, affecting cell growth and proliferation, and regulating feedback loops [Minden A. *et al.,* 1995]. Rac and cdc42 inhibition is necessary for cytokinesis completion [Davies T. and Canman J.C. 2012; Atkins B.D. *et al.,* 2013].

3.3.8. p38α in cancer

The tumour-suppressive activity of p38α is attributed to its inhibitory effects in cell cycle checkpoints [Ambrosino A. and Nebreda A.R. 2001] as well as to the induction of apoptosis [Hui K. *et al.,* 2014; Lu X. *et al.,* 2014; Zhang Y. *et al.,* 2014] and cellular senescence [Zhang Y. *et al.,* 2013; Davies T. *et al*., 2014; Harrada G. *et al.,* 2014]. Indeed, it has been observed that inactivation of this pathway promotes cellular transformation *in vitro* and cancer development in mouse models [Han J. and Sun P. 2007].

In the tumour environment, the increase in ROS is shown to activate p38α promoting cell cycle arrest and apoptosis. Mechanisms that allow cancerous cells to decouple oxidative stress with p38α activation have been already described [Dolado I. *et al.,* 2007].

However, the ability of p38α to suppress the development of tumours is also due to its novel role in the regulation of cell invasion and metastasis [Küper C. *et al.,* 2014; Lin L.C. *et al.,* 2014; Ma X.M. *et al.,* 2014; Ren H. *et al.,* 2014; Wu X. *et al.,* 2014]. Tumour cells need p38 MAPK activity to successfully trigger metastasis [del Barco Barrantes I and Nebreda A.R. 2012]. p38 MAPK allows the acquisition of migrating and invasion capabilities [Dreissigacker U. et al., 2006; Hsieh Y.H. *et al.,* 2007; Strippoli R. *et al.,* 2010; Hong J. *et al.,* 2011; Villares G.J. *et al.,* 2011] but, in contrast, p38 MAPK inhibition allows circulating cancer cells to survive [Lagadec C. *et al.,* 2009; Owens T.W. *et al.,* 2009; Zhang Y. *et al.,* 2009].

3.4. p38α and oxidative stress

p38α acts as a REDOX sensitive kinase, and thus, it can be activated by ROS [Dolado I. et al., 2007].

3.4.1. p38α, oxidative stress and cell cycle

Under physiological conditions, p38α can function as a mediator of ROS signaling and either promote or inhibit cell cycle progression depending on the cell type and the activation stimulus.

Low levels of ROS seem to be needed to activate several signaling pathways in response to hepatectomy and to orchestrate liver regeneration. However, liver regeneration may be impaired by permanent oxidative stress [Dayoub R. *et al*., 2013]. Mice lacking nuclear factor (erythroid-derived-2)-like 2 (Nrf-2) suffered from delayed liver regeneration [Beyer T.A. *et al.,* 2008] and Kelch-like ECH-associated protein 1 (Keap1) knock out regenerating livers showed severe disruption on the REDOX regulation and delayed cell cycle progression [Hu M. *et al.,* 2014].

The inactivation of p38 MAPK might be necessary for the early stages of liver regeneration after partial hepatectomy [Campbell J.S. *et al.,* 2011] and it is conceivable that ROS-dependent activation of p38α during liver regeneration may inhibit hepatocyte proliferation. In fact, the activation of p38 MAPK in hepatocytes rarely leads to proliferation, with exception of the human hepatocytes stimulated with palmitic acid in which ROS induced the p38/ERK-AKT cascade and promoted cell cycle progression [Wang X. *et al.,* 2011].

Finally, considering that ROS are involved in various aspects of cancer, cells that have developed mechanisms to uncouple p38 MAPK activation from oxidative stress are more likely to become tumorigenic [Dolado I. *et al.,* 2007; Faust D. *et al.,* 2012]. Oxidative stress resistance together with inflammation and cell death is the factor that stimulates compensatory hepatocyte proliferation as a response that maintains liver mass and may drive hepatocarcinogenesis [Rozga J. 2012].

3.4.2. p38α and antioxidant defense

p38α deficiency has been reported to cause enhancement in ROS production in cancer, such as, HCC [Sakurai T. *et al*., 2013], ovarian tumours [Mateescu B. *et al*., 2011], epidermoid squamous cells carcinoma [Liu L. et al., 2014], breast and colon cancer cells [Pereira L. *et al*., 2013].

In addition, there is evidence that p38α signaling may impair ROS generation by up-regulating the antioxidant defense. Previous works have already showed that p38α induced expressions of Nrf-2 and hemoxygenase 1

(HO1) [Kim H.S. *et al*., 2013; Chen X.Q. *et al.,* 2013; Lee H.S. *et al*., 2014; Man W. *et al.,* 2014; Rubio N. *et al.,* 2014]. Recently, it has been assessed that p38α activates the antioxidant defenses, such as SOD1 (superoxide dismutase 1), SOD2 and catalase through a direct regulation of transcription mediated by ATF2 or regulation of protein stability and mRNA in MEFs [Gutierrez-Uzquiza A. *et al.,* 2012]. So far, p38α influences the REDOX balance, determining proliferation, cell survival and terminal differentiation.

OBJECTIVES

Chapter 2

II. OBJECTIVES

The aims of the present Thesis are as follows:

1. To elucidate the role of p38α in the regulation of cytokinesis in hepatocytes with age

2. To determine whether p38α affects hepatocyte cytokinesis in liver regeneration induced by partial hepatectomy

3. To study the regulation of cytokinesis by p38α in liver disease induced by chronic cholestasis

4. To asses the role of reactive oxygen species in cytokinesis upon hepatocyte isolation

MÉTODOS

Capítulo 3

III. MÉTODOS

1. Aparatos

- Agitador magnético Selecta Agimatic-S
- Agitador orbital marca Stuart Rocket SSL3
- Agitador orbital STS5 CAT
- Agitador orbital Stuart gyro-rocker SSL3
- Autoclave Selecta Autester-G
- Balanza Kern 440-23
- Balanzas de precisión SARTORIUS TECATOR 6110 y PT 1200
- Baño con termostato, provisto de agitación automática regulable, SBS BT
- Baño con ultrasonidos Ultrasons P-Selecta
- Baño húmedo Precisterm P-Selecta
- Bibbyjet Pipetboy Fisher Scientific
- Cámara digital para microscopio Leica DFC 300 FX
- Cámara húmeda para inmunohistoquímica hecha artesanalmente
- Cámara Neubauer para contaje de células
- Cámara seca de incubación para inmunohistoquímica Simport
- Campana de flujo laminar vertical CULTAIR B100
- Campana de flujo laminar vertical Telstar AV-100
- Cánulas de jeringa BD Microlance 3
- Centrífuga HermLe Z216 MK
- Centrífuga refrigerada HETTICH Rotina 420R
- Citómetro Amnis FlowSight
- Citómetro BD FACSCanto
- Citómetro BD FACSVerse

- Cubetas de electroforesis y electrotransferencia de BIORAD Mini-PROTEAN 3 Cell
- Destilador de agua Millipore
- Espectrofotómetro HALO RB-10 Dynamica
- Espectrofotómetro Multiscan Thermo Scientific
- Émbolo de teflón para homogeneizar
- Equipo *real time* PCR Biorad I-Cycler + IQ Multicolor Real Time OCR Detection System
- Filtros 50 μM no estériles BD 340631
- Filtros acetato de celulosa estériles 0,22 μm Jet Biofil FCA-206-025
- Filtros Syringe Filter Nylon estériles 0,22 μm Thermos Scientific 195-2520
- Fuente de alimentación de electroforesis SIGMA PS 250-2, y BIO-RAD 200/2.0 Power Supply
- Homogeneizador Heidolph RZR 2021
- Incubador con agitación Innova 4000 incubator shaker New Brunswick Scientific
- Incubador termostatizado de cultivos NAPCO 5415IR CO_2 System
- Jeringas BD Plastic
- Microscopio Leica DM 4500B
- pHmetro CRISON Microph 2001 con un electrodo incorporado INGLOD
- Pipetas de 1000, 200, 20, 10, 5 y 2 μl Thermo Scienctific
- Potter Elvehjem de 2mL
- Placas Petri desechables Raypa 1.90131347
- Rasurador de pelo para ratones
- Set de material quirúrgico: pinzas de clamp, tijeras con puntas rectas, tijeras con puntas roma, pinzas rectas, pinzas curvas, porta agujas, y seda trenzada Aragó estéril para sutura 3/0 y 6/0

- Sistema anestesia para ratones Veterinary fluosorber Harvard Apparatus
- Sistema captador de quimioluminiscencia para *Western blot* Biorad ChemiDoc XRS+ Molecular Imager
- Sistema cromatográfico formado por espectrómetro de masas triple-cuadrupolo MicromassQuatro^{TM} equipado con una fuente de ionización Z-spray operando en modo ion positivo con un LC-10A Shimadzu acoplado al software MassLynx y columna C18 Teknokroma Mediterranean Sea con 3 µm de tamaño de partícula
- Sistema de ósmosis inversa MiliQ Plus
- Sistema para el aislamiento de hepatocitos: Baño termostatizado con bomba peristáltica UNI-100 Raypa, mesa de quirófano elevada con sistema para el desaguado, tubos de PVC estériles para el circuito de perfusión y calefacción, sistema de canulación Braun Introcan Safety 4353523-01, sistema de ajuste de caudal Braun Intrafix Primeline 4062181, camisa calefactora y circuito de suministro de carbógeno (5% CO_2 y 95%O_2)
- Termobloque Accu-Block Digital Dry Bath Labnet
- Termobloque Thermoshaker TS-100C Biosan
- TermocicladorBiorad C1000 Thermal Cycler
- Termociclador TC-312 Techne
- Ultracentrífuga Beckman Coulter Optima TLX
- Ultracongelador SC-420 NewBrunswick
- Vortex Ika Genius 3

2. Reactivos

- 4',6-Diamidino-2-Phenylindole, Dihydrochloride (DAPI) Life Technologies D1306
- Agua ultrapura libre de ARNasas y ADNasas Gibco 10977035
- Anestesia: Isoflurano Laboratorios Esteve Veterinaria
- Anticuerpos Biolegend, Bioworld, Cell signaling, Jackson Inmunoresearch, Life Techonologies, Millipore, Novus y Santa Cruz Biotechnology.
- ARNasa Sigma Aldrich R4642
- Azul Tripán Life Techonologies 15250061
- BCA Protein Assay Thermo Scientific 23223
- Buprex, buprenorfina inyectable 0,3 mg/ 1 mL Laboratorios Esteve
- CellROX® Deep Red Life Technologies C10422
- Colagenasa tipo IV (≥125 CDU/mg sólido) Sigma Aldrich C5138
- DNasa I Roche 04716728001
- Eosina Sigma Aldrich HT110216
- Etanol absoluto CSA-ACS-ISO Panreac 131086.1214
- Formaldehído 35-38% Sigma Aldrich 15513
- Gasas estériles Aragó
- Hematoxilina de Mayer Sigma Aldrich MHS16
- Heparina 5% (5000U /mL) Leo
- Histo-clear National Diagnostics HS-200
- Inhibidores de fosfatasas: fluoruro sódico, pirofosfato sódico, ortovanadato sódico Sigma Aldrich
- Inhibidores de proteasas (*cocktail*) : leupeptina, bestatina, aprotinina, E64, pepstatina A y AEBSF Sigma Aldrich P8340
- Ketamina Imalgene 1000 Laboratorios Merial

- Kit de determinación de actividad alanino amino transferasa en suero Spinreact 41280
- Kit de determinación de actividad gamma glutamil transpeptidasa en plasma Spinreact 1001185
- Kit de determinación de bilirrubina total en suero Thermo Scientific TO32102
- Kit de revelado de *Western blot*: Lumigen Thermo Scientific KJ134089 y Luminol Reagent Santa Cruz Biotechnology sc-2048
- Kit F-actina: G-actin/f-actin *in vivo* assay biochem Cytoskeleton BK037
- Kit TUNEL: *In situ* cell detection kit Roche 11 684 817 910
- Master Mix Universal con fluorocromo SYBR Green Takara RR820L
- Medio de montaje estándar Eukitt Labolan 28100
- Medio de cultivo para hepatocitos primarios compuesto por: 50% v/v Medio Williams Life Technologies 22551 y 50% v/v medio Ham-F12 Life Technologies 11765. Enriquecido con: insulina 9,03 10^{-8} M (Life Technologies 12585), transferrina 0,025 mg/mL (Sigma Aldrich A4503), etanolamina 66,8 μM (Sigma Aldrich 110167), L-glutamina 2,5 mM (Life Technologies 25030), ácido linolénico 7,17 μM (Sigma Aldrich L1376), glucosa 17 mM (Sigma Aldrich G7021), ácido ascórbico 0,62 mM (Sigma Aldrich A4403), *L-NG-Nitroarginine Methyl Ester* 0,64 mM (L-NAME Sigma Aldrich N5751), penicilina/streptomicina 1% (Life Technologies 15140), albúmina sérica bovina 1 g/L (Sigma aldrich A9418), suero bovino fetal 2% (Life Tecnologies 16000044) y dexametasona 10^{-7} M (Fortecortin ® Merck Farma)
- Membranas de transferencia de nitrocelulosa 0,45 µm Schleicher & Schuell Bioscience
- N-acetil cisteína Sigma Aldrich A7250
- Patrón GSH Sigma Aldrich G6013

- Patrón GSSG Sigma Aldrich G4626
- Pipetas de 25, 10, 5 mL Dispenser Nirco
- Ponceau S Sigma Aldrich P7170
- Povidona yodada Betadine®
- *Primers* Agilent y Sigma Aldrich
- ProLong Antifade Life Technologies P36934
- Proteinasa K Thermo Scientific EO 0491
- Reactivos para electroforesis de proteínas: Acrilamida, tetrametiletilendiamina (TEMED), persulfato amónico (APS), dodecilsulfato sódico (SDS), DL–Ditiotreitol (DTT), albúmina de suero fetal (BSA) obtenidos de Sigma-Aldrich Quimica, β-mercaptoetanol, dual color protein molecular marker (Biorad)
- Reservorios para reactivos Matrix Thermo Scientific
- Sytox Green Nucleic Acid Stain® Life Technologies S7020
- Tampón TAE 50x, Running 10x, Transfer 10x National Diagnostics
- Tampón Tris-EDTA 10x pH 8 Gibco AM9849
- Trizol Reagent Life Technologies 15596026
- Tubos de plástico de 50 y 15 mL Labbox
- Xilacina Xilagesic 2% Laboratorios Calier
- Xilol Carlo Erba Reagents 492301

3. Animales de experimentación y cirugía

Para este trabajo se han utilizado ratones macho *knock out* para p38α en células parenquimales hepáticas (p38α *liver parenchymal cells* -LPC-) condicionales de hígado, suministrados por el Dr. Ángel Nebreda y procedentes del IRB Barcelona (*Institute for Research in Biomedicine*). Los ratones se mantuvieron en el estabulario de la Facultad de Farmacia de la Universidad de Valencia, bajo condiciones de temperatura 23 ± 1°C, humedad relativa 60% y ciclos de luz/oscuridad 12h/12h constantes. Además, bebieron y se alimentaron con pienso estándar *ad libitum*.

Tal como se ha descrito anteriormente [Takamura K. *et al.,* 2009], la delección del gen de p38α es letal durante el desarrollo embrionario. Por ello, para estudiar el papel de p38α en el hígado se utilizaron ratones p38α *knock out* condicionales en hígado.

La estrategia empleada por el Dr. Ángel Nebreda, que nos suministró los ratones, se basa en el sistema Cre/LoxP [Heinrichsdorff J. *et al.,* 2008], que permite la recombinación del ADN en lugares específicos. Este sistema está compuesto por una enzima denominada Cre recombinasa que cataliza la recombinación del ADN entre dos dominios de secuencia específica llamados LoxP. Un dominio LoxP consta de 34 pares de bases, distribuidas de forma que en la región central se encuentra una secuencia de 8 pares de bases flanqueada en ambos lados por secuencias palindrómicas de 13 bases. Las secuencias palindrómicas son el sitio de unión para la Cre recombinasa. La recombinación sucede, por tanto, en la zona central asimétrica. Es importante conocer que para que se produzca la deleción de parte de un gen los dos sitios LoxP deben estar localizados en el mismo brazo del cromosoma, tener la misma dirección y flanquear la región que se desee eliminar.

Con el objetivo de obtener ratones p38α *knock out* específicos de hígado, se cruzaron ratones p38α^{FL} (*floxed*: con sitios LoxP entre el exón 2 y 3 del gen para p38α) con ratones portadores del transgén Alfp Cre (en los cuales la Cre recombinasa está regulada por el promotor de la albúmina y los elementos potenciadores de la expresión de albúmina y α-fetoproteína) [Kellendonk C. *et al.*, 2000] específico para hepatocitos y células del ducto biliar. Del cruce entre ambos obtenemos los p38α condicionales p38α$^{LPCc\ P38KO}$ (Figura 10 y 11).

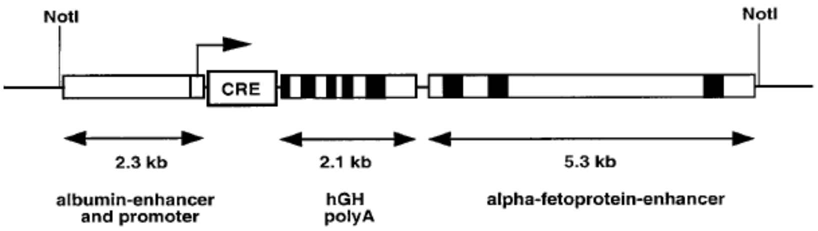
NotI
NotI
CRE
2.3 kb
2.1 kb
5.3 kb
albumin-enhancer and promoter
hGH polyA
alpha-fetoprotein-enhancer

Figura 10. Descripción esquemática del transgén Alfp Cre [Heinrichsdorff J. *et al.*, 2010].

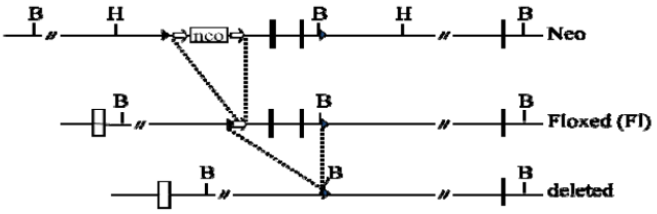
B
H
neo
B
H
B
Neo
B
B
B
Floxed (Fl)
B
B
B
deleted

Figura 11. Descripción esquemática de la estrategia LoxP para obtener el ratón *knock out* de p38α. Los exones 2 y 3 se eliminan ya que están flanqueados por secuencias LoxP (flechas en negro). Ambos codifican para el sitio de unión del ATP de la kinasa. La letra B representa sitios de restricción de la enzima BamHI [Heinrichsdorff J. et al., 2010].

Los ratones p38α $^{\text{LPC-P38KO}}$ son animales viables y fértiles, que no muestran alteraciones hepáticas en condiciones normales. A partir de ahora, para simplificar, a estos ratones se les denominará p38α *knock out*.

Los procedimientos quirúrgicos que se realizaron en los p38α *knock out*: ligadura del ducto biliar (*Bile duct ligation* -BDL-) y hepatectomía parcial del 70% (*Partial hepatectomy* -HPx-) se aprobaron por el Comité de Ética y Experimentación Animal de la Universidad de Valencia. Todos los experimentos se diseñaron con un grupo control o SHAM.

Las edades y “n” para cada uno de los grupos fueron las siguientes (Tabla 2):

Tabla 2. Distribución de grupos para los experimentos de citoquinesis y p38α.

ESTUDIO	**WT destetado**	**KO destetado**	**WT adulto**	**KO adulto**	**WT viejo**	**KO viejo**
	4 semanas	4 semanas	5 meses	5 meses	2 años	2 años
Citoquinesis hepática con la edad	n=8	n=7	n=8	n=8	n=6	n=4
Citoquinesis hepática tras HPx	n=8 SHAM n=4 HPx 24h n=6 HPx 72h	n=7 SHAM n=4 HPx 24h n=6 HPx 72h				
Citoquinesis hepatica tras BDL			n=8 SHAM n=4 BDL12d n=6 BDL28d n=20 para supervivencia	n=8 SHAM n=4 BDL12d n=6 BDL28d n=18 para supervivencia		

WT (*wild type*), KO (p38α *knock out*), SHAM (control), HPx (hepatectomía parcial), BDL (*bile duct ligation*), h (horas), d (días).

Puntualmente, para el aislamiento de hepatocitos, se utilizaron ratones machos de 4 semanas de edad de la cepa C57BL/6.

3.1. Técnicas quirúrgicas

3.1.1. Laparotomía y extracción del hígado en ratones viejos

Los animales fueron sacrificados bajo anestesia (isoflurano al 3% en oxígeno). El abdomen del animal se rasuró y desinfectó (EtOH al 70%) para mantener una condición de semi-esterilidad, necesaria para disminuir el riesgo de infecciones post-operatorias. Se procedió a la laparotomía mediante incisión abdominal y se extrajo el hígado con precaución, para no dañarlo. Los ratones fueron sacrificados por exanguinación.

3.1.2. Ligadura del ducto biliar (BDL)

Las operaciones BDL se realizaron con los animales bajo anestesia (isoflurano al 3% en oxígeno). El abdomen del animal se rasuró y desinfectó (EtOH al 70%) para mantener una condición de semi-esterilidad. Para tener acceso a los órganos abdominales, se realizó una incisión en el abdomen longitudinalmente por la línea alba; siendo la longitud del corte de unos 2 cm. Para tener un mejor acceso al ducto biliar, se colocó un tubo de 5 mm de diámetro detrás del dorso del animal que lo obliga a arquearse.

Después de haber desplazado el hígado en dirección craneal con ayuda de un disector estéril, se aisló el ducto biliar por apertura de la membrana que lo tiene en contacto con los vasos adyacentes. A continuación, se realizaron dos ligaduras dobles con seda trenzada 6/0, una arriba y una debajo del *clamp*. Terminadas las ligaduras se cortó el ducto biliar entre las dos ligaduras, y se cortaron las excedencias de los hilos. Al acabar se quitó el tubo detrás del dorso del animal (Figura 12).

Se concluyó la operación quirúrgica con una sutura continua (seda trenzada 5/0) de la capa muscular y sucesivamente una sutura de la capa cutánea con dos puntos de fijación, uno al inicio y el otro al finalizar la sutura. El animal fue desinfectado con tintura de yodo y colocado sobre una manta eléctrica a 37°C, con el objetivo de que recuperara la temperatura corporal. Finalmente, se les colocó en una jaula limpia. Tanto animales SHAM como BDL fueron tratados con analgesia (Buprex®) durante todo el periodo de tiempo posterior a la operación (tanto 12 como 28 días, teniendo en cuenta que la semivida de eliminación del analgésico es de 12h).

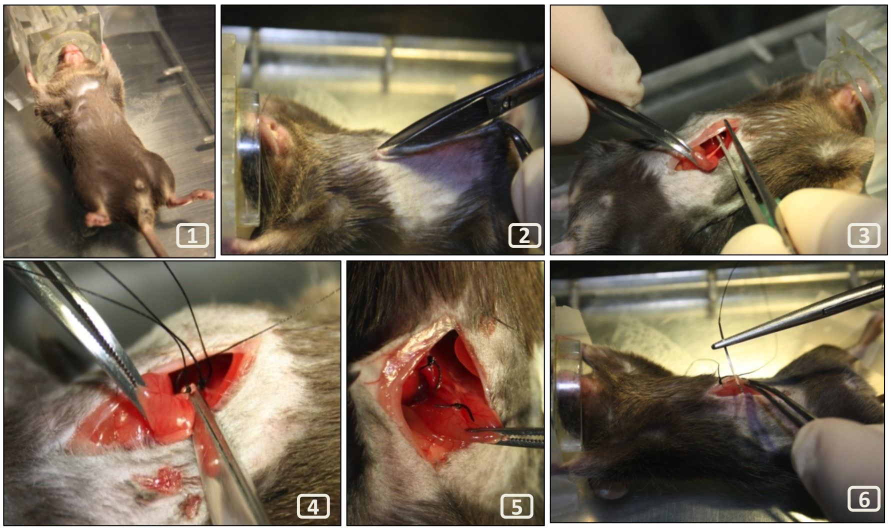

Figura 12. Técnica quirúrgica: ligadura del ducto biliar común. Sistema de anestesia inhalada para ratón (1). Laparotomía (2). Exposición del ducto biliar común (3). Ligadura del ducto (4). Aspecto de un ducto ya ligado y cortado (5). Sutura abdominal (6).

Los animales fueron sacrificados a los 12 días y 28 días después de haber sido operados. La correcta inducción de la colestasis biliar se comprobó mediante la medida de parámetros de daño hepático en sangre como concentración de bilirrubina y actividad de enzimas hepáticas.

3.1.3. Hepatectomía parcial

La hepatectomía realizada en estos ratones consistió en la reducción del hígado en un 70%. Los ratones fueron operados bajo anestesia (isoflurano al 3% en oxígeno) y con el uso de una manta calefactora a 37° C. El abdomen del animal se rasuró y desinfectó (EtOH al 70%) para mantener una condición de semi-esterilidad. Se realizó una incisión en el abdomen longitudinalmente por la línea alba, de unos 2 cm; acercándose lo máximo posible al final del esternón, evitando dañar el diafragma. Para tener un mejor acceso al hígado, se colocó un tubo de 5 mm de diámetro detrás del dorso del animal que lo obliga a arquearse.

Para la resección, se dividió imaginariamente el hígado en 6 secciones o segmentos, lo cual simplificó la operación [Hori T. *et al.,* 2012]. Las secciones se denominan (en inglés): *right anterior segment* (RAS), right middle segment (RMS), *right posterior segment* (RPS*), left anterior segment* (LAS), *left posterior segment* (LPS), y *omental segment* (OS). Las secciones reseccionadas fueron: RAS, LAS y LPS (Figura 13). De hecho, OS, RPS y RMS constituyen en torno a 35,5 ± 7,7% del hígado [Hori T. *et al.,* 2012].

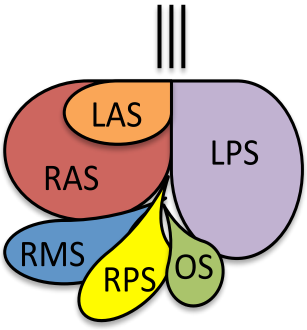

Figura 13. Representación esquemática de los segmentos hepáticos en ratón.

Una vez identificados las secciones hepáticas, el hígado se desplaza hacia el exterior con ayuda de una torunda estéril. A continuación, se ligaron las secciones a reseccionar con seda trenzada 6/0, de forma que se bloquea el flujo sanguíneo para poder eliminarlas sin riesgo de hemorragia. Tras la resección, se lavó la cavidad abdominal con NaCl 0,9% atemperado a 37°C, con la ayuda de una gasa y se quitó el tubo de detrás del dorso del animal.

Se finalizó con el cierre de la cavidad abdominal con una sutura continua (seda trenzada 5/0) de la capa muscular y capa cutánea con dos puntos de fijación, uno al inicio y el otro al finalizar la sutura. El animal fue desinfectado con tintura de yodo y colocado sobre una manta eléctrica a 37°C (Figura 14).

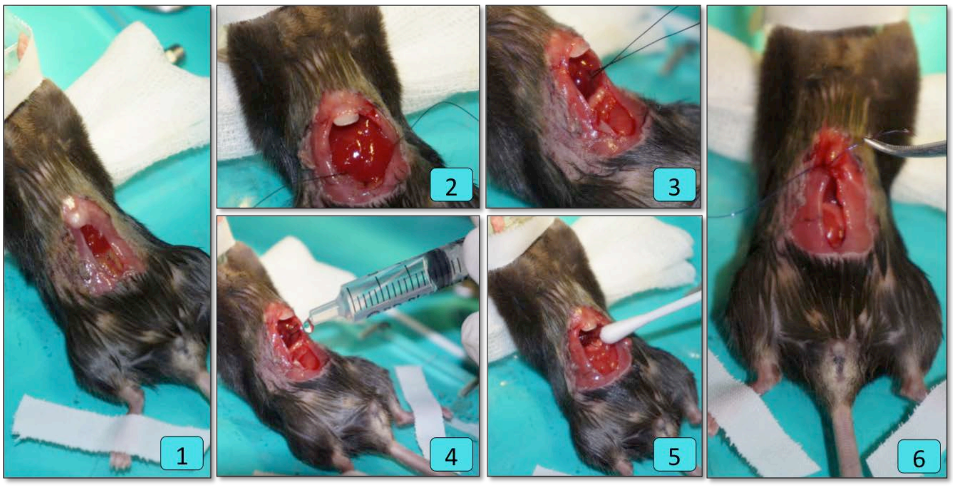

Figura 14. Técnica quirúrgica: hepatectomía parcial. Laparotomía abdominal (1). Exposición del hígado (2). Ligadura de los 3 lóbulos a reseccionar (3). Limpieza de la cavidad abdominal (4 y 5). Sutura abdominal (6). Nótese la presencia de la manta calefactora.

Tanto animales SHAM como hepatectomizados (HPx) fueron tratados con analgesia durante todo el tiempo posterior a la operación (Buprex®).

Los animales fueron sacrificados a las 24 o 72 horas de la operación. La correcta resección del hígado se manifiesta rápidamente tras la operación, observándose tras el sacrificio un claro aumento en la masa de los lóbulos no reseccionados.

3.1.4. Aislamiento de hepatocitos primarios murinos

Para este experimento se utilizaron ratones macho C57BL/6 de 4 semanas de edad. Los ratones utilizados para el aislamiento se dividieron en dos grupos diferentes: hepatocitos aislados sin N-acetil cisteína (NAC) y hepatocitos aislados con NAC 5mM. Cada grupo estuvo formado por 6 ratones en los que la viabilidad de los hepatocitos aislados fue siempre superior al 80%.

El aislamiento de los hepatocitos fue descrito por Berry y Friend en 1969 [Berry M.N. y Friend D.S. 1969]. Nuestro método se basa en una estrategia mejorada de éste, el cual combina la técnica de perfusión con el uso de enzimas disgregadoras.

Una vez preparado el sistema para el aislamiento, y tras haber comprobado que la velocidad de perfusión (3,5 mL/min) y la temperatura del agua circulante (37°C) fuera la adecuada, se procedió a anestesiar al ratón. Los ratones fueron anestesiados con una mezcla de xilacina y ketamina (100/10 mg/kg respectivamente) inyectada via subcutánea.

Tras la inducción de la anestesia, el animal fue rasurado en la zona abdominal y se colocó en la mesa de quirófano, completamente esterilizada. Se inyectaron 25 µL de heparina sódica al 0,5% por la vena femoral del ratón y se procedió a hacer la laparotomía (Figura 15).

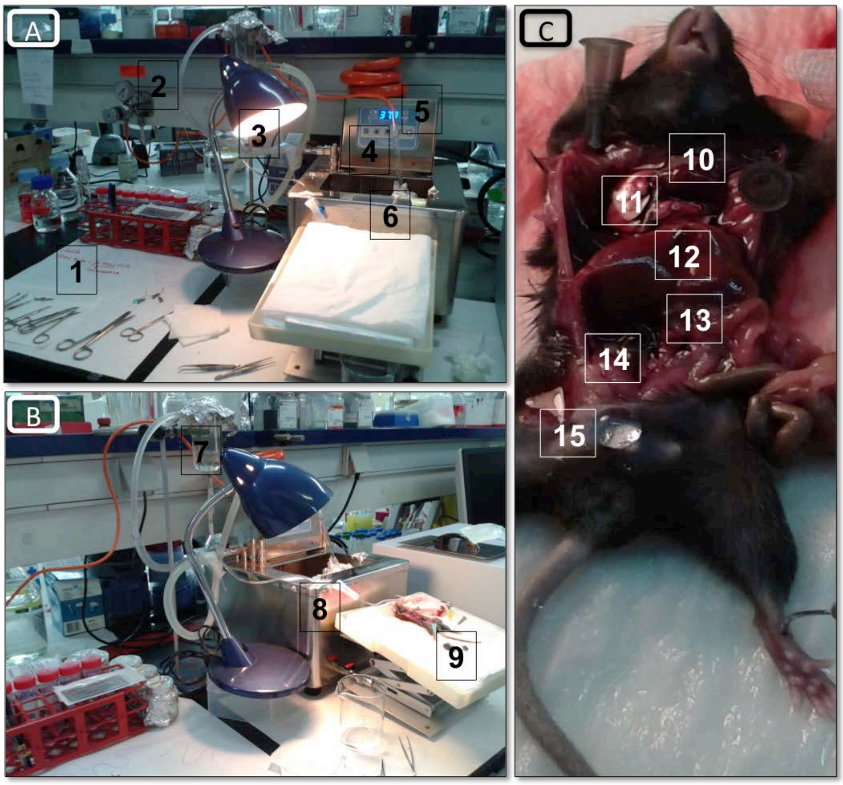

Figura 15. Aislamiento de hepatocitos murinos. Descripción del sistema utilizado para el aislamiento de hepatocitos desde diferentes perspectivas (A,B): material quirúrgico estéril (1), instalación de gas carbógeno (2), sistema de iluminación que ayuda a mantener al animal caliente (3), salida de gas carbógeno (4), baño termostatizado a 37 grados (5), soluciones Krebs-Ringer (6), camisa calefactora (7), regulador del caudal para la perfusión (8), mesa de qurófano de altura regulable y con sistema de evacuación de líquidos (9). Partes claves en la anatomía murina para el aislamiento de hepatocitos (C): corazón (10), vena cava superior (11), hígado (12), vena porta (13), vena cava inferior (14), vena femoral (15).

Para comenzar, vena cava inferior y vena porta se localizaron y aislaron con hilo de sutura (no ligadas) para una vez iniciada la perfusión, ser capaces de localizar con precisión ambas vías. Después de haber abierto el diafragma y cortado las costillas (proceso que duró menos de un minuto para evitar la isquemia del tejido), el hígado se canuló desde la vena cava superior, entrando la cánula por el atrio derecho del corazón. Cuando se inició la perfusión, la vena cava inferior fue ligada y la vena porta se cortó para favorecer el desagüe.

La perfusión constó de dos fases:

Fase 1 (10-15 minutos): lavado con solución Krebs-Ringer (con o sin NAC 5mM) que contenía EGTA 80 µM (*ethylene glycol tetraacetic acid*). La solución Krebs-Ringer se prepara en el día y se compone de: NaCl 118 mM, KCl 4,7 mM, H_3PO_4 1,2 mM, $MgSO_4$ 1,2 mM, $NaHCO_3$ 25 mM y glucosa 10 mM. Además debe filtrarse para que permanezca estéril y el pH se ajusta a 7,4. Todas las soluciones se mantuvieron a 37°C y se burbujearon en carbógeno.

Fase 2 (10 minutos): digestión con solución Krebs-Ringer (con o sin NAC 5 mM) con $CaCl_2$ 2,5mM y colagenasa.

Una vez finalizada la digestión, el hígado se cortó en pequeñas porciones en medio de cultivo de hepatocitos y se filtró a través de una gasa estéril dispuesta en triple capa. La suspensión celular fue centrifugada 3 veces a 100 *g* durante 1 minuto a temperatura ambiente. El número de células y viabilidad se determinó con Azul Tripán y con la ayuda de una cámara Neubauer en un microscopio.

Si se requirió, algunas alícuotas de hepatocitos fueron sembradas. Las placas de cultivo se recubrieron con colágeno y los hepatocitos se sembraron en medio de cultivo especial para hepatocitos primarios, descrito previamente en el apartado de reactivos. Para mantenerlos, se utilizó un incubador de células de uso exclusivo para cultivos primarios.

4. Técnicas de laboratorio

4.1. Medida de la masa hepática

Los ratones se pesaron antes de ser intervenidos quirúrgicamente y después de la intervención -si procedía- en el momento previo al sacrificio. El hígado también se pesó tras el sacrificio.

Con los datos obtenidos se calculó la masa hepática expresada en porcentaje en relación a la masa corporal, con la siguiente fórmula:

$$\frac{\text{peso hígado (g)}}{\text{peso animal (g)}} \text{ x } 100$$

4.2. Técnicas de bioquímica hemática

4.2.1. Obtención del suero

La sangre del ratón extraída sin heparina durante el sacrificio (hasta 1mL) se dejó coagular a temperatura ambiente durante 45 minutos y se centrifugó en tubos de 1,5 mL a 1800 rpm durante 20 minutos, a temperatura ambiente. El suero, que correspondió con el sobrenadante, se recogió y guardó a -80°C hasta su análisis.

En el suero de los ratones sometidos a la ligadura del ducto biliar se realizaron las siguientes determinaciones con el fin de establecer la correcta inducción de la colestasis y valorar el daño hepático tras la intervención:

- Determinación de la concentración de bilirrubina total
- Determinación de la actividad alanina aminotransferasa
- Determinación de la actividad gamma glutamil transpeptidasa

4.2.2.Determinación de bilirrubina total

(REFERENCIA: Thermo Scientific TO32102)

A. PRINCIPIO

La bilirrubina se conjuga con la sal estabilizada del diazonium, esta conjugación forma azobilirrubina, que tiene absorbancia máxima a 540 nm. El diazonium tiene color claro, pálido, ligeramente amarillo. Su absorbancia a 540 nm es normalmente inferior a 0,1. Es importante proteger las muestras de la luz porque la exposición del suero a la luz durante 1 hora puede degradar la bilirrubina en un 50%.

$$Bilirrubina + ácido\ sulfanílico\ diazotizado \rightarrow azobilirrubina$$

B. PROCEDIMIENTO

1. Ajustar a “0” el espectrofotómetro con agua desionizada.
2. Poner 1 mL de reactivo en un tubo de ensayo.
3. Agregar 50 µL de la muestra, del calibrador, o de agua desionizada según la muestra.
4. Mezclar inmediatamente.
5. Incubar a temperatura ambiente durante 5 minutos.
6. Medir la absorbancia de las muestras a 540 nm.

C. INTERPRETACIÓN DE RESULTADOS

El patrón es bilirrubina disuelta en agua, a pH 7,6. Dado que la reacción es lineal hasta 340 µM, la casa comercial recomienda poner sólo un punto de calibración y utilizarlo de la siguiente manera:

[Bilirrubina total] (mg /dL) = (Abs A / Abs B) x [B, en mg/dL]

Donde A = muestra, y B = patrón

La concentración del patrón, y en consecuencia de la bilirrubina se expresa en mg/dL. Sin embargo, es posible efectuar la conversión a molaridad según la siguiente fórmula: 1 mg/dL = 17,1 µM.

Para eliminar posibles interferencias de absorbancia de las muestras hemolizadas o turbias, se mide la absorbancia de la muestra (50 µL) a 540 nm, diluida en 1 mL de agua desionizada. El valor obtenido se restará al valor medido en presencia del reactivo.

4.2.3. Determinación de actividad alanina aminotransferasa (ALT)

(REFERENCIA: Spinreact 41280)

A. PRINCIPIO

La determinación se basa en la transaminación de la alanina y el α-cetoglutarato mediada por la ALT, para formar glutamato y piruvato (que es convertido por la lactato deshidrogenasa) en lactato y NADH.

La medida de la actividad ALT se refleja en la oxidación del NADH a NAD+, que se acompaña con un aumento de absorbancia del cromóforo del kit, medido a 340 nm. La disminución de NADH es proporcional al incremento de actividad de la enzima en la muestra.

$$L-alanina+\ \alpha-cetoglutarato\xrightarrow{ALT}\ Glutamato+Piruvato$$

$$Piruvato+NADH\xrightarrow{LDH}\ Lactato+NAD$$

B. PROCEDIMIENTO

1. Ajustar a “0” el espectrofotómetro con agua desionizada.
2. Pipetear en un tubo de ensayo 100 µL de muestra y 1 mL de solución de trabajo.
3. Mezclar e incubar un minuto a temperatura ambiente.
4. Transferir a la cubeta y medir la absorbancia cada minuto durante 3 minutos a 340 nm.
5. Calcular el promedio de incremento de absorbancia por minuto.

C. INTERPRETACIÓN DE RESULTADOS

La actividad enzimática se calcula como el producto de la disminución de la absorbancia por minuto y se multiplica por el factor corrector 1750 que indica el fabricante del kit.

$$\frac{\Delta A}{min}x\ 1750=\frac{U}{L}de\ ALT$$

4.2.4. Determinación de actividad γ-glutamil transpeptidasa (γ-GT)

(REFERENCIA: Spinreact 1001185)

A. PRINCIPIO

Para la detección de la actividad de la γ-GT se utilizó una modificación del método de Szasz [Szasz G. *et al.,* 1969].

$$L - glutamil - 4 - nitroanilida + Glicilglicina \rightarrow$$
$$L - g - Glutamilglicina + 4 - nitroanilida.$$

Además de hidrolizar el glutatión, la γ-glutamil transpeptidasa también cataliza la transferencia del grupo glutamilo de la γ-glutamyl-4-p-nitroanilida. El rango de liberación 4-*p*-nitroanilida es directamente proporcional a la actividad de la γ-glutamil transpeptidasa en la muestra y se cuantifica midiendo el incremento a 405 nm.

B. PROCEDIMIENTO

1. Se prepara la solución de reacción para la γ-GT: γ-glutamyl-3-carboxi-4-nitroanilida 2,9 mM y glicilglicina 100 mM en tris 0,1 M a pH 8,25. Para disolverlo bien, se calienta durante 30 minutos en un baño con agua a ebullición.

2. Se mezclan 1 mL de la solución reactiva para la γ-GT y 50 µL de cada muestra de suero. Cada muestra se analizó por duplicado y se realizaron dos blancos a los que se les añadió 50 µL de agua.

3. Se incuban las muestras y los blancos a 37°C.

4. Se para la reacción a los 5 minutos de incubación.

5. Se centrifugan las muestras 10 minutos a 3.500 *g*. Se recoge el sobrenadante.
6. Ajustar a “0” el espectrofotómetro con agua desionizada.
7. Medir la absorbancia de las muestras a 405 nm.

C. INTERPRETACIÓN DE RESULTADOS

Para calcular la concentración de 4-*p*-nitroanilida, se utiliza el coeficiente de extinción molar de la 4-p-nitroanilida a 405 nm ($\varepsilon = 9{,}2\ \mathrm{mM}^{-1}\ \mathrm{cm}^{-1}$), utilizando la siguiente fórmula:

$$[4 - p - nitroanilida] = \frac{(E1 - E0)}{9{,}2} \mathrm{x} \frac{V\ total}{Vmuestra}$$

(siendo E1 la absorbancia de la muestra y E0 la absorbancia del blanco. Se expresó la concentración de la 4-p-nitroanilida en µmoL/mL).

La actividad γ-GT se determinó restando la concentración inicial de 4-p-nitroanilida a la concentración final de 4-*p*-nitroanilida en las muestras, y se dividió por los 5 minutos de incubación. Los valores de la actividad γ-glutamiltranspeptidasa (o tasa de formación de 4-*p*-nitroanilida) se expresaron en nmol min^{-1} mg^{-1} de proteína.

4.3. Técnicas de análisis histológico

4.3.1. Preparación del tejido para histología

Se utilizó el protocolo de Junqueira [Junqueira L.C. *et al.,* 1978] con el fin de obtener las preparaciones para histología.

1. En el momento de la extracción del hígado, se prepararon secciones de tejido de aproximadamente 1 cm^3 en paraformaldehido al 4% tamponado en *phosphate buffered saline* (PBS) pH 7,4. A las 24 horas, se sustituye el tampón por paraformaldehido al 0,5%. Después que la muestra ha sido fijada se elimina el fijador y se deshidrata. Debido a que una gran parte del tejido está constituida por agua, se aplica una serie gradual de soluciones de menor a mayor proporción de agente deshidratante (etanol 30%, etanol 50%, etanol 70%, etanol 96%, etanol 100% en etapas de 10 minutos). No se puede colocar el tejido directamente en 100% etanol, ya que el agua se extraería muy rápido del tejido y éste se deformaría.

Después de deshidratar el tejido, se pasa a una solución de una sustancia que es miscible tanto con el alcohol como con el medio de inclusión a utilizar (en la mayoría de los casos se utiliza como medio de inclusión parafina líquida). La sustancia comúnmente utilizada es el xileno o xilol. Se coloca la muestra de tejido en un recipiente con xilol, el cual sólo es soluble en alcohol al 100%. Este proceso se denomina aclaramiento, ya que el tejido se torna transparente o claro en el xilol, esto se debe a que cambia su índice de refracción. En el caso de las preparaciones en las que se estudió la polimerización de la actina, el xilol se sustituyó por Histo-clear (National Diagnostics HS-200).

2. A fin de que se puedan obtener cortes suficientemente finos para ser observados al microscopio, los tejidos deben incluirse y envolverse con una sustancia de consistencia firme (parafina). Por lo general, se coloca la muestra de tejido en un recipiente y se le agrega la parafina fundida a 60°C, se mantienen en estufa durante 5 horas a la temperatura a 60°C. Debido al calor, el xilol se evapora y los espacios anteriormente ocupados por él son ahora ocupados por la parafina. Después se coloca la pieza y un poco de parafina fundida en un molde de papel o metal de forma rectangular, y se deja solidificar a temperatura ambiente, formándose un bloque sólido de parafina con el trozo de tejido incluido, a este bloque se le denomina taco.

3. El taco ahora se puede cortar con un microtomo en secciones lo suficientemente delgadas como para permitir el paso de la luz. La mayor parte de los preparados para microscopia óptica tienen un grosor entre 3 a 10 micrómetros.

4. Los cortes todavía no son aptos para su examen con el microscopio, puesto que los tejidos se hallan infiltrados en parafina y carecen de color. Los cortes se colocan sobre un portaobjetos a los que se les agrega una pequeña cantidad de albúmina, la cual actúa como adhesivo.

5. Previo al análisis histológico, la parafina se elimina con xilol, y la muestra se rehidrata haciéndola pasar por una serie de graduaciones decrecientes de etanol (etanol 100%, etanol 96%, etanol 70%, etanol 50%, etanol 30% en etapas de 10 minutos) hasta llegar a PBS.

Sobre los cortes histológicos se realizaron bien tinciones para el estudio de la inflamación y/o fibrosis, o bien inmunohistoquímica con anticuerpos de la proteína de interés. Todas las técnicas inmunológicas utilizaron fluorescencia como sistema de revelado. Debido a los problemas de autoflorescencia que aparecen en el hígado, las muestras requirieron el uso de Sudan Black (solución saturada en EtOH al 70%), previo a la toma de imágenes.

4.3.2. Estudio de la inflamación hepática por tinción con hematoxilina-eosina

Una vez rehidratado el tejido, se tiñó con hematoxilina de Harris durante 2 minutos y se lavó con agua corriente. Después, se sumergió en alcohol ácido al 1% durante 5 a 3 segundos, controlando con el microscopio. Se azuló en agua corriente y lavó abundantemente. A continuación, se coloreó con eosina durante 2 minutos y se volvió a lavar hasta que la intensidad del color rojo fuera la adecuada. Por último se deshidrató utilizando una serie gradual de soluciones de menor a mayor porcentaje de etanol (etanol 30%, etanol 50%, etanol 70%, etanol 96%, etanol 100% en etapas de 10 minutos) y montó con medio de montaje estándar Eukitt Labolan (28100). Las muestras se almacenaron a temperatura ambiente.

Para la visualización de la preparación se utilizó un microscopio Leica DM 4500B con filtro polarizado. Las imágenes se capturaron con una cámara digital Leica DFC 300 FX.

4.3.3. Estudio de la fibrosis hepática mediante tinción rojo Sirio

Una vez rehidratado el tejido se tiñó con rojo Sirio. Para ello, se incubó el corte durante 2 horas a temperatura ambiente en una solución de rojo Sirio al 1% en ácido pícrico y agua destilada. Se eliminó el exceso de rojo Sirio con 3 lavados en agua destilada. Posteriormente, se tiñó con hematoxilina de Harris, y se volvió a eliminar el exceso con agua destilada (1 lavado). El viraje se realizó en agua corriente, en carbonato de litio al 5% en agua. Posteriormente, se efectuó una tinción rápida con eosina durante 60 segundos seguida del lavado con agua destilada. Finalmente, se deshidrataron los cortes con una serie de alcoholes de concentración creciente (etanol 30%, etanol 50%, etanol 70%, etanol 96%, etanol 100% en etapas de 10 minutos), de tal manera que pudo fijarse de modo permanente el cubreobjetos con medio de montaje estándar Eukitt Labolan (28100). El microscopio utilizado fue el modelo Leica DM 4500B, con cámara Leica DFC 300 FX. Las muestras se almacenaron a temperatura ambiente.

4.3.4. Inmunohistoquímica

Tras rehidratar el tejido, las muestras, sumergidas en tampón citrato pH 6 con Tween 20 al 0,2%, se introdujeron en el autoclave hasta alcanzar los 100°C y se mantuvieron durante 15 segundos. De esta forma se facilita la exposición del epiítopo del antígeno, facilitando el reconocimiento por el anticuerpo.

Cuando el tampón estuvo atemperado, se procedió al bloqueo de las muestras con BSA al 5%, durante una hora, en agitación y a temperatura ambiente.

Después del bloqueo se añadió el anticuerpo primario (Tabla 3). A la incubación le siguieron tres lavados con PBS y el anticuerpo secundario (Tabla 4), seguido de otros 3 lavados con PBS.

Los núcleos se tiñeron con DAPI, una vez lavado el anticuerpo secundario. Los cortes se montaron con ProLong Antifade Life Technologies (P36934). Se utilizó el microscopio Leica DM 4500B, con cámara Leica DFC 300 FX. Las muestras se conservaron a -20°C.

Tabla 3. Anticuerpos primarios utilizados en inmunohistoquímica.

Antígeno	Referencia	Especie	Dilución	Incubación
β catenina	Cell signaling 9587	Conejo	1/100 en BSA 1% tritón 0,3%	Toda la noche 4°C
F-actina	Acris SM1349	Conejo	1/10 en BSA 1% tritón 0,3%	Toda la noche 4°C
p-H3 (Ser10)	Cell signaling 9701	Conejo	1/50 en BSA 1% tritón 0,3%	Toda la noche 4°C
Ki67	Millipore AB9260	Ratón	1/200 en BSA 1% triton 0,3%	Toda la noche 4°C
PCNA	Cell signaling 2586	Ratón	1/100 en BSA 1% tritón 0,3%	Toda la noche, 4°C

BSA, *bovine serum albumin*; p-H3*, phosphorylated histone 3*; Ki67, *cellular marker for proliferation 67 discovered in Kiel* y PCNA, *proliferating cell nuclear antigen*.

Tabla 4. Anticuerpos secundarios utilizados en inmunohistoquímica.

Antígeno	Referencia	Especie	Color	Dilución	Incubación
Alexa Fluor 488 anti conejo	Life Technologies A-21206	Burro	Verde	1/100 en PBS	1 hora temperatura ambiente
Alexa Fluor 532 anti ratón	Life Technologies A-11002	Cabra	Rojo	1/100 en PBS	1 hora temperatura ambiente

4.3.5. Detección de apoptosis por método TUNEL

(REFERENCIA: Roche 11 684 817 910)

A. PRINCIPIO

La apoptosis es un tipo de muerte celular programada que da lugar a la ruptura o digestión del ADN nuclear, originando fragmentos de bajo peso molecular y doble hebra. Estos pequeños fragmentos pueden ser detectados mediante la adición de nucleótidos marcados con fluorescencia al extremo libre OH en 3'.

B. PROCEDIMIENTO

Una vez rehidratados los cortes histológicos, que han sido previamente embebidos en parafina, se procede a realizar la técnica:

1. Permeabilización de las muestras con tampon citrato y proteinasa K (0,1% de citrato sódico 0,1% de Tritón X-100, al que se le han añadido 10 µg/mL de proteinasa K). Se incuban las muestras a 37°C durante 30 minutos en una cámara húmeda hecha artesanalmente.

2. Lavar 3 veces con PBS.

3. Se selecciona una muestra para control positivo. El control positivo se obtiene mediante digestión con DNasa (DNasa 1 recombinante, 3000 U/mL) durante 10 minutos a 37°C en la cámara húmeda.

4. Lavar el control positivo 3 veces con PBS.

5. Se adiciona la reacción de polimerización de nucleótidos (nucleótidos marcados con fluorescencia y polimerasa) a las muestras de estudio y al control positivo. Antes de este paso, se debe haber seleccionado una

muestra como control negativo en la que se añadirán nucleótidos pero no polimerasa. Se incuban todas las muestras y controles en la cámara húmeda durante 1 hora a 37°C.

6. Lavar 3 veces con PBS.

7. Añadir DAPI. Los cortes se montan con ProLong Antifade Life Technologies (P36934). Se utilizó el microscopio Leica DM 4500B, con cámara Leica DFC 300 FX. Para su correcta conservación, las muestras se almacenaron a -20°C.

C. INTERPRETACIÓN DE RESULTADOS

En los cortes histológicos las células apoptóticas tiñen sus núcleos de verde. Dado que los núcleos se han teñido con DAPI, se puede establecer un cociente entre núcleos positivos para apoptosis (verdes) y núcleos totales (azules).

4.4. Técnicas de *Western blot*

4.4.1. Extracción de proteínas tisulares

Se homogeneizó el tejido hepático con tampón fosfato según una proporción de 1 mL cada 30 mg de tejido. El proceso se realizó con homogeneizador mecánico y un *potter Elvehjem* de 2mL con émbolo de teflón. La composición del tampón hipotónico Hepes *Lysis Buffer* pH 7,48 fue la siguiente: *Hepes buffer* 1X, DTT 1 mM, pirofosfato sódico 30 mM, ortovanadato sódico 1 mM, fluoruro sódico 50 mM e inhibidores de proteasas (*cocktail* de inhibidores de proteasas estándar de Sigma Aldrich P8340 para células de mamífero, en una proporción de 5 µL por 1mL de tampón), siendo la composición del Hepes buffer 2X: NaCl 150 mM, $MgCl_2$ 1,5 mM, Hepes pH 7,4 50 mM, EGTA 1 mM, glicerol 10% p/p e igepal 1% (p/p). Tras una centrifugación del homogenado a 15000 *g* durante 15 minutos a 4°C, se alicuotó el sobrenadante y se congeló a -80°C. A partir de los sobrenadantes se determinó la concentración de proteínas mediante el método BCA y se analizaron específicamente mediante *Western blot.*

4.4.2. Aislamiento de núcleos

Los núcleos del tejido hepático fueron aislados para la determinación de proteínas reguladoras del ciclo celular y otras proteínas nucleares mediante *Western blot.*

El tejido hepático fue homogeneizado -con el mismo sistema utilizado para la extracción de proteínas tisulares- en tampón NIM isotónico (Sacarosa 0,25M, KCl 25 mM, $MgCl_2$ 5 mM y Tris-HCl 10 mM pH 7,4) en proporción 1 mL de tampón por cada 100 mg de tejido. La homogeneización fue suave, 600 rpm, con el objetivo de mantener intactas las membranas nucleares. Una vez homogeneizado, el lisado se filtró para obtener un eluato clarificado (paso de filtro 50 µM).

El eluato fue centrifugado a 800 *g*, durante 10 minutos a 4°C. El sobrenadante obtenido corresponde con el citoplasma de las células, mientras que el precipitado se compone fundamentalmente de núcleos.

El precipitado se volvió a lavar con tampón NIM (800 *g*, durante 10 minutos a 4°C) y sobre él se realizó la lisis del material nuclear.

Para lisar los núcleos se empleó tampón Hepes tal y como se describe en el apartado de extracción de proteínas totales (apartado 4.4.1).

4.4.3. Determinación de proteínas con método BCA

(REFERENCIA: Thermo Fisher 23223)

Para la determinación de la concentración de las proteínas totales se empleó el método del BCA. Se eligió este método porque no se ve afectado por la alta concentración de sales biliares y bilirrubina que encontramos en el hígado colestásico.

A. PRINCIPIO

Se trata de un método basado en la reacción de Biuret, en la que los péptidos que contienen tres o más aminoácidos forman un complejo con los cationes Cu^{2+} en un medio alcalino (contiene tartrato sódico y potásico). El cobre se reduce desde el estado +II a +I, y genera un color azul violáceo que se puede medir 540 nm. La intensidad del color es proporcional al número de enlaces peptídicos presentes en la reacción.

El ensayo BCA asocia la reacción de Biuret a la interacción del Cu^{+1} con el ácido bicinchonínico (*bicinchoninic acid*, BCA). Lo que sucede en esta segunda reacción es la formación del complejo Cu-BCA que produce una coloración mucho más intensa. Por cada catión Cu reaccionan dos moléculas de BCA, y el complejo resultante absorbe intensamente luz a 562 nm.

Este ensayo puede verse afectado por la presencia de aminoácidos libres tales como triptófano, cisteína/cistina y tirosina, que también pueden formar quelatos con el Cu^{+1}. Sin embargo, contribuye mucho más el efecto del enlace peptídico sobre la intensidad de la absorbancia final. El ensayo de BCA no se interfiere por detergentes y detecta concentraciones de proteínas entre 5 y 160 mg/mL, y 100 veces más sensible que el método Biuret por sí solo.

B. PROCEDIMIENTO

1. Preparar una mezcla de la solución A con 1/50 de la solución B del kit. Si se hace en placas de 96 pocillos, necesitamos 260 µL de la mezcla por pocillo.
2. Elaborar la recta patrón: para este método empleamos diluciones ½ de una madre 16 mg/mL hasta 0,25 mg/mL de un patrón de BSA. Preparar un blanco con el agua con la que se diluye el estándar.
3. Dosificar tanto el patrón como las muestras por triplicado (2,7 µl por pocillo).
4. Añadir la mezcla preparada anteriormente a cada muestra, e incubar en agitación durante 30 minutos a 37°C.
5. Medir la absorbancia de las muestras a 540 nm.

C. INTERPRETACIÓN DE RESULTADOS

Extrapolar en la curva de calibrado los valores de absorbancia de cada muestra. Los resultados se expresan en mg de proteína por mL de volumen de muestra.

4.4.4. Determinación de proteínas específicas mediante *Western blot*

4.4.4.1. Electroforesis de proteínas

La electroforesis de proteínas se hizo en geles con una matriz de poliacrilamida (PAGE, *poliacrilamide gel electrophoresis*) en un rango del 10 hasta el 13% de acrilamida (13% para proteínas de peso molecular inferior a 20kDa, 12% para proteínas de peso molecular comprendido entre 20 kDa y 70kDa y 10% para proteínas de peso molecular superior a 70 kDa) con un 0,1% de SDS, sobre los que se aplicó un campo eléctrico de intensidad constante de 40 mA hasta completar la electroforesis. El tampón utilizado en la cámara de transferencia fue, glicina 200 mM, 0,1% SDS, Tris-HCl 25 mM pH 8,3. La electroforesis se hizo en condiciones desnaturalizantes de las proteínas. La eliminación de la estructura nativa de las proteínas se obtiene por combinación de un detergente desnaturalizante (SDS) y un agente reductor (β-mercaptoetanol).

Los complejos SDS-proteína se separan estrictamente según su tamaño molecular y así, es posible estimar su masa molecular. En presencia de una concentración de SDS superior a 8 mM, las proteínas unen 1,4 g de SDS por gramo de proteínas, lo que equivale a la unión de una molécula de SDS por cada 2 aminoácidos. Las cargas propias de las proteínas quedan así enmascaradas o anuladas. Debido a que cada molécula de SDS proporciona una carga negativa (del grupo $SO4^{2-}$), los complejos proteína-SDS están cargados negativamente de forma uniforme.

4.4.4.2. Transferencia de proteínas a membrana

Generalmente se empleó el sistema de transferencia húmeda, debido a su mejor rendimiento. Consiste en transferir las proteínas a una membrana de nitrocelulosa o bien de PVDF (*polivinilidene fluorure*), mediante electrotransferencia en condiciones húmedas por medio del sistema Mini-protean II (Bio-Rad, USA). La transferencia se efectuó durante 1 hora a una temperatura de 4°C, una intensidad de corriente de 180 mA, en el siguiente tampón de transferencia: glicina 192 mM, metanol 20 % v/v, Tris-HCl 25 mM pH 8,3.

4.4.4.3. Detección de proteínas con tinción Ponceau

Esta tinción se utiliza para teñir las membranas de nitrocelulosa y PVDF, cuando las proteínas ya han sido transferidas. Es una tinción reversible, de modo que una vez observados los *blots* de proteínas, se puede eliminar lavando con *Tris Buffered Saline-Tween* 0,05% (TBS-T) durante 5 minutos. Se emplea como control de carga del *Western blot* y para verificar que la transferencia ha sucedido con éxito.

Para obtener la coloración se introduce la membrana en una bandeja de plástico con el colorante rojo Ponceau (0,1% p/v Ponceau S en 5/5% v/v ácido acético) adquirido en Sigma Aldrich (P7170) y se incuba durante 10 segundos. Luego se lava con TBS-T 0,05% y se escanea la imagen.

4.4.4.4. Reconocimiento de la proteína de estudio con anticuerpos específicos

Tras la transferencia, las membranas se incubaron durante 1 hora a temperatura ambiente en tampón de bloqueo que fue diferente según las recomendaciones del fabricante del anticuerpo:

- 5% p/v de leche en polvo desnatada en TBS (Tris 20 mM, NaCl 137 mM, pH 7,6) con Tween 0,05%.
- 5% p/v de BSA en TBS-T 0,05%

A continuación, se realizan 3 lavados de 5 minutos cada uno con 15mL de TBS-T 0,05%. Posteriormente las membranas se incubaron durante toda la noche a 4°C con agitación orbital en tampón de anticuerpo (5%/1% BSA o 5% leche desnatada disuelto en TBS-T 0,05%) con la dilución de anticuerpo primario correspondiente. Al día siguiente se realizan 3 lavados de 5 minutos con 15 mL de TBS-T 0,05%. Tras los lavados, se incubaron las membranas con el anticuerpo secundario en agitación durante 1 hora a temperatura ambiente. El anticuerpo secundario se diluyó en TBS-T 0,05% con BSA o leche según el anticuerpo primario utilizado. Para eliminarlo, se realizaron 3 lavados de 5 minutos con 15mL de TBS-T 0,05%. En las tablas siguientes se muestran las proteínas estudiadas, junto con los anticuerpos primarios y secundarios, y diluciones utilizadas (Tabla 5 y 6).

Tabla 5. Anticuerpos primarios utilizados para *Western blot*.

Antígeno	Referencia	Especie	Dilución
α tubulina	Sigma Aldrich T6074	Ratón	1/1000 en 1% BSA TBS-T
AKT	Cell signaling 9272	Conejo	1/1000 en 5% BSA TBS-T
p-AKT (Ser473)	Cell signaling 4070	Conejo	1/1000 en 5% BSA TBS-T
AKT (Thr308)	Cell signaling 13038	Conejo	1/1000 en 5% BSA TBS-T
β catenin	Cell signaling 9587	Conejo	1/1000 en 5% BSA TBS-T
BAD	Cell signaling 9292	Conejo	1/1000 en 5% BSA TBS-T
BAX	Biolegend 625101	Conejo	1/1000 en 1% BSA TBS-T
BCL-2	Cell signaling 2870	Conejo	1/1000 en 5% BSA TBS-T
BCL-XL	Cell signaling 2762	Conejo	1/1000 en 5% BSA TBS-T
Caspasa 3 clivada	Cell signaling 9664	Conejo	1/1000 en 5% leche TBS-T
Caspasa 3	Cell signaling 9665	Conejo	1/1000 en 5% leche TBS-T
Cofilina	Cell signaling 5175	Conejo	1/1000 en 5% leche TBS-T
p-cofilina (Ser 3)	Cell signaling 3313	Conejo	1/1000 en 5% BSA TBS-T
Ciclina B1	Santa Cruz Biotechnology sc-245	Ratón	1/500 en 1% BSA TBS-T
Ciclina D1	Santa Cruz Biotechnology sc-20044	Ratón	1/500 en 1% BSA TBS-T
GSK3β	Santa Cruz Biotechnology sc-9166	Conejo	1/1000 en 1% BSA TBS-T
p- GSK3β (Ser 9)	Bioworld BS4084	Conejo	1/1000 en 1% BSA TBS-T
Histona 3	Cell signaling 4499	Conejo	1/1000 en 5% leche TBS-T
p-H3 (Ser 10)	Cell signaling 9701	Conejo	1/1000 en 5% BSA TBS-T
p-HSP27 (Ser 82)	Cell signaling 2401	Conejo	1/1000 en 5% BSA TBS-T

MK2	Santa Cruz Biotechnology sc-7871	Ratón	1/1000 en 1% BSA TBS-T
p-MK2 (Thr222)	Cell signaling 3116	Conejo	1/1000 en 5% BSA TBS-T
p-MK2 (Thr334)	Cell signaling 3007	Conejo	1/1000 en 5% BSA TBS-T
MNK1	Novus H00008569-M14	Ratón	1/1000 en 1% BSA TBS-T
p-MNK1 (Thr197/202)	Cell signaling 2111	Conejo	1/1000 en 5% BSA TBS-T
mTOR	Cell signaling 2972	Conejo	1/1000 en 5% BSA TBS-T
p-mTOR (Ser2448)	Cell signaling 5536	Conejo	1/1000 en 5% BSA TBS-T
PCNA	Cell signaling 2586	Ratón	1/1000 en 5% leche TBS-T
PRK2	Cell signaling 2612	Conejo	1/1000 en 5% BSA TBS-T
Phospho-PRK1 (Thr774)/PRK2 (Thr816)	Cell signaling 2611	Conejo	1/1000 en 5% BSA TBS-T
p21	Santa Cruz Biotechnology sc-6246	Ratón	1/1000 en 1% BSA TBS-T
p27	Cell signaling 3698	Ratón	1/1000 en 5% leche TBS-T
p38α	Santa Cruz Biotechnology sc-535	Ratón	1/1000 en 1% BSA TBS-T
p-p38 (Thr180/Thr182)	Cell signaling 4511	Conejo	1/1000 en 5% BSA TBS-T
TATA-binding protein	Abcam ab818	Ratón	1/1000 en 1% BSA TBS-T

BAD, *Bcl-2-associated death promoter*; BAX, *Bcl-2-associated X protein* y BCL-XL, *B-cell lymphoma-extra large.*

Tabla 6. Anticuerpos secundarios utilizados para el *Western blot*.

Antígeno	Referencia	Dilución
Anticuerpo secundario hecho en burro anti conejo	Jackson Inmunoresearch 711-035-152	1/40000
Anticuerpo secundario hecho en burro anti ratón	Jackson Inmunoresearch 711-035-151	1/40000
Anticuerpo secundario hecho en burro anti cabra	Jackson Inmunoresearch 705-035-003	1/40000

4.4.4.5. Captura de imagen digital

Se incubó la membrana 1 minuto con 2 mL de reactivo Luminol (Santa Cruz Biotechnology sc-2048). Si al revelar la señal era muy tenue, se añadió al reactivo anterior 30 µL de Lumigen (Thermo Scientific KJ134089) que incrementa la intensidad de la señal.

Se capturó la imagen digital mediante el captador de quimioluminiscencia para *Western* Biorad ChemiDoc XRS+ Molecular Imager, cuyo software (Image Lab Biorad) permite realizar las densitometrías pertinentes.

4.4.5. Estudio de la polimerización de la actina

(REFERENCIA: Cytoeskeleton BK037)

A. PRINCIPIO

La actina en las células eucariotas existe en dos formas: globular o G-actina y filamentosa o F-actina. La forma filamentosa es el componente mayoritario del citoesqueleto en cuanto a actina se refiere.

El tejido se lisa en un tampón que solubiliza y mantiene tanto la G como la F-actina. Posteriormente se ultracentrifuga para diferenciar ambas fracciones y se despolimeriza la F-actina, que al ser de mayor peso molecular queda en el precipitado tras la ultracentrifugación. Ambas fracciones se separan por electroforesis de proteínas y se analizan por *inmunoblotting.*

B. PROCEDIMIENTO

1. Añadir a la muestra de tejido el tampón estabilizador de actina precalentado a 37°C (1 mL de tampón por cada 100 mg de tejido).
2. Homogeneizar las muestras con el sistema ya descrito para la extracción de proteínas a 800 rpm.
3. Centrifugar 100 µL del lisado a 350 *g* durante 5 minutos a temperatura ambiente para precipitar el debris tisular y las células que no se hayan roto. Desechar el precipitado.
4. Con el sobrenadante se realiza la ultracentrifugación a 100000 *g*, 37°C durante 1h que permite separar ambas fracciones de la actina. El resultado es la presencia de G-actina en el sobrenadante y F-actina en el precipitado.
5. Añadir 100 µL de tampón desnaturalizador de la actina al precipitado, e incubar durante una hora en hielo para facilitar la despolimerización. Pipetear cada 15 minutos para disgregar.
6. Adicionar a las diferentes fracciones tampón de carga (tampón de muestra 5X con SDS) y cargar en el gel de electroforesis.
7. Tras la electroforesis, transferir las proteínas a una membrana de nitrocelulosa y seguir la técnica de *Western blot*.

8. El kit viene previsto de unos patrones de G-actina para cuantificar los blots (10, 20 y 50 ng de G-actina) y un control de F-actina para comprobar que esta fracción ha sido precipitada eficientemente.

C. INTERPRETACIÓN DE RESULTADOS

Las diferentes fracciones se cuantifican con el patrón de G-actina y se calcula el cociente G-actina/ F-actina, que equivale al grado de despolimerización de esta.

4.5. Técnica de Real Time Polymerase Chain Reaction (RT- PCR)

4.5.1. Extracción de ácido ribonucleico (ARN)

Las extracciones de ARN se efectuaron a partir de tejido hepático utilizando el reactivo TRIZOL. Este reactivo es una solución monofásica de fenol y guanidina isotiocianato que permite mejorar el método de extracción propuesto por Chomczynsksi y Sacchi [Chomczynski P. y Sacchi N. 1987]. Durante la homogeneización del tejido, el reactivo TRIZOL, mantiene la integridad del RNA, y al mismo tiempo rompe la célula y disuelve sus componentes. La adición de cloroformo seguida de centrifugación separa la solución en dos fases: una fase acuosa y una fase orgánica. El ARN se queda exclusivamente en la fase acuosa. Tras la transferencia de la fase acuosa a un tubo estéril, el ARN se recupera por precipitación con isopropilalcohol.

El ARN total aislado con este método puede llegar a estar prácticamente ausente de contaminaciones de ADN y proteínas. La pureza del ARN aislado se valora generalmente por espectrofotometría, midiendo la absorbancia de los ácidos nucleicos (A =260 nm) y del material proteico (A =280 nm). El cociente entre los dos (A260/A280) se utiliza como índice de la contaminación de la muestra con proteínas; valores comprendidos entre 1,8 y 2,0 indican que la muestra es de calidad adecuada.

4.5.2. Diseño de *primers*

Los oligonucleótidos o *primers* utilizados para este trabajo se diseñaron a partir de la secuencia del correspondiente transcrito (ARNm), disponible en *Entrez Gene*, NCBI *Reference Sequences*. Una vez obtenida la secuencia codificante para la proteína, y dentro del menú "analizar secuencia", seleccionamos la opción "escoger *primers*". El mismo programa realiza una alineación en base lógica (BLAST) en el genoma de la especie para la que diseñamos los *primers* (Tabla 7). En este punto, sugerimos al generador de *primers* que nuestros oligos tengan las siguientes características:

- Temperatura de *melting* (50% de las hebras están desapareadas) entre los 55 y los 59°C
- Longitud de cada *primer* entre 20 y 24 pares de bases
- Longitud del tránscrito entre 70 y 130 pares de bases
- Porcentaje de guanina y citosina comprendido entre el 40 y el 65%
- Secuencia poco repetida en cuanto a tipo de nucleótido
- Escasa complementariedad entre los dos *primers*

Intentaremos diseñar *primers* que cubrieran los extremos de dos exones contiguos. En casos más complejos, se diseñan *primers* que se pegan en dos exones distintos y que entre ellos haya un intrón de tamaño superior a 1000 pb. Estos criterios perimitieron eligir aquellas secuencias que amplificaban exclusivamente ADN complementario (ADNc), no pudiendo por lo tanto amplificar las eventuales contaminaciones del ADN.

En el caso de que existiera más de una pareja de secuencias posibles, se eligieron las parejas de *primers* con la menor diferencia de temperatura, y las que tenían menor probabilidad de formar *primer-dimer*, es decir, que los *primers forward* y *reverse* se unan entre ellos y *self-annealing* (que un mismo primer se pliegue sobre sí mismo).

4.5.3. Retrotranscripción del ARN a ADN complementario

Consiste en la obtención del ADNc a partir de un ARN mensajero (ARNm), el proceso inverso de la transcripción. Para ello son necesarias unas ADN polimerasas particulares, llamadas transcriptasas inversas o retrotranscriptasas. Las enzimas utilizadas proceden de algunos retrovirus, que son virus que presentan ARN como genoma, en vez de ADN. La retrotranscriptasa utilizada es la Multiscribe (Applied Biosystems). Para la síntesis de ADNc a partir de ARN utilizamos una mezcla de productos que incluye *primers*, deoxinucleótidos (*dNTPs*), un tampón 10x para la enzima, una solución de magnesio 25 mM, inhibidor de ARNasa y agua destilada estéril.

4.5.4. Puesta a punto de *primers*

Para cada pareja de *primers* se comprobó experimentalmente la temperatura de *annealing* o anillamiento, haciendo un gradiente de temperaturas; las temperaturas escogidas fueron 60, 62, 64 y 66°C.

4.5.5. Eficiencia de la reacción de PCR

Una vez elegida la temperatura de hibridación, se calculó la eficiencia de cada pareja de *primers,* utilizando una curva de concentraciones de ADNc. La concentración más alta de ADNc elegida fue la correspondiente a una cantidad de ARNm de 2,5 ng/µL. Las amplificaciones con menor cantidad de muestra se efectuaron con diluciones 1/2 de la anterior (en concreto se eligieron las siguientes concentraciones: 1/10, 1/20, 1/40, 1/80, 1/160 ng/µL de ARNm). Los cálculos de la eficiencia se efectuaron a partir de los valores de Ct. Todas las parejas de *primers* utilizadas tenían eficiencias de amplificación entre 1,9 y 2,1. Por lo tanto se propuso utilizar el método del delta-delta Ct, explicado a continuación.

Tabla 7. ***Primers*** **para la cuantificación de ARNm por RT-PCR.**

Gen	Función	Secuencia (5’→3’)
Bcl2	Apoptosis	**F:**TGGACAACATCGCCCTGTGGATG **R:**CACAAAGGCATCCCAGCCTCCGTTA
Birc2	Apoptosis	**F:** GCTGTTGTCCACTTCAGACACCCC **R:**GGCCAAAATGCACCACTGTCTCTGT
Gas2	Apoptosis	**F:**TTCCTATCCTGGTGCCGAGA **R:**ACCATACCTGGCTGCAATCC
Cdc25b	Ciclo celular	**F:** AAACTGAAGCAGGCTACCGA **R:** TGGTAAGACACCTTCTCTCCC
Ciclina A1	Ciclo celular	**F:** GTCAACCCCGAAAAACTGGC **R:** GAGCAACCCGTCGAGTCTT
Ciclina B1	Ciclo celular	**F:** GCACTTCCTCCGTAGAGCAT **R:** CTTTGTGAGGCCACAGTTCA
Ciclina B2	Ciclo celular	**F:** ACCCACAGCCTCTGTGAAAC **R:** CTTGCAGAGCAGAGCATCAG
Ciclina D1	Ciclo celular	**F:** GCAAGCATGCACAGACCTT **R:** GCAGGAGAGGAAGTTGTTGG
Ciclina F	Ciclo celular	**F:** TTTCTGTTGGGGACATCCTT **R:** GAGCTTCAGGTTCTGTGGAGA
Catalasa	Defensa antioxidante	**F:** GGAGCAGGTGCTTTTGGATA **R**: GAGGGTCACGAACTGTGTCA
CuZn Sod	Defensa antioxidante	**F:** TTTTTGCGCGGTCCTTTC **R:** CCATACTGATGGACGTGGAA
Gclc	Defensa antioxidante	**F:** CCATCACTTCATTCCCCAGA **R:** GATGCCGGATGTTTCTTGTT
Gpx	Defensa antioxidante	**F:** ATCAGTTCGGACACCAGGAG **R**: TTCCGCAGGAAGGTAAAGAG
Mn Sod	Defensa antioxidante	**L:** GGCCAAGGGAGATGTTACAA **R:** GAACCTTGGACTCCCACAGA
Col1	Fibrosis	**F**: CTGGACAACGTGGTGTGGTC **R**: TTGCCAGGTTCACCAGAGGG

Timp1	Fibrosis	**F:** ACAGCCTTCTGCAACTCGGA **R:** CATGACTGGGGTGTAGGCGT
Tata-binding protein	Housekeeping (control)	**F:** GCTCTGGAATTGTACCGCAGC **R:** GCAGTTGTCCGTGGCTCTCT
Il10	Inflamación	**F:** GGCTGAGGCGCTGTCATCGAT **R:** TCACTCTTCACCTG CTCCACTGCC
Il6	Inflamación	**F:**CTCTCTGCAAGAGACTTCCATCCAG **R:** AGTAGGGAAG GCCGTGGTTGT
Tnfα	Inflamación	**F:** CCACCACGCTCTTCTGTCTAC **R:** CCACCACGCTCTTCTG TCTAC

Birc2, baculoviral IAP repeat-containing protein 2; Gas2, growth arrest-specific protein 2; Cdc25, cell division cycle 2; Gpx, glutathione peroxidase; Cu Zn Sod, copper zinc superoxide dismutase; Gclc, glutamate cysteine ligase catalytic subunit; Mn Sod, manganese superoxide dismutase; Col1, colágeno1; Timp1, tissue inhibitor of metalloproteinases-1.

4.5.6. Amplificacion del ADNc por PCR cuantitativa a tiempo real

Una vez sintetizado el ADNc, lo amplificamos por medio de la PCR. Éste es un método que permite amplificar de forma selectiva secuencias específicas de ADN. El método de PCR está basado en la amplificación de una secuencia de ADNc utilizando una cadena simple como molde. La PCR utiliza dos fragmentos cortos de ADN (oligonucleótidos) como cebadores de la síntesis. Estos cebadores o *primers* se unen específicamente a secuencias que flanquean la región a amplificar, uno en cada una de las cadenas del ADN. El proceso básico se desarrolla en tres pasos (desnaturalización, hibridación y extensión) que se repiten sucesivas veces, según el gen a amplificar. La repetición del procedimiento un número determinado de veces produce un aumento exponencial de la cantidad de la región diana del ADN, que viene dado por la expresión 2^n (siendo n el número de ciclos) hasta que se llega a un punto en que disminuye la eficiencia de la enzima, y la reacción deja de ser exponencial.

La detección directa del producto de amplificación durante la fase exponencial de la reacción se realiza a través del empleo de compuestos con propiedades fluorescentes que sólo emiten fluorescencia cuando el ADN está en forma de doble cadena, de modo que determinando el incremento de fluorescencia se puede determinar la cantidad de producto formado. La sustancia fluorescente utilizada en nuestros experimentos fue SYBR Green I, el cual se une al ADN y emite fluorescencia sólo en el caso de que las dos hebras complementarias de ADN estén unidas. Este método nos permite seguir la reacción a medida que transcurre a través del incremento de fluorescencia y controlar la reacción en todo momento (aumento del nº de ciclos, repetición de ciclos, pausa, etc.).

El software del equipo construye estas curvas de amplificación a partir de los datos de emisión de fluorescencia recogidos durante la reacción en tiempo real. Así, al final obtenemos con la fluorescencia en el eje de ordenadas y el número de ciclos transcurridos en el eje de abcisas. Una vez obtenida la representación, el eje de ordenadas se transforma en logarítmico para su mejor interpretación.

En el caso de la PCR a tiempo real, el parámetro de medida de la expresión de un determinado gen no es la fluorescencia, sino el ciclo en el que la amplificación comienza a ser exponencial. Este ciclo se denomina ciclo umbral (*threshold cycle*, Ct), a partir del cual la amplificación empieza a ser realmente medible. De este modo, los valores de ciclo umbral decrecerán linealmente conforme aumenta la cantidad de ADNc de partida, puesto que cuantas más copias de ARNm de partida del gen estudiado haya, más ADNc se obtendrá en la retrotranscripción, y antes comenzará la amplificación a ser exponencial.

Para la reacción de PCR a tiempo real se utilizó la Master Mix Universal con fluorocromo SYBR Green I y agua libre de ARNasas (agua DEPC). La reacción se llevó a cabo con una concentración de *primers* de 165nM y un volumen final de 20 µL. Para obtener resultados más reales, todas las muestras de ADNc se diluyeron 1/20 en agua destilada estéril. Esto permite diluir considerablemente todo tipo de compuesto que pueda inhibir la reacción de PCR. Debido a la alta sensibilidad de la técnica, esta operación no compromete la amplificación de las muestras.

La ecuación que permite la cuantificación por el método de comparación de Ct viene dada por:

ΔΔCt→ Donde ΔCt = Ct gen diana – Ct gen referencia

Se realiza esta operación 2 veces: una para el grupo de estudio (Ct1), la otra para el grupo de control (Ct2). Luego se calcula la media y la desviación estándar de cada grupo. Así, ΔΔCt es la diferencia entre la media del ΔCt del grupo de estudio y el ΔCt del grupo control (ΔCt1 –ΔCt2). El método se acaba calculando la potencia en base 2 del valor negativo del ΔΔCt obtenido ($2^{-\Delta\Delta Ct}$). En el caso del grupo control se obtiene siempre un valor arbitrario de 1, ya que la potencia en base 2 de -0 es igual a 1. Se utilizó como referencia el gen de la *TATA-binding protein* (tbp).

4.6. Citometría de flujo

Con las suspensiones de hepatocitos primarios murinos se realizó *Western blot* y RT-PCR siguiendo los pasos que se han mencionado en los apartados anteriores (Apartados 4.4 y 4.5, respectivamente).

Sin embargo, la técnica de citometría de flujo se realizó exclusivamente en estas suspensiones celulares, con el objetivo de estudiar el ciclo celular y determinar la producción de radicales libres del oxígeno.

4.6.1. Estudio del ciclo celular con Sytox green®

Una vez aislados, los hepatocitos se fijaron en una solución al 4% de paraformaldehido en PBS durante 12 horas a 4°C. La tinción de ADN se realizó con *Sytox Green Nucleic Acid Stain*®. La permeabilización con Triton-X y tratamiento enzimático para degradar el ARN (RNase Sigma Aldrich R4642) se empleó durante la tinción.

Para esta determinación se utilizó un citómetro convencional BD FACSVerse y un citómetro con análisis por imagen Amnis FlowSight.

4.6.2. Cuantificación de la producción de radicales libres del oxígeno con Cell Rox®

CellROX® Deep Red fue el fluorocromo indicado para esta determinación. Los hepatocitos fueron incubados con el fluorocromo durante 30 minutos a 37°C en un incubador de células. La suspension celular se lavó 3 veces con PBS antes de ser analizado con el citómetro. Para esta determinación se utilizó un citómetro convencional BD FACSCanto.

4.7. Determinación de GSH y GSSG por espectrofotometría de masas

La determinación de GSH y GSSG en el tejido hepático y hepatocitos se realizó mediante cromatografía líquida de alta resolución acoplada a un tándem de espectrometría de masas (HPLC-MS/MS). El sistema cromatográfico consta de un espectrómetro de masas triple-cuadrupolo MicromassQuatro^{TM} (Micromass) equipado con una fuente de ionización Z-spray operando en modo ion positivo con un LC-10A Shimadzu (Shimadzu) acoplado al software MassLynx 4.1 para el procesado de los datos. Las muestras fueron analizadas por HPLC en fase reversa con una columna C18 Mediterranean Sea (Teknokroma) (5.0 x 0.21 cm) con 3 µm de tamaño de partícula.

Las muestras de tejido congelado se homogenizaron en 400 µL de PBS y N-etilmaleimida (NEM) 11 mM. Después, se añadió ácido perclórico (*Perchloric Acid,* PCA) para obtener una concentración final de 4% y se centrifugaron durante 15 min a 15000 *g* (4°C). Las concentraciones de GSH y GSSG se determinaron en los sobrenadantes. En la columna analítica se inyectaron 20 µl de sobrenadante. La fase móvil consistió en el sistema de gradiente (min/%A/%B) (A, 0,5% ácido fórmico; B, isopropanol/acetonitrilo 50/50; 0,5% ácido fórmico): 5/100/0, 10/0/100, 15/0/100, 15/100/0 y 60/100/0. El flujo fue de 0,2ml/min. Como gas secante y nebulizante se utilizó nitrógeno en un flujo de 500 y 30 L/h, respectivamente. Se empleó argón a $1{,}5\text{x}10^{-3}$ mbar como gas de colisión. Para caracterizar los distintos metabolitos se utilizó un ensayo basado en LC-MS/MS con monitorización de reacción múltiple, usando transiciones m/z, energía cono (V), energía de colisión (eV) y tiempo de retención (min).

Las curvas de calibración se obtienen usando seis puntos (0,01 a 100 µmol/L) estándar que utilizan GSH y GSSG adquiridos en Sigma Aldrich (G6013 y G4626 respectivamente). Los distintos picos se integran en el software *MassLynx* 4.1. Los resultados se expresan en nanomoles por miligramo de proteína.

5. Análisis estadístico

Todos los resultados se expresan como media y desviación estándar. Para el análisis de la significación, se utilizó el tratamiento estadístico ANOVA (*one-way analysis of variance*) seguido por Tukey's *post-hoc* test. Una *P* de 0,05 se utilizó como límite para la aceptación de diferencias estadísticamente significativas.

Las curva de supervivencia se construyó mediante el método de Kaplan-Meyer y el análisis estadístico de basó en el test Mantel-Cox.

El manejo de los resultados se realizó con hojas de cálculo de Microsoft Excel y con el software SPSS, versión 17.

RESULTS

Chapter 4

IV. RESULTS

1. p38α regulates cytokinesis in hepatocytes upon aging

We will begin this chapter with the study of p38α function during liver development and aging. Previous studies about p38 MAPK in hepatocyte proliferation were controversial, so the characterization of the p38α function in liver development was established before proceeding with models of liver proliferation.

1.1. p38α deficiency caused a decrease in liver mass in old mice

Liver growth is achieved during embryonic development and after birth, and it is kept quiescent since adulthood [Gupta S. 2000]. Therefore, we set three time points during mice life (after weaning, 4-week-old; adulthood, 5-month-old; and senescence, 24-month-old) in order to characterize the evolution of the liver mass and the effect of p38α inhibition.

Total liver homogenates where analyzed to determine the activation of p38α by phosphorylation, and to ensure that knock out mice did not express p38α (Figure 16).

As only hepatocytes and cholangiocytes have the deletion for p38α MAPK [Heinrichdorff J. *et al.,* 2008], some background can be observed in these blots and it should be ascribed to other cell types, such as Kupffer cells and endothelial cells, and to other p38 isoforms recognized by the p-p38 antibody.

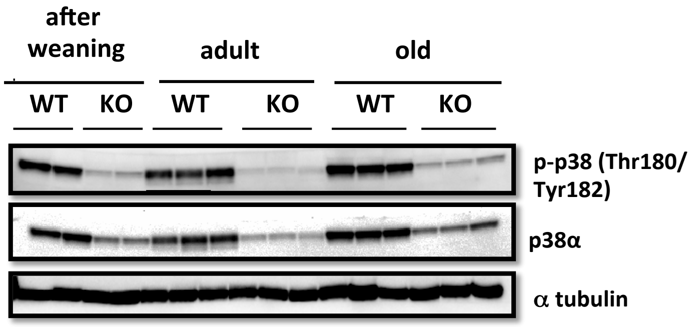

Figure 16. p38 in liver homogenates with age. Representative Western blot images for p-p38 and p38α in wild type and p38α knock out liver extracts. Three stages of liver development were represented: after weaning, adult and old mice. α tubulin was used as a loading control. WT, wild type; KO, p38α knock out. n(after weaning WT)=8, n(after weaning KO)=7, n(adult WT)=8, n(adult KO)=8, n(old WT)=6, n(old KO)=4.

We firstly proceeded with the antropometric analysis of these mice. The evolution of liver mass ratio (liver weight/body weight) showed a significant decrease in liver mass of old p38α liver specific knock out mice when compared to wild type old mice (Figure 17).

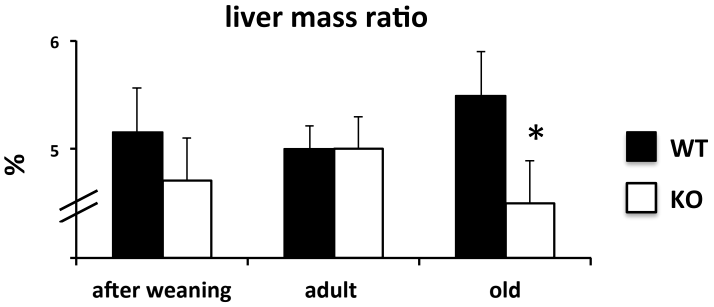

Figure 17. Liver mass ratio (%) with age. Data are shown as mean and standard deviation (SD). Black, wild type (WT); white, p38α knock out (KO). *$P < 0,05$ WT *versus* KO. n(after weaning WT)=8, n(after weaning KO)=7, n(adult WT)=8, n(adult KO)=8, n(old WT)=6, n(old KO)=4.

If a decrease in liver mass was observed in old p38α knock out mice compared to old wild type, two main causes could be responsible for this effect: the hepatocytes could get smaller in size, or the proliferation would be somehow compromised. Nevertheless, a potential increase in apoptosis in p38α knock out mice should be considered.

1.2. Hepatocyte size in wild type and p38α knock out mice

The number of hepatocytes per field was counted to get an indirect measure of hepatocyte size. Thus, the higher number of hepatocytes we counted, the smaller the hepatocytes were. However, no statistical differences were found between wild type and p38α knock out old livers (Figure 18), concluding that p38α knock out mice did not seem to exhibit smaller hepatocytes.

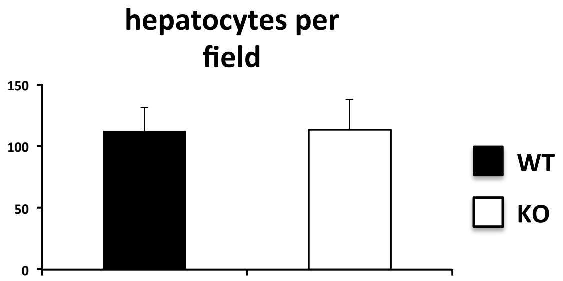

Figure 18. Count of hepatocytes per field from old wild type and p38α knock out mouse liver immunohistochemistry. Data are shown as mean and SD. n(old WT)=6, n(old KO)=4.

1.3. Increase in binucleation rate in p38α knock out mouse liver

Once concluding that hepatocyte size was not the cause, hepatocyte immunohistochemistry was performed in order to observe morphologic changes in these cells. As binucleation is an hepatocyte feature that evolves within age [Gupta S. 2000], and reflects the quality of the mitotic performance, binucleation rates were counted by immunohistochemistry (Figure 19).

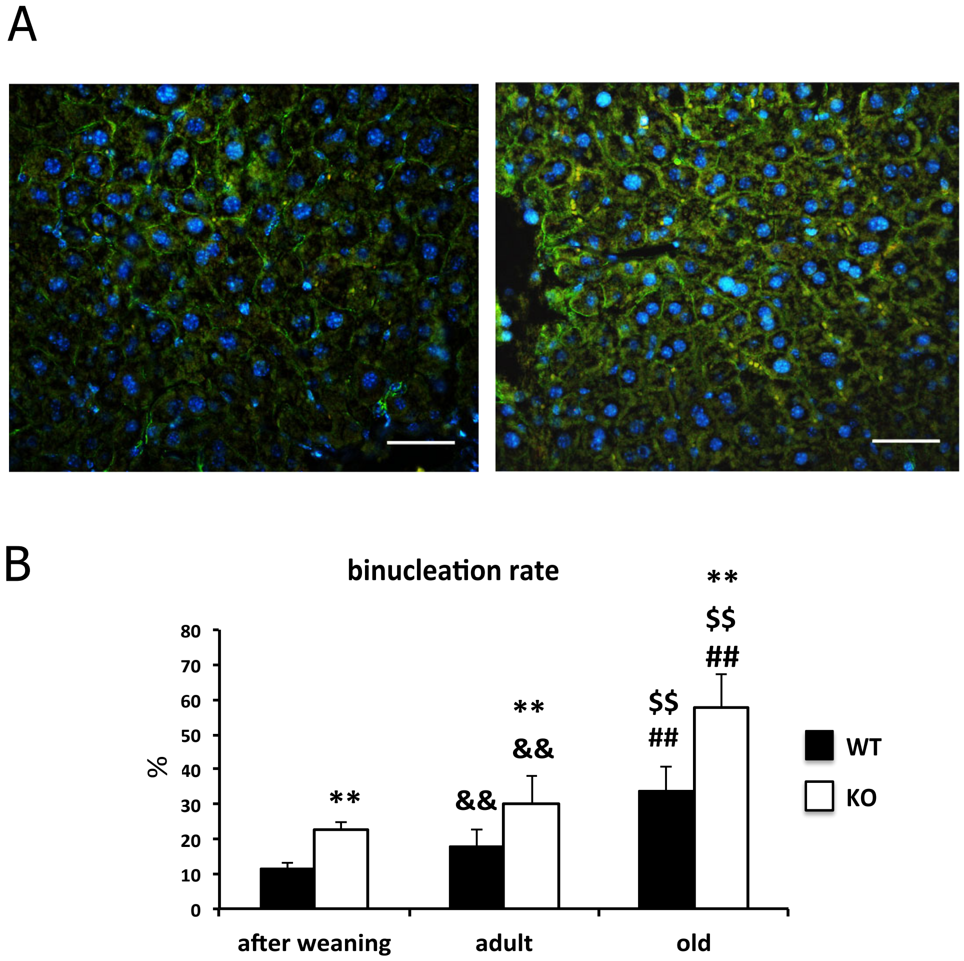

Figure 19. Binucleation in old liver. Representative DAPI (blue) and β catenin (green) staining image of wild type and knock out old liver. A minimum of four experiments were performed for each groups of animals. Scale bars = 50 μm (A). Ratio of binucleated hepatocytes per field was based on immunohistochemistry analysi. At least 20 fields per animal were examined (B). Data are shown as mean and SD. ***P* < 0,01 WT *versus* KO, &&*P* < 0,01 adult *versus* after weaning, $$*P* < 0,01 old *versus* adult, ##*P* < 0,01 old *versus* after weaning. n(after weaning WT)=8, n(after weaning KO)=7, n(adult WT)=8, n(adult KO)=8, n(old WT)=6, n(old KO)=4.

p38α knock out liver had significantly higher binucleation rates comparing to their wild type littermates. Surprisingly, the highest binucleation rates were found in p38α old knock out livers.

1.4. Apoptosis in p38α knock out mice

The blockade of cell cycle can lead to apoptosis [Hartwell L.H. and Kastan M.B. 1994; Adhami V.M. *et al.,* 2004; Ho Y.F. *et al.*, 2013]. Furthermore, apoptosis could be the cause for the loss of liver mass in p38α knock out aged livers. No significant differences in apoptosis were found between old wild type and old p38α knock out mice. Caspase-3-induced cleavage of PARP was not affected by p38α deficiency and no changes were found in steady state levels of pro-apoptotic (Bad, Bax) and anti-apoptotic proteins (Bcl-2, Bcl-XL) (Figure 20).

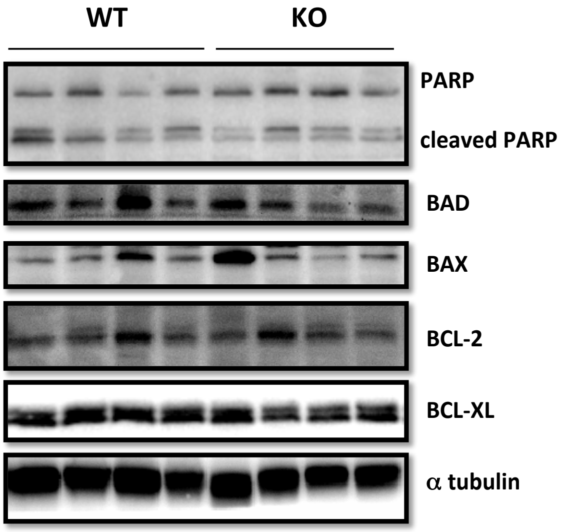

Figure 20. Apoptosis mediators in old liver. Representative Western blot images for pro- (Bad, Bax) and anti-apoptotic (Bcl-2, Bcl-XL) markers in wild type and p38α knock out total liver homogenates. α tubulin was used as loading control. n(old WT)=6, n(old KO)=4.

Apoptosis was also analyzed by TUNEL (Figure 21). No statistical differences were found comparing both aged livers. Interestingly, positive cells for apoptosis-induced DNA fragmentation did not correspond with binucleated cells.

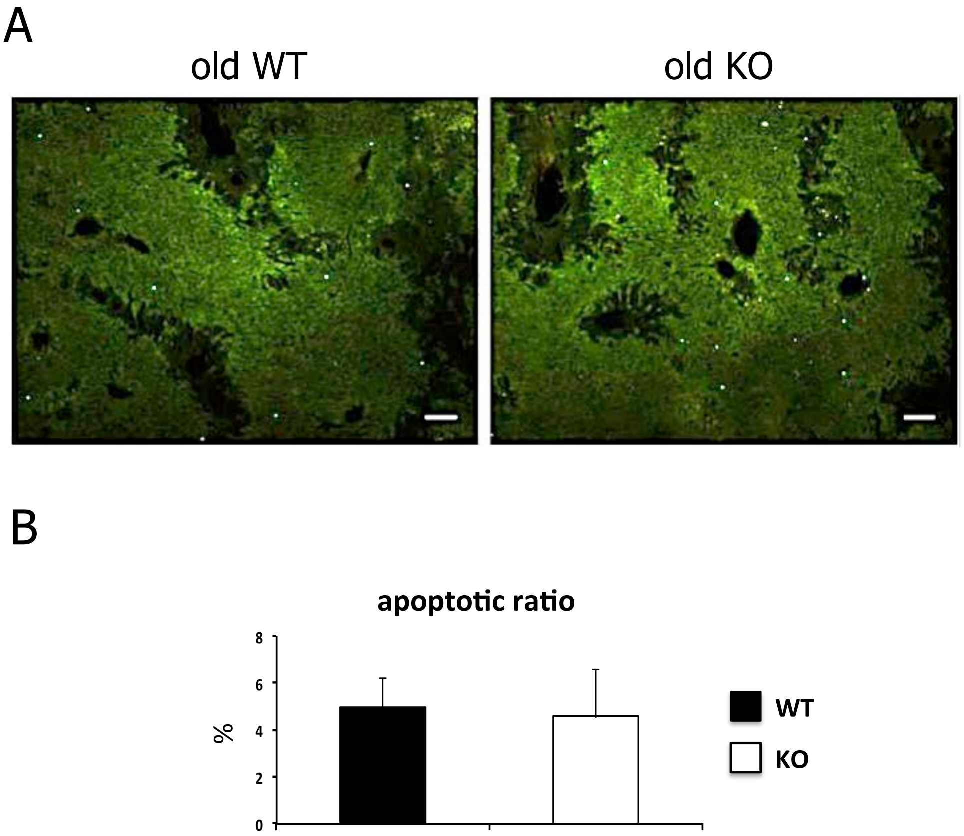

Figure 21. Apoptosis quantification by TUNEL in old liver. Representative inmunohystochemistry images of TUNEL from old wild type and p38α knock out liver. A minimum of four experiments were performed for each groups of animals. Scale bars = 100 µm (A). Ratio of apoptotic hepatocytes per field in old mouse liver (B). Apoptotic rate count percentage in hepatocytes was based on immunohistochemistry analysis. At least 20 fields per animal were examined. Data are shown as mean and SD. n(old WT)=6, n(old KO)=4.d. Data are shown as mean and SD. n(old WT)=6, n(old KO)=4.

To complete the apoptosis characterization, we determined mRNA levels of growth arrest-specific gene 2 (*Gas2*), a protein that is involved in the defense against apoptosis in polyploid (binucleated) cells [Lu P. *et al.,* 2007] (Figure 22). Interestingly, mRNA levels of *Gas2* were up-regulated in p38α knock out old livers. This may provide protection to p38α knock out aged hepatocytes against high binucleation rates.

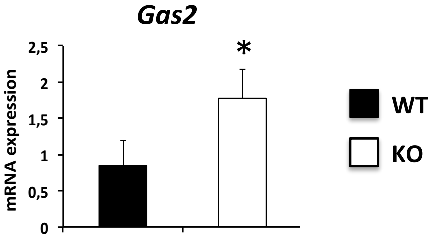

Figure 22. Real-time PCR analysis of the expressions of mRNA for *Gas2*. Data (mean and SD) are shown as fold increase in mRNA level compared to the control and were normalized by TATA-binding protein mRNA. *P < 0,05 WT *versus* KO. n(old WT)=6, n (old KO)=4.

1.5. Hepatocyte proliferation in old p38α knock out livers

Subsequently, we decided to study other parameters that could support the hypothesis that hepatocytes from p38α knock out mice got progressively comprised cell proliferation.

As it has been defined in the introduction section (see 3.3.7), p38α mainly regulates checkpoints G_0/G_1 and G_2/M under physiological conditions [Stepniak E. *et al.,* 2006]. We chose representative cyclins for both checkpoints: cyclin D1 for G_0/G_1, and cyclin B1 for G_2/M progression. Interestingly, a significant increase of cyclin B1 was found in nuclear extracts from p38 knock out old livers (Figure 23). The accumulation of cyclin B1 could point out hepatocyte difficulties in going through mitosis. No signifficant differences were found in cyclin D1 levels.

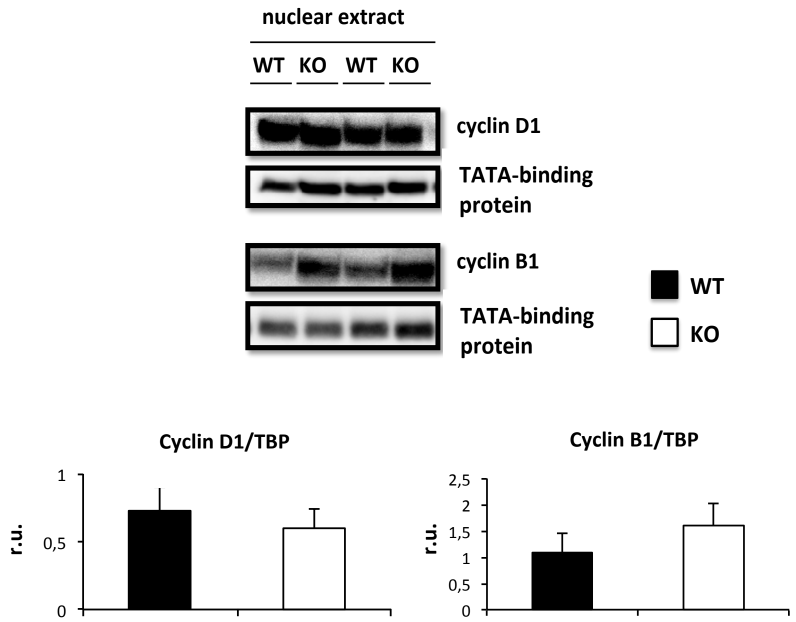

Figure 23. Cell cycle study in old liver. Representative Western blot images for cyclin D1 and cyclin B1 in nuclear homogenates from wild type or p38α knock out old liver. Western blot densitometries used TATA-binding protein as loading control. Data are shown as mean and SD. **P* < 0,05 WT *versus* KO. n(old WT)=6, n(old KO)=4.

1.6. The absence of p38α blocked pathways required for hepatocyte cytokinesis completion: MNK1

MNK1 is a direct target of p38 MAPK that is involved in cytokinesis completion and, hence, inactivation of MNK1 could lead to the formation of multinucleated cells [Rannou Y. *et al.,* 2012]. MNK1 phosphorylation was markedly inhibited in p38α knock out livers (Figure 24), but there was no significant differences between after weaning and adult p38α knock out livers when measured by Western blot.

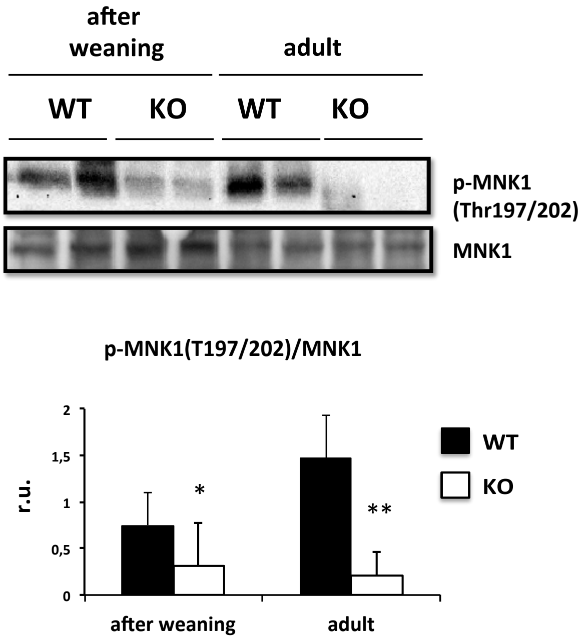

Figure 24. MNK1 activation in after weaning and adult livers. Representative Western blot images for p-MNK1 and MNK1 in homogenates from wild type or p38α knock out after weaning and adult liver. Western blot densitometries used α tubulin as loading control. Data are shown as mean and SD. **P* < 0,05 WT *versus* KO, ***P* < 0,01 WT *versus* KO. n(after weaning WT)=8, n(after weaning KO)=7, n(adult WT)=8, n(adult KO)=8.

Then, we analyzed activation of MNK1 in wild type and p38α knock out old livers (Figure 25).

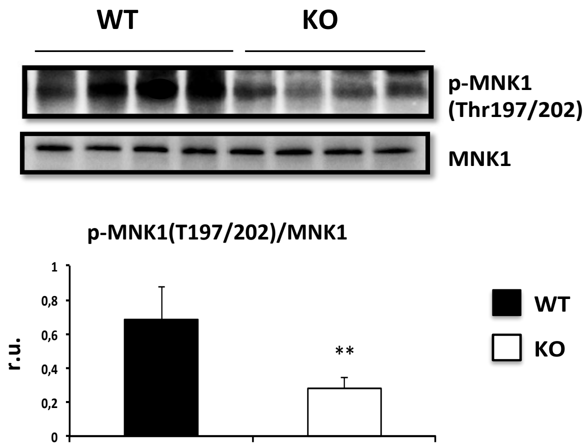

Figure 25. MNK1 activation in old liver. Representative Western blot images for p-MNK1 and MNK1 in homogenates from wild type or p38α knock out old liver. Western blot densitometries used α tubulin as loading control. Data are shown as mean and SD. $^{**}P < 0{,}01$ WT *versus* KO. n(old WT)=6, n(old KO)=4.

1.7. Actin polymerization was abrogated by p38α deficiency in old hepatocytes

Inactivation of MNK1 could induce binucleation in p38α knock out mice but it was unable to explain the progressive increase in binucleated hepatocytes upon age, which was exacerbated in old p38α knock out mice.

Inhibition of p38α seemed to affect mitosis by blocking the separation of the two daughter cells. We hypothesized that p38α knock out hepatocytes could go through mitosis but when they were ready to divide the cytoplasm to give birth to two new cells, the absence of p38α hindered cytokinesis.

Among the proteins that have been described to have a role in cytokinesis, we focused on the ones that could be regulated by p38α. One protein that accomplishes all these requirements is actin. Actin cytoskeleton rearrangement is a well-known target of p38 signaling [Dalle-Donne I. *et al.*, 2001; Chae K.S.

and Dryer S.E. 2005; Zuluaga S. *et al.,* 2007; Corrêa S.A and Eales K.L. 2012].

The quantification of the different conformational fractions of actin in wild type and p38α knock out old mice by ultracentrifugation followed by Western blot showed that p38α knock out mice had higher levels of G-actin and lower levels of F-actin, indicating an alteration in actin polymerization (Figure 26).

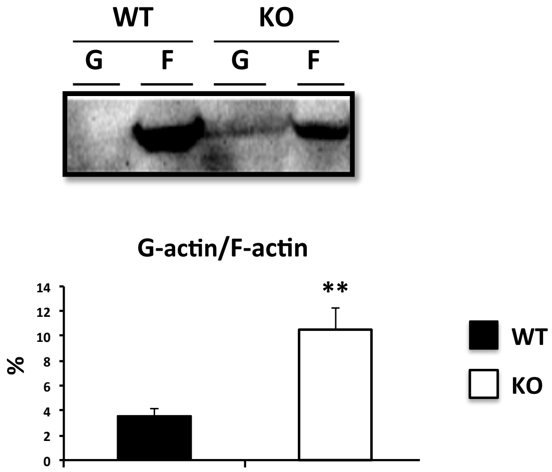

Figure 26. Actin polymerization in aging. Representative Western blot images for G and F-actin in old wild type and p38α knock out total liver homogenates. G= G-actin, F= F-actin. Western blot densitometry of G-actin/F-actin ratio was also calculated. Data are shown as mean and SD. **$P <$ 0,01 WT *versus* KO. n(old WT)=6, n(old KO)=4.

Once estimating actin polymerization with the ratio G-actin/F-actin, we checked the F-actin immunostaining in liver slides (Figure 27) . Livers from p38α knock out old mice exhibited a severe impairment in the polymerization of F-actin.

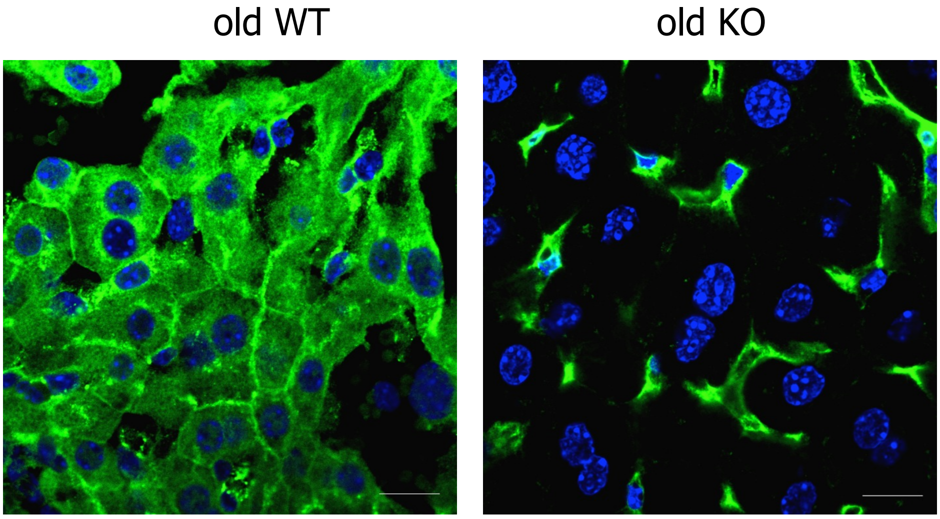

Figure 27. F-actin staining in old liver slides. Representative immunohistochemistry for F-actin (green) and DAPI (blue) staining image of wild type and p38α knock out old liver. A minimum of four experiments were performed for each group of animals. Scale bars =10 μm. n(old WT)=6, n(old KO)=4.

1.8. Progressive impairment of actin polymerization in p38α knock out liver with age

If the binucleation rate was higher in p38α knock out livers in all stages of development in comparison to wild type, actin polymerization may be already damaged in younger p38α knock out livers. Thus, we kept looking for any disregulation. We also performed F-actin immunohistochemistry in after weaning and adult liver (Figure 28). Although p38α knock out adult mice showed diminished F-actin positive cells, p38α knock out after weaning mice did not show any difference when comparing with their wild type littermates.

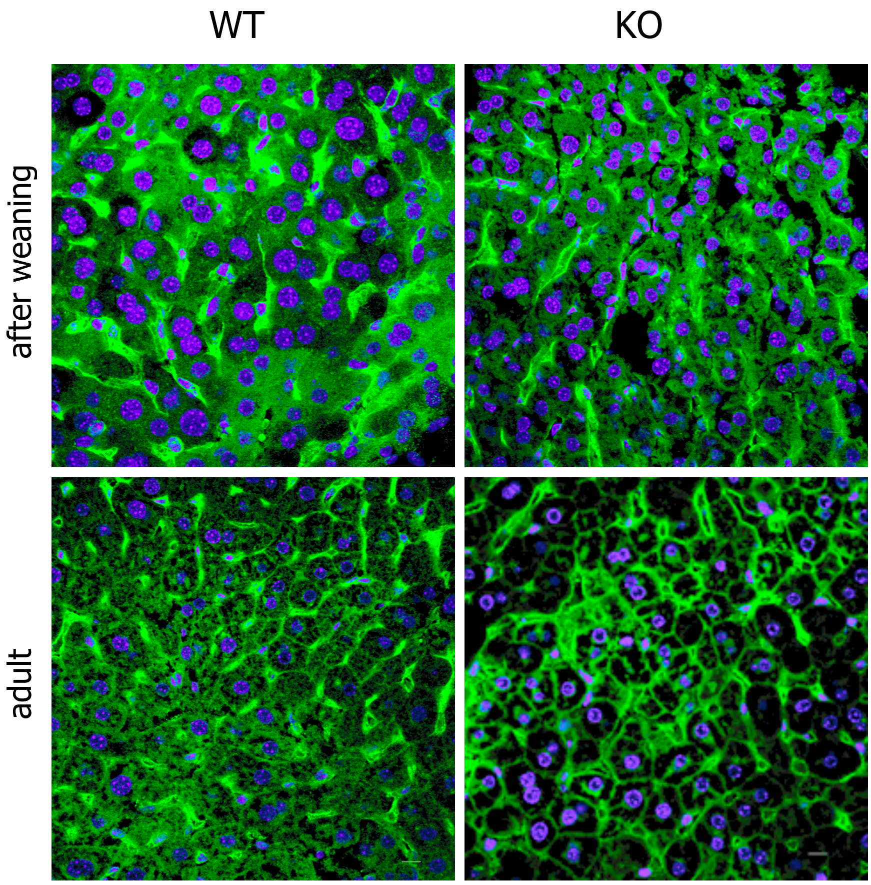

Figure 28. F-actin staining in after weaning and adult liver slides. Representative immunohistochemistry for F-actin (green) and DAPI (blue) staining image of wild type and knock out after weaning and adult liver. A minimum of 4 experiments were performed for each group of animals. Scale bars=10 µm. n(after weaning WT)=8, n(after weaning KO)=7, n(adult WT)=8, n(adult KO)=8.

Not only did adult knock out hepatocytes show a decrease in F-actin staining, but they also showed morphological changes in the intracellular F-actin distribution. Interestingly, F-actin in adult wild type livers was located around the nucleus and occupying all the cytoplasm (Figure 29). However, F-actin distribution in adult p38α knock out mice was more peripheral next to the plasmatic membrane.

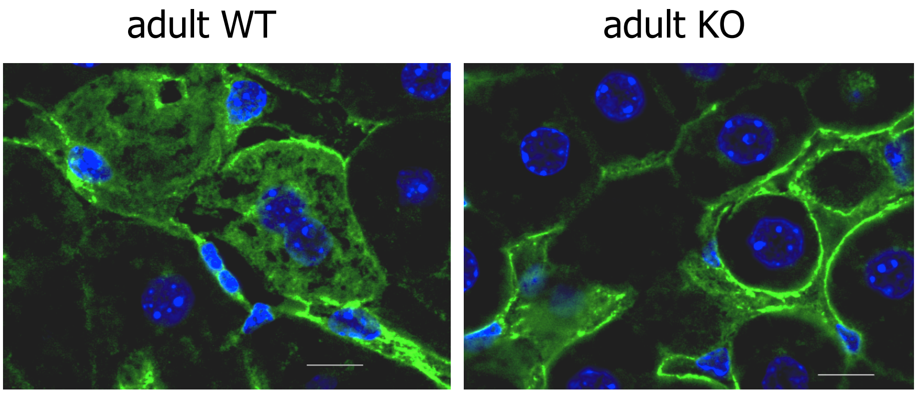

Figure 29. F-actin distribution in adult liver slides. Representative immunohistochemistry for F-actin (green) and DAPI (blue) staining image of wild type and knock out adult mouse liver. A minimum of 4 experiments were performed for each group of animals. Scale bars = 5 µm. n(adult WT)=8, n(adult KO)=8.

1.9. Blockade of actin polymerization pathways in p38α knock out livers: Role of HSP27

Absence of p38α progressively impaired the proper polymerization and distribution of F-actin in p38α knock out adult and, was almost blocked it in aged liver. Therefore, we went further with the identification of the pathways that could be inactivated after the deletion of p38α in liver. We focused on old livers as first approach.

First of all, we analyzed the proteins that are direct targets of p38α and could be involved in actin polymerization, such as MK2, a downstream kinase of p38α, and HSP27, which have often been found to be dephosphorylated in absence of p38α [Pichon S. *et al.,* 2004; Gamell C. *et al.,* 2011; Shiryaev A. *et al.,* 2011]. In our work, lack of MK2 phosphorylation on Thr334 was observed when p38α was deleted (Figure 30).

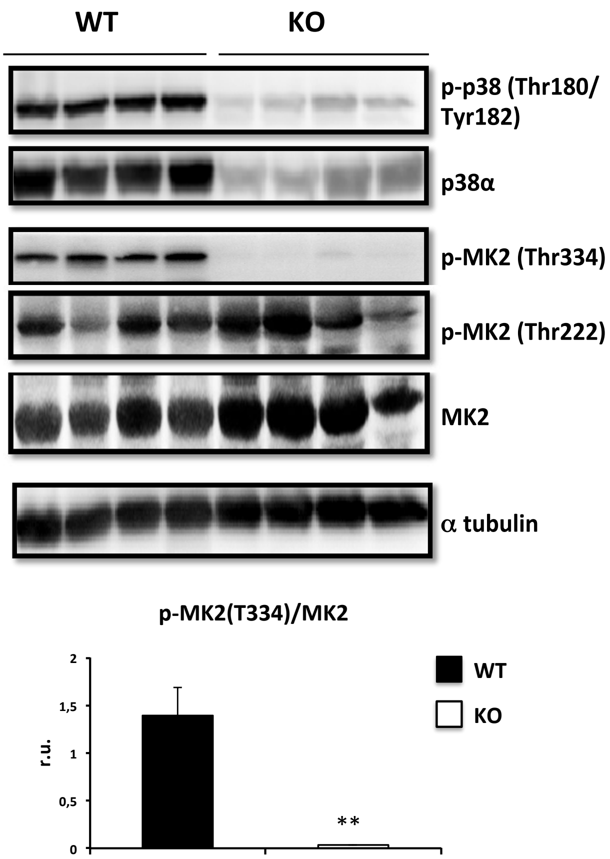

Figure 30. p38α downstream pathway in aging: MK2. Representative Western blot images for p-p38, p38α, p-MK2, and MK2 in homogenates from wild type or p38α knock out old liver. Western blot densitometry used α tubulin as a loading control. Data are shown as mean and SD. $^{**}P < 0{,}01$ WT *versus* KO. n(old WT)=6, n(old KO)=4.

The p38α downstream axis MK2/HSP27 could provide an explanation of why actin polymerization was failing in p38α knock out mice (Figure 31). As we had already checked by immunohistochemistry, the highest binucleation rate and the most deficient F-actin polymerization was significantly found in p38α knock out old livers.

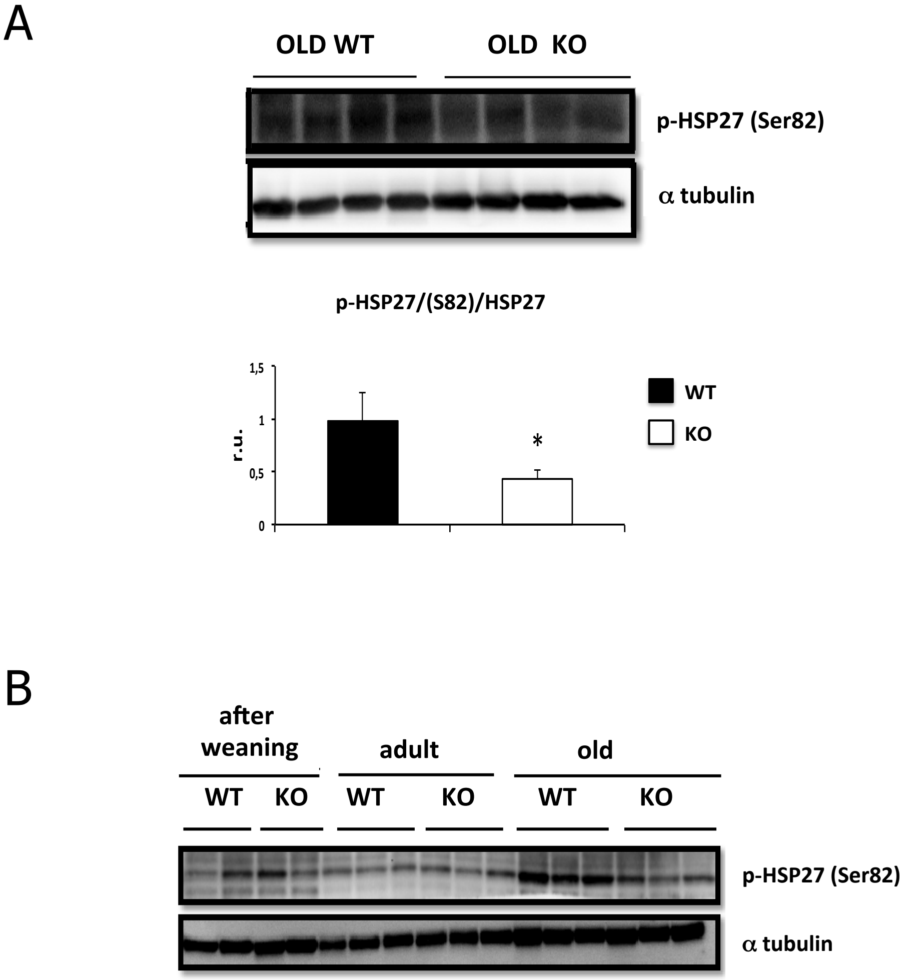

Figure 31. HSP27 phosphorylation within age. Representative Western blot images for p-HSP27 from wild type or p38α knock out old liver (A). α tubulin was used as loading control in denstritometry. Data are shown as mean and SD. *$P < 0,05$ WT *versus* KO. Representative Western blot images for p-HSP27 from after weaning, adult and old wild type and p38α knock out total liver homogenates (B). α tubulin was used as loading control. n(after weaning WT)=8, n(after weaning KO)=7, n(adult WT)=8, n(adult KO)=8, n(old WT)=6, n(old KO)=4.

Accordingly to our F-actin polymerization results, only old p38α knock out livers showed a significant reduction in F-actin and a decrease in HSP27 phosphorylation levels, comparing with their wild type littlermates. Both features accompanied the reduction in liver mass. However, the exclusive activation of HSP27 in old wild type mice seemed hard to be attributed to p-MK2, which was also downregulated in after weaning and adult p38α knock out mice (Figures 47 and 58).

1.10. p38α regulated the RhoA pathway in old livers

Significant deficiencies in F-actin polymerization could also involve inactivation of the RhoA pathway [Sit S.T. and Manser E. 2011]. In addition, RhoA can promote p38α-mediated HSP27 phosphorylation [Zhang S. *et al.,* 1995; Katoh K. *et al.,* 2001; Dubroca C. *et al.,* 2005]. The association between HSP27 and RhoA has been described in muscle cells [Bitar K.N. *et al.,* 1985; Patil S.B. *et al.,* 2004] modulating actin-myosin interaction [Bitar K.N. 2002].

To begin with, we performed some immunoblots of RhoA targets in old mice. We found a significant dephosphorylation and, hence, inactivation of PRK2 in p38α knock out old liver. Moreover, p38α knock out old livers showed accumulation of p-cofilin in the nucleus and p27 in the cytoplasm (Figure 32).

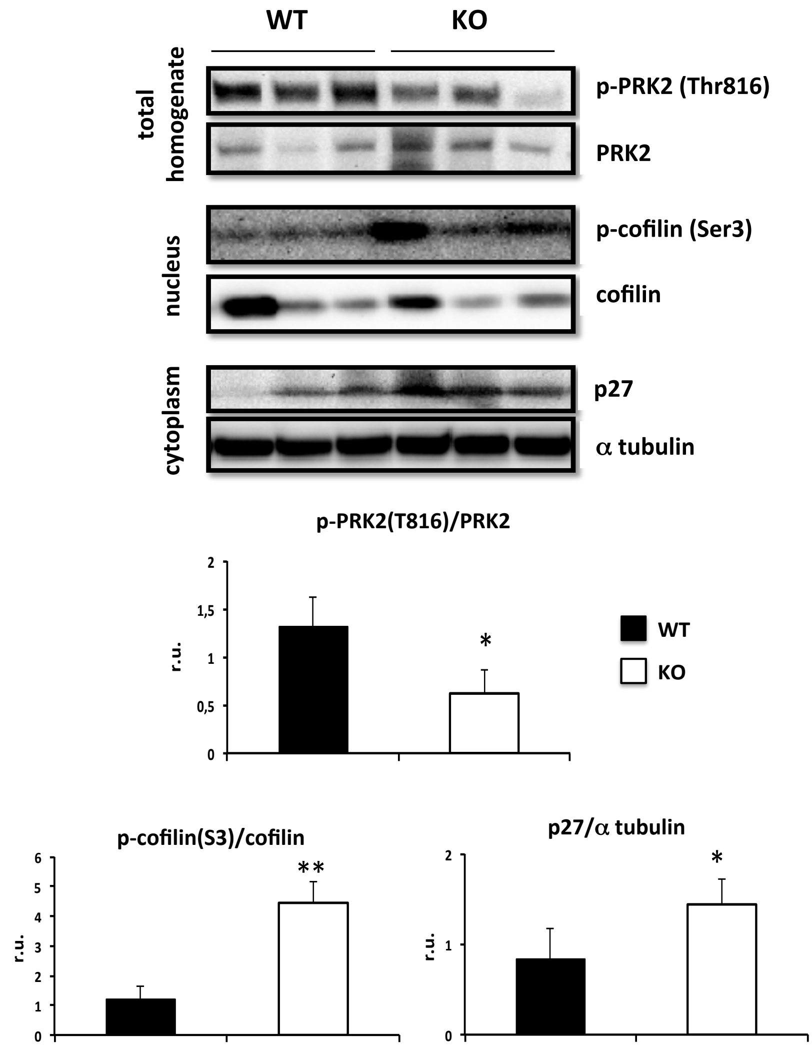

Figure 32. RhoA pathway regulation by p38α in aging liver. Representative Western blot images of key regulators of the pathway such as: p-PRK2 and PRK2 in total homogenate; p-cofilin and cofilin in the nucleus, and p27 in the cytosolic fraction. α tubulin was used as loading control for the cytosolic fraction. Western blot densitometry data are shown as mean and SD. **P* < 0,05 WT *versus* KO. ***P* < 0,01 WT *versus* KO. n(old WT)=6, n(old KO)=4.

1.11. p38α deficiency led to a decrease in GSH levels in adulthood

Because binucleation may, in part, be induced by oxidative stress, we determined liver GSH and GSSG levels in the three different groups of animals. No correlation between binucleation and oxidative stress in p38α knock out livers was found. Interestingly, adult p38α knock out exhibited an unexpected decrease in the levels of reduced glutathione. Meanwhile, old p38α knock out showed decreased GSSG/GSH ratio (Figure 33).

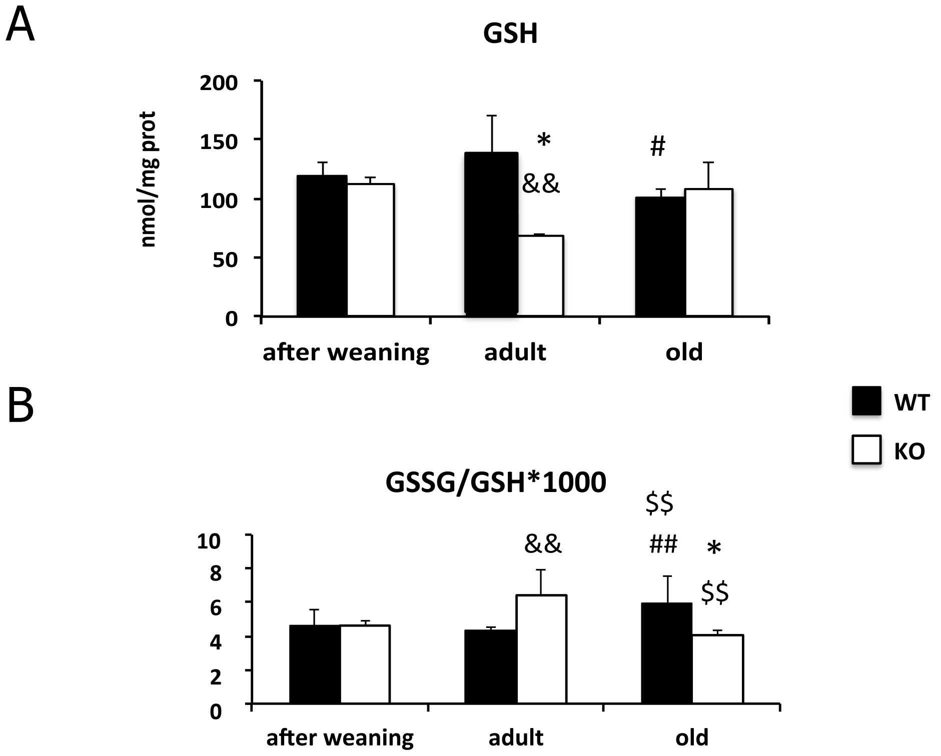

Figure 33. REDOX variations in liver with age. GSH (A) and GSSG/GSH ratio (B) measurement in wild type and p38α knock out mouse liver tissue. Data are shown as mean and SD. **P* < 0,05 WT versus KO, #*P* < 0,05 old versus after weaning, ##*P* < 0,01 old versus after weaning, $$*P* < 0,01 old versus adult, &&*P* < 0,01 adult versus after weaning. n(after weaning WT)=8, n(after weaning KO)=7, n(adult WT)=8, n(adult KO)=8, n(old WT)=6, n(old KO)=4.

1.12. p38α induced the liver antioxidant defense in adulthood but not in old livers

Preliminary results showed that the regulation of certain cytosolic and mitochondrial antioxidant enzymes perfectly matched with the evolution of the REDOX balance (Figure 34).

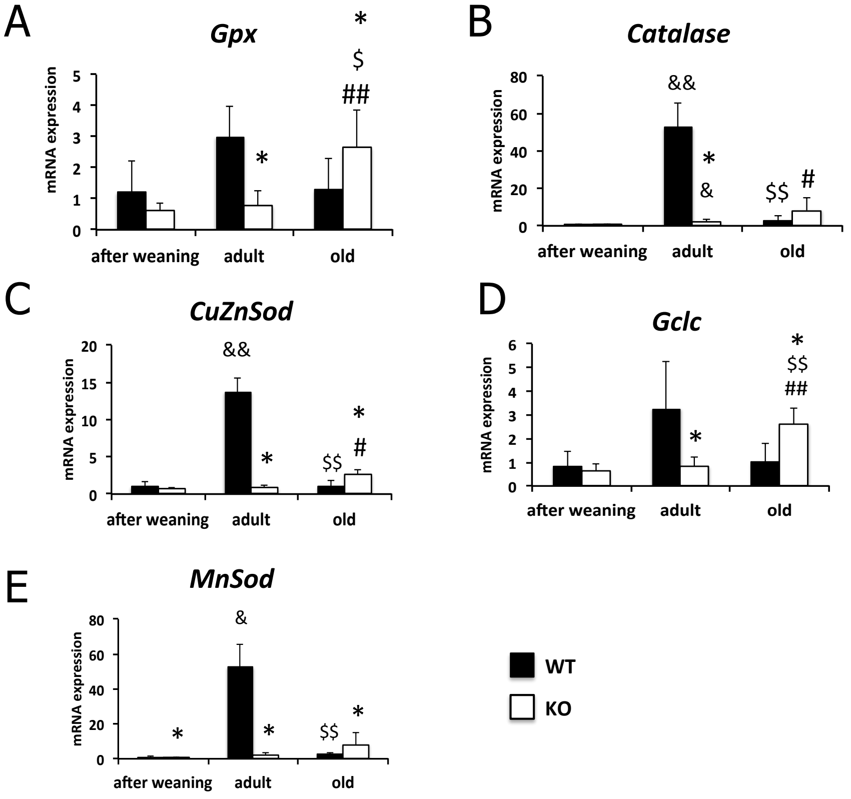

Figure 34. Real-time PCR analysis of antioxidant enzymes. The expressions of mRNA for glutathione peroxidase (*Gpx*) (A), *Catalase* (B), copper zinc superoxide dismutase (*Cu Zn Sod)* (C), glutamate cysteine ligase catalytic subunit (*Gclc*) (D) and manganese superoxide dismutase (*Mn Sod*) (E). Data (mean and SD) are shown as fold increase in mRNA level compared to the control and were normalized by TATA-binding protein mRNA. *P < 0,05 WT *versus* KO, **P < 0,01 WT *versus* KO, &P < 0,05 adult *versus* after weaning, &&P < 0,01 adult *versus* after weaning, $\$P$ < 0,05 old *versus* adult, $\$\$P$ < 0,01 old *versus* adult, #P < 0,05 old *versus* after weaning ##P < 0,01 old *versus* after weaning. n(after weaning WT)=8, n(after weaning KO)=7, n(adult WT)=8, n(adult KO)=8, n(old WT)=6, n(old KO)=4.

1.13. NF-κB nuclear traslocation and activation correlated with the REDOX oscilations

Our last results about the role of p38α in the regulation of the antioxidant defense with age directed us to evaluate the activity of some transcription factors, such as PGC-1α, Nrf-2 and p65, which could regulate liver antioxidant defense, in the groups where more differences were observed. In adult livers, p65 subunit of NF-κB was significantly phosphorylated in nuclear extracts from wilt type livers. Neither PGC-1α nor Nrf-2 seemed to be involved in this regulation (Figure 35).

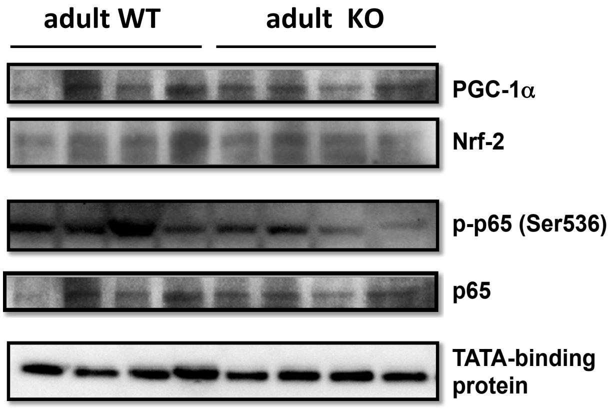

Figure 35. Transcription factors mediating antioxidant defense in adult liver. Representative Western blot images for PGC-1α, Nrf-2, p-p65 and p65 in wild type and p38α knock out adult liver nuclear extracts. TATA-binding protein was used as a loading control. n (adult WT)=8, n(adult KO)=8.

In old livers, p38α knock out mice exhibited higher phosphorylation and traslocation of p65 to the nucleus. In addition, Nrf-2 decreased its nuclear levels in old p38α knock out mice (Figure 36).

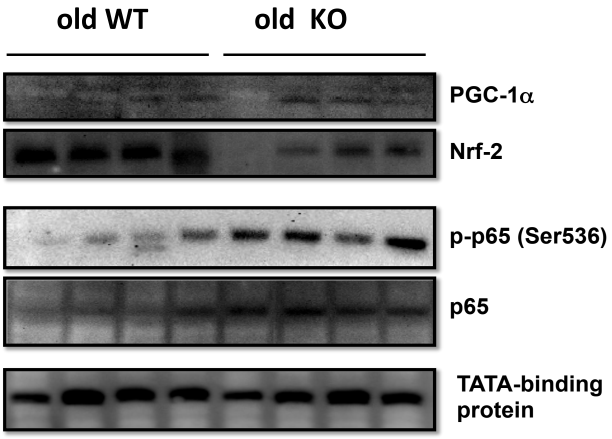
old WT
old KO
PGC-1α
Nrf-2
p-p65 (Ser536)
p65
TATA-binding protein

Figure 36. Transcription factors mediating antioxidant defense in old liver. Representative Western blot images for PGC1α, Nrf-2, p-p65 and p65 in wild type and p38α knock out old liver nuclear extracts. TATA-binding protein was used as a loading control. n(old WT)=6, n(old KO)=4.

2. p38α in hepatocyte proliferation after partial hepatectomy

The next step in the characterization of the role of p38α in hepatocyte cytokinesis was liver regeneration. Therefore, we studied the consequences of the deletion of p38α in an acute model of liver proliferative response: after 70% resection of liver mass.

2.1. p38α deficiency reduced liver mass recovery after partial hepatectomy

Liver mass ratio after partial hepatectomy was calculated in order to assess the effects of p38α on liver regeneration. p38α deletion significantly reduced liver growth at 72h after partial hepatectomy. Nevertheless, it seemed that deletion of p38α during the first hours after hepactectomy did not completely block the priming and initial proliferation of hepatocytes (Figure 37).

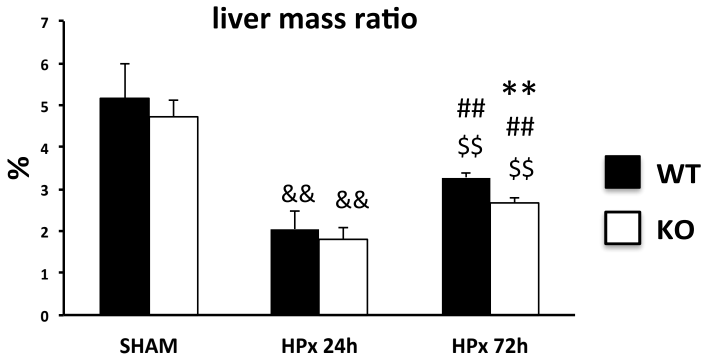

Figure 37. Liver mass ratio (%) in SHAM and after 24 and 72h of partial hepatectomy. Data are shown as mean and SD. $^{**}P < 0{,}01$ WT *versus* KO, &&$P < 0{,}01$ HPx 24h *versus* SHAM, $$$P < 0{,}01$ HPx 72h *versus* HPx 24h, ##$P < 0{,}01$ HPx 24h *versus* SHAM. n(WT SHAM)=6, n(KO SHAM)=6, n(WT HPx 24h)=4, n(KO HPx 24h)=4, n(WT HPx 72h)=6, n(KO HPx 72h)=6.

2.2. Binucleation after partial hepatectomy

Following the assessment of liver mass ratio, we calculated the binucleation rate by inmunohystochemistry (β catenin and DAPI staining), in order to check if cytokinesis impairment was behind this proliferation pattern after 72 hours of partial hepatectomy.

Binucleation rate in hepatocytes was reduced at 72h after partial hepatectomy in both groups, but p38α knock out hepatectomized livers had higher rates of binucleation when compared with hepatectomized wild type livers (Figure 38). Interstingly, p38α knock out hepatocytes were able to perform ploidy reversal as wild type mice did [Duncan A.W. *et al.,* 2000] converting themselves into less complex mononuclear shapes.

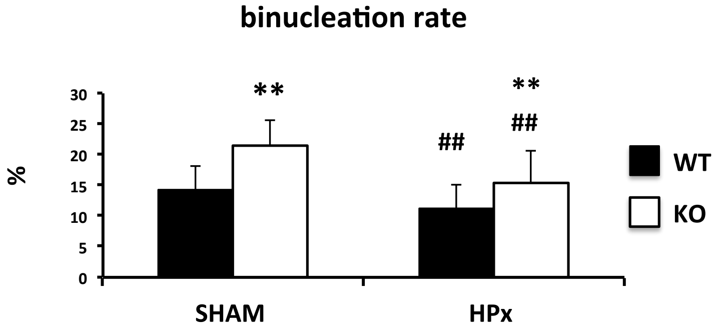

Figure 38. Binucleation rate (%) in SHAM and after 72h of partial hepatectomy. Data are shown as mean and SD. *$P < 0,05$ WT *versus* KO. **$P < 0,01$ WT *versus* KO, ##$P < 0,01$ HPx 24h *versus* SHAM. n(WT SHAM)=6, n(KO SHAM)=6, n(WT HPx 72h)= 6, n(KO HPx 72h)=6.

2.3. Effect of p38α deletion on cell cycle transitions after partial hepatectomy

To obtain a broad overview of the role of p38α on cell cycle regulation under proliferative conditions, we determined the mRNA expression and protein levels of cyclins and other proteins involved in cell cycle checkpoints

G1/S transition

The G_1/S checkpoint was markedly altered by deletion of p38α. A significant increase in mRNA levels of *CyclinD1* was found in hepatectomized p38α knock out livers after 72 hours when compared with livers from wild type mice. In addition, knock out mice also exhibited higher *CyclinD1* expression under basal conditions (Figure 39).

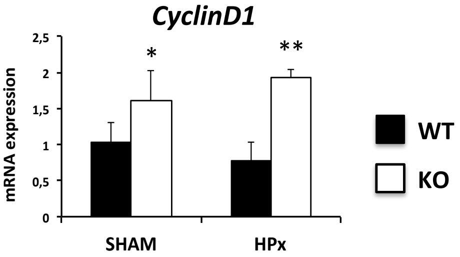

Figure 39. Real-time PCR analysis of the expressions of mRNA for *CyclinD1* after 72 hours partial hepactectomy. Data (mean and SD) are shown as fold increase in mRNA level compared to the control and were normalized by TATA-binding protein mRNA. **P* < 0,05 WT versus KO. ***P* < 0,01 WT *versus* KO. n(WT SHAM)=6, n(KO SHAM)=6, n(WT HPx 72h)= 6, n(KO HPx 72h)=6.

However, protein levels of cyclin D1 were also assessed by Western blot, and nuclear extracts did not show any differences in cyclin D1 (Figure 40).

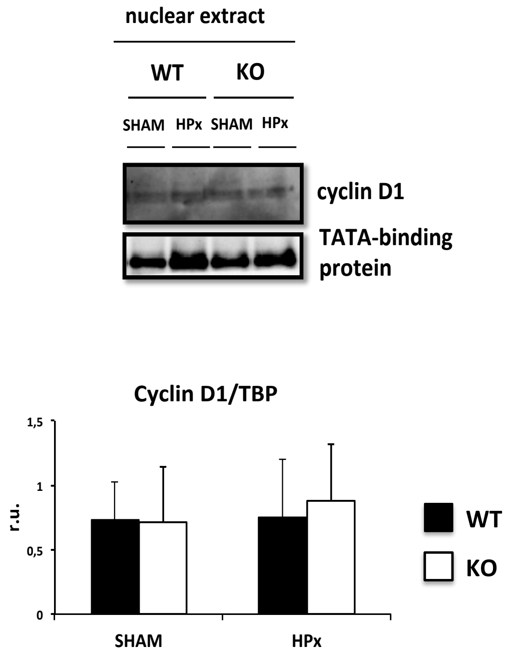

Figure 40. Cyclin D1 protein levels after partial hepatectomy. Representative Western blot for cyclin D1 in SHAM and after 72h of partial hepatectomy in wild type and p38α knock out liver nuclear extracts. Western blot densitometry used TATA-binding protein as a loading control. Data are shown as mean and SD. n(WT SHAM)=6, n(KO SHAM)=6, n(WT HPx 72h)=6, n(KO HPx 72h)=6.

S phase progression

Furthermore, a significant rise in mRNA levels of *CyclinA1* was observed in hepatectomized p38α knock out livers after 72 hours. This increase was also assessed in p38α deficiency under basal conditions (Figure 41).

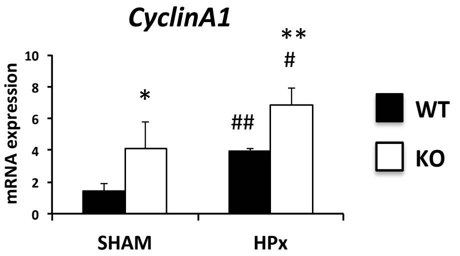

Figure 41. Real-time PCR analysis of the expressions of mRNA for *CyclinA1* after 72 hours partial hepactectomy. Data (mean and SD) are shown as fold increase in mRNA level compared to the control and were normalized by TATA-binding protein mRNA. *$P < 0,05$ WT *versus* KO. **$P < 0,01$ WT *versus* KO. n(WT SHAM)=6, n(KO SHAM)=6, n(WT HPx 72h)=6, n(KO HPx 72h)=6.

G_2/M transition

The absence of p38α also disturbed the regulation of the G_2/M transition. A significant increase in mRNA levels of *Cdc25* and *CyclinB2* was found in p38α knock out mice after 72 hours hepatectomy. p38α knock out mice also showed higher *CyclinB2* expression under basal conditions. No differences were observed in *CyclinB1* mRNA expression when comparing between wild type and p38α knock out (Figure 42).

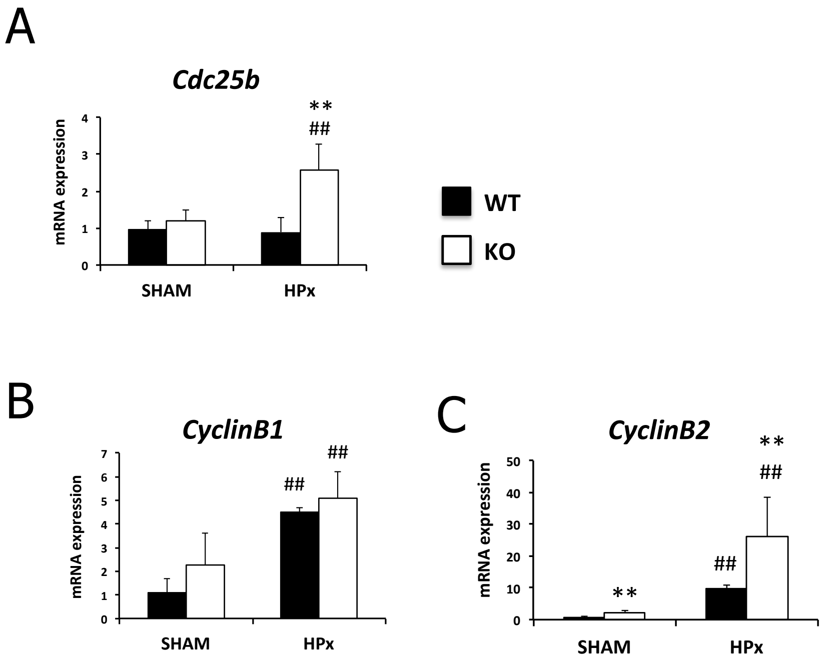

Figure 42. Real-time PCR analysis of the expressions of mRNA for G_2/M regulators after 72 hours partial hepatectomy. *Cdc25b* (A), *CyclinB1* (B) and *CyclinB2* (C) mRNA expression are represented as mean and SD and shown as fold increase in mRNA level compared to the control. mRNA levels were normalized by TATA-binding protein mRNA. ***P* < 0,01 WT *versus* KO, #*P* < 0,05 HPx *versus* SHAM, ##*P* < 0,01 HPx *versus* SHAM. (WT SHAM)=6, n(KO SHAM)=6, n(WT HPx 72h)=6, n(KO HPx 72h)=6.

The enhancement of cyclin B1 nuclear protein levels in p38α knock out mice was confirmed by Western blot (Figure 43).

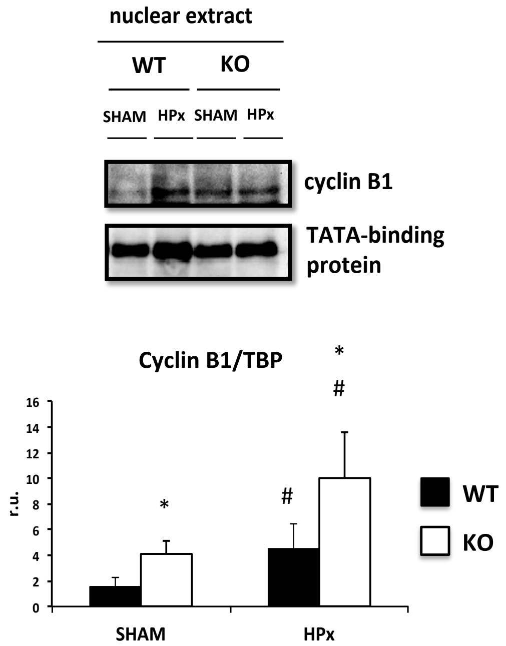

Figure 43. Cyclin B1 protein levels after partial hepatectomy. Representative Western blot for cyclin B1 in SHAM and after 72h of partial hepatectomy wild type and p38α knock out liver nuclear extracts. TATA-binding protein was used as a loading control. Western blot densitometry used TATA-binding protein as a loading control. Data are shown as mean and SD. *P < 0,05 WT *versus* KO, #P < 0,05 HPx *versus* SHAM. n(WT SHAM)=6, n(KO SHAM)=6, n(WT HPx 72h)=6, n(KO HPx 72h)=6.

Mitotic progression

The mitotic stage was significantly affected by the absence of p38α. A rise in mRNA levels of *CyclinF* was confirmed in p38α knock out mice after 72 hours hepatectomy and also in basal conditions (Figure 44).

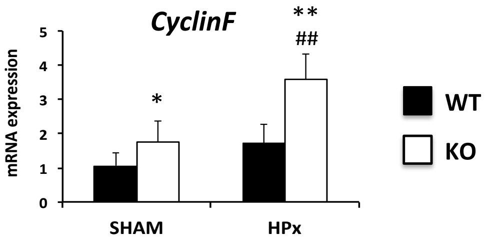

Figure 44. Real-time PCR analysis of the expressions of mRNA for *CyclinF* 72 hours after partial hepatectomy. Data (mean and SD) are shown as fold increase in mRNA level compared to the control and were normalized by TATA-binding protein mRNA. $^{**}P < 0{,}01$ WT *versus* KO, $\#P < 0{,}05$ HPx *versus* SHAM, $\#\#P < 0{,}01$ HPx *versus* SHAM. n(WT SHAM)=6, n(KO SHAM)=6, n(WT HPx 72h)= 6, n(KO HPx 72h)=6.

Finally, the ratio p-H3/PCNA was also calculated. This index is called mitotic index and allows determining which cells are going through mitosis (they are positive for phosphorylated histone 3 on Ser 10) from the ones that are proliferating (positive for PCNA) [Cha H. *et al.,* 2007].

The mitotic index was initially determined by Western blot (Figure 45). Nuclear extracts from hepatectomized livers showed high variability, and thus no significant changes were assesed. Moreover, p38α knock out mice expressed higher p21, a mito-inhibitor protein in hepatocytes that blocks hepatocyte mitosis preventing premature hepatocyte re-entry into cell cycling [Clouston A.D. *et al.,* 2005].

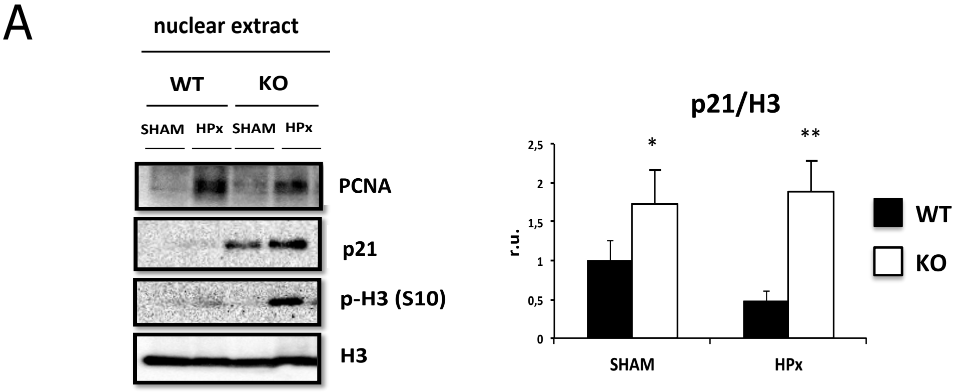

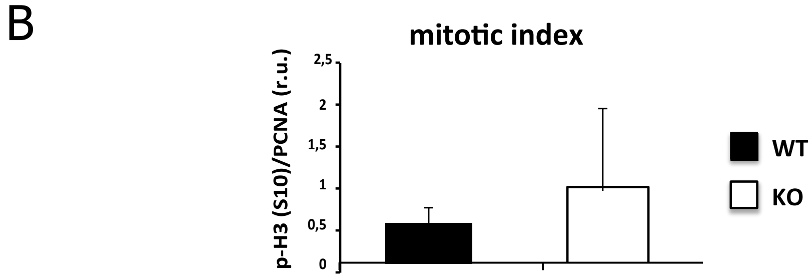

Figure 45. Mitotic index quantification after hepatectomy by Western blot. Representative western blot and densitometry for PCNA, p21, p-H3 and H3 in nuclear extracts of SHAM and 72 hours after hepatectomy. H3 was used as a loading control. **P* < 0,05 WT versus KO. ***P* < 0,01 WT versus KO (A). Mitotic index calculated from Western blot (B). n(WT SHAM)=6, n(KO SHAM)=6, n(WT HPX 72h)=6, n(KO HPx 72h)=6.=6.

Then, we proceed with mitotic index analysis by inmunohystochemistry: p38α knock out mice exhibited higher p-H3/PCNA ratio when they underwent partial hepatectomy (Figure 46).

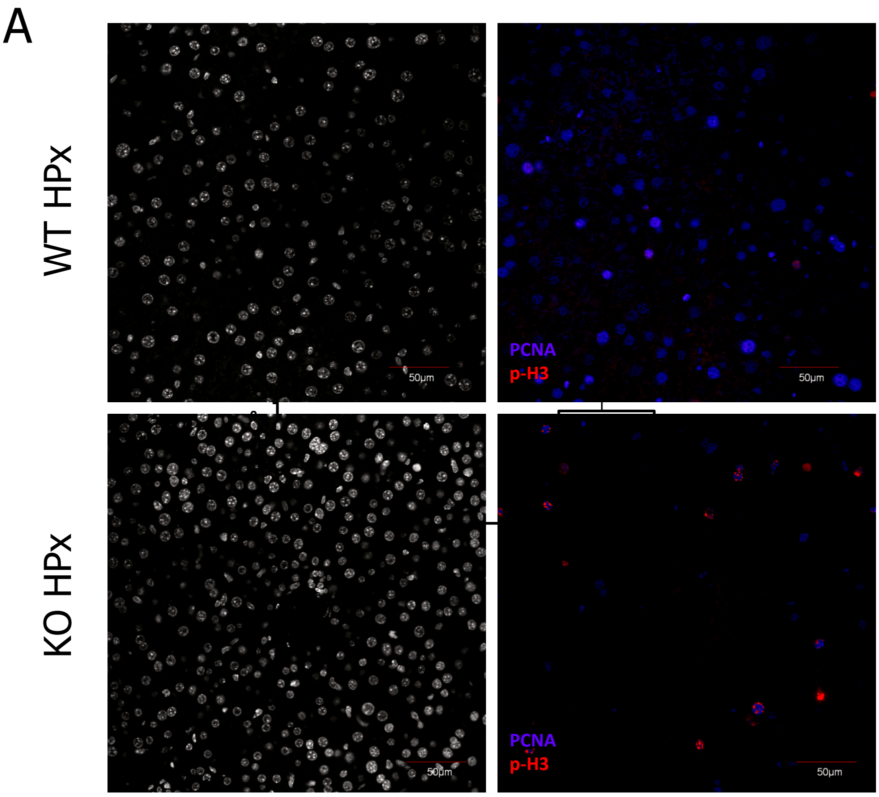

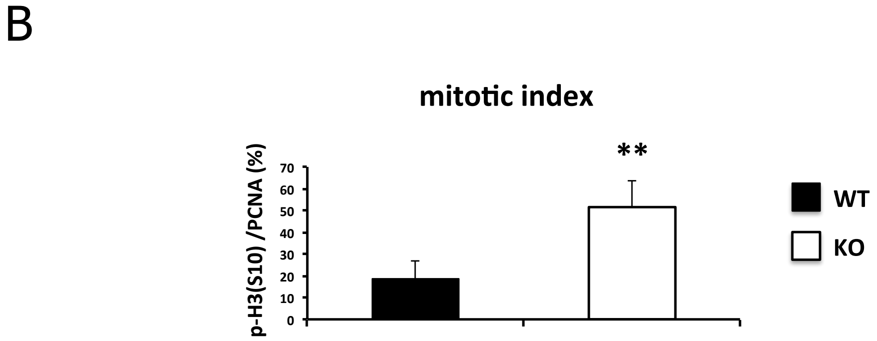

Figure 46. Mitotic index quantification after hepatectomy by immunohistochemistry. Representative immunohistochemistry images of wild type and p38α knock out liver sections after partial hepatectomy. Red, phosphorylated histone 3; blue, PCNA; white, DAPI. A minimum of four experiments were performed for each groups of animals. Scale bars = 50 µm (A). Mitotic index representation as the p-H3/PCNA ratio expressed in percentage of positive cells (B). Data are shown as mean and SD. $^{**}P < 0{,}01$ WT versus KO. n(WT HPx 72h)=6, n(KO HPx 72h)=6.

2.4. p38α downstream pathways involved in cytokinesis completion

Since p38α knock out liver still exhibited higher binucleation rates when compared with wild type after partial hepactectomy, we investigated potential actin abnormalities. The MK2 pathway and HSP27 activation were analysed by Western blot (Figure 47). After 72 hours partial hepatectomy, both mice showed phosphorylation of HSP27. However, activation of HSP27 was not affected by MK2 phosphorylation on Thr334.

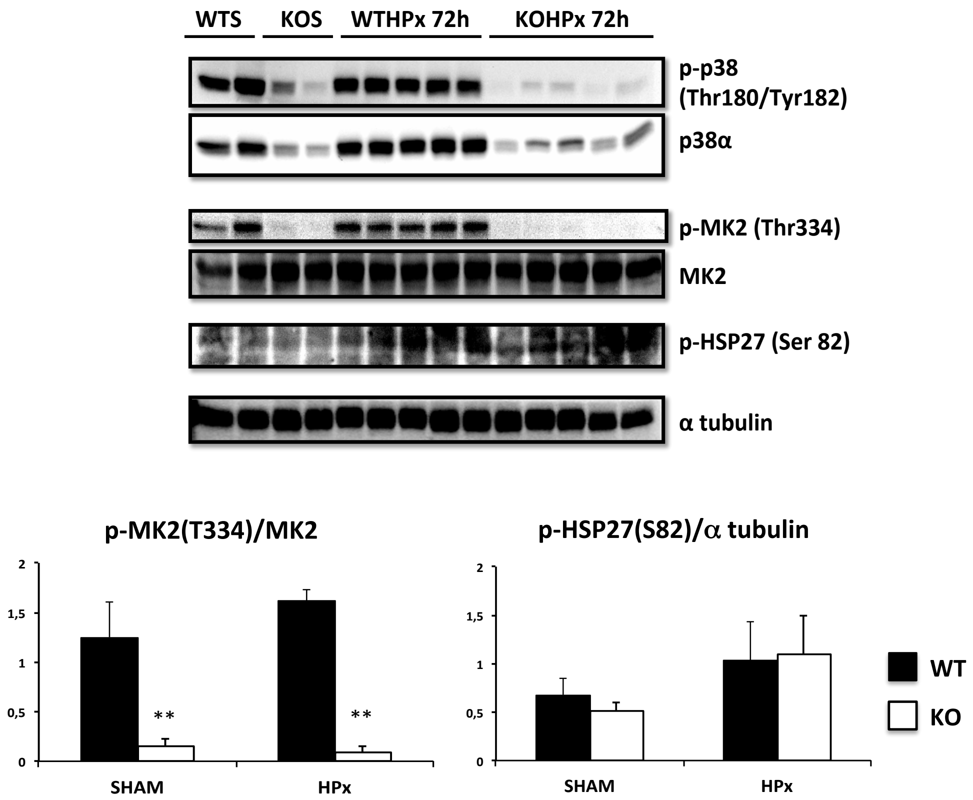

Figure 47. p38α downstream pathway after partial hepatectomy: MK2 and HSP27. Representative Western blot for p-p38, p38α, p-MK2, MK2 and p-HSP27 in SHAM and after 72h of partial hepatectomy wild type and p38α knock out total liver homogenates. Western blot densitometry used α tubulin as a loading control. Data are shown as mean and SD. $^{**}P < 0{,}01$ WT *versus* KO. n(WT SHAM)=6, n(KO SHAM)=6, n(WT HPx 72h)=6, n(KO HPx 72h)=6.

Nevertheless, MNK1 phosphorylation did significantly decreased in p38α knock out mice (Figure 48).

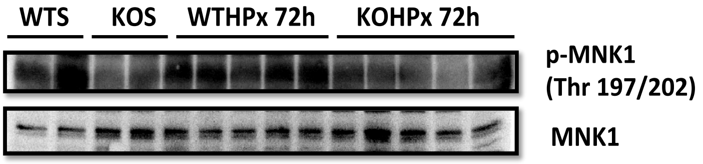

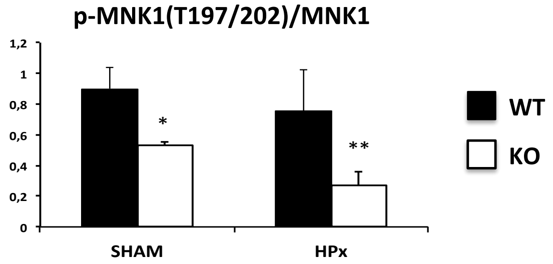

Figure 48. Phosphorylation of MNK1 after partial hepatectomy. Representative Western blot for p-MNK1 and MNK1 in SHAM and after 72h of partial hepatectomy wild type and p38α knock out total liver homogenates. α tubulin was used as a loading control in Western blot densitometry. Data are shown as mean and SD. *P < 0,05 WT *versus* KO. **P < 0,01 WT *versus* KO. n(WT SHAM)=6, n(KO SHAM)=6, n(WT HPx 72h)=6, n(KO HPx 72h)=6.

2.5. Consequences of the deletion of p38α on the REDOX balance after partial hepatectomy

Lastly, and following the same analysis as in p38α regulation of the REDOX status in aging livers, we quantified the GSSG/GSH ratio in order to assess the consequences of p38α deficiency after 72h of partial hepatectomy. Hepatectomy acted as a pro-oxidant stimuli and p38α knock out mice suffer from higher levels of oxidative stress (Figure 49).

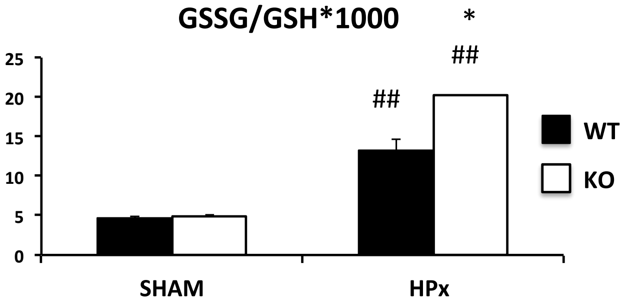

Figure 49. REDOX status variations 72 hours after partial hepatectomy. GSSG/GSH ratio measurement in wild type and p38α knock out mouse liver tissue after partial hepatectomy. Data are shown as mean and SD. *P < 0,05 WT *versus* KO, ##P < 0,05 HPx *versus* SHAM. n(WT SHAM)=6, n(KO SHAM)=6, n(WT HPx 72h)=6, n(KO HPx 72h)=6.

3. p38α in hepatocyte proliferation in liver disease induced by chronic cholestasis

We had already found that p38α knock out hepatocytes had difficulties to complete mitosis but we wondered if p38α would affect the progression of biliary cirrhosis induced by BDL. To this end, we proceed by performing BDL to wild type and p38α knock out mice.

3.1. Liver damage in wild type and p38α knock out mice after BDL

Serum markers of cholestasis were measured in order to confirm the proper induction of liver cholestasis. Hepatocellular injury was also assessed. No significant differences were found between wild type BDL and p38α knock out BDL (Table 8).

Table 8. Serum biochemistry in SHAM and BDL mice.

	Total bilirubin (mg/dL)	ALT (U/L)	γ-GT (U/L)
WT SHAM	0,3±0,1; n=8	27,5±2,4; n=8	5,8±1,5; n=8
KO SHAM	0,2± 0,0; n=8	35,3±8,8; n=8	7,0±0,8; n=8
WT BDL 12 days	21,2±4,8; n=4	183,3±23,0; n=4	17,8±3,6; n=4
KO BDL 12 days	30,7±1,0; n=4	189,0±29,0; n=4	16,5±3,7; n=4
WT BDL 28 days	24,0±1,9; n=6	179,3± 39,9; n=6	18,75±1,7; n=6
WT BDL 28 days	26,5±3,0; n=6	171,8±22,3; n=6	19,0±2,9; n=6

ALT, alanine amino transferase; γ–GT, gamma glutamil transpeptidase.

3.2. p38α knock out BDL mice exhibited reduced survival after BDL

We expected that p38α would have an effect on cell cycle and this deficiency may trigger a decrease in the recovery capacity of the liver in severe inflammatory conditions. The survival curve showed that p38α was necessary to deal with the cholestatic disorder better (Figure 50). Thus, we kept on searching for the potential pathways that p38α activated in order to promote survival after severe liver injury.

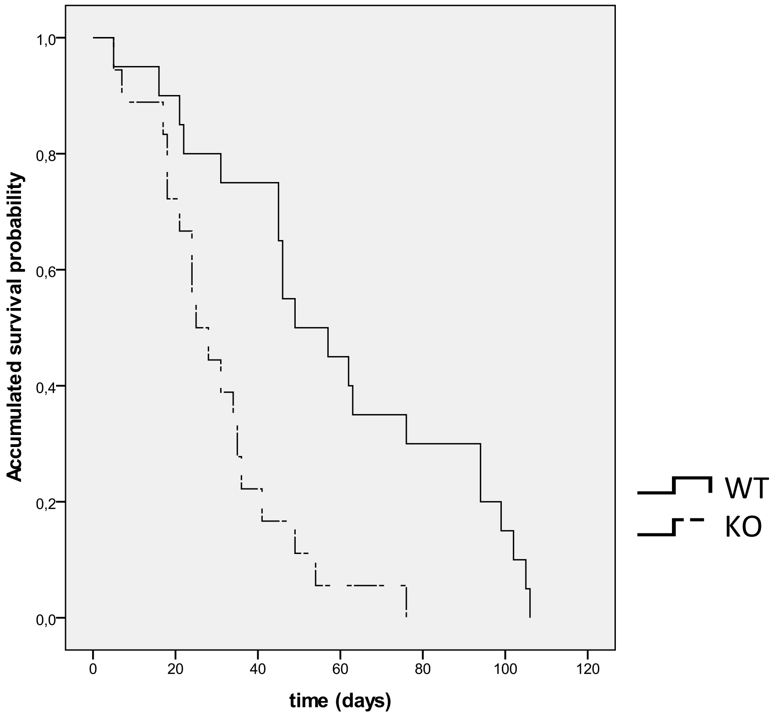

Figure 50. Survival curve after cholestasis induction in wild type and p38α knock out mice. Both groups of mice, WT (n=20) and p38α KO (n=18), underwent BDL. Statistical differences in animal survival were found between groups following a Kaplan-Meier test. *P* < 0,001 was obtained using the score test of the Mantel-Cox proportional hazards model for grouped data.

3.3. p38α knock out BDL mice did not exhibit reduced inflammatory response

As p38α is known to have an important role in the inflammatory response, we expected to get a less severe proinflammatory profile in p38α knock out BDL mice. In contrast, no significant increase in the inflammatory response was found in p38α knock out BDL livers.

The pro-inflammatory *Il6* and *Tnfα* were analyzed by RT-PCR during BDL progression (Figure 51).

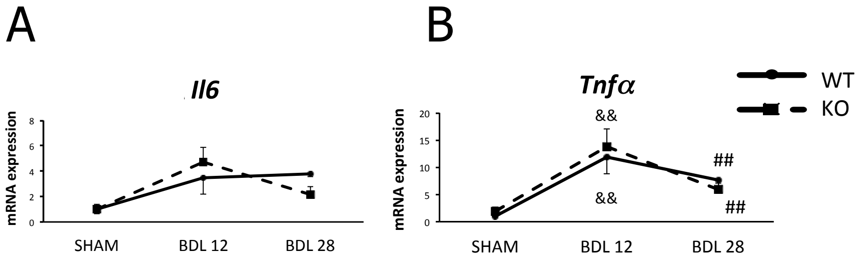

Figure 51. Real-time PCR analysis of the expressions of mRNA for pro-inflammatory cytokines. *Il6* (A) and *Tnfα* (B) mRNA levels after BDL. Data (mean and SD) are shown as fold increase in mRNA level compared to the control and were normalized by TATA-binding protein mRNA. ##*P* < 0,01 BDL 28 days *versus* SHAM, &&*P* < 0,01 BDL 12 days *versus* SHAM. n(WTS)=8, n(KOS)=8, n(WTB 12 days)=4, n(WTB 28 days)=6, (KOB 12 days)=4, n(KOB 28 days)=6.

In parallel, the anti-inflammatory *Il10,* was measured by RT-PCR. A marked increase in *Il10* was found in p38α knock out mice after 12 days of BDL (Figure 52). However, this difference was lost 28 days after BDL.

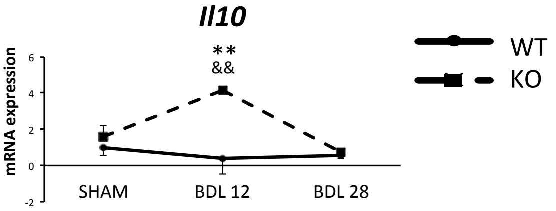

Figure 52. Real-time PCR analysis of the expressions of mRNA for *Il10* after BDL. Data (mean and SD) are shown as fold increase in mRNA level compared to the control and were normalized by TATA-binding protein mRNA. ***P* < 0,01 WT *versus* KO, &&*P* < 0,01 BDL 12 days *versus* SHAM. n(WTS) =8, n(KOS)=8, n(WTB 12 days)=4, n(WTB 28 days)= 6, (KOB 12 days)=4, n(KOB 28 days)=6.

Histological analysis was performed after BDL ligation by haematoxylin eosin staining of liver sections. No differences were found in the inflammatory infiltration (Figure 53).

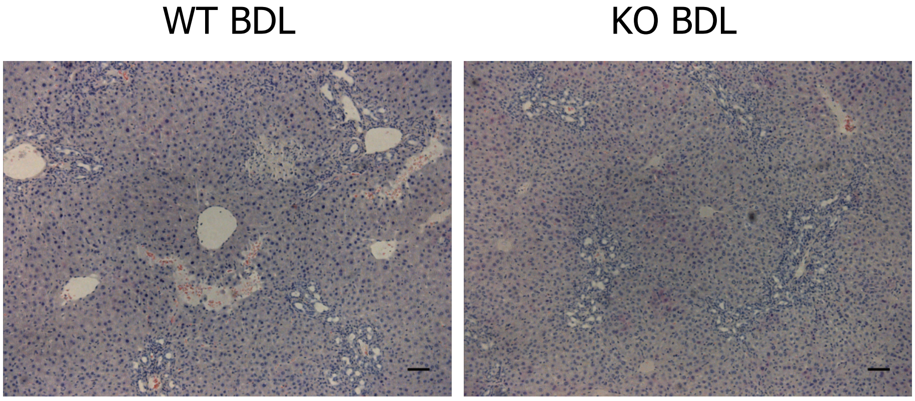

Figure 53. Representative liver sections of haematoxylin and eosin staining in BDL mice, after 28 days BDL. A minimum of 4 experiments were performed for each group of animals. Scale bars=100 µm. n(WTB 28 days)=6, n(KOB 28 days)=6.

3.4. p38α knock out BDL mice developed the same degree of profibrotic response as wild type BDL

Quantitative RT-PCR was also used to determine the time course of two markers of fibrosis: *Colagen1* and *Timp1*. No differences were found in the mRNA expression of both fibrosis markers (Figure 54).

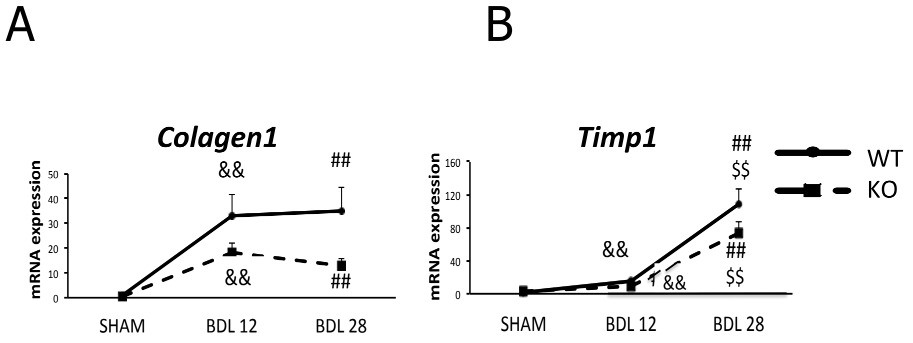

Figure 54. Real-time PCR analysis of the expressions of mRNA for pro-fibrotic factors. *Colagen1* (A) and *Timp1* (B) in SHAM and BDL wild type and p38α knock out mouse liver. Data (mean and SD) are shown as fold increase in mRNA level compared to the control and were normalized by TATA-binding protein mRNA. ##*P* < 0,01 BDL 28 days *versus* SHAM, $$*P* < 0,01 BDL 28 days *versus* BDL 12 days, &&*P* < 0,01 BDL 12 days *versus* SHAM. n(WTS)=8, n(KOS)=8, n(WTB 12 days)=4, n(WTB 28 days)=6, (KOB 12 days)=4, n(KOB 28 days)=6.

Sirius Red staining for fibrosis completed the study with no differences between groups (Figure 55).

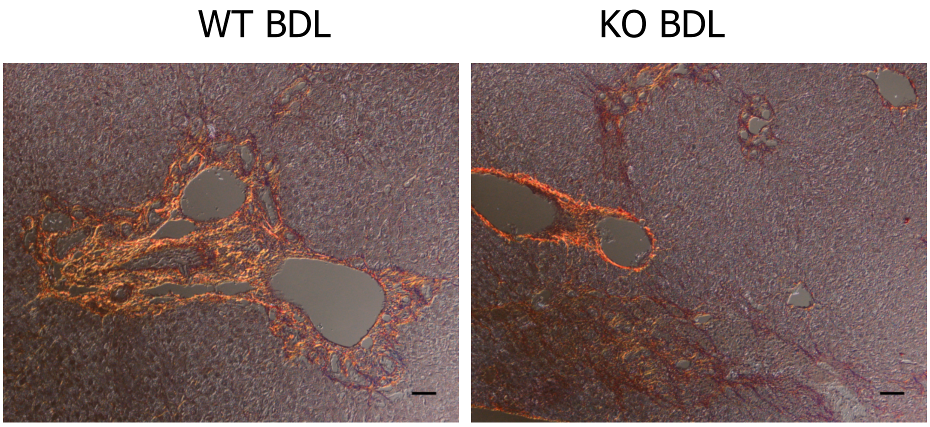

Figure 55. Representative liver sections of Sirius Red staining in BDL mice, after 28 days BDL. A minimum of 4 experiments were performed for each groups of animals. Scale bars=100 µm. n(WTB 28 days)=6, n(KOB 28 days)=6.

3.5. p38α ablation did not cause an increase in apoptosis after BDL

Characterization of our model included a study of apoptosis. As we were interested in determining liver mass evolution and cell death, apoptosis could be a major factor in this regard. To begin with, we performed immunoblotting for cleavage of caspase 3 (Figure 56). No differences between wild type and p38α knock out were found in the cleavage of caspase 3.

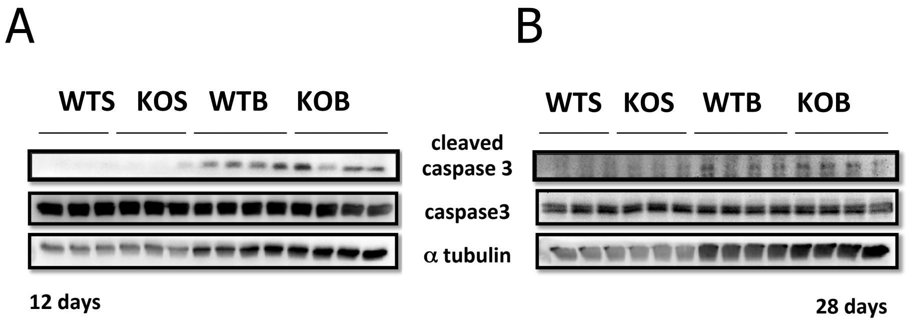

Figure 56. Cleavage of caspase 3 after BDL. Representative Western blot for cleaved caspase3 and caspase 3 in SHAM, 12 days BDL(A) and 28 days BDL (B) wild type and p38α knock out total liver homogenates. α tubulin was used as a loading control. n(WTS)=8, n(KOS) =8, n(WTB 12 days)=4, n(WTB 28 days)=6, (KOB 12 days) =4, n(KOB 28 days)=6.

Secondly, mRNA expression of other proteins involved in apoptosis was quantified during BDL progression in wild type and p38α knock out mice. No significant differences in *Bcl2* and *Birc2* expression between genotypes were found (Figure 57).

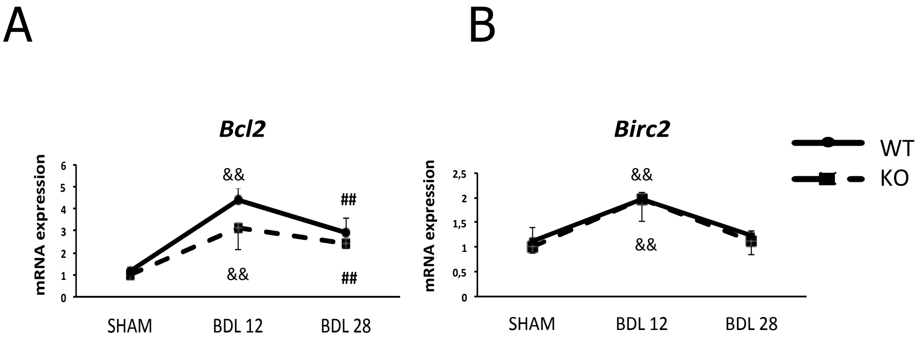

Figure 57. Real-time PCR analysis of the expressions of mRNA of pro-apoptotic factors. *Bcl2* (A) and *Birc2* (B) in SHAM and BDL wild type and p38α knock out mouse liver. Data (mean and SD) are shown as fold increase in mRNA level compared to the control and were normalized by TATA-binding protein ##*P* < 0,01 BDL 28 days *versus* SHAM, $$*P* < 0,01 BDL 28 days *versus* BDL 12 days. n(WTS)=8, n(KOS)=8, n(WTB 12 days)=4, n(WTB 28 days)=6, (KOB 12 days =4, n(KOB 28 days)=6.

3.6. p38α downstream pathways after BDL. Role of Akt

In order to study the role of p38α in BDL survival, we analysed by Western blot levels steady states of proteins downstream of p38α involved in prosurvival pathways. We started by determining proteins levels and activation of p38α downstream kinases, such as MK2. Activation of MK2 by phosphorylation on Thr334 was only found in wild type livers (Figure 58).

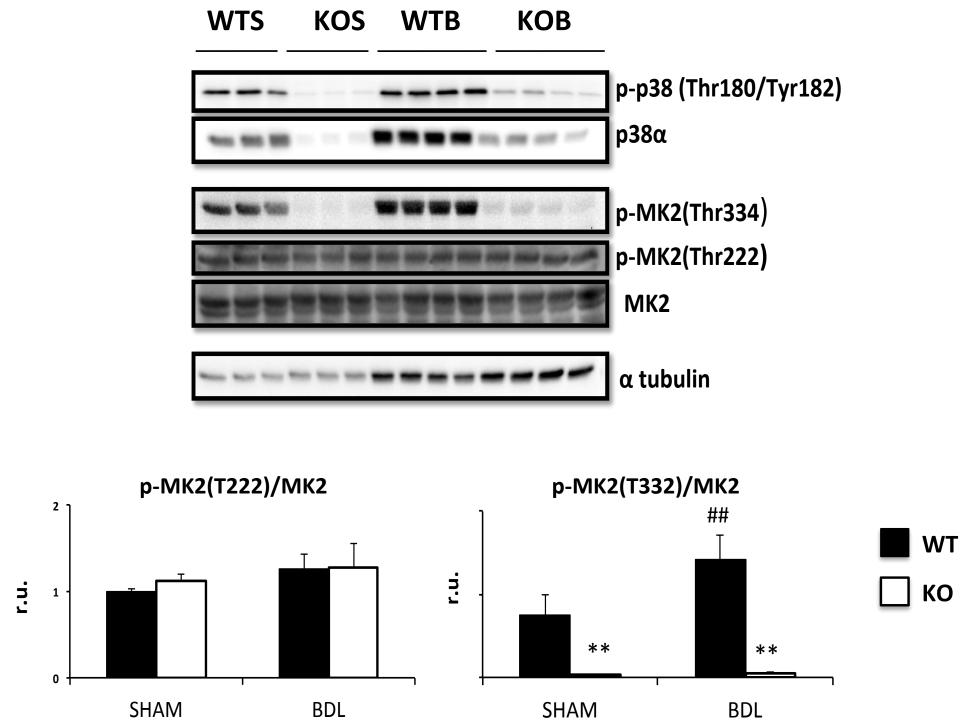

Figure 58. p38α downstream pathway after BDL: MK2. Representative Western blot for p-p38, p38α, p-MK2, and MK2 in SHAM and after 28 days of BDL wild type and p38α knock out total liver homogenates. α tubulin was used as a loading control in Western blot densitometry. ** P < 0,01 WT *versus* KO, ## P < 0,01 BDL 28 days *versus* SHAM. n(WTS)=8, n(KOS)=8, n(WTB 28 days) =6, n(KOB 28 days)=6.

Secondly, we studied the p38α-mediated phosphorylation of AKT and its downstream targets mTOR, GSK3β and β catenin (Figure 59 and 60). We confirmed that wild type BDL mice activated the AKT pathway after 28 days of cholestasis induction.

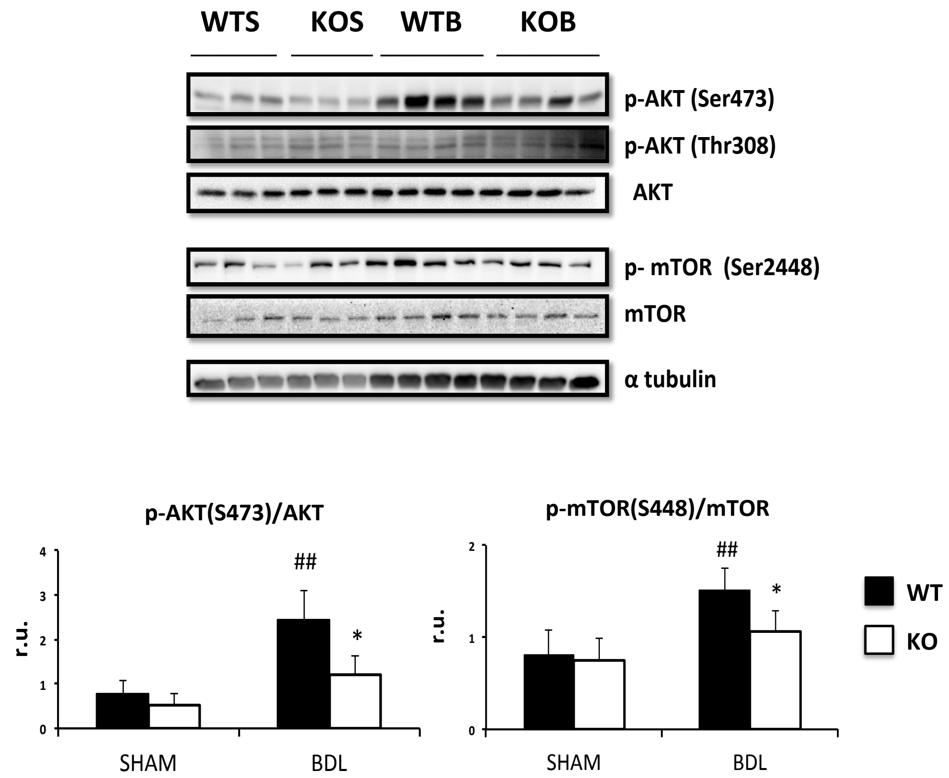

Figure 59. p38α downstream pathway after BDL: AKT and mTOR. Representative Western blot for p-AKT, AKT, p-mTOR and mTOR in SHAM and after 28 days of BDL wild type and p38α knock out total liver homogenates. α tubulin was used in Western blot densitometry as a loading control. Data are shown as mean and SD. *P < 0,05 WT *versus* KO, ##P < 0,01 BDL 28 days *versus* SHAM. n(WTS)=8, n(KOS)=8, n(WTB 28 days)=6, n(KOB 28 days)=6.

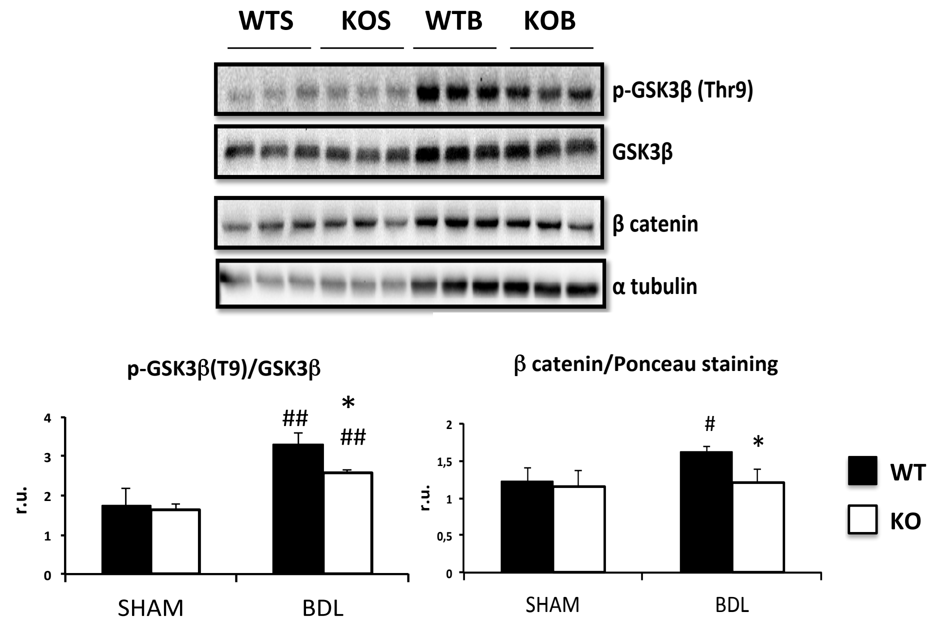

Figure 60. p38α downstream pathway after BDL: GSK3β and βcatenin. Representative western blot for p-GSK3β, GSK3β and β catenin in SHAM and after 28 days of BDL wild type and p38α knock out total liver homogenates. α tubulin and Ponceau staining were used as a loading control in Western blot densitometry. Data are shown as mean and SD. *$P < 0,05$ WT *versus* KO, #$P < 0,05$ BDL 28 days *versus* SHAM, ##$P < 0,01$ BDL 28 days *versus* SHAM. n(WTS)=8, n(KOS)=8, n(WTB 28 days)=6, n(KOB 28 days)=6.

3.7. HSP27 phosphorylation after BDL

Phosphorylation levels of HSP27 in total nuclear extracts were measured by Western blot. Significant dephosphorylation of HSP27 was found in p38α knock out mice (Figure 61).

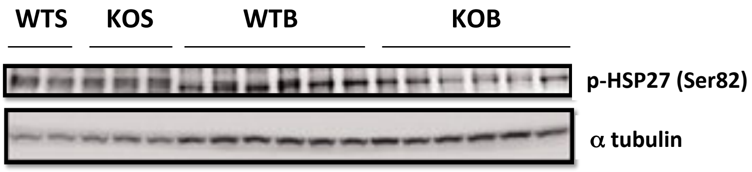

Figure 61. HSP27 phosphorylation after BDL. Representative Western blot for HSP27 in liver extracts of SHAM and BDL wild type and p38α knock out livers. α tubulin was used as a loading control. n(WTS)=8, n(KOS)=8, n(WTB 28 days)=6, n(KOB 28 days)=6.

3.8. p38α deficiency in liver abrogates compensatory hepatomegaly after BDL

p38α knock out livers could not compensate the liver loss of function after severe injury. Indeed, they got a significant liver weight reduction of 20% comparing to the initial mass by day 28, when they were sacrificed (Figure 62).

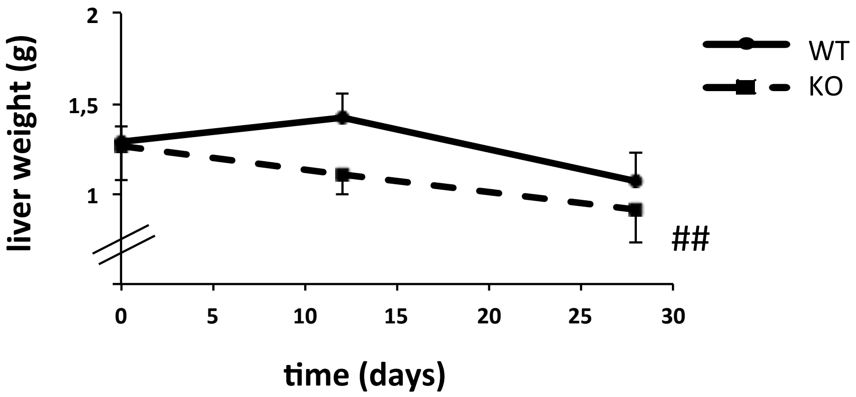

Figure 62. Evolution of liver weight after 28 days of cholestasis induction. Data are shown as mean and SD. ##*P* < 0,01 BDL 28 days *versus* SHAM. n(WTS)=8, n(KOS)=8, n(WTB 12 days)=4, n(WTB 28 days)=6, (KOB 12 days)=4, n(KOB 28 days)=6.

In addition, liver mass ratio was also calculated at 28 days of BDL. A significant decrease in liver mass ratio was also found in p38α knock out BDL mice (Figure 63).

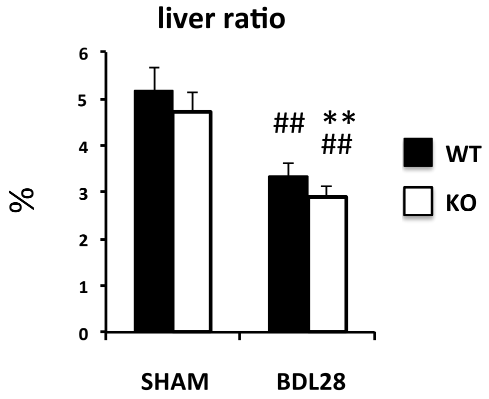

Figure 63. Liver mass ratio after 28 days BDL. Liver mass ratio was calculated in wild type and p38α knock out mice SHAM and after 28 days of BDL. Data are shown as mean and SD. Black, WT; white, KO. **P* < 0,05 WT *versus* KO. ***P* < 0,01 BDL 28 days *versus* SHAM. n(WTS)=8, n(KOS)=8, n(WTB 28 days)=6, n(KOB 28 days)=6.

3.9. Deficiency of p38α in liver induced hepatocyte binucleation that was enhanced after BDL

After finding the loss of compensatory hepatomegaly in p38α knock out mice we suspected that cytokinesis impairment and subsequent binucleation might be the fact that was behind the early death when p38α was absent. Interestingly, p38α knock out mice were not able to reduce the binucleation in their hepatocytes in order to induce compensatory hepatomegaly (Figure 64).

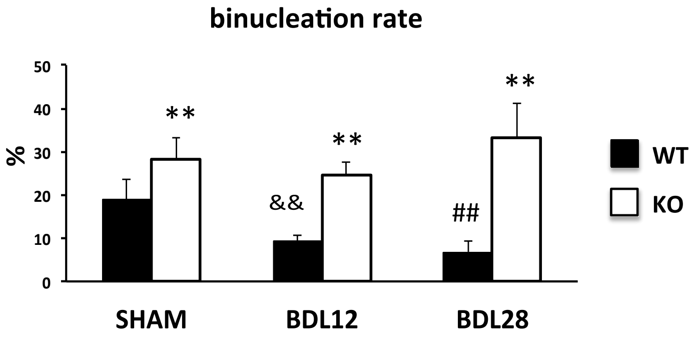

Figure 64. Binucleation rate (%) in SHAM and after 12 and 28 days BDL. Data are shown as mean and SD. ***P* < 0,01 WT *versus* KO, ##*P* < 0,01 BDL 28 days *versus* SHAM, && *P* < 0,01 BDL 12 days *versus* SHAM n(WTS) 8, n(KOS)=8, n(WTB 12 days)=4, n(WTB 28 days) = 6, (KOB 12 days)=4, n(KOB 28 days)=6.

3.10. Increased hepatocyte binucleation rate was associated with restrained cell proliferation after BDL

We determined levels of PCNA -as a general activation of cell cycle entry- and p-H3 -as a marker of mitosis- in liver extracts by Western blot. Although the induction of liver injury by BDL is supposed to be a stimulus for liver regeneration, there was a blockade of proliferation in p38α knock out mice after BDL (as evidenced by decreased PCNA in knock out *versus* wild type). Indeed, less mitotic marker (i.e. p-H3) was found in knock out mice. Then, the p-H3/PCNA ratio, also called mitotic index, was determined (Figure 65).

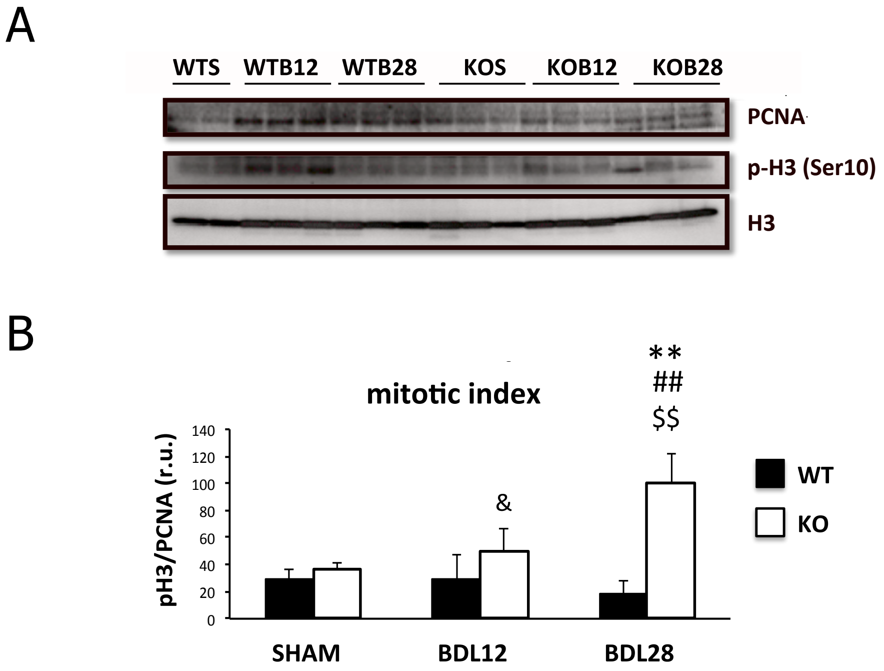

Figure 65. Quantification of mitotic index in BDL mice by Western blot. Representative Western blot for PCNA, p-H3, H3 and PCNA in nuclear extracts of SHAM and BDL wild type and p38α knock out livers (A). H3 was used as a loading control. Mitotic index calculated from inmunoblots (B). Data are shown as mean and SD. **P < 0,01 WT *versus* KO, ##P < 0,01 BDL 28 days *versus* SHAM, &P < 0,05 BDL 12 days *versus* SHAM, $$$P$< 0,01 BDL 28 days *versus* BDL 12 days. n(WTS)=8, n(KOS)8, n(WTB 12 days)=4, n(WTB 28 days)=6, (KOB 12 days)=4, n(KOB 28 days)=6.

If mitosis was impaired, we had to look what happened with the very less nuclei that were proliferating in p38α knock out mice. For this approach, we performed liver immunohistochemistry with ki67, a proliferative marker such as PCNA, which was combined with p-H3 (Figure 66).

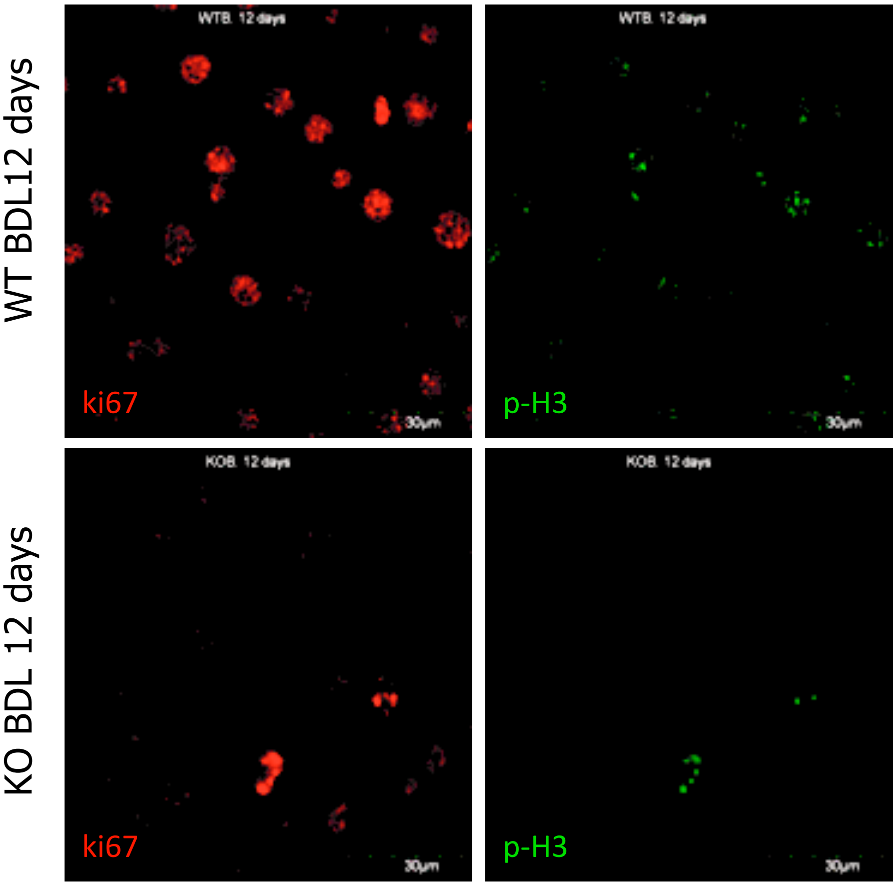
WT BDL12 days
KO BDL 12 days
WTB. 12 days
WTB. 12 days
ki67
p-H3
30µm
30µm
KOB. 12 days
KOB. 12 days
ki67
p-H3
30µm
30µm

Figure 66. Mitotic index in 12 days BDL mice by immunohistochemistry. Representative immunohistochemistry for ki67 (red) and p-H3 (green) in wild type and p38α knock out mice after 12 days of BDL. 4 experiments were performed for each groups of animals. Scale bars=30 µm. n(WTS)=8, n(KOS)=8, n(WTB 12 days)=4, n(KOB 12 days)=4.

After 12 days BDL, the majority of wild type hepatocytes kept on proliferating but only a few knock out hepatocytes did. Interestingly, all the p38α knock out hepatocytes that were positive for ki67 were also positive for phosphorylated histone 3. It seemed that those hepatocytes that were able to enter cell cycle were stacked during mitosis.

3.11. Increased cyclin B1 and p21 in p38α knock out mice

In order to further assess a possible mitotic failure, we quantified the levels of key cell cycle regulators -cyclin D1, cyclin B1 and p21- in these mice. The aim was to clarify the relationship between hepatocyte p38α expression and markers of cell cycle progression after liver injury.

Interestingly, as we already found in old mice, p38α knock out BDL livers had significantly higher expression of cyclin B1 when comparing with SHAM mice (Figure 67). Moreover, p38α knock out mice after 28 days of BDL expressed higher p21, a mito-inhibitor protein in hepatocytes that blocks hepatocyte mitosis preventing premature hepatocyte re-entry into cell cycle.

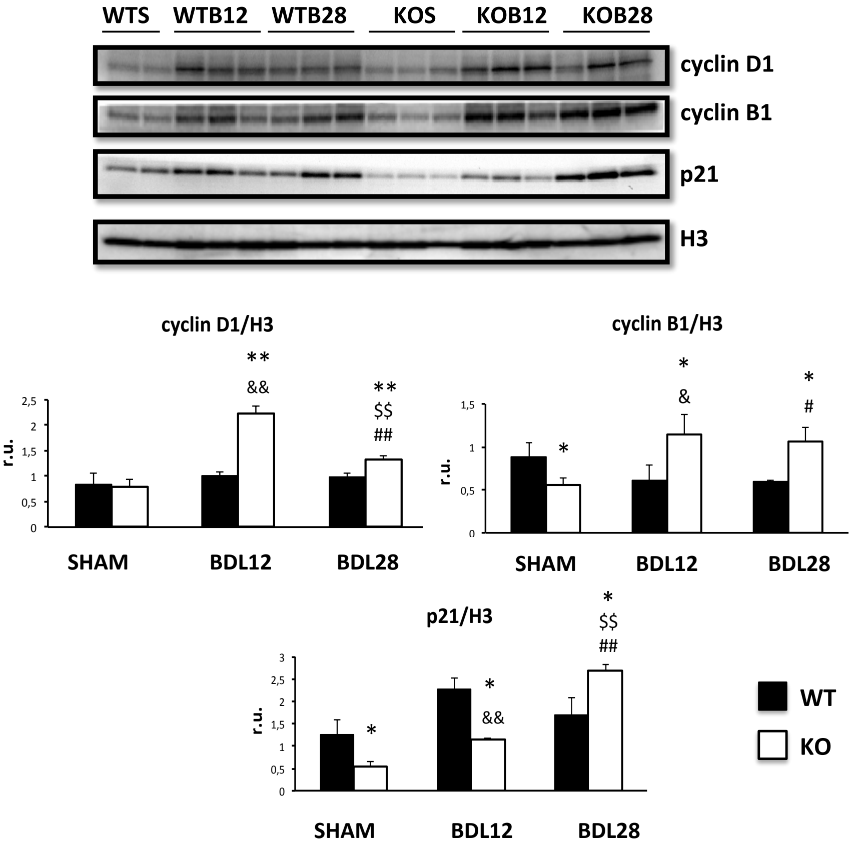

Figure 67. Cell cycle study in BDL nuclear extracts by Western blot. Representative Western blot for cyclin D1, cyclin B1 and p21 in nuclear extracts of wild type and p38α knock out SHAM and BDL liver. H3 was used as a loading control in Western blot densitometries. Data are shown as mean and SD. **P* < 0,05 WT *versus* KO, ***P* < 0,01 WT *versus* KO, #*P* < 0,05 BDL 28 days *versus* SHAM, ##P< 0,01 BDL 28 days *versus* SHAM, &*P* < 0,05 BDL 12 days *versus* SHAM, &&*P* < 0,01 BDL 12 days *versus* SHAM, $*P* < 0,05 BDL 28 days *versus* BDL 12 days, $$ *P*< 0,01 BDL 28 days *versus* BDL 12 days. n(WTS)=8, n(KOS)=8, n(WTB 12 days)=4, n(WTB 28 days) =6, (KOB 12 days)=4, n(KOB 28 days)=6.

3.12. p38α deficiency decreased the hepatic proliferative response after BDL

The parameters that were firstly used to assess the impairment in cell cycle progression were also useful for the establishment of the hepatocyte proliferative response after the induction of cholestasis. As showed (Figure 68), p38α knock out liver suffer from certain difficulties when trying to recover the liver mass loss after BDL.

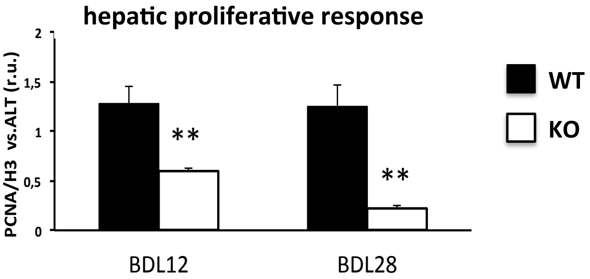

Figure 68. Hepatic proliferative response to liver injury after BDL. It was established with the PCNA (normalized by H3) and ALT enzymatic activity in wild type and p38α knock out mice. Data are shown as mean and SD. Black, WT; white, KO. *P < 0,05 WT *versus* KO, **P < 0,01 WT *versus* KO. n(WTB 12 days)=4, n(WTB 28 days)=6, (KOB 12 days)=4, n(KOB 28 days)=6.

3.13. Oxidative stress after BDL

Levels of GSH and GSSG were determined in SHAM and BDL animals by mass spectrometry and the GSSG/GSH ratio was calculated (Figure 69). A significant increase in this ratio was found in p38α knock out mice when comparing with p38α knock out SHAM livers and wilt type BDL.

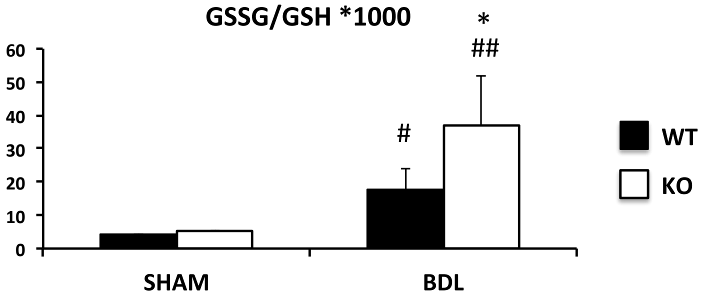

Figure 69. GSSG/GSH ratio quantification in wild type and p38α knock out SHAM and 28 days BDL mice. Data are shown as mean and SD. Black, WT; white, KO. *P < 0,05 WT *versus* KO, ##P < 0,01 BDL 28 days *versus* SHAM. n(WTS)=8, n(KOS)=8, n(WTB 28 days)=6, n(KOB 28 days)=6.

4. Cytokinesis failure upon hepatocyte isolation

4.1. Hepatocyte isolation triggers an increase in binucleation in primary hepatocytes, which can be inhibited by NAC addition to the perfusion media

Hepatocyte cultures had high binucleation rates but we wanted to confirm that binucleation was already induced during the hepatocyte isolation procedure (Figure 70).

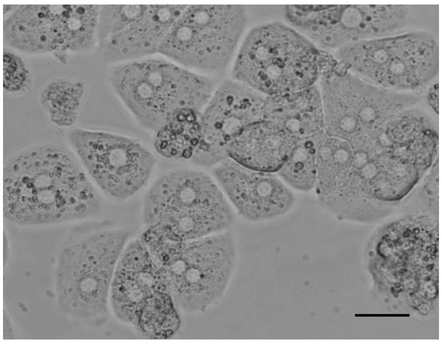

Figure 70. Hepatocyte binucleation during culture. Isolated hepatocytes culture (without NAC) microscopy image. Scale bar=20 µm.

Therefore, we assessed the rates of binucleation and polyploidy in freshly isolated hepatocytes. We combined two methods: Isolation with an antioxidant, such as NAC, and normal isolation without antioxidant. Ploidy measurement was performed by conventional cytometry, and binucleation quantification by image cytometry (Figure 71).

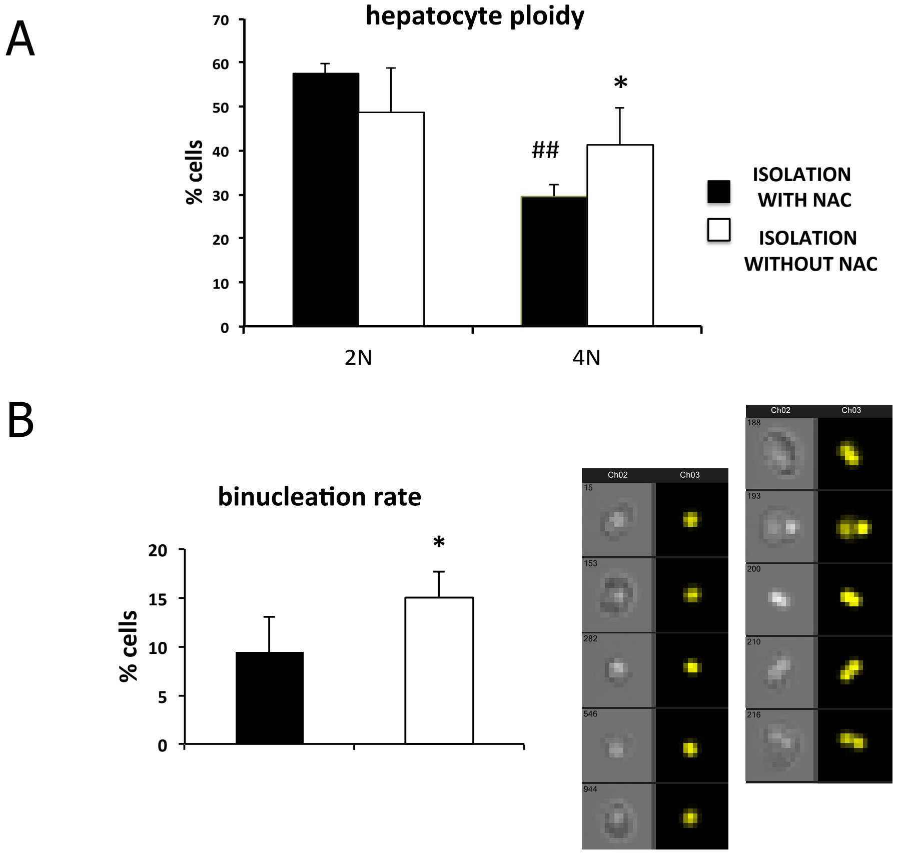

Figure 71. Isolated hepatocyte ploidy analysis by flow cytometry. Hepatocyte ploidy representation of ploidy results obtained by conventional flow cytometry (A). Binucleation rate comparing hepatocytes isolated with NAC and without NAC, determined by image flow cytometry (B). Representative images of the hepatocytes that belong to the mononucleated and binucleated populations. Data are shown as mean and SD. *P < 0,05 hepatocytes isolated with NAC *versus* hepatocytes isolated without NAC, **P < 0,01 hepatocytes isolated with NAC *versus* hepatocytes isolated without NAC. n=8 in both groups, ##P < 0,01 hepatocytes population 4N *versus* 2N.

4.2. Hepatocyte isolation leads to an increase in ROS and promotes oxidative stress in primary hepatocytes, prevented by NAC

Considering that binucleation as a result of oxidative stress generation has been described [Nakatani T. *et al.,* 1997; Gorla G.R. *et al.*, 2001] and hepatocyte disintegration from liver induced oxidative stress generation, we secondly assessed the generation of oxidative stress after liver disgregation. NAC addition not only increased the GSSG/GSH ratio but also decreased the generation of ROS (Figure 72).

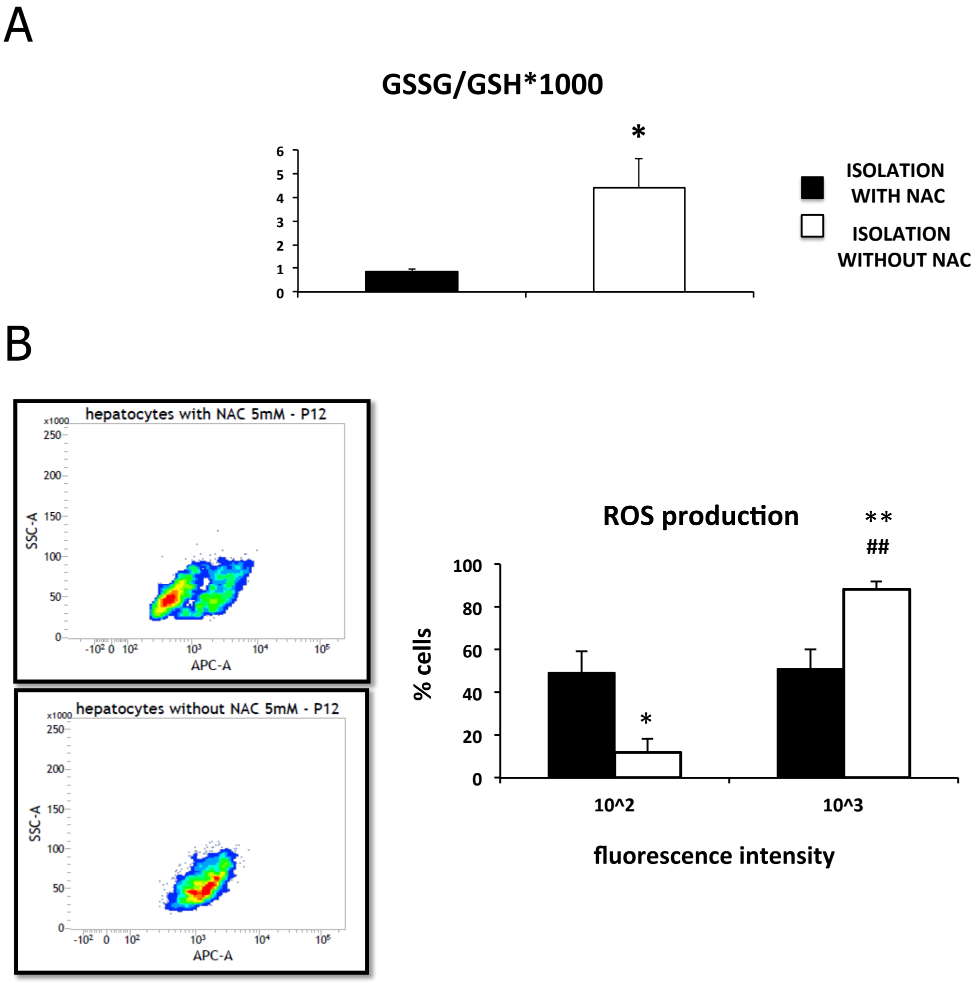

Figure 72. Oxidative stress upon hepatocyte isolation. GSSG/GSH ratio determination by mass spectrometry (A). ROS production measurement by flow cytometry. Cell ROX Deep Red (APC-A) was used to measure ROS (B). Density plot representation of ROS production in hepatocytes isolated with NAC and without NAC. Each dot or point represents an individual cell. (ROS production representation. Two populations with different APC intensity were found. Data are shown as mean and SD. *P < 0,05 hepatocytes isolated with NAC *versus* hepatocytes isolated without NAC, **P < 0,01 hepatocytes isolated with NAC *versus* hepatocytes isolated without NAC. ##P < 0,01 hepatocytes population 10^3 *versus* 10^2 (fluorescence intensity). n=8 in both groups.

4.3. Hepatocyte isolation promotes cell cycle entry, palliated by NAC

Western blot of key regulators of cell cycle showed the down-regulation of cyclin B1 levels in hepatocytes isolated with NAC, at the same time that they expressed lower PCNA protein levels. Moreover mRNA levels of the mitotic transition promoter *CyclinF* were overexpressed in hepatocytes isolated with NAC (Figure 73).

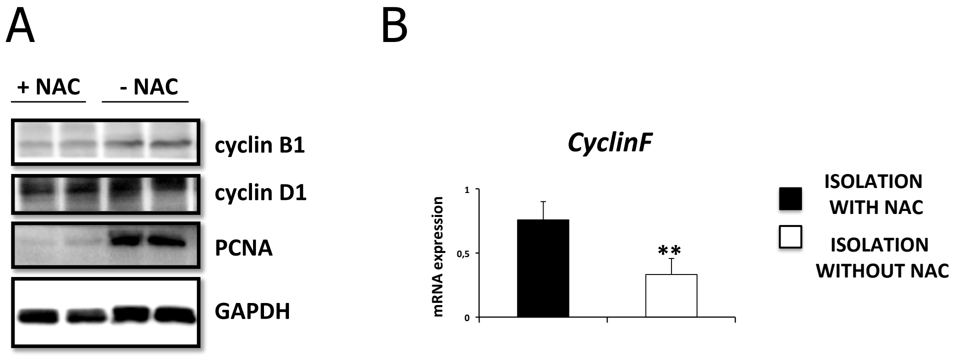

Figure 73. Cell cycle study in isolated hepatocytes. Representative western blot images of cyclin B1, cyclin D1 and PCNA protein levels. GAPDH was used as a loading control (A). Mitotic transition was analyzed by mRNA levels of *CyclinF* (B). Data (mean and SD) are shown as fold increase in mRNA level compared to a pool of control livers and were normalized by TATA-binding protein mRNA. ***P* < 0,01 hepatocytes isolated with NAC *versus* hepatocytes isolated without NAC.

DISCUSSION

Chapter 5

V. DISCUSSION

When we started this work, we dealt with the premise that REDOX-sensitive p38α would be activated as an adaptive mechanism in liver disease associated with oxidative stress, such as biliary cirrhosis, and hence it might contribute to survival.

Our preliminary results showed that the lack of p38α specifically in the liver increased the mortality rate after bile duct ligation and surprisingly, it promoted hepatocyte binucleation. We had the hypothesis that p38α deficiency could impair cytokinesis, the last step of mitosis [Slonim D.K. *et al.,* 2009, Chua A. *et al.,* 2014] consequently leading to the generation of binucleated hepatocytes [Nakatani T. *el al.,* 1997; Gorla G.R. *et al.,* 2001; Park J.K. *et al.,* 2010]. In addition, we enquired: Is there a role for oxidative stress in cytokinesis failure induced by p38α deficiency? (Figure 74).

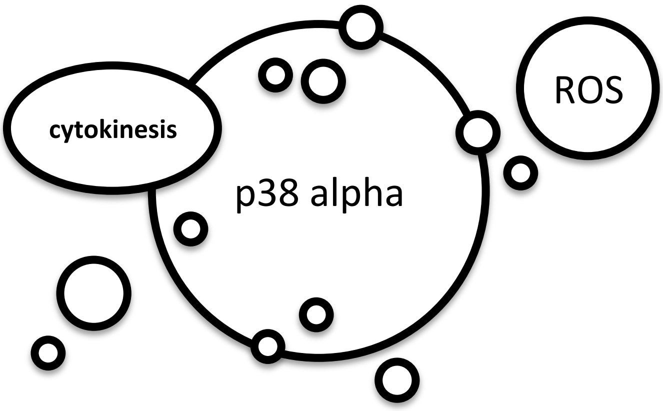

Figure 74. p38α regulation of cytokinesis: is there a role for oxidative stress?

1. p38α and cytokinesis regulation in aging liver: proper actin polymerization maintains physiological binucleation rates and liver mass

1.1. p38α regulates hepatocyte cytokinesis during physiological liver development maintaining liver size

Binucleation is a nuclear physiological phenomenon during liver development [Guidotti J. *et al.,* 2003]. In our work, p38α deficiency led to a higher increase in liver binucleation, reaching the highest rate in old mice, when comparing with liver from wild type mice. Therefore, the role of p38α as a modulator of binucleation has been confirmed in 3 different ages. Our findings showed the other face of p38α, as a regulator of hepatocyte cell cycle transition and cytokinesis.

Not many studies have been published about pathways involved in the regulation of liver binucleation. It is known that the insulin/AKT pathway induces liver binucleation by cytokinesis failure during liver maturation [Celton-Morizur S. *et al.,* 2010] and that p53 prevents binucleation after hepatocyte DNA damage [Nuñez F. *et al.,* 2000].

Firstly, we focused on the aging liver, the stage of liver development that presented the highest binucleation rate. Wild type mouse liver exhibited around 30% of binucleated hepatocytes and p38α knock out mice did significantly duplicate this rate. In addition, p38α knock out old liver ratios were smaller in size than their littermates’. Once apoptosis and hepatocyte size reduction were discarded, we went further into the analysis of the mitotic performance, which could be behind the loss of liver ratio. Interestingly, p38α knock out old hepatocytes, as they were polyploid, should be prone to have higher apoptotic rates, but overexpression of *Gas2* seemed to protect these hepatocytes from apoptosis.

By that time, we could assert that p38α knock out mice had some difficulties when undergoing cytokinesis. We analyzed the main checkpoints of the cell cycle regulated by p38α: cyclin D1, which is known to be a key regulator in the G_1/S checkpoint and it is also influenced by p38α [Thoms H.C. *et al.,* 2007; Parekh P. *et al.,* 2011]; and cyclin B1, which controls G_2/M transition [Chow J.P. *et al.,* 2003]. As we expected, p38α knock out mice expressed higher levels of cyclin B1 that would lead to the blockade of the mitotic progression by stopping them at the G_2/M checkpoint. The increase in cyclin B1 nuclear protein levels pointed out the necessity of preventing mitotic entry in p38α knock out hepatocytes.

1.2. MNK1 and liver binucleation

We moved forward to the main pathways that being regulated by p38α could trigger cytokinesis impairment. As it has been described by Rannou and collaborators [Rannou Y. *et al.,* 2012], dephosphorylation of MNK1 leads to the generation of multinucleated cells by deregulating centriolin localization and thus, affecting cytokinesis [Gromley A. *et al.,* 2005]. The absence of MNK1 phosphorylation was confirmed in p38α knock out mice, and thus, it would contribute to binucleation.

p38α does clearly target MNK1 in the liver. Lack of MNK1 is not exclusive of p38α knock out aging liver and its inactivation could not be the only explanation for the decrease in liver mass ratio in old p38α knock out liver. Therefore, we looked for other possible pathways that could contribute to the formation of binucleated cells, at least in aging liver.

1.3. p38α controls actin polymerization in aging liver: Role of the MK2/HSP27 axis

Old wild type liver exhibited a dense network of F-actin when performing immunohistochemistry. On the contrary, F-actin almost disappeared in old knock out hepatocytes.

We also analyzed F-actin by ultracentrifugation and observed that F-actin was present in p38α knock out hepatocytes, but probably not well polymerized. By ultracentrifugation, we separated the filamentous fraction (that is heavier and goes to the bottom) from the globular actin (lighter and remains on the supernatant). Digestion of F-actin allowed the recognition of this fraction with antibody for G-actin and thus, we calculated the G-actin/F-actin ratio. p38α knock out old livers exhibited less F-actin polymerization, which supported the results obtained by immunohistochemistry.

This surprising actin depolymerization finding has also been reported in mouse embryos that were treated with p38 inhibitors SB220025 and SB203580. These embryos displayed a severe loss of F-actin and suffered from mitotic delay when comparing to controls, although they were viable [Natale D.R. *et al.,* 2004; Paliga A.J.M. *et al.,* 2005]. Moreover, these studies, which firstly introduced the role of p38 MAPK in the regulation of F-actin during early development, also confirmed the actin polymerization axis: p38/MK2/HSP27 [Stokoe D. *et al.* 1992; Rouse J. *et al.* 1994]. Thus, inhibition of p38 blocked MK2 and HSP27 phosphorylation. The role of the p38/MK2/HSP27 axis in the regulation of actin polymerization has also been reported in the loss of proliferative potential in cancerous cells after p38α inhibition [Gibert B. *et al.,* 2012].

HSP27 was clearly affected by p38α deficiency in p38α knock out mouse liver. Old wild type mice exhibited an activation of HSP27, while p38α knock out ones did not. HSP27 could be activated by MK2, which is a downstream target of p38α, and was only active in wild type mice. However, the MK2-mediated HSP27 phosphorylation was not so clear when studying younger p38α knock out mice. Although MK2 was apparently not a mediator of HSP27 phosphorylation in our model, phosphorylation of MK2 is essential for p38 traslocation to the cytosol and its regulation of cytoskeleton dynamics [Ronkina N. *et al.,* 2008].

Anyway, lower levels in HSP27 phosphorylation were exhibited in old p38α knock out mice. Lack of Ser 82 phosphorylation on HSP27 inhibits actin polymerization like capping proteins do [Miron T. *et al.,* 1991; Benndorf R. *et al.,* 1994]. In fact, non-phosphorylated HSP27 acts as an actin sequester, maintaining the G-actin pool, required for a high rate of actin filament turnover [Pollard T.D. and Borisy G.G. 2003]. Only when HSP27 is phosphorylated, it binds F-actin and promotes F-actin stabilization [Mounier N. and Arrigo A.P. 2002].

The impairment of F-actin polymerization may affect multiple cell functions. However, it kept p38α knock out animals alive. We hypothesize that alterations in actin polymerization were compatible with life but not with cell cycle progression.

1.4. p38α controls actin polymerization in aging liver: Role of the RhoA pathway

Actin polymerization can also be regulated by the RhoA pathway. Therefore, we performed some preliminary Western blots to assess the activation of the

RhoA pathway. RhoA pathway plays an essential role on furrow initiation, furrow ingression and actomyosin ring formation- always mediating actin polymerization [Normand G. and King R.W. 2010].

Our preliminary results about Rho GTPases suggested that p38α knock out hepatocytes did not show a complete activation of the RhoA pathway. This inactivation could be reflected by the lack of phosphorylated PRK2 (RhoA effector in charge of the midbody abcission and G_2/M transition) [Schmidt A. *et al.,* 2007] and the cytosolic accumulation of p27 (whose expression leads to cell division impairment) [Serres M.P. *et al.,* 2012]. In addition, the enhancement of phosphorylated levels of cofilin in the nucleus would inhibit the nuclear actin-depolymerizing activity of cofilin [Katoh K. *et al.,* 2010] and protect F-actin polymerization in the nucleus, which is supposed to be fundamental for the regulation of transcription and gene expression [Pederson T. 2008; Zheng B. *et al.,* 2009]. In fact, cofilin promotes F-actin nuclear transport [Berstein B.W. and Bambrug, J.R. 2010]. This mechanism would also explain why p38α knock out mice had a significant F-actin fraction isolated by ultracentrifugation.

The link between the RhoA signaling pathway and HSP27 in actin polymerization remains unknown. On the one hand, results obtained in HeLa cells [Zhang S. *et al.,* 1995], in rabbit facial vein [Dubroca C. *et al.,* 2005], and in osteoblasts [Katoh K. *et al.,* 2010] showed that RhoA activation was upstream of p38 and induced its phosphorylation and the following HSP27 activation. Thus, HSP27 would be considered as an effector of the RhoA pathway. On the other hand, the p38 activation seems to affect actin polymerization independently of the RhoA pathway [Guay J. *et al.,* 1997]. For instance, CCl39 cells were unable to activate p38 or to induce phosphorylation of HSP27 but expressed the RhoA pathway [Guay J. *et al.,* 1997].

Therefore, our results suggest that p38α is able to activate HSP27 and potentially induce the retroactivation of RhoA in order to keep the appropriate F-actin network for successful cytokinetic performances in aging, whereas p38α deficiency induces progressive binucleation with age. The abnormalities in actin polymerization start in adult p38α knock out hepatocytes. Abnormal or severe depolymerization of F-actin that occurs in old p38α knock out is compatible with life (Figure 75).

1.5. Oxidative stress is not the cause of liver binucleation in p38α knock out mice

The aged tissue develops a state of chronic oxidative stress as a consequence of mitochondrial dysfunction [Hsieh C.C. *et al.,* 2003] and the mitochondrial release of ROS leads to the oxidation of macromolecules such as DNA, RNA, proteins and lipids [Finkel T. and Holbrook N.J. 2000]. Thus, in normal liver and hepatic mitochondria the GSSG/GSH ratio and peroxide levels increase with age [Sastre J. *et al.,* 1996; Hsieh C.C. *et al.,* 2003]. Accordingly, livers from our wild type aged mice showed an increase in GSSG/GSH levels. Contrarily, p38α knock out mice recovered their hepatic GSSG/GSH ratio when they got older.

It has been reported that oxidative stress may increase the rate of binucleation [Chipchase M.D. *et al.,* 2003; Lu P. *et al.,* 2007]. On the one hand, it seems that increase in gene copies -because of polyploidization- could be a pro-survival mechanism induced by oxidative stress [Lu P. *et al.,* 2007]. On the other hand, oxidative stress can lead to DNA damage and promote polyploidization [Chipchase M.D. *et al.,* 2003]. However, old p38α knock out mice exhibited lower GSSG/GSH ratio as well as higher binucleation rate in comparison with younger knock out mice. Therefore, our results suggest that oxidative stress is not the cause of binucleation upon p38α deficiency in old mice.

1.6. Oxidative stress may be the activator of RhoA in wild type old hepatocytes

Recent *in vitro* studies have indicated that GTPases, such as RhoA, are directly regulated by oxidative stress. This REDOX-based mechanism might affect F-actin dynamics [Aghajanian A. *et al.,* 2009; Soliman H. *et al.,* 2012]. Therefore, we hipotesize that physiological increase in ROS levels because of aging could mediate RhoA activation in wild type liver and would keep the cytoskeleton properly in order to maintain liver mass.

1.7. p38α, alternatively with NF-κB, regulates the antioxidant defense in the liver with age

Studies in mice have indicated that during aging, the GSSG/GSH ratio in liver shifts towards oxidation [Rebrin I. *et al.,* 2003]. Although antioxidant cell defense system could increase with age, the rate of ROS generation exceeds the induced antioxidant ability, as it has been seen in rats [Sanz N. *et al.,* 1997]. Overall, aging mouse liver shows an increase in oxidative stress generation that is also related to the increase in inflammatory and stress response genes [Lebel M. *et al.,* 2011].

p38α knock out livers are exposed to a pro-oxidant REDOX status when they are younger. However, this pro-oxidant status was completely abrogated when mice got older: p38α knock out old hepatocytes up-regulated their antioxidant capacity, and thus decreased their GSSG/GSH ratio. The reduced environment excluded oxidative stress as responsible for the binucleation evolution, but highlighted one transcription factor that is involved in multiple liver processes that are related to oxidative stress: NF-κB. Our very last results demonstrated that p-p65 migrated to a nuclear location when wild type hepatocytes were younger and it did the same when p38α knock out hepatocytes were older. Some other transcription factors may be required for the regulation of the liver antioxidant defense with age, but based on previous works NF-κB may up-regulate antioxidant enzymes such as Mn SOD, Cu Zn SOD, GPx and GCL [Rojo A.I. *et al.,* 2004; George L.E. *et al.,* 2009; George L.E. *et al.,* 2012].

Therefore, p38α regulates the antioxidant defense and the intracellular REDOX status in adult liver, but it does not seem to be necessary for up-regulation of liver antioxidant defense in aging.

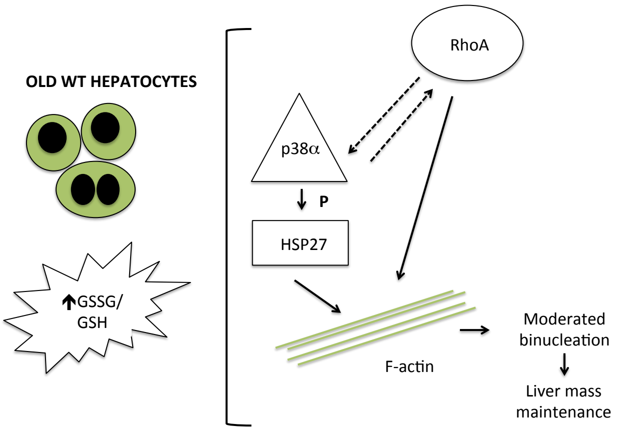

Figure 75. SNAPSHOT: F-actin polymerization pathways in wild type old hepatocytes. Our results suggest that hepatocyte binucleation progressively increases with age and it is enhanced by p38α deficiency. In aging, p38α activates HSP27 and RhoA axis in order to keep the proper F-actin network for successful cytokinetic performances. Although MK2 could not be the regulator of p38α-induced HSP27 activation, MK2 could mediate p38 traslocation to the cytosol. The inactivation of MNK1 phosphorylation is always assessed in p38α knock out mice, and thus, it would contribute to binucleation.

2. p38α and partial hepactectomy: binucleation, ploidy reversal and oxidative stress

Binucleation has its prons and cons. It has some clear advantages, such as gain of function or genetic protection [Lu P. *et al.,* 2007]; but it is considered a disadvantage when liver needs to grow [Gentric G. *et al.,* 2012]. It was thought that binucleated hepatocytes, as they have more complexity, meet more difficulties when undergoing cell cycle [Gentric G. *et al.,* 2012]. This hypothesis is nowadays in question since Duncan and collaborators [Duncan A.W. *et al.,* 2010] reported that hepatocytes are able to reverse its ploidy. Ploidy reversal has casted doubt upon classical hepatocyte proliferation principles that affirmed that polyploid hepatocytes are a growing disadvantage. Moreover, ploidy reversal would provide an explanation for the success obtained in continuous hepatectomy.

Aged p38α knock out livers in basal conditions can stand high rates of binucleation. However: what would happen when highly binucleated hepatocytes face liver regeneration? Is there a role for p38α in this fascinating ploidy reversal?

2.1. p38α deficiency increases binucleation rate in after weaning hepatocytes

In order to get a better response to hepatectomy, we started this study with highly proliferative young hepatocytes. In fact, postnatal period exhibits the most of liver growth and the after weaning stage corresponds with the maximum binucleation induction [Celton-Morizur S. *et al.,* 2010].

p38α knock out after weaning hepatocytes exhibited more frequent binucleated shapes, but neither actin polymerization disarrangements nor pro-oxidant REDOX status were observed.

No differences in basal HSP27 phosphorylation were found between wild type and knock out mice, and partial hepatectomy induced phosphorylation of HSP27 in both groups. However, activation of the MK2 pathway was only observed in wild type mice.

2.2. p38α deficiency reduces liver growth after partial hepatectomy

It is well known that partial hepatectomy is a proliferative stimulus that induces compensatory growth in the liver. It represents the most commonly used intervention for studying liver regeneration because it lacks of massive necrosis or inflammation [Zou Y. *et al.,* 2012]. Between 5 to 7 days after partial hepatectomy, rodents have usually recovered most of the original liver mass [Fabrikant J.I. 1968]. Intense liver growth takes place on the first 6 days and many mitotic processes are completed by day 3 [Zou Y. *et al.,* 2012].

Although p38α knock out hepatocytes did not reverse binucleation during cholestasis, partial hepatectomy let binucleated p38α knock out hepatocytes convert into mononuclear hepatocytes, in order to efficiently proliferate. Interstingly, 3 days after liver resection, liver mass ratio in p38α knock out mice was significantly lower when comparing to wild type.

2.3. p38α is not needed for ploidy reversal in hepatocytes

p38α knock out after weaning mice could reduce their binucleation rates in hepatocytes when it was necessary to carry out a compensatory hepatomegaly after liver resection. Although the mechanisms responsible for ploidy reversal remain quite unknown, we can be sure that activation of p38α is not required for the formation of bipolar spindles and the clustering of centrosomes [Duncan A.W. *et al*., 2010], at least, under partial hepatectomy.

However, p38α knock out hepatocytes are still more binucleated after partial hepatectomy. Ploidy reversal is known to be followed by cytokinesis, but the lack of p38α could be impairing this last stage leading to failed cytokinesis (Figure 76).

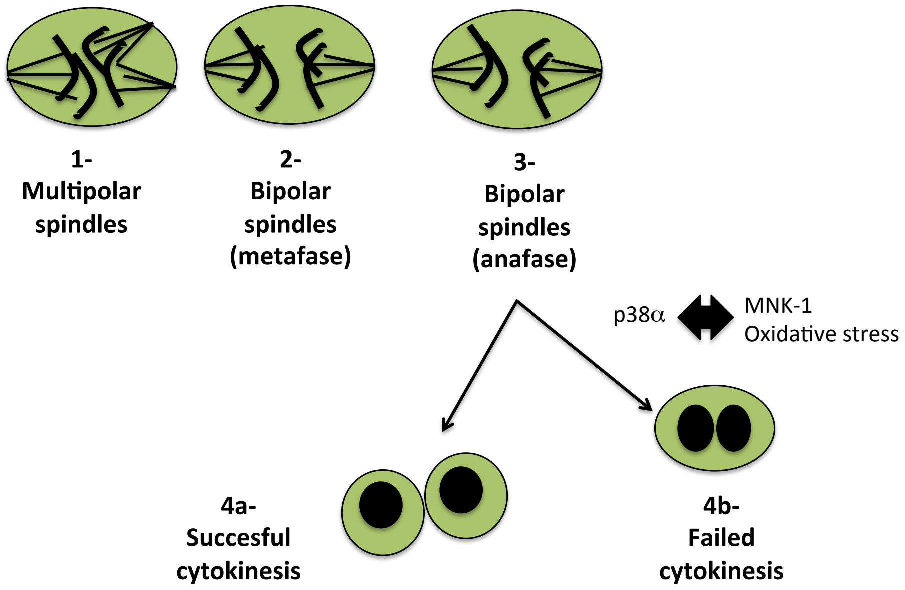
1- Multipolar spindles
2- Bipolar spindles (metafase)
3- Bipolar spindles (anafase)
p38α
MNK-1
Oxidative stress
4a- Succesful cytokinesis
4b- Failed cytokinesis

Figure 76. Ploidy reversal upon p38α deficiency.

This partial decrease in binucleation in p38α knock out hepatectomized hepatocytes could be ascribed to:

- Dephosphorylation of MNK1. In fact, the MNK1 ortologue in *Drosophila melanogaster* (Lk6) interacts with microtubules and localizes in the centrosomes [Kidd and Raff, 1997; Reiling J.H. *et al.,* 2005] and it is necessary for cell abscission [Rannou Y. *et al.,* 2010].

- Oxidative stress-mediated failed ploidy reversal cytokinesis. As we will discuss, p38α knock out mice exhibited higher GSSG/GSH ratio after partial hepatectomy.

2.4. p38α deficiency blocks mitotic progression during hepatocyte cell cycle after partial hepatectomy

Campbell and collaborators [Campbell J.S. *et al.,* 2011] reported that p38 is rapidly inactivated after 30 minutes partial hepatectomy (corresponding with the activation of protein synthesis) and re-activated after 12 hours, concluding that p38 activity does not appear to be required for DNA replication *in vivo* during liver regeneration. In agreement with these findings, low p38 MAPK activity was found during embryonic development [Awad M.M. *et al.* 2000]. Therefore, p38α may not be required for DNA synthesis in hepatocytes, but its effects on the regulation of mitotic transition and cytokinesis need to be clarified.

After weaning p38α knock out mice already exhibited significantly higher *CyclinD1, A1, B2* and *F* mRNA levels, as well as increased cyclin B1 protein levels under basal conditions. Some of these differences were enhanced when partial hepatectomy was performed and thus, hepatectomyzed p38α knock out mice showed a considerable blockade in the G_2/M transition. Overexpression of those cyclins that stop the cell cycle at the mitotic entry would trigger an accumulation of hepatocytes at the mitotic stage [Cha H. *et al*., 2005]. In fact, after 72 hours hepatectomy, p38α knock out hepatocytes displayed higher nuclear levels of phosphorylated H3 in comparision with wild type hepatocytes.

Furthermore, p38α knock out hepatocytes overexpressed p21 protein levels, a marker of replicative arrest [Clouston A.D. *et al.,* 2005] and universal mitoinhibitor [d'Adda di Fagagna F. *et al.,* 2008], which can bind to cyclin B1 inhibiting cell cycle progression [Dash B.C. and El-Deiry W.S. 2005].

Previous works have reported the requirement of p38α when entering mitosis, for proper spindle assembly and checkpoint function in human, mouse, rat-kangaroo cells [Lee K. *et al*., 2010] and HCT116 cells [Cha H. *et al.,* 2005]. This function remains controversial, although our results about p38α deletion in hepatocytes could support this hypothesis.

2.5. Oxidative stress after partial hepatectomy in p38α knock out mice

The lack of p38α is clearly affecting mitotic progression in our model, as it has been supported [Cha H. *et al.,* 2005; Lee K. *et al*., 2010]. Nevertheless, p38α deficiency during the mitotic transit did not trigger binucleated cells [Cha H. *et al.,* 2005; Lee K. *et al*., 2010]. Therefore, we wanted to find an explanation for the higher binucleation rates found in p38α knock out hepatocytes after hepatectomy.

After weaning p38α knock out mice did not show any significant inhibition in the phosphorylation of HSP27 and thus, potential defects in actin polymerization should not be ascribed to this mechanism. F-actin proper polymerization was assessed under basal conditions by immunohistochemistry. Then, we looked for other factors that could be behind the cytokinetic blockade.

We cannot discard that oxidative stress is behind cytokinetic impairment in p38α deficiency. The same REDOX status was found in both wild type and p38α knock out mice under basal conditions, but p38α knock out hepatectomized mice exhibited higher glutathione oxidation and consequently more oxidative stress. Therefore, the impact of the pro-oxidant REDOX disbalance on the induction of failed cytokinesis in ploidy reversal should not be discarded (Figure 77).

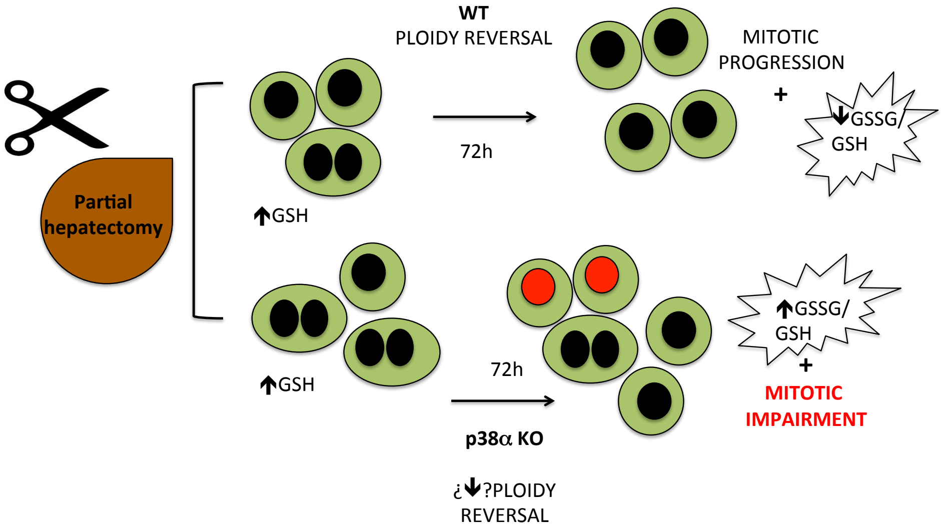
WT
PLOIDY REVERSAL
MITOTIC PROGRESSION
+
↓GSSG/GSH
Partial hepatectomy
↑GSH
72h
↑GSSG/GSH
+
MITOTIC IMPAIRMENT
↑GSH
72h
p38α KO
¿↓?PLOIDY REVERSAL

Figure 77. SNAPSHOT: after weaning liver wild type and p38α knock out upon 72 hours partial hepatectomy. Our results suggest that p38α modulates mitotic transit and recovery of liver mass after 72 hours partial hepatectomy. p38α is not essential for ploidy reversal but it could contribute to ploidy reversal's-coupled cytokinesis. Moreover, p38α regulates hepatocyte cell cycle after partial hepatectomy promoting the mitotic progression.

3. p38α in chronic liver injury: binucleation and survival during chronic cholestasis

The next part of the discussion deals with the experiments carried out in adult liver injury induced by chronic cholestasis. Chronic cholestasis was induced by bile duct ligation, and combined liver regeneration with leukocyte infiltration, fibrosis and necrosis [Fickert, P. *et al.,* 2002; Georgiev P. *et al.,* 2008; Heinrich S. *et al.,* 2012]. As a reminder, it is important to know that p38α knock out adult hepatocytes had higher rates of binucleation, less phosphorylation of MNK1 and inappropriate F-actin arrangement in comparison with wild type mice under basal conditions.

3.1. p38α knock out adult mice exhibited decreased survival after chronic cholestasis

Chronic cholestasis induced by BDL is a much more aggressive model than partial hepatectomy. Chronic cholestasis induces a severe hepatocellular injury that eventually leads to liver failure and death [Miyoshi H. *et al.,* 1999]. Because of this, we began with the study of survival after the cholestasis induction. BDL produces immediate jaundice, with elevated bilirubin serum levels, and release of transaminases. Preliminary results of liver damage analyzed in serum, such as bilirubin, ALT and γ-GT did not exhibit significant differences between groups. In spite of the lack of changes in serum biochemical parameters, p38α knock out hepatocytes dealt worse with BDL damage: by day 30, half of the p38α knock out population had died, while 75% wild type mice survived.

3.2. The absence of p38α did not affect inflammation, neither fibrosis nor apoptosis after chronic cholestasis

In the next part we will discuss about three main features of the cholestasis progression (inflammation, fibrosis, and apoptosis) and the role that p38α exerts on them.

Since p38α is considered a mediator of inflammation [Schieven G.L. *et al.,* 2005] a pro-survival advantage in p38α knock out mice might be expected. Analysis of pro-inflammatory cytokines and liver histology did not show differences between groups. It is known that MAPK are activated after extrahepatic biliary obstruction [Samuel I. 2008] and p38 is reported to up-regulate IL-10 synthesis 14 days after BDL [Morita Y. *et al.,* 2008; Waseem T. *et al.*, 2008]. However, our results showed that p38α knock out mice exhibited higher mRNA expression of the anti-inflammatory cytokine *Il10* by day 12, but this protection was lost in the long term.

Regarding fibrosis and apoptosis, p38α liver-deficient mice did not show higher degree of apoptosis nor fibrosis after 28 days of cholestasis induction compared to wild type mice.

3.3. p38α-dependent activation of the MK2 pathway after chronic cholestasis

Wild type adult livers exhibited marked phosphorylation of MK2 on Thr334 after chronic cholestasis. Phosphorylation of p38α seemed to activate three different targets: HSP27, AKT and GSK3β, only after BDL, independent of MK2 phosphorylation on Thr334.

HSP27 phosphorylation was only observed in BDL wild type animals. According to Mounier and Arrigo [Mounier N. and Arrigo A.P. 2002], the activation of this small heat shock protein would provide these mice with an appropriate network of F-actin for proliferation and efficient cell division.

Phosphorylation of AKT on Ser473 was markedly reduced in liver of p38α-deficient mice upon chronic cholestasis. The consequences of inactivating this pathway might mainly be down-regulation of cell size through mTOR-dependent and mTOR-independent pathways, promotion of protein degradation, inhibition of protein synthesis [Faridi J. *et al.,* 2003], and indeed, deregulation of the actin cytoskeleton [Jacinto E. *et al*., 2004].

Regarding GSK3β, p38α is able to inactivate GSK3β by direct or AKT-mediated phosphorylation leading to β catenin accumulation. Thus, p38 modulated the canonical Wnt/β catenin signaling after BDL, which is critical for normal cell proliferation and homeostasis [Bikavilli R.K. *et al.,* 2008].

3.4. p38α knock out mice maintained their high binucleation levels after chronic cholestasis

Inactivation of the AKT pro-survival pathway in p38α knock out mice could contribute to the high mortality induced by cholestasis in these mice. However, a very interesting and surprising finding appeared when analyzing binucleation. As we have already discussed, p38α knock out mice at the after weaning period were able to perform ploidy reversal. However, after induction of chronic cholestasis, adult knock out mice were not. Indeed, p38α knock out mice did not modify their binucleation rate after cholestasis induction. In contrast, wild type mice gradually reduced their binucleation levels with the progression of the disease. In this case, wild type hepatocytes did reverse their ploidy in order to proliferate after the regenerative stimulus. Regarding the maintenance of binucleation in p38α knock out mice, we should keep in mind that these mice already had actin polymerization deficiencies under basal conditions and displayed lower levels of phosphorylated HSP27 after BDL.

The increase in binucleation in chronic disorders may be considered a bad prognostic and an index of severity. In fact, binucleation is a severity index in progressive chronic hepatitis and cirrhosis [Grizzi F. *et al.,* 2007; Celton-Morizur S and Desdouets C. 2010]; and it is completely avoided in HCC. Accordingly, BDL knock out mice died before than their littermates.

3.5. p38α knock out mice did not develop compensatory hepatomegaly after BDL

The evolution of liver weight after cholestasis induction displayed a phenomenon with potential deleterious consequences: p38α knock out livers were not able to increase their mass as a compensatory mechanism after liver injury. In fact, the ratio PCNA/AST activity indicated that p38α knock out livers did not respond adequately to liver injury for ensuring their survival.

The potentially fatal combination of loss of compensatory hepatomegaly and absence of ploidy reversal prompted us to study the cell cycle.

3.6. Delayed mitotic transition in p38α knock out mice after chronic cholestasis

p38α knock out BDL livers were highly binucleated and unable to recover the loss of liver mass. Accordingly, PCNA expression in p38α knock out BDL liver was almost abrogated, but nuclear extracts still exhibited p-H3 positivity. The same analysis was performed by immunohistochemistry, and confirmed that only a few p38α knock out hepatocytes underwent cell cycle after 12 days of

BDL, and most of them were stacked in mitosis, as reflected by p-H3 positive staining.

Cyclin B1 protein levels were higher in p38α knock out BDL mice after 12 days, which confirmed the mitotic delay. Hence, p38α deficiency blockades progression of mitosis towards the S phase in hepatocytes during the course of chronic cholestasis.

3.7. p38α deficiency enhances oxidative stress after chronic cholestasis

p38α knock out BDL mice exhibited an enhanced pro-oxidant status when compared to wild type mice, which was evidenced by increased glutathione oxidation in the liver. In this context, we should consider that basal levels of GSH were decreased and could inhibit proliferation [Markovic J. *et al.,* 2007; Markovic J. *et al.,* 2009], whereas oxidative stress could promote oxidation of proteins involved in cytokinesis [Hayashi M.T. and Karlseder J. 2013; Burruel V. *et al.,* 2014] (Figure 78).

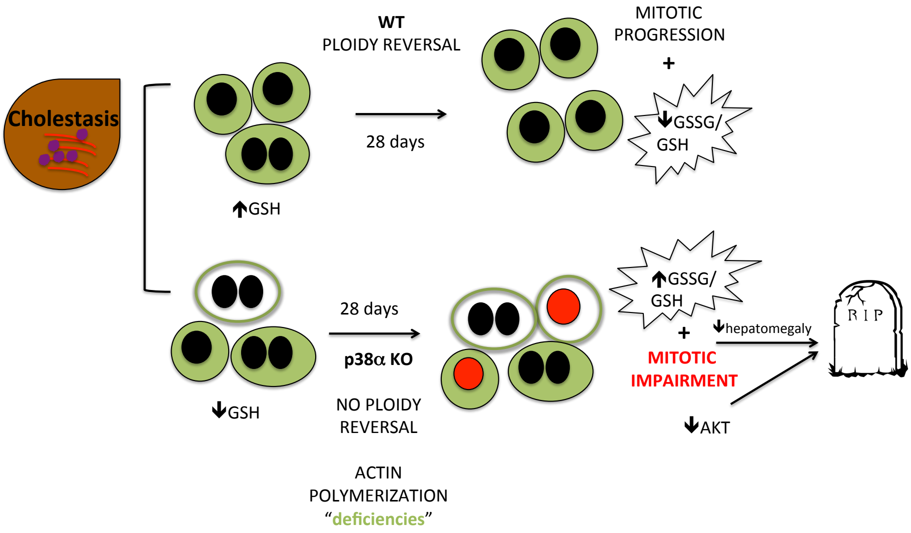

Cholestasis
WT
PLOIDY REVERSAL
28 days
↑GSH
MITOTIC
PROGRESSION
+
↓GSSG/
GSH
↓GSH
28 days
p38α KO
NO PLOIDY
REVERSAL
ACTIN
POLYMERIZATION
"deficiencies"
↑GSSG/
GSH
+
MITOTIC
IMPAIRMENT
↓hepatomegaly
↓AKT
RIP

Figure 78. SNAPSHOT: adult hepatocytes from wild type and p38α knock out mice after BDL. Our results suggest that loss of compensatory hepatomegaly, probably induced by ploidy reveral's coupled cytokinesis and delayed mitosis, together with enhanced oxidative stress resulted in a lethal combination for p38α knock out mice when inducing chronic cholestasis. Moreover, the mechanisms of this accelerated mortality may be mediated by HSP27 and the AKT/GSK3β axis.

4. Hepatocyte isolation: when oxidative stress orchestrates binucleation

The model of hepatocyte binucleation induction upon isolation is a simple *in vitro* model that permitted us to clarify some preliminary information about oxidative stress and cell cycle progression.

The collagenase-mediated digestion of the liver stimulates hepatocyte G_0/G_1 cell cycle transition [Etienne P.L. *et al.,* 1988; Loyer P. *et al.,* 1996]. However, freshly isolated primary hepatocytes face difficulties when trying to divide *in vitro.* Although hepatocytes are very versatile in terms of cell division (they are able to become polyploidy cells, to reverse polyploidy, to complete mitosis and indeed, to suffer from mitosis impairment [Duncan A.W. *et al.,* 2010]), they seem to do it better *in vivo*. *In vitro*, adult hepatocytes have limited proliferation capacity [Block G.D. *et al.*, 1996; Runge D.M. 1999].

After isolation, primary hepatocytes express several proto-oncogenes that make them undergo mid-late G_1 phase [Loyer P. *et al.,* 1996; Corlu A. and Loyer P. 2012], but progression towards the G_1/S cell cycle is only possible after stimulation with appropriate growth factors to overcome the mitogen-dependent mid-late G1 restriction point [Loyer P. *et al.,* 1996]. In addition, we have found that the rates of binucleation increase after hepatocyte isolation.

4.1. Collagenase digestion triggers oxidative stress

In our model, we confirm that hepatocytes are exposed to oxidative stress during isolation that is revealed by the increase in the GSSG/GSH ratio and by ROS production. This pro-oxidant status can be avoided by the addition of an antioxidant, such as NAC. In fact, NAC is commonly used to preserve the metabolic activity and to obtain high viabilities during the isolation procedure [Sagias F.G. *et al.,* 2010; Bartlett D.C. *et al.,* 2014], to avoid the activation of apoptosis and the associated lipid peroxidation [Abrahamse S.L. *et al.,* 2003; Lai P.H., *et al.,* 2005], and to prevent the isquemia-reperfusion injury in isolated liver too [Dunne J.B. *et al.,* 1994]. Hence, it has been postulated the use of NAC in liver surgery as well as in hepatocyte and liver transplantation [Gomez-Lechon M. *et al*., 2008].

4.2. Oxidative stress promotes hepatocyte cell cycle entry but blocks cytokinesis upon hepatocyte isolation

ROS may trigger cytokinesis blockade and it is very frequent in senescent cells [Takahashi A. *et al.,* 2007]. In fact, cells exposed to high levels of ROS block their proliferative potential and activate pro-survival pathways to avoid cell death [Finkel T. 2003]. Accordingly, NAC lowered the percentage of hepatocytes that entered the cell cycle and prevented cytokinetic impairments (calculated by the binucleation rate). Hepatocytes isolated with NAC scarcely underwent cell proliferation. If they did, *CyclinF* mRNA levels were up-regulated fatilitating mitotic transition.

In the contrary, hepatocytes isolated without NAC had significantly enhanced binucleation rate and exhibited higher levels of PCNA. At the same time that hepatocytes tried to proliferate, cyclin B1 protein levels were overexpressed, blocking the mitotic phase entry [Chow J.P. *et al.,* 2003]. Overexpression of cyclin B1 may be blocking hepatocyte entry into mitosis, indicating that a potential mitotic impairment, such as cytokinesis blockade, should be overtaken. Hepatocytes isolated without NAC also exhibited lower mRNA levels of *Cyclin F*, which is usually degraded before cyclin B1 expression in the mitotic checkpoint [Bai C. *et al.,* 1994].

To conclude, our results suggest that oxidative stress during hepatocyte isolation induced cell cycle entry but caused hepatocyte cytokinesis failure (Figure 79). According to these findings, primary hepatocytes are recommended to be isolated from the tissue by collagenase digestion with 5 mM NAC in order to avoid the loss of replicating capacity of the cells, which may be of critical interest for clinical applications. The addition of 5 mM NAC abrogates defective cytokinesis and the generation of binucleated daughter cells, which exhibit high frequency of mitotic failure when they go to the next round of mitosis [Ganem N.J. *et al.,* 2009; Silkworth W.T. *et al.,* 2009]. This procedure may be of critical interest for clinical applications.

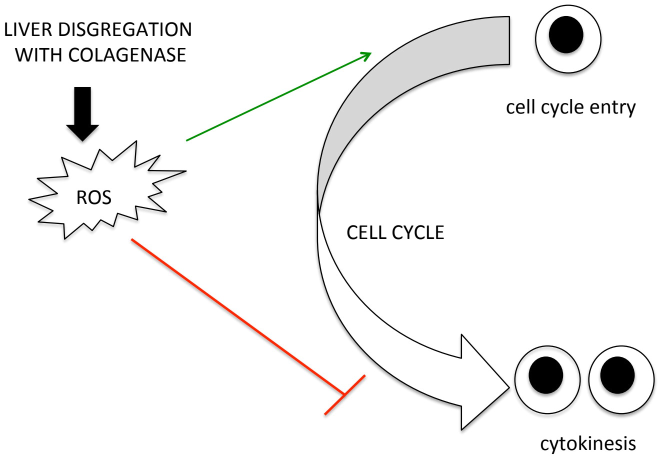

Figure 79. ROS generation upon hepatocyte isolation and their effects on hepatocyte cell cycle.

CONCLUSIONS

Chapter 6

VI. CONCLUSIONS

1. Hepatocyte binucleation progressively increases with age and it is enhanced by p38α deficiency. In fact, p38α activates the HSP27 and RhoA pathways in order to keep the appropriate F-actin network for successful cytokinesis upon aging. The lack of p38α blocks MNK1 activation, which would contribute to increased binucleation.

2. p38α modulates mitotic transit and it is needed for complete recovery of liver mass after partial hepatectomy. p38α is not essential for ploidy reversal but it is likely to contribute to ploidy reversal's coupled cytokinesis and to S-phase followed cytokinesis either by activating MNK1 or by REDOX modulation.

3. p38α deficiency restrains compensatory hepatomegaly after chronic cholestasis, causing failed cytokinesis in ploidy reversal and delayed mitosis, leading to increased mortality. The mechanisms involved seem to be reduced HSP27 phosphorylation and inactivation of the AKT/GSK3β axis.

4. Hepatocyte isolation triggers oxidative stress cell cycle entry as well as cytokinesis failure, which are prevented by the addition of N-acetyl cysteine.

REFERENCES

Chapter 7

VII. REFERENCES

Abrahamse SL, van Runnard Heimel P, Hartman RJ, Chamuleau RA, van Gulik TM. Induction of necrosis and DNA fragmentation during hypothermic preservation of hepatocytes in UW, HTK, and Celsior solutions. Cell Transplant 2003;12(1):59-68.

Abdelhalim MA, Jarrar BM. Histological alterations in the liver of rats induced by different gold nanoparticle sizes, doses and exposure duration. J Nanobiotechnology 2012; 25;10:5-3155-10-5.

Adams RH, Porras A, Alonso G, Jones M, Vintersten K, Panelli S, et al. Essential role of p38alpha MAP kinase in placental but not embryonic cardiovascular development. Mol Cell 2000; 6(1):109-116.

Adhami VM, Aziz MH, Reagan-Shaw SR, Nihal M, Mukhtar H, Ahmad N. Sanguinarine causes cell cycle blockade and apoptosis of human prostate carcinoma cells via modulation of cyclin kinase inhibitor-cyclin-cyclin-dependent kinase machinery. Mol Cancer Ther 2004; 3(8):933-940.

Aghajanian A, Wittchen ES, Campbell SL, Burridge K. Direct activation of RhoA by reactive oxygen species requires a REDOX-sensitive motif. PLoS One 2009;26;4(11).

Alison MR and Wright NA. The Biology of Epithelial Cell Populations. Oxford: Oxford University Press; 1985.

Allen M, Svensson L, Roach M, Hambor J, McNeish J, Gabel CA. Deficiency of the stress kinase p38alpha results in embryonic lethality: characterization of the kinase dependence of stress responses of enzyme-deficient embryonic stem cells. J Exp Med 2000; 6;191(5):859-870.

Alonso A, Sasin J, Bottini N, Friedberg I, Friedberg I, Osterman A, et al. Protein tyrosine phosphatases in the human genome. Cell 2004; 11;117(6):699-711.

Alpini G, Roberts S, Kuntz SM, Ueno Y, Gubba S, Podila PV, et al. Morphological, molecular, and functional heterogeneity of cholangiocytes from normal rat liver. Gastroenterology 1996;110(5):1636-1643.

Alpini G, Ulrich C, Roberts S, Phillips JO, Ueno Y, Podila PV, et al. Molecular and functional heterogeneity of cholangiocytes from rat liver after bile duct ligation. Am J Physiol 1997;272(2 Pt 1):G289-97.

Ambrosino C, Nebreda AR. Cell cycle regulation by p38 MAP kinases. Biol Cell 2001;93(1-2):47-51.

Aouadi M, Bost F, Caron L, Laurent K, Le Marchand Brustel Y, Binetruy B. P38 Mitogen-Activated Protein Kinase Activity Commits Embryonic Stem Cells to either Neurogenesis Or Cardiomyogenesis. Stem Cells 2006; 24(5):1399-1406.

Arthur JS. MSK activation and physiological roles. Front Biosci 2008; 13:5866-5879.

Atkins BD, Yoshida S, Saito K, Wu CF, Lew DJ, Pellman D.Inhibition of Cdc42 during mitotic exit is required for cytokinesis. J Cell Biol. 2013; 202(2):231-40.

Awad MM, Enslen H, Boylan JM, Davis RJ, Gruppuso PA. Growth regulation via p38 mitogen-activated protein kinase in developing liver. J Biol Chem 2000;275(49):38716-38721.

Bai C, Richman R, Elledge SJ. Human cyclin F. EMBO J 1994;13(24):6087-6098.

Barr FA, Gruneberg U. Cytokinesis: placing and making the final cut. Cell 2007;131(5):847-860.

Bartlett DC, Hodson J, Bhogal RH, Youster J, Newsome PN. Combined use of N-acetylcysteine and Liberase improves the viability and metabolic function of human hepatocytes isolated from human liver. Cytotherapy 2014;16(6):800-809.

Bataller R, Brenner DA. Liver fibrosis. J Clin Invest 2005;115(2):209-218.

Beenstock J, Ben-Yehuda S, Melamed D, Admon A, Livnah O, Ahn NG, et al. The p38beta mitogen-activated protein kinase possesses an intrinsic autophosphorylation activity, generated by a short region composed of the alpha-G helix and MAPK insert. J Biol Chem 2014; 289(34):23546-23556.

Ben-Levy R, Hooper S, Wilson R, Paterson HF, Marshall CJ. Nuclear export of the stress-activated protein kinase p38 mediated by its substrate MAPKAP kinase-2. Curr Biol 1998;8(19):1049-1057.

Benndorf R, Hayess K, Ryazantsev S, Wieske M, Behlke J, Lutsch G. Phosphorylation and supramolecular organization of murine small heat shock protein HSP25 abolish its actin polymerization-inhibiting activity. J Biol Chem 1994; 269(32):20780-20784.

Bermudez O, Pages G, Gimond C. The dual-specificity MAP kinase phosphatases: critical roles in development and cancer. Am J Physiol Cell Physiol 2010; 299(2):C189-202.

Bernstein BW, Bamburg JR. ADF/cofilin: a functional node in cell biology. Trends Cell Biol 2010; 20(4):187-195.

Berry MN, Friend DS. High-yield preparation of isolated rat liver parenchymal cells: a biochemical and fine structural study. J Cell Biol 1969; 43(3):506-520.

Beyer HS, Sherman R, Zieve L. Aging is associated with reduced liver regeneration and diminished thymidine kinase mRNA content and enzyme activity in the rat. J Lab Clin Med 1991; 117(2):101-108.

Beyer TA, Xu W, Teupser D, auf dem Keller U, Bugnon P, Hildt E, et al. Impaired liver regeneration in Nrf2 knockout mice: role of ROS-mediated insulin/IGF-1 resistance. EMBO J 2008;27(1):212-223.

Bikkavilli RK, Feigin ME, Malbon CC. p38 mitogen-activated protein kinase regulates canonical Wnt-beta-catenin signaling by inactivation of GSK3beta. J Cell Sci 2008; 121(Pt 21):3598-3607.

Block GD, Locker J, Bowen WC, Petersen BE, Katyal S, Strom SC, et al. Population expansion, clonal growth, and specific differentiation patterns in primary cultures of hepatocytes induced by HGF/SF, EGF and TGF alpha in a chemically defined (HGM) medium. J Cell Biol 1996;132(6):1133-1149.

Boivin B, Khairallah M, Cartier R, Allen BG. Characterization of hsp27 kinases activated by elevated aortic pressure in heart. Mol Cell Biochem 2012; 371(1-2):31-42.

Bonavita AG, Quaresma K, Cotta-de-Almeida V, Pinto MA, Saraiva RM, Alves LA. Hepatocyte xenotransplantation for treating liver disease. Xenotransplantation 2010;17(3):181-187.

Borowiak M, Garratt AN, Wustefeld T, Strehle M, Trautwein C, Birchmeier C. Met provides essential signals for liver regeneration. Proc Natl Acad Sci U S A 2004;101(29):10608-10613.

Bouwens L, Wisse E. Pit cells in the liver. Liver 1992;12(1):3-9.

Boyer JL. Tight junctions in normal and cholestatic liver: does the paracellular pathway have functional significance? Hepatology 1983;3(4):614-617.

Bradham CA, Foltz KR, Beane WS, Arnone MI, Rizzo F, Coffman JA, et al. The sea urchin kinome: a first look. Dev Biol 2006;300(1):180-193.

Braet F, Wisse E. Structural and functional aspects of liver sinusoidal endothelial cell fenestrae: a review. Comp Hepatol 2002; 23;1(1):1.

Bucher NL, Swaffield MN, Ditroia JF. The Influence of Age upon the Incorporation of Thymidine-2-C14 into the Dna of Regenerating Rat Liver. Cancer Res 1964;24:509-512.

Budziszewska B, Szymanska M, Leskiewicz M, Basta-Kaim A, Jaworska-Feil L, Kubera M, et al. The decrease in JNK- and p38-MAP kinase activity is accompanied by the enhancement of PP2A phosphate level in the brain of prenatally stressed rats. J Physiol Pharmacol 2010; 61(2):207-215.

Bulavin DV, Amundson SA, Fornace AJ. p38 and Chk1 kinases: different conductors for the G(2)/M checkpoint symphony. Curr Opin Genet Dev 2002;12(1):92-97.

Bulavin DV, Phillips C, Nannenga B, Timofeev O, Donehower LA, Anderson CW, et al. Inactivation of the Wip1 phosphatase inhibits mammary tumorigenesis through p38 MAPK-mediated activation of the p16(Ink4a)-p19(Arf) pathway. Nat Genet 2004;36(4):343-350.

Burruel V, Klooster K, Barker CM, Pera RR, Meyers S. Abnormal early cleavage events predict early embryo demise: sperm oxidative stress and early abnormal cleavage. Sci Rep 2014;4:6598.

Burt AD, Mutton A, Day CP. Diagnosis and interpretation of steatosis and steatohepatitis. Semin Diagn Pathol 1998;15(4):246-258.

Buttrick GJ, Wakefield JG. PI3-K and GSK-3: Akt-ing together with microtubules. Cell Cycle 2008;7(17):2621-2625.

Buxade M, Parra-Palau JL, Proud CG. The Mnks: MAP kinase-interacting kinases (MAP kinase signal-integrating kinases). Front Biosci 2008;13:5359-5373.

Campbell JS, Argast GM, Yuen SY, Hayes B, Fausto N. Inactivation of p38 MAPK during liver regeneration. Int J Biochem Cell Biol 2011;43(2):180-188.

Campo-Ruiz V, Lauwers GY, Anderson RR, Delgado-Baeza E, Gonzalez S. In vivo and ex vivo virtual biopsy of the liver with near-infrared, reflectance confocal microscopy. Mod Pathol 2005;18(2):290-300.

Cara DC, Kaur J, Forster M, McCafferty DM, Kubes P. Role of p38 mitogen-activated protein kinase in chemokine-induced emigration and chemotaxis in vivo. J Immunol 2001;167(11):6552-6558.

Cargnello M, Roux PP. Activation and function of the MAPKs and their substrates, the MAPK-activated protein kinases. Microbiol Mol Biol Rev 2011;75(1):50-83.

Cavalli V, Vilbois F, Corti M, Marcote MJ, Tamura K, Karin M, et al. The stress-induced MAP kinase p38 regulates endocytic trafficking via the GDI:Rab5 complex. Mol Cell 2001;7(2):421-432.

Cave M, Deaciuc I, Mendez C, Song Z, Joshi-Barve S, Barve S, et al. Nonalcoholic fatty liver disease: predisposing factors and the role of nutrition. J Nutr Biochem 2007;18(3):184-195.

Celton-Morizur S, Desdouets C. Polyploidization of liver cells. Adv Exp Med Biol 2010;676:123-135.

Celton-Morizur S, Merlen G, Couton D, Desdouets C. Polyploidy and liver proliferation: central role of insulin signaling. Cell Cycle 2010;9(3):460-466.

Cha H, Wang X, Li H, Fornace AJ,Jr. A functional role for p38 MAPK in modulating mitotic transit in the absence of stress. J Biol Chem 2007;282(31):22984-22992.

Chae KS, Dryer SE. The p38 mitogen-activated protein kinase pathway negatively regulates Ca2+-activated K+ channel trafficking in developing parasympathetic neurons. J Neurochem 2005;94(2):367-379.

Chang E, Heo KS, Woo CH, Lee H, Le NT, Thomas TN, et al. MK2 SUMOylation regulates actin filament remodeling and subsequent migration in endothelial cells by inhibiting MK2 kinase and HSP27 phosphorylation. Blood 2011;117(8):2527-2537.

Chang L, Karin M. Mammalian MAP kinase signalling cascades. Nature 2001;410(6824):37-40.

Chaudhuri S, Smith PG. Cyclic strain-induced HSP27 phosphorylation modulates actin filaments in airway smooth muscle cells. Am J Respir Cell Mol Biol 2008;39(3):270-278.

Chen RH, Sarnecki C, Blenis J. Nuclear localization and regulation of erk- and rsk-encoded protein kinases. Mol Cell Biol 1992;12(3):915-927.

Chen XQ, Wu SH, Zhou Y, Tang YR. Lipoxin A4-induced heme oxygenase-1 protects cardiomyocytes against hypoxia/reoxygenation injury via p38 MAPK activation and Nrf2/ARE complex. PLoS One 2013;8(6):e67120.

Chen Z, Gibson TB, Robinson F, Silvestro L, Pearson G, Xu B, et al. MAP kinases. Chem Rev 2001;101(8):2449-2476.

Cheung PC, Campbell DG, Nebreda AR, Cohen P. Feedback control of the protein kinase TAK1 by SAPK2a/p38alpha. EMBO J 2003;22(21):5793-5805.

Cheung WD, Hart GW. AMP-activated protein kinase and p38 MAPK activate O-GlcNAcylation of neuronal proteins during glucose deprivation. J Biol Chem 2008;283(19):13009-13020.

Chipchase MD, O'Neill M, Melton DW. Characterization of premature liver polyploidy in DNA repair (Ercc1)-deficient mice. Hepatology 2003;38(4):958-966.

Chomczynski P, Sacchi N. Single-step method of RNA isolation by acid guanidinium thiocyanate-phenol-chloroform extraction. Anal Biochem 1987;162(1):156-159.

Chopra P, Kanoje V, Semwal A, Ray A. Therapeutic potential of inhaled p38 mitogen-activated protein kinase inhibitors for inflammatory pulmonary diseases. Expert Opin Investig Drugs 2008;17(10):1411-1425.

Chow JP, Siu WY, Fung TK, Chan WM, Lau A, Arooz T, et al. DNA damage during the spindle-assembly checkpoint degrades CDC25A, inhibits cyclin-CDC2 complexes, and reverses cells to interphase. Mol Biol Cell 2003;14(10):3989-4002.

Chua A, Thomas P, Wijesundera C, Clifton P, Fenech M. Effect of docosahexaenoic acid and furan fatty acids on cytokinesis block micronucleus cytome assay biomarkers in astrocytoma cell lines under conditions of oxidative stress. Environ Mol Mutagen 2014;55(7):573-590.

Clouston AD, Powell EE, Walsh MJ, Richardson MM, Demetris AJ, Jonsson JR. Fibrosis correlates with a ductular reaction in hepatitis C: roles of impaired replication, progenitor cells and steatosis. Hepatology 2005;41(4):809-818.

Coe SJ, Kapur R, Luthardt F, Rabinovitch P, Kramer D. Prenatal diagnosis of tetraploidy: a case report. Am J Med Genet 1993;45(3):378-382.

Comai L. The advantages and disadvantages of being polyploid. Nat Rev Genet 2005;6(11):836-846.

Comes F, Matrone A, Lastella P, Nico B, Susca FC, Bagnulo R, et al. A novel cell type-specific role of p38alpha in the control of autophagy and cell death in colorectal cancer cells. Cell Death Differ 2007;14(4):693-702.

Conlin LK, Thiel BD, Bonnemann CG, Medne L, Ernst LM, Zackai EH, et al. Mechanisms of mosaicism, chimerism and uniparental disomy identified by single nucleotide polymorphism array analysis. Hum Mol Genet 2010;19(7):1263-1275.

Corey KE, Kaplan LM. Obesity and liver disease: the epidemic of the twenty-first century. Clin Liver Dis 2014;18(1):1-18.

Corlu A, Loyer P. Regulation of the g1/s transition in hepatocytes: involvement of the cyclin-dependent kinase cdk1 in the DNA replication. Int J Hepatol 2012;2012:689324.

Correa SA, Eales KL. The Role of p38 MAPK and Its Substrates in Neuronal Plasticity and Neurodegenerative Disease. J Signal Transduct 2012;2012:649079.

Coulthard LR, White DE, Jones DL, McDermott MF, Burchill SA. p38(MAPK): stress responses from molecular mechanisms to therapeutics. Trends Mol Med 2009;15(8):369-379.

Crofton RW, Diesselhoff-den Dulk MM, van Furth R. The origin, kinetics, and characteristics of the Kupffer cells in the normal steady state. J Exp Med 1978;148(1):1-17.

Crosby HA, Nijjar SS, de Goyet Jde V, Kelly DA, Strain AJ. Progenitor cells of the biliary epithelial cell lineage. Semin Cell Dev Biol 2002;13(6):397-403.

Cuadrado A, Lafarga V, Cheung PC, Dolado I, Llanos S, Cohen P, et al. A new p38 MAP kinase-regulated transcriptional coactivator that stimulates p53-dependent apoptosis. EMBO J 2007;26(8):2115-2126.

Cuadrado A, Nebreda AR. Mechanisms and functions of p38 MAPK signalling. Biochem J 2010;429(3):403-417.

Cuenda A, Rouse J, Doza YN, Meier R, Cohen P, Gallagher TF, et al. SB 203580 is a specific inhibitor of a MAP kinase homologue which is stimulated by cellular stresses and interleukin-1. FEBS Lett 1995;364(2):229-233.

Cuenda A, Rousseau S. p38 MAP-kinases pathway regulation, function and role in human diseases. Biochim Biophys Acta 2007;1773(8):1358-1375.

Cuevas BD, Abell AN, Johnson GL. Role of mitogen-activated protein kinase kinase kinases in signal integration. Oncogene 2007;26(22):3159-3171.

d'Adda di Fagagna F. Living on a break: cellular senescence as a DNA-damage response. Nat Rev Cancer 2008;8(7):512-522.

Dahm F, Georgiev P, Clavien PA. Small-for-size syndrome after partial liver transplantation: definition, mechanisms of disease and clinical implications. Am J Transplant 2005;5(11):2605-2610.

Dalakas E, Newsome PN, Harrison DJ, Plevris JN. Hematopoietic stem cell trafficking in liver injury. FASEB J 2005;19(10):1225-1231.

Dalle-Donne I, Rossi R, Milzani A, Di Simplicio P, Colombo R. The actin cytoskeleton response to oxidants: from small heat shock protein phosphorylation to changes in the REDOX state of actin itself. Free Radic Biol Med 2001;31(12):1624-1632.

Dash BC, El-Deiry WS. Phosphorylation of p21 in G2/M promotes cyclin B-Cdc2 kinase activity. Mol Cell Biol 2005;25(8):3364-3387.

Davies T, Canman JC. Stuck in the middle: Rac, adhesion, and cytokinesis.J Cell Biol. 2012;198(5):769-71.

Davies SP, Reddy H, Caivano M, Cohen P. Specificity and mechanism of action of some commonly used protein kinase inhibitors. Biochem J 2000;351(Pt 1):95-105.

Davis T, Rokicki MJ, Bagley MC, Kipling D. The effect of small-molecule inhibition of MAPKAPK2 on cell ageing phenotypes of fibroblasts from human Werner syndrome. Chem Cent J 2013;7(1):18-153X-7-18.

Davis T, Tivey HS, Brook AJ, Kipling D. Nijmegen breakage syndrome fibroblasts expressing the C-terminal truncated NBN protein undergo p38/MK2-dependent premature senescence. Biogerontology 2014, *in press.*

Dayoub R, Vogel A, Schuett J, Lupke M, Spieker SM, Kettern N, et al. Nrf2 activates augmenter of liver regeneration (ALR) via antioxidant response element and links oxidative stress to liver regeneration. Mol Med 2013;19:237-244.

de Nadal E, Posas F. Multilayered control of gene expression by stress-activated protein kinases. EMBO J 2010;29(1):4-13.

del Barco Barrantes I, Nebreda AR. Roles of p38 MAPKs in invasion and metastasis. Biochem Soc Trans 2012;40(1):79-84.

Delhaye M, Louis H, Degraef C, Le Moine O, Deviere J, Peny MO, et al. Hepatocyte proliferative activity in human liver cirrhosis. J Hepatol 1999;30(3):461-471.

Denu JM, Dixon JE. Protein tyrosine phosphatases: mechanisms of catalysis and regulation. Curr Opin Chem Biol 1998;2(5):633-641.

Desbois-Mouthon C, Wendum D, Cadoret A, Rey C, Leneuve P, Blaise A, et al. Hepatocyte proliferation during liver regeneration is impaired in mice with liver-specific IGF-1R knockout. FASEB J 2006;20(6):773-775.

Desmet VJ. Histopathology of cholestasis. Verh Dtsch Ges Pathol 1995;79:233-240.

Dhawan A, Strom SC, Sokal E, Fox IJ. Human hepatocyte transplantation. Methods Mol Biol 2010;640:525-534.

Dickinson RJ, Keyse SM. Diverse physiological functions for dual-specificity MAP kinase phosphatases. J Cell Sci 2006;119(Pt 22):4607-4615.

Diehl AM. Cytokine regulation of liver injury and repair. Immunol Rev 2000;174:160-171.

Dinarello CA, Pomerantz BJ. Proinflammatory cytokines in heart disease. Blood Purif 2001;19(3):314-321.

Dolado I, Nebreda AR. AKT and oxidative stress team up to kill cancer cells. Cancer Cell 2008;14(6):427-429.

Dolado I, Swat A, Ajenjo N, De Vita G, Cuadrado A, Nebreda AR. p38alpha MAP kinase as a sensor of reactive oxygen species in tumorigenesis. Cancer Cell 2007;11(2):191-205.

Dreissigacker U, Mueller MS, Unger M, Siegert P, Genze F, Gierschik P, et al. Oncogenic K-Ras down-regulates Rac1 and RhoA activity and enhances migration and invasion of pancreatic carcinoma cells through activation of p38. Cell Signal 2006;18(8):1156-1168.

Dubroca C, You D, Levy BI, Loufrani L, Henrion D. Involvement of RhoA/Rho kinase pathway in myogenic tone in the rabbit facial vein. Hypertension 2005;45(5):974-979.

Duch A, de Nadal E, Posas F. The p38 and Hog1 SAPKs control cell cycle progression in response to environmental stresses. FEBS Lett 2012;586(18):2925-2931.

Duncan AW, Hanlon Newell AE, Smith L, Wilson EM, Olson SB, Thayer MJ, et al. Frequent aneuploidy among normal human hepatocytes. Gastroenterology 2012;142(1):25-28.

Duncan AW, Soto-Gutierrez A. Liver repopulation and regeneration: new approaches to old questions. Curr Opin Organ Transplant 2013;18(2):197-202.

Duncan AW, Taylor MH, Hickey RD, Hanlon Newell AE, Lenzi ML, Olson SB, et al. The ploidy conveyor of mature hepatocytes as a source of genetic variation. Nature 2010;467(7316):707-710.

Dunne JB, Davenport M, Williams R, Tredger JM. Evidence that S-adenosylmethionine and N-acetylcysteine reduce injury from sequential cold and warm ischemia in the isolated perfused rat liver. Transplantation 1994;57(8):1161-1168.

Dutkowski P, Linecker M, DeOliveira ML, Mullhaupt B, Clavien PA. Challenges to Liver Transplantation and Strategies to Improve Outcomes. Gastroenterology 2014, *in press.*

Eferl R, Ricci R, Kenner L, Zenz R, David JP, Rath M, et al. Liver tumor development. c-Jun antagonizes the proapoptotic activity of p53. Cell 2003;112(2):181-192.

Engel FB, Schebesta M, Duong MT, Lu G, Ren S, Madwed JB, et al. p38 MAP kinase inhibition enables proliferation of adult mammalian cardiomyocytes. Genes Dev 2005;19(10):1175-1187.

Engelman JA, Lisanti MP, Scherer PE. Specific inhibitors of p38 mitogen-activated protein kinase block 3T3-L1 adipogenesis. J Biol Chem 1998;273(48):32111-32120.

Enomoto A, Murakami H, Asai N, Morone N, Watanabe T, Kawai K, et al. Akt/PKB regulates actin organization and cell motility via Girdin/APE. Dev Cell 2005;9(3):389-402.

Etienne PL, Baffet G, Desvergne B, Boisnard-Rissel M, Glaise D, Guguen-Guillouzo C. Transient expression of c-fos and constant expression of c-myc in freshly isolated and cultured normal adult rat hepatocytes. Oncogene Res 1988;3(3):255-262.

Everson GT, Lawson MJ, McKinley C, Showalter R, Kern F,Jr. Gallbladder and small intestinal regulation of biliary lipid secretion during intraduodenal infusion of standard stimuli. J Clin Invest 1983;71(3):596-603.

Fabrikant JI. The kinetics of cellular proliferation in regenerating liver. J Cell Biol 1968;36(3):551-565.

Faggioli F, Vezzoni P, Montagna C. Single-cell analysis of ploidy and centrosomes underscores the peculiarity of normal hepatocytes. PLoS One 2011;6(10).

Fan L, Yang X, Du J, Marshall M, Blanchard K, Ye X. A novel role of p38 alpha MAPK in mitotic progression independent of its kinase activity. Cell Cycle 2005;4(11):1616-1624.

Faridi J, Fawcett J, Wang L, Roth RA. Akt promotes increased mammalian cell size by stimulating protein synthesis and inhibiting protein degradation. Am J Physiol Endocrinol Metab 2003;285(5):E964-72.

Faust D, Schmitt C, Oesch F, Oesch-Bartlomowicz B, Schreck I, Weiss C, et al. Differential p38-dependent signalling in response to cellular stress and mitogenic stimulation in fibroblasts. Cell Commun Signal 2012;10:6-811X-10-6.

Fausto N. Liver regeneration. J Hepatol 2000;32(1 Suppl):19-31.

Ferrari G, Terushkin V, Wolff MJ, Zhang X, Valacca C, Poggio P, et al. TGF-beta1 induces endothelial cell apoptosis by shifting VEGF activation of p38(MAPK) from the prosurvival p38beta to proapoptotic p38alpha. Mol Cancer Res 2012;10(5):605-614.

Fickert P, Zollner G, Fuchsbichler A, Stumptner C, Weiglein AH, Lammert F, et al. Ursodeoxycholic acid aggravates bile infarcts in bile duct-ligated and Mdr2 knockout mice via disruption of cholangioles. Gastroenterology 2002;123(4):1238-1251.

Finkel T. Oxidant signals and oxidative stress. Curr Opin Cell Biol 2003;15(2):247-254.

Finkel T, Holbrook NJ. Oxidants, oxidative stress and the biology of ageing. Nature 2000 Nov 9;408(6809):239-247.

Freund A, Patil CK, Campisi J. p38MAPK is a novel DNA damage response-independent regulator of the senescence-associated secretory phenotype. EMBO J 2011;30(8):1536-1548.

Friedman SL. Liver fibrosis -- from bench to bedside. J Hepatol 2003;38 Suppl 1:S38-53.

Fujii R, Yamashita S, Hibi M, Hirano T. Asymmetric p38 activation in zebrafish: its possible role in symmetric and synchronous cleavage. J Cell Biol 2000 150(6):1335-1348.

Funayama R, Ishikawa F. Cellular senescence and chromatin structure. Chromosoma 2007;116(5):431-440.

Gaestel M. MAPKAP kinases - MKs - two's company, three's a crowd. Nat Rev Mol Cell Biol 2006;7(2):120-130.

Gallardo MH, Gonzalez CA, Cebrian I. Molecular cytogenetics and allotetraploidy in the red vizcacha rat, Tympanoctomys barrerae (Rodentia, Octodontidae). Genomics 2006;88(2):214-221.

Gamell C, Susperregui AG, Bernard O, Rosa JL, Ventura F. The p38/MK2/Hsp25 pathway is required for BMP-2-induced cell migration. PLoS One 2011;6(1):e16477.

Gandillet A, Alexandre E, Royer C, Cinqualbre J, Jaeck D, Richert L. Hepatocyte ploidy in regenerating livers after partial hepatectomy, drug-induced necrosis, and cirrhosis. Eur Surg Res 2003;35(3):148-160.

Ganem NJ, Godinho SA, Pellman D. A mechanism linking extra centrosomes to chromosomal instability. Nature 2009;460(7252):278-82.

Gao Y, Gao G, Long C, Han S, Zu P, Fang L, et al. Enhanced phosphorylation of cyclic AMP response element binding protein in the brain of mice following repetitive hypoxic exposure. Biochem Biophys Res Commun 2006;340(2):661-667.

Gardiner TA, Gibson DS, de Gooyer TE, de la Cruz VF, McDonald DM, Stitt AW. Inhibition of tumor necrosis factor-alpha improves physiological angiogenesis and reduces pathological neovascularization in ischemic retinopathy. Am J Pathol 2005;166(2):637-644.

Ge B, Gram H, Di Padova F, Huang B, New L, Ulevitch RJ, et al. MAPKK-independent activation of p38alpha mediated by TAB1-dependent autophosphorylation of p38alpha. Science 2002;295(5558):1291-1294.

Gebhardt R, Ueberham E. Zonal gene expression in murine liver: Are tumors helping us to solve the mystery? Hepatology 2006; 44(2):512; author reply 512-3.

Gentric G, Celton-Morizur S, Desdouets C. Polyploidy and liver proliferation. Clin Res Hepatol Gastroenterol 2012;36(1):29-34.

Gentric G, Desdouets C, Celton-Morizur S. Hepatocytes polyploidization and cell cycle control in liver physiopathology. Int J Hepatol 2012;2012:282430.

George L, Lokhandwala MF, Asghar M. Exercise activates REDOX-sensitive transcription factors and restores renal D1 receptor function in old rats. Am J Physiol Renal Physiol 2009;297(5):F1174-80.

George LE, Lokhandwala MF, Asghar M. Novel role of NF-kappaB-p65 in antioxidant homeostasis in human kidney-2 cells. Am J Physiol Renal Physiol 2012 J;302(11):F1440-6.

Georgiev P, Jochum W, Heinrich S, Jang JH, Nocito A, Dahm F, et al. Characterization of time-related changes after experimental BDL. Br J Surg 2008;95(5):646-656.

(Gerits N, Mikalsen T, Kostenko S, Shiryaev A, Johannessen M, Moens U. Modulation of F-actin rearrangement by the cyclic AMP/cAMP-dependent protein kinase (PKA) pathway is mediated by MAPK-activated protein kinase 5 and requires PKA-induced nuclear export of MK5. J Biol Chem 2007; 282(51):37232-37243.

Gerlyng P, Abyholm A, Grotmol T, Erikstein B, Huitfeldt HS, Stokke T, et al. Binucleation and polyploidization patterns in developmental and regenerative rat liver growth. Cell Prolif 1993;26(6):557-565.

Gerlyng P, Grotmol T, Seglen PO. Effect of 4-acetylaminofluorene and other tumour promoters on hepatocellular growth and binucleation. Carcinogenesis 1994;15(2):371-379.

Gibert B, Eckel B, Fasquelle L, Moulin M, Bouhallier F, Gonin V, et al. Knock down of heat shock protein 27 (HspB1) induces degradation of several putative client proteins. PLoS One 2012;7(1):e29719.

Girard J, Ferre P, Pegorier JP, Duee PH. Adaptations of glucose and fatty acid metabolism during perinatal period and suckling-weaning transition. Physiol Rev 1992;72(2):507-562.

Goedert M, Cuenda A, Craxton M, Jakes R, Cohen P. Activation of the novel stress-activated protein kinase SAPK4 by cytokines and cellular stresses is mediated by SKK3 (MKK6); comparison of its substrate specificity with that of other SAP kinases. EMBO J 1997;16(12):3563-3571.

Goldstein DM, Kuglstatter A, Lou Y, Soth MJ. Selective p38alpha inhibitors clinically evaluated for the treatment of chronic inflammatory disorders. J Med Chem 2010; 53(6):2345-2353.

Gomez-Lechon MJ, Lahoz A, Jimenez N, Bonora A, Castell JV, Donato MT. Evaluation of drug-metabolizing and functional competence of human hepatocytes incubated under hypothermia in different media for clinical infusion. Cell Transplant 2008;17(8):887-897.

Goncharova EA, Vorotnikov AV, Gracheva EO, Wang CL, Panettieri RA,Jr, Stepanova VV, et al. Activation of p38 MAP-kinase and caldesmon phosphorylation are essential for urokinase-induced human smooth muscle cell migration. Biol Chem 2002;383(1):115-126.

Gordon GJ, Coleman WB, Grisham JW. Temporal analysis of hepatocyte differentiation by small hepatocyte-like progenitor cells during liver regeneration in retrorsine-exposed rats. Am J Pathol 2000;157(3):771-786.

Gorla GR, Malhi H, Gupta S. Polyploidy associated with oxidative injury attenuates proliferative potential of cells. J Cell Sci 2001;114(Pt 16):2943-2951.

Grisham JW. A morphologic study of deoxyribonucleic acid synthesis and cell proliferation in regenerating rat liver; autoradiography with thymidine-H3. Cancer Res 1962;22:842-849.

Grizzi F, Chiriva-Internati M. Human binucleate hepatocytes: are they a defence during chronic liver diseases? Med Hypotheses 2007;69(2):258-261.

Gromley A, Yeaman C, Rosa J, Redick S, Chen CT, Mirabelle S, et al. Centriolin anchoring of exocyst and SNARE complexes at the midbody is required for secretory-vesicle-mediated abscission. Cell 2005;123(1):75-87.

Grompe M. Pancreatic-hepatic switches in vivo. Mech Dev 2003;120(1):99-106.

Guay J, Lambert H, Gingras-Breton G, Lavoie JN, Huot J, Landry J. Regulation of actin filament dynamics by p38 map kinase-mediated phosphorylation of heat shock protein 27. J Cell Sci 1997;110 (Pt 3)(Pt 3):357-368.

Guidotti JE, Bregerie O, Robert A, Debey P, Brechot C, Desdouets C. Liver cell polyploidization: a pivotal role for binuclear hepatocytes. J Biol Chem 2003;278(21):19095-19101.

Guo JH, Wang HY, Malbon CC. Conditional, tissue-specific expression of Q205L Galphai2 in vivo mimics insulin activation of c-Jun N-terminal kinase and p38 kinase. J Biol Chem 1998;273(26):16487-16493.

Gupta S. Hepatic polyploidy and liver growth control. Semin Cancer Biol 2000;10(3):161-171.

Gutierrez-Uzquiza A, Arechederra M, Bragado P, Aguirre-Ghiso JA, Porras A. p38alpha mediates cell survival in response to oxidative stress via induction of antioxidant genes: effect on the p70S6K pathway. J Biol Chem 2012;287(4):2632-2642.

Halawani D, Mondeh R, Stanton LA, Beier F. p38 MAP kinase signaling is necessary for rat chondrosarcoma cell proliferation. Oncogene 2004;23(20):3726-3731.

Halilbasic E, Baghdasaryan A, Trauner M. Nuclear receptors as drug targets in cholestatic liver diseases. Clin Liver Dis 2013;17(2):161-189.

Han J, Lee JD, Bibbs L, Ulevitch RJ. A MAP kinase targeted by endotoxin and hyperosmolarity in mammalian cells. Science 1994;265(5173):808-811.

Han J, Sun P. The pathways to tumor suppression via route p38. Trends Biochem Sci 2007;32(8):364-371.

Hartwell LH, Kastan MB. Cell cycle control and cancer. Science 1994;266(5192):1821-1828.

Hayashi MT, Karlseder J. DNA damage associated with mitosis and cytokinesis failure. Oncogene 2013;32(39):4593-4601.

Hedges JC, Dechert MA, Yamboliev IA, Martin JL, Hickey E, Weber LA, et al. A role for p38(MAPK)/HSP27 pathway in smooth muscle cell migration. J Biol Chem 1999;274(34):24211-24219.

Heinrich S, Georgiev P, Weber A, Vergopoulos A, Graf R, Clavien PA. Partial BDL in mice: a novel model of acute cholestasis. Surgery 2011;149(3):445-451.

Higgins, G. M., and Anderson, R. M. Experimental pathology of the liver. 1. Restoration of the liver of the white rat following partial surgical removal. Arch. Pathol. 1931;186-202.

Heinrichsdorff J, Luedde T, Perdiguero E, Nebreda AR, Pasparakis M. p38 alpha MAPK inhibits JNK activation and collaborates with IkappaB kinase 2 to prevent endotoxin-induced liver failure. EMBO Rep 200;9(10):1048-1054.

Hillebrandt S, Goos C, Matern S, Lammert F. Genome-wide analysis of hepatic fibrosis in inbred mice identifies the susceptibility locus Hfib1 on chromosome 15. Gastroenterology 2002;123(6):2041-2051.

Hillebrandt S, Wasmuth HE, Weiskirchen R, Hellerbrand C, Keppeler H, Werth A, et al. Complement factor 5 is a quantitative trait gene that modifies liver fibrogenesis in mice and humans. Nat Genet 2005;37(8):835-843.

Hirschfield GM, Heathcote EJ, Gershwin ME. Pathogenesis of cholestatic liver disease and therapeutic approaches. Gastroenterology 2010;139(5):1481-1496.

Hixon ML, Muro-Cacho C, Wagner MW, Obejero-Paz C, Millie E, Fujio Y, et al. Akt1/PKB upregulation leads to vascular smooth muscle cell hypertrophy and polyploidization. J Clin Invest 2000;106(8):1011-1020.

Hixon ML, Obejero-Paz C, Muro-Cacho C, Wagner MW, Millie E, Nagy J, et al. Cks1 mediates vascular smooth muscle cell polyploidization. J Biol Chem 2000;275(51):40434-40442.

Ho YF, Karsani SA, Yong WK, Abd Malek SN. Induction of apoptosis and cell cycle blockade by helichrysetin in a549 human lung adenocarcinoma cells. Evid Based Complement Alternat Med 2013;2013:857257.

Hoare M, Das T, Alexander G. Ageing, telomeres, senescence, and liver injury. J Hepatol 2010;53(5):950-961.

Hochedlinger K, Wagner EF, Sabapathy K. Differential effects of JNK1 and JNK2 on signal specific induction of apoptosis. Oncogene 2002;21(15):2441-2445.

Hoenerhoff MJ, Pandiri AR, Lahousse SA, Hong HH, Ton TV, Masinde T, et al. Global gene profiling of spontaneous hepatocellular carcinoma in B6C3F1 mice: similarities in the molecular landscape with human liver cancer. Toxicol Pathol 2011;39(4):678-699.

Hong J, Zhou J, Fu J, He T, Qin J, Wang L, et al. Phosphorylation of serine 68 of Twist1 by MAPKs stabilizes Twist1 protein and promotes breast cancer cell invasiveness. Cancer Res 2011;71(11):3980-3990.

Hori T, Ohashi N, Chen F, Baine AM, Gardner LB, Hata T, et al. Simple and reproducible hepatectomy in the mouse using the clip technique. World J Gastroenterol 2012;18(22):2767-2774.

Hsieh CC, Rosenblatt JI, Papaconstantinou J. Age-associated changes in SAPK/JNK and p38 MAPK signaling in response to the generation of ROS by 3-nitropropionic acid. Mech Ageing Dev 2003;124(6):733-746.

Hsieh YH, Wu TT, Huang CY, Hsieh YS, Hwang JM, Liu JY. p38 mitogen-activated protein kinase pathway is involved in protein kinase Calpha-regulated invasion in human hepatocellular carcinoma cells. Cancer Res 2007;67(9):4320-4327.

Hu M, Zou Y, Nambiar SM, Lee J, Yang Y, Dai G. Keap1 modulates the REDOX cycle and hepatocyte cell cycle in regenerating liver. Cell Cycle 2014;13(15).

Hu P, Nebreda AR, Liu Y, Carlesso N, Kaplan M, Kapur R. p38alpha protein negatively regulates T helper type 2 responses by orchestrating multiple T cell receptor-associated signals. J Biol Chem 2012;287(40):33215-33226.

Huang C, Borchers CH, Schaller MD, Jacobson K. Phosphorylation of paxillin by p38MAPK is involved in the neurite extension of PC-12 cells. J Cell Biol 2004;164(4):593-602.

Hughes RD, Mitry RR, Dhawan A, Lehec SC, Girlanda R, Rela M, et al. Isolation of hepatocytes from livers from non-heart-beating donors for cell transplantation. Liver Transpl 2006;12(5):713-717.

Huh CG, Factor VM, Sanchez A, Uchida K, Conner EA, Thorgeirsson SS. Hepatocyte growth factor/c-met signaling pathway is required for efficient liver regeneration and repair. Proc Natl Acad Sci U S A 2004;101(13):4477-4482.

Hui K, Yang Y, Shi K, Luo H, Duan J, An J, et al. The p38 MAPK-regulated PKD1/CREB/Bcl-2 pathway contributes to selenite-induced colorectal cancer cell apoptosis in vitro and in vivo. Cancer Lett 2014;354(1):189-199.

Hui L, Bakiri L, Mairhorfer A, Schweifer N, Haslinger C, Kenner L, et al. p38alpha suppresses normal and cancer cell proliferation by antagonizing the JNK-c-Jun pathway. Nat Genet 2007;39(6):741-749.

Hui L, Bakiri L, Stepniak E, Wagner EF. P38alpha: a Suppressor of Cell Proliferation and Tumorigenesis. Cell Cycle 2007;6(20):2429-2433.

Huot J, Houle F, Rousseau S, Deschesnes RG, Shah GM, Landry J. SAPK2/p38-dependent F-actin reorganization regulates early membrane blebbing during stress-induced apoptosis. J Cell Biol 1998;143(5):1361-1373.

Im JS, Lee JK. ATR-dependent activation of p38 MAP kinase is responsible for apoptotic cell death in cells depleted of Cdc7. J Biol Chem 2008;283(37):25171-25177.

Jacinto E, Loewith R, Schmidt A, Lin S, Ruegg MA, Hall A, et al. Mammalian TOR complex 2 controls the actin cytoskeleton and is rapamycin insensitive. Nat Cell Biol 2004;6(11):1122-1128.

Jans R, Atanasova G, Jadot M, Poumay Y. Cholesterol depletion upregulates involucrin expression in epidermal keratinocytes through activation of p38. J Invest Dermatol 2004;123(3):564-573.

Jeffrey KL, Camps M, Rommel C, Mackay CR. Targeting dual-specificity phosphatases: manipulating MAP kinase signalling and immune responses. Nat Rev Drug Discov 2007;6(5):391-403.

Jiang Y, Gram H, Zhao M, New L, Gu J, Feng L, et al. Characterization of the structure and function of the fourth member of p38 group mitogen-activated protein kinases, p38delta. J Biol Chem 1997;272(48):30122-30128.

Jirmanova L, Sarma DN, Jankovic D, Mittelstadt PR, Ashwell JD. Genetic disruption of p38alpha Tyr323 phosphorylation prevents T-cell receptor-mediated p38alpha activation and impairs interferon-gamma production. Blood 2009;113(10):2229-2237.

Jirmanova L, Bulavin DV, Fornace AJ,Jr. Inhibition of the ATR/Chk1 pathway induces a p38-dependent S-phase delay in mouse embryonic stem cells. Cell Cycle 2005; 4(10):1428-1434.

Johnson GL, Lapadat R. Mitogen-activated protein kinase pathways mediated by ERK, JNK, and p38 protein kinases. Science 2002 Dec 6;298(5600):1911-1912.

Jones NC, Tyner KJ, Nibarger L, Stanley HM, Cornelison DD, Fedorov YV, et al. The p38alpha/beta MAPK functions as a molecular switch to activate the quiescent satellite cell. J Cell Biol 2005;169(1):105-116.

Jorns C, Ellis EC, Nowak G, Fischler B, Nemeth A, Strom SC, et al. Hepatocyte transplantation for inherited metabolic diseases of the liver. J Intern Med 2012;272(3):201-223.

Junqueira LC, Cossermelli W, Brentani R. Differential staining of collagens type I, II and III by Sirius Red and polarization microscopy. Arch Histol Jpn 1978;41(3):267-274.

Kakinuma N, Roy BC, Zhu Y, Wang Y, Kiyama R. Kank regulates RhoA-dependent formation of actin stress fibers and cell migration via 14-3-3 in PI3K-Akt signaling. J Cell Biol 2008;181(3):537-549.

Kang JS, Bae GU, Yi MJ, Yang YJ, Oh JE, Takaesu G, et al. A Cdo-Bnip-2-Cdc42 signaling pathway regulates p38alpha/beta MAPK activity and myogenic differentiation. J Cell Biol 2008;182(3):497-507.

Karageorgos N, Patsoukis N, Chroni E, Konstantinou D, Assimakopoulos SF, Georgiou C. Effect of N-acetylcysteine, allopurinol and vitamin E on jaundice-induced brain oxidative stress in rats. Brain Res 2006;1111(1):203-212.

Karin M. Nuclear factor-kappaB in cancer development and progression. Nature 2006;441(7092):431-436.

Kato K, Tokuda H, Natsume H, Adachi S, Matsushima-Nishiwaki R, Minamitani C, et al. Rho-kinase regulates prostaglandin D(2)-stimulated heat shock protein 27 induction in osteoblasts. Exp Ther Med 2010;1(4):579-583.

Katoh K, Kano Y, Amano M, Onishi H, Kaibuchi K, Fujiwara K. Rho-kinase--mediated contraction of isolated stress fibers. J Cell Biol 2001;153(3):569-584.

Kellendonk C, Opherk C, Anlag K, Schutz G, Tronche F. Hepatocyte-specific expression of Cre recombinase. Genesis 2000;26(2):151-153.

Khurana A, Nakayama K, Williams S, Davis RJ, Mustelin T, Ronai Z. Regulation of the ring finger E3 ligase Siah2 by p38 MAPK. J Biol Chem 2006;281(46):35316-35326.

Kidd D, Raff JW. LK6, a short lived protein kinase in Drosophila that can associate with microtubules and centrosomes. J Cell Sci 1997;110: 209-219.

Kim C, Sano Y, Todorova K, Carlson BA, Arpa L, Celada A, et al. The kinase p38 alpha serves cell type-specific inflammatory functions in skin injury and coordinates pro- and anti-inflammatory gene expression. Nat Immunol 2008;9(9):1019-1027.

Kim HS, Park EJ, Park SW, Kim HJ, Chang KC. A tetrahydroisoquinoline alkaloid THI-28 reduces LPS-induced HMGB1 and diminishes organ injury in septic mice through p38 and PI3K/Nrf2/HO-1 signals. Int Immunopharmacol 201;17(3):684-692.

(Kim L, Del Rio L, Butcher BA, Mogensen TH, Paludan SR, Flavell RA, et al. p38 MAPK autophosphorylation drives macrophage IL-12 production during intracellular infection. J Immunol 2005;174(7):4178-4184.

Kinosita R. Studies on the cancerogenic chemical substances. Trans Soc Pathol Jpn. 1937;27:329–334

Koniaris LG, McKillop IH, Schwartz SI, Zimmers TA. Liver regeneration. J Am Coll Surg 2003;197(4):634-659.

Koshikawa M, Mukoyama M, Mori K, Suganami T, Sawai K, Yoshioka T, et al. Role of p38 mitogen-activated protein kinase activation in podocyte injury and proteinuria in experimental nephrotic syndrome. J Am Soc Nephrol 2005;16(9):2690-2701.

Kotlyarov A, Neininger A, Schubert C, Eckert R, Birchmeier C, Volk HD, et al. MAPKAP kinase 2 is essential for LPS-induced TNF-alpha biosynthesis. Nat Cell Biol 1999;1(2):94-97.

Kouroumalis E, Notas G. Pathogenesis of primary biliary cirrhosis: a unifying model. World J Gastroenterol 2006;12(15):2320-2327.

Krupczak-Hollis K, Wang X, Dennewitz MB, Costa RH. Growth hormone stimulates proliferation of old-aged regenerating liver through forkhead box m1b. Hepatology 2003;38(6):1552-1562.

Kudryavtsev BN, Kudryavtseva MV, Sakuta GA, Stein GI. Human hepatocyte polyploidization kinetics in the course of life cycle. Virchows Arch B Cell Pathol Incl Mol Pathol 1993;64(6):387-393.

Kuma Y, Campbell DG, Cuenda A. Identification of glycogen synthase as a new substrate for stress-activated protein kinase 2b/p38beta. Biochem J 2004;379(Pt 1):133-139.

Kuma Y, Sabio G, Bain J, Shpiro N, Marquez R, Cuenda A. BIRB796 inhibits all p38 MAPK isoforms in vitro and in vivo. J Biol Chem 2005;280(20):19472-19479.

Kumar S, Jiang MS, Adams JL, Lee JC. Pyridinylimidazole compound SB 203580 inhibits the activity but not the activation of p38 mitogen-activated protein kinase. Biochem Biophys Res Commun 1999;263(3):825-831.

Kumar S, McDonnell PC, Gum RJ, Hand AT, Lee JC, Young PR. Novel homologues of CSBP/p38 MAP kinase: activation, substrate specificity and sensitivity to inhibition by pyridinyl imidazoles. Biochem Biophys Res Commun 1997;235(3):533-538.

Kummer JL, Rao PK, Heidenreich KA. Apoptosis induced by withdrawal of trophic factors is mediated by p38 mitogen-activated protein kinase. J Biol Chem 1997; 272(33):20490-20494.

Kuper C, Beck FX, Neuhofer W. NFAT5-mediated expression of S100A4 contributes to proliferation and migration of renal carcinoma cells. Front Physiol 2014;5:293.

Kyriakis JM, Avruch J. Mammalian mitogen-activated protein kinase signal transduction pathways activated by stress and inflammation. Physiol Rev 2001;81(2):807-869.

Kyriakis JM and Avruch J.. Sounding the alarm: protein kinase cascades activated by stress and inflammation. J Biol Chem. 1996;271(40):24313-6.

Lagadec C, Meignan S, Adriaenssens E, Foveau B, Vanhecke E, Romon R, et al. TrkA overexpression enhances growth and metastasis of breast cancer cells. Oncogene 2009;28(18):1960-1970.

Lahousse SA, Hoenerhoff M, Collins J, Ton TV, Masinde T, Olson D, et al. Gene expression and mutation assessment provide clues of genetic and epigenetic mechanisms in liver tumors of oxazepam-exposed mice. Vet Pathol 2011;48(4):875-884.

Lai PH, Sielaff TD, Hu WS. Sustaining a bioartificial liver under hypothermic conditions. Tissue Eng 2005;11(3-4):427-437.

Lavoie JN, L'Allemain G, Brunet A, Muller R, Pouyssegur J. Cyclin D1 expression is regulated positively by the p42/p44MAPK and negatively by the p38/HOGMAPK pathway. J Biol Chem 1996;271(34):20608-20616.

Lebel M, de Souza-Pinto NC, Bohr VA. Metabolism, genomics, and DNA repair in the mouse aging liver. Curr Gerontol Geriatr Res 2011;2011:859415.

Lee HS, Lee GS, Kim SH, Kim HK, Suk DH, Lee DS. Anti-oxidizing effect of the dichloromethane and hexane fractions from Orostachys japonicus in LPS-stimulated RAW 264.7 cells via upregulation of Nrf2 expression and activation of MAPK signaling pathway. BMB Rep 2014;47(2):98-103.

Lee K, Kenny AE, Rieder CL. P38 mitogen-activated protein kinase activity is required during mitosis for timely satisfaction of the mitotic checkpoint but not for the fidelity of chromosome segregation. Mol Biol Cell 2010;21(13):2150-2160.

Lemaigre F, Zaret KS. Liver development update: new embryo models, cell lineage control, and morphogenesis. Curr Opin Genet Dev 2004;14(5):582-590.

Lemire JM, Shiojiri N, Fausto N. Oval cell proliferation and the origin of small hepatocytes in liver injury induced by D-galactosamine. Am J Pathol 1991;139(3):535-552.

Li J, Miller EJ, Ninomiya-Tsuji J, Russell RR,3rd, Young LH. AMP-activated protein kinase activates p38 mitogen-activated protein kinase by increasing recruitment of p38 MAPK to TAB1 in the ischemic heart. Circ Res 2005;97(9):872-879.

Li M, Liu J, Zhang C. Evolutionary history of the vertebrate mitogen activated protein kinases family. PLoS One 2011;6(10).

Liang J, Slingerland JM. Multiple roles of the PI3K/PKB (Akt) pathway in cell cycle progression. Cell Cycle 2003;2(4):339-345.

Lin LC, Hsu SL, Wu CL, Hsueh CM. TGFbeta can stimulate the p/beta-catenin/PPARgamma signaling pathway to promote the EMT, invasion and migration of non-small cell lung cancer (H460 cells). Clin Exp Metastasis 2014, *in press.*

Liu L, Rezvani HR, Back JH, Hosseini M, Tang X, Zhu Y, et al. Inhibition of p38 MAPK signaling augments skin tumorigenesis via NOX2 driven ROS generation. PLoS One 2014;9(5).

Liu X, Ma B, Malik AB, Tang H, Yang T, Sun B, et al. Bidirectional regulation of neutrophil migration by mitogen-activated protein kinases. Nat Immunol 2012;13(5):457-464.

Llanos S, Cuadrado A, Serrano M. MSK2 inhibits p53 activity in the absence of stress. Sci Signal 2009;2(89).

Loyer P, Cariou S, Glaise D, Bilodeau M, Baffet G, Guguen-Guillouzo C. Growth factor dependence of progression through G1 and S phases of adult rat hepatocytes in vitro. Evidence of a mitogen restriction point in mid-late G1. J Biol Chem 1996; 271(19):11484-11492.

Lu P, Prost S, Caldwell H, Tugwood JD, Betton GR, Harrison DJ. Microarray analysis of gene expression of mouse hepatocytes of different ploidy. Mamm Genome 2007;18(9):617-626.

Lu X, Li C, Wang YK, Jiang K, Gai XD. Sorbitol induces apoptosis of human colorectal cancer cells via p38 MAPK signal transduction. Oncol Lett 2014;7(6):1992-1996.

Ma XM, Shen ZH, Liu ZY, Wang F, Hai L, Gao LT, et al. Heparanase promotes human gastric cancer cells migration and invasion by increasing Src and p38 phosphorylation expression. Int J Clin Exp Pathol 2014;7(9):5609-5621.

MacGowan GA, Mann DL, Kormos RL, Feldman AM, Murali S. Circulating interleukin-6 in severe heart failure. Am J Cardiol 1997;79(8):1128-1131.

Magadum S, Banerjee U, Murugan P, Gangapur D, Ravikesavan R. Gene duplication as a major force in evolution. J Genet 2013;92(1):155-161.

Mahtani KR, Brook M, Dean JL, Sully G, Saklatvala J, Clark AR. Mitogen-activated protein kinase p38 controls the expression and posttranslational modification of tristetraprolin, a regulator of tumor necrosis factor alpha mRNA stability. Mol Cell Biol 2001;21(19):6461-6469.

Malan V, Vekemans M, Turleau C. Chimera and other fertilization errors. Clin Genet 2006;70(5):363-373.

Malhi H, Gores GJ. Cellular and molecular mechanisms of liver injury. Gastroenterology 2008;134(6):1641-1654.

Malarkey DE, Johnson K, Ryan L, Boorman G, Maronpot RR. New insights into functional aspects of liver morphology. Toxicol Pathol 2005;33(1):27-34.

Malumbres M, Barbacid M. Cell cycle, CDKs and cancer: a changing paradigm. Nat Rev Cancer 2009;9(3):153-166.

Man W, Ming D, Fang D, Chao L, Jing C. Dimethyl sulfoxide attenuates hydrogen peroxide-induced injury in cardiomyocytes via heme oxygenase-1. J Cell Biochem 2014;115(6):1159-1165.

Mao SA, Glorioso JM, Nyberg SL. Liver regeneration. Transl Res 2014;163(4):352-362.

Margall-Ducos G, Celton-Morizur S, Couton D, Bregerie O, Desdouets C. Liver tetraploidization is controlled by a new process of incomplete cytokinesis. J Cell Sci 2007;120(Pt 20):3633-3639.

Marino IR, Doyle HR, Aldrighetti L, Doria C, McMichael J, Gayowski T, et al. Effect of donor age and sex on the outcome of liver transplantation. Hepatology 1995; 22(6):1754-1762.

Markovic J, Borras C, Ortega A, Sastre J, Vina J, Pallardo FV. Glutathione is recruited into the nucleus in early phases of cell proliferation. J Biol Chem 2007;282(28):20416-20424.

Markovic J, Mora NJ, Broseta AM, Gimeno A, de-la-Concepcion N, Vina J, et al. The depletion of nuclear glutathione impairs cell proliferation in 3t3 fibroblasts. PLoS One 2009;4(7):e6413.

Mateescu B, Batista L, Cardon M, Gruosso T, de Feraudy Y, Mariani O, et al. miR-141 and miR-200a act on ovarian tumorigenesis by controlling oxidative stress response. Nat Med 2011;17(12):1627-1635.

Matsuyama W, Faure M, Yoshimura T. Activation of discoidin domain receptor 1 facilitates the maturation of human monocyte-derived dendritic cells through the TNF receptor associated factor 6/TGF-beta-activated protein kinase 1 binding protein 1 beta/p38 alpha mitogen-activated protein kinase signaling cascade. J Immunol 2003;171(7):3520-3532.

Mattos LJ, Valenca SS, Azevedo SM, Soares RM. Dualistic evolution of liver damage in mice triggered by a single sublethal exposure to Microcystin-LR. Toxicon 2014; 83:43-51.

Mead JE, Fausto N. Transforming growth factor alpha may be a physiological regulator of liver regeneration by means of an autocrine mechanism. Proc Natl Acad Sci U S A 1989;86(5):1558-1562.

Meier R, Rouse J, Cuenda A, Nebreda AR, Cohen P. Cellular stresses and cytokines activate multiple mitogen-activated-protein kinase kinase homologues in PC12 and KB cells. Eur J Biochem 1996;236(3):796-805.

Miller AL, Bement WM. Regulation of cytokinesis by Rho GTPase flux. Na Cell Biol 2009;11(1):71-77.

Minden A, Lin A, Claret FX, Abo A, Karin M. Selective activation of the JNK signaling cascade and c-Jun transcriptional activity by the small GTPases Rac and Cdc42Hs.Cell. 1995;81(7):1147-57.

Miron T, Vancompernolle K, Vandekerckhove J, Wilchek M, Geiger B. A 25-kD inhibitor of actin polymerization is a low molecular mass heat shock protein. J Cell Biol 1991;114(2):255-261.

Mitchell C, Nivison M, Jackson LF, Fox R, Lee DC, Campbell JS, et al. Heparin-binding epidermal growth factor-like growth factor links hepatocyte priming with cell cycle progression during liver regeneration. J Biol Chem 2005;280(4):2562-2568.

Mitry RR, Dhawan A, Hughes RD, Bansal S, Lehec S, Terry C, et al. One liver, three recipients: segment IV from split-liver procedures as a source of hepatocytes for cell transplantation. Transplantation 2004;77(10):1614-1616.

Miyoshi H, Rust C, Roberts PJ, Burgart LJ, Gores GJ. Hepatocyte apoptosis after BDL in the mouse involves Fas. Gastroenterology 1999;117(3):669-677.

Morita Y, Yoshidome H, Kimura F, Shimizu H, Ohtsuka M, Takeuchi D, et al. Excessive inflammation but decreased immunological response renders liver susceptible to infection in bile duct ligated mice. J Surg Res 2008;146(2):262-270.

Morrison DK, Davis RJ. Regulation of MAP kinase signaling modules by scaffold proteins in mammals. Annu Rev Cell Dev Biol 2003;19:91-118.

Mounier N, Arrigo AP. Actin cytoskeleton and small heat shock proteins: how do they interact? Cell Stress Chaperones 2002;7(2):167-176.

Mudgett JS, Ding J, Guh-Siesel L, Chartrain NA, Yang L, Gopal S, et al. Essential role for p38alpha mitogen-activated protein kinase in placental angiogenesis. Proc Natl Acad Sci U S A 2000;97(19):10454-10459.

Mukherjee A, Misra S, Howlett NG, Karmakar P. Multinucleation regulated by the Akt/PTEN signaling pathway is a survival strategy for HepG2 cells. Mutat Res 2013;755(2):135-140.

Nakatani T, Inouye M, Mirochnitchenko O. Overexpression of antioxidant enzymes in transgenic mice decreases cellular ploidy during liver regeneration. Exp Cell Res 1997;236(1):137-146.

Nascimento FA, Barbosa-da-Silva S, Fernandes-Santos C, Mandarim-de-Lacerda CA, Aguila MB. Adipose tissue, liver and pancreas structural alterations in C57BL/6 mice fed high-fat-high-sucrose diet supplemented with fish oil (n-3 fatty acid rich oil). Exp Toxicol Pathol 2010;62(1):17-25.

Natale DR, Paliga AJ, Beier F, D'Souza SJ, Watson AJ. p38 MAPK signaling during murine preimplantation development. Dev Biol 2004;268(1):76-88.

Nebreda AR, Porras A. p38 MAP kinases: beyond the stress response. Trends Biochem Sci 2000;25(6):257-260.

Normand G, King RW. Understanding cytokinesis failure. Adv Exp Med Biol 2010;676:27-55.

Nunez F, Chipchase MD, Clarke AR, Melton DW. Nucleotide excision repair gene (ERCC1) deficiency causes G(2) arrest in hepatocytes and a reduction in liver binucleation: the role of p53 and p21. FASEB J 2000;14(9):1073-1082.

Oe S, Lemmer ER, Conner EA, Factor VM, Leveen P, Larsson J, et al. Intact signaling by transforming growth factor beta is not required for termination of liver regeneration in mice. Hepatology 2004;40(5):1098-1105.

Oh SH, Hatch HM, Petersen BE. Hepatic oval 'stem' cell in liver regeneration. Semin Cell Dev Biol 2002;13(6):405-409.

Okamoto CT. HSP27 and signaling to the actin cytoskeleton focus on "HSP27 expression regulates CCK-induced changes of the actin cytoskeleton in CHO-CCK-A cells". Am J Physiol 1999;277(6 Pt 1):C1029-31.

Ono K, Han J. The p38 signal transduction pathway: activation and function. Cell Signal 2000;12(1):1-13.

Overturf K, Al-Dhalimy M, Tanguay R, Brantly M, Ou CN, Finegold M, et al. Hepatocytes corrected by gene therapy are selected in vivo in a murine model of hereditary tyrosinaemia type I. Nat Genet 1996;12(3):266-273.

Owens DM, Keyse SM. Differential regulation of MAP kinase signalling by dual-specificity protein phosphatases. Oncogene 2007;26(22):3203-3213.

Owens TW, Valentijn AJ, Upton JP, Keeble J, Zhang L, Lindsay J, et al. Apoptosis commitment and activation of mitochondrial Bax during anoikis is regulated by p38MAPK. Cell Death Differ 2009;16(11):1551-1562.

Pages G, Berra E, Milanini J, Levy AP, Pouyssegur J. Stress-activated protein kinases (JNK and p38/HOG) are essential for vascular endothelial growth factor mRNA stability. J Biol Chem 2000;275(34):26484-26491.

Paliga AJ, Natale DR, Watson AJ. p38 mitogen-activated protein kinase (MAPK) first regulates filamentous actin at the 8-16-cell stage during preimplantation development. Biol Cell 2005;97(8):629-640.

Parekh P, Motiwale L, Naik N, Rao KV. Downregulation of cyclin D1 is associated with decreased levels of p38 MAP kinases, Akt/PKB and Pak1 during chemopreventive effects of resveratrol in liver cancer cells. Exp Toxicol Pathol 2011; 63(1-2):167-173.

Pargellis C, Tong L, Churchill L, Cirillo PF, Gilmore T, Graham AG, et al. Inhibition of p38 MAP kinase by utilizing a novel allosteric binding site. Nat Struct Biol 2002;9(4):268-272.

Park JK, Hong IH, Ki MR, Chung HY, Ishigami A, Ji AR, et al. Vitamin C deficiency increases the binucleation of hepatocytes in SMP30 knock-out mice. J Gastroenterol Hepatol 2010; 25(11):1769-1776.

Parker CG, Hunt J, Diener K, McGinley M, Soriano B, Keesler GA, et al. Identification of stathmin as a novel substrate for p38 delta. Biochem Biophys Res Commun 1998; 249(3):791-796.

Patterson KI, Brummer T, O'Brien PM, Daly RJ. Dual-specificity phosphatases: critical regulators with diverse cellular targets. Biochem J 2009;418(3):475-489.

Pearson G, Robinson F, Beers Gibson T, Xu BE, Karandikar M, Berman K, et al. Mitogen-activated protein (MAP) kinase pathways: regulation and physiological functions. Endocr Rev 2001;22(2):153-183.

Pederson T. As functional nuclear actin comes into view, is it globular, filamentous, or both? J Cell Biol 2008;180(6):1061-1064.

Perdiguero E, Ruiz-Bonilla V, Gresh L, Hui L, Ballestar E, Sousa-Victor P, et al. Genetic analysis of p38 MAP kinases in myogenesis: fundamental role of p38alpha in abrogating myoblast proliferation. EMBO J 2007;26(5):1245-1256.

Perdiguero E, Ruiz-Bonilla V, Serrano AL, Muñoz-Cánoves P. Genetic deficiency of p38alpha reveals its critical role in myoblast cell cycle exit: the p38alpha-JNK connection. Cell Cycle. 2007;6(11):1298-303.

Pennisi PA, Kopchick JJ, Thorgeirsson S, LeRoith D, Yakar S. Role of growth hormone (GH) in liver regeneration. Endocrinology 2004;145(10):4748-4755.

Pereira L, Igea A, Canovas B, Dolado I, Nebreda AR. Inhibition of p38 MAPK sensitizes tumour cells to cisplatin-induced apoptosis mediated by reactive oxygen species and JNK. EMBO Mol Med 2013;5(11):1759-1774.

Phong MS, Van Horn RD, Li S, Tucker-Kellogg G, Surana U, Ye XS. p38 mitogen-activated protein kinase promotes cell survival in response to DNA damage but is not required for the G(2) DNA damage checkpoint in human cancer cells. Mol Cell Biol 2010;30(15):3816-3826.

Pichon S, Bryckaert M, Berrou E. Control of actin dynamics by p38 MAP kinase - Hsp27 distribution in the lamellipodium of smooth muscle cells. J Cell Sci 2004; 117(Pt 12):2569-2577.

Piekny A, Werner M, Glotzer M. Cytokinesis: welcome to the Rho zone. Trends Cell Biol 2005;15(12):651-658.

Piekny AJ, Glotzer M. Anillin is a scaffold protein that links RhoA, actin, and myosin during cytokinesis. Curr Biol 2008;18(1):30-36.

Platanias LC. Map kinase signaling pathways and hematologic malignancies. Blood 2003;101(12):4667-4679.

Pollard TD, Borisy GG. Cellular motility driven by assembly and disassembly of actin filaments. Cell 2003;112(4):453-465.

Raingeaud J, Gupta S, Rogers JS, Dickens M, Han J, Ulevitch RJ, et al. Pro-inflammatory cytokines and environmental stress cause p38 mitogen-activated protein kinase activation by dual phosphorylation on tyrosine and threonine. J Biol Chem 1995;270(13):7420-7426.

Rannou Y, Salaun P, Benaud C, Khan J, Dutertre S, Giet R, et al. MNK1 kinase activity is required for abscission. J Cell Sci 2012;125(Pt 12):2844-2852.

Rebrin I, Kamzalov S, Sohal RS. Effects of age and caloric restriction on glutathione REDOX state in mice. Free Radic Biol Med 2003;35(6):626-635.

Recio JA, Merlino G. Hepatocyte growth factor/scatter factor activates proliferation in melanoma cells through p38 MAPK, ATF-2 and cyclin D1. Oncogene 2002;21(7):1000-1008.

Regan J, Breitfelder S, Cirillo P, Gilmore T, Graham AG, Hickey E, et al. Pyrazole urea-based inhibitors of p38 MAP kinase: from lead compound to clinical candidate. J Med Chem 2002;45(14):2994-3008.

Reiling JH, Doepfner KT, Hafen E, Stocker H. Diet-dependent effects of the Drosophila Mnk1/Mnk2 homolog Lk6 on growth via eIF4E. Curr Biol 2005;15(1):24-30.

Ren H, Zhang S, Ma H, Wang Y, Liu D, Wang X, et al. Matrine reduces the proliferation and invasion of colorectal cancer cells via reducing the activity of p38 signaling pathway. Acta Biochim Biophys Sin (Shanghai) 2014 Oct 27.

Richter JD, Sonenberg N. Regulation of cap-dependent translation by eIF4E inhibitory proteins. Nature 2005;433(7025):477-480.

Ricote M, Garcia-Tunon I, Bethencourt F, Fraile B, Onsurbe P, Paniagua R, et al. The p38 transduction pathway in prostatic neoplasia. J Pathol 2006;208(3):401-407.

Rikans LE, Moore DR, Snowden CD. Sex-dependent differences in the effects of aging on antioxidant defense mechanisms of rat liver. Biochim Biophys Acta 1991;1074(1):195-200.

Rodriguez-Garay EA. Cholestasis: human disease and experimental animal models. Ann Hepatol 2003;2(4):150-158.

Rojo AI, Salinas M, Martin D, Perona R, Cuadrado A. Regulation of Cu/Zn-superoxide dismutase expression via the phosphatidylinositol 3 kinase/Akt pathway and nuclear factor-kappaB. J Neurosci 2004;24(33):7324-7334.

Ronkina N, Kotlyarov A, Gaestel M. MK2 and MK3--a pair of isoenzymes? Front Biosci 2008;13:5511-5521.

Roskams T. Liver stem cells and their implication in hepatocellular and cholangiocarcinoma. Oncogene 2006;25(27):3818-3822.

Roskams T, Cassiman D, De Vos R, Libbrecht L. Neuroregulation of the neuroendocrine compartment of the liver. Anat Rec A Discov Mol Cell Evol Biol 2004;280(1):910-923.

Roth S, Stein D, Nusslein-Volhard C. A gradient of nuclear localization of the dorsal protein determines dorsoventral pattern in the Drosophila embryo. Cell 1989 Dec 22;59(6):1189-1202.

Rouse J, Cohen P, Trigon S, Morange M, Alonso-Llamazares A, Zamanillo D, et al. A novel kinase cascade triggered by stress and heat shock that stimulates MAPKAP kinase-2 and phosphorylation of the small heat shock proteins. Cell 1994 Sep 23;78(6):1027-1037.

Rousseau S, Dolado I, Beardmore V, Shpiro N, Marquez R, Nebreda AR, et al. CXCL12 and C5a trigger cell migration via a PAK1/2-p38alpha MAPK-MAPKAP-K2-HSP27 pathway. Cell Signal 2006;18(11):1897-1905.

Rousseau S, Houle F, Kotanides H, Witte L, Waltenberger J, Landry J, et al. Vascular endothelial growth factor (VEGF)-driven actin-based motility is mediated by VEGFR2 and requires concerted activation of stress-activated protein kinase 2 (SAPK2/p38) and geldanamycin-sensitive phosphorylation of focal adhesion kinase. J Biol Chem 2000;275(14):10661-10672.

Roux PP, Blenis J. ERK and p38 MAPK-activated protein kinases: a family of protein kinases with diverse biological functions. Microbiol Mol Biol Rev 2004;68(2):320-344.

Rozga J. Liver support technology--an update. Xenotransplantation 2006;13(5):380-389.

Rozga J. Hepatocyte proliferation in health and in liver failure. Med Sci Monit 2002;8(2).

Rubio N, Verrax J, Dewaele M, Verfaillie T, Johansen T, Piette J, et al. p38(MAPK)-regulated induction of p62 and NBR1 after photodynamic therapy promotes autophagic clearance of ubiquitin aggregates and reduces reactive oxygen species levels by supporting Nrf2-antioxidant signaling. Free Radic Biol Med 2014;67:292-303.

Runge DM, Runge D, Dorko K, Pisarov LA, Leckel K, Kostrubsky VE, et al. Epidermal growth factor- and hepatocyte growth factor-receptor activity in serum-free cultures of human hepatocytes. J Hepatol 1999;30(2):265-274.

Rushlow CA, Han K, Manley JL, Levine M. The graded distribution of the dorsal morphogen is initiated by selective nuclear transport in Drosophila. Cell 1989;59(6):1165-1177.

Saeter G, Schwarze E, Seglen O. Shift from polyploidizing to nonpolyploidizing growth in carcinogen-treated rat liver. J Natl Cancer Inst 1988;80(12):950-958.

Sagias FG, Mitry RR, Hughes RD, Lehec SC, Patel AG, Rela M, et al. N-acetylcysteine improves the viability of human hepatocytes isolated from severely steatotic donor liver tissue. Cell Transplant 2010;19(11):1487-1492.

Sakurai T, Kudo M, Umemura A, He G, Elsharkawy AM, Seki E, et al. P38alpha Inhibits Liver Fibrogenesis and Consequent Hepatocarcinogenesis by Curtailing Accumulation of Reactive Oxygen Species. Cancer Res 2013;73(1):215-224.

Salinthone S, Ba M, Hanson L, Martin JL, Halayko AJ, Gerthoffer WT. Overexpression of human Hsp27 inhibits serum-induced proliferation in airway smooth muscle myocytes and confers resistance to hydrogen peroxide cytotoxicity. Am J Physiol Lung Cell Mol Physiol 2007;293(5):L1194-207.

Salvador JM, Mittelstadt PR, Belova GI, Fornace AJ,Jr, Ashwell JD. The autoimmune suppressor Gadd45alpha inhibits the T cell alternative p38 activation pathway. Nat Immunol 2005;6(4):396-402.

Salvador JM, Mittelstadt PR, Guszczynski T, Copeland TD, Yamaguchi H, Appella E, et al. Alternative p38 activation pathway mediated by T cell receptor-proximal tyrosine kinases. Nat Immunol 2005;6(4):390-395.

Samuel I. Bile and pancreatic juice exclusion activates acinar stress kinases and exacerbates gallstone pancreatitis. Surgery 2008;143(3):434-440.

Sanz N, Diez-Fernandez C, Alvarez A, Cascales M. Age-dependent modifications in rat hepatocyte antioxidant defense systems. J Hepatol 1997;27(3):525-534.

Sarbassov DD, Ali SM, Kim DH, Guertin DA, Latek RR, Erdjument-Bromage H, et al. Rictor, a novel binding partner of mTOR, defines a rapamycin-insensitive and raptor-independent pathway that regulates the cytoskeleton. Curr Biol 2004; 14(14):1296-1302.

Sastre J, Pallardo FV, Pla R, Pellin A, Juan G, O'Connor JE, et al. Aging of the liver: age-associated mitochondrial damage in intact hepatocytes. Hepatology 1996; 24(5):1199-1205.

Satyanarayana A, Kaldis P. Mammalian cell-cycle regulation: several Cdks, numerous cyclins and diverse compensatory mechanisms. Oncogene 2009; 28(33):2925-2939.

Schaeffer HJ, Weber MJ. Mitogen-activated protein kinases: specific messages from ubiquitous messengers. Mol Cell Biol 1999;19(4):2435-2444.

Schiel JA, Prekeris R. Making the final cut - mechanisms mediating the abscission step of cytokinesis. ScientificWorldJournal 2010;10:1424-1434.

Schieven GL. The biology of p38 kinase: a central role in inflammation. Curr Top Med Chem 2005;5(10):921-928.

Schmidt A, Durgan J, Magalhaes A, Hall A. Rho GTPases regulate PRK2/PKN2 to control entry into mitosis and exit from cytokinesis. EMBO J 2007;26(6):1624-1636.

Schmucker DL. Hepatocyte fine structure during maturation and senescence. J Electron Microsc Tech 1990;14(2):106-125.

Schneider S, Steinbeisser H, Warga RM, Hausen P. Beta-catenin translocation into nuclei demarcates the dorsalizing centers in frog and fish embryos. Mech Dev 1996;57(2):191-198.

Schwartz M. Rho signalling at a glance. J Cell Sci. 2004 Nov 1;117(Pt 23):5457-8.

Seger R, Krebs EG. The MAPK signaling cascade. FASEB J 1995;9(9):726-735.

Seglen PO. DNA ploidy and autophagic protein degradation as determinants of hepatocellular growth and survival. Cell Biol Toxicol 1997;13(4-5):301-315.

Sell S. The role of progenitor cells in repair of liver injury and in liver transplantation. Wound Repair Regen 2001 Nov-Dec;9(6):467-482.

Serenari M, Cescon M, Cucchetti A, Pinna AD. Liver function impairment in liver transplantation and after extended hepatectomy. World J Gastroenterol 2013;19(44):7922-7929.

Serres MP, Kossatz U, Chi Y, Roberts JM, Malek NP, Besson A. p27(Kip1) controls cytokinesis via the regulation of citron kinase activation. J Clin Invest 2012;122(3):844-858.

Seternes OM, Johansen B, Hegge B, Johannessen M, Keyse SM, Moens U. Both binding and activation of p38 mitogen-activated protein kinase (MAPK) play essential roles in regulation of the nucleocytoplasmic distribution of MAPK-activated protein kinase 5 by cellular stress. Mol Cell Biol 2002;22(20):6931-6945.

Shafritz DA, Dabeva MD. Liver stem cells and model systems for liver repopulation. J Hepatol 2002;36(4):552-564.

Shahabuddin S, Ji R, Wang P, Brailoiu E, Dun N, Yang Y, et al. CXCR3 chemokine receptor-induced chemotaxis in human airway epithelial cells: role of p38 MAPK and PI3K signaling pathways. Am J Physiol Cell Physiol 2006; 291(1):C34-9.

Shi Y, Gaestel M. In the cellular garden of forking paths: how p38 MAPKs signal for downstream assistance. Biol Chem 2002;383(10):1519-1536.

Shi Y, Kotlyarov A, Laabeta K, Gruber AD, Butt E, Marcus K, et al. Elimination of protein kinase MK5/PRAK activity by targeted homologous recombination. Mol Cell Biol 2003;23(21):7732-7741.

Shiryaev A, Dumitriu G, Moens U. Distinct roles of MK2 and MK5 in cAMP/PKA- and stress/p38MAPK-induced heat shock protein 27 phosphorylation. J Mol Signal 2011;6(1):4-2187-6-4.

Shiryaev A, Moens U. Mitogen-activated protein kinase p38 and MK2, MK3 and MK5: menage a trois or menage a quatre? Cell Signal 2010;22(8):1185-1192.

Siegel AB, Zhu AX. Metabolic syndrome and hepatocellular carcinoma: two growing epidemics with a potential link. Cancer 2009;115(24):5651-5661.

Sigal SH, Rajvanshi P, Gorla GR, Sokhi RP, Saxena R, Gebhard DR,Jr, et al. Partial hepatectomy-induced polyploidy attenuates hepatocyte replication and activates cell aging events. Am J Physiol 1999;276(5 Pt 1):G1260-72.

Silkworth WT, Nardi IK, Scholl LM, Cimini D. Multipolar spindle pole coalescence is a major source of kinetochore mis-attachment and chromosome mis-segregation in cancer cells. PLoS One 2009;4(8).

Simon C, Goepfert H, Boyd D. Inhibition of the p38 mitogen-activated protein kinase by SB 203580 blocks PMA-induced Mr 92,000 type IV collagenase secretion and in vitro invasion. Cancer Res 1998;58(6):1135-1139.

Simpson GE, Finckh ES. The Pattern of Regeneration of Rat Liver After Repeated Partial Hepatectomies. J Pathol Bacteriol 1963;86:361-370.

Sit ST, Manser E. Rho GTPases and their role in organizing the actin cytoskeleton. J Cell Sci 2011;124(Pt 5):679-683.

Soliman H, Gador A, Lu YH, Lin G, Bankar G, MacLeod KM. Diabetes-induced increased oxidative stress in cardiomyocytes is sustained by a positive feedback loop involving Rho kinase and PKCbeta2. Am J Physiol Heart Circ Physiol 2012;303(8):H989-H1000.

Slonim DK, Koide K, Johnson KL, Tantravahi U, Cowan JM, Jarrah Z, et al. Functional genomic analysis of amniotic fluid cell-free mRNA suggests that oxidative stress is significant in Down syndrome fetuses. Proc Natl Acad Sci U S A 2009;106(23):9425-9429.

Solopaev BP, Bobyleva NA. Liver regeneration following multiple resections. Biull Eksp Biol Med 1972;73(10):88-91.

Song G, Sharma AD, Roll GR, Ng R, Lee AY, Blelloch RH, et al. MicroRNAs control hepatocyte proliferation during liver regeneration. Hepatology 2010;51(5):1735-1743.

Song L, Dai T, Xiong H, Lin C, Lin H, Shi T, et al. Inhibition of centriole duplication by centrobin depletion leads to p38-p53 mediated cell-cycle arrest. Cell Signal 2010; 22(5):857-864.

Spear BT, Jin L, Ramasamy S, Dobierzewska A. Transcriptional control in the mammalian liver: liver development, perinatal repression, and zonal gene regulation. Cell Mol Life Sci 2006;63(24):2922-2938.

Standring S. Gray’s Anathomy. The Anatomical Basis of Clinical Practice, Expert Consult. 40th Edition. Amsterdam: Elsevier, 2008.

Steiling H, Wustefeld T, Bugnon P, Brauchle M, Fassler R, Teupser D, et al. Fibroblast growth factor receptor signalling is crucial for liver homeostasis and regeneration. Oncogene 2003;22(28):4380-4388.

Stock M, Lamatsch DK. Why comparing polyploidy research in animals and plants? Cytogenet Genome Res 2013;140(2-4):75-78.

Streetz KL, Luedde T, Manns MP, Trautwein C. Interleukin 6 and liver regeneration. Gut 2000;47(2):309-312.

Stepniak E, Ricci R, Eferl R, Sumara G, Sumara I, Rath M, et al. c-Jun/AP-1 controls liver regeneration by repressing p53/p21 and p38 MAPK activity. Genes Dev 2006; 20(16):2306-2314.

Steward R. Relocalization of the dorsal protein from the cytoplasm to the nucleus correlates with its function. Cell 1989;59(6):1179-1188.

Stocker E, Heine WD. Regeneration of liver parenchyma under normal and pathological conditions. Beitr Pathol 1971;144(4):400-408.

Stoker AW. Protein tyrosine phosphatases and signalling. J Endocrinol 2005; 185(1):19-33.

Stokoe D, Engel K, Campbell DG, Cohen P, Gaestel M. Identification of MAPKAP kinase 2 as a major enzyme responsible for the phosphorylation of the small mammalian heat shock proteins. FEBS Lett 1992;313(3):307-313.

Strippoli R, Benedicto I, Foronda M, Perez-Lozano ML, Sanchez-Perales S, Lopez-Cabrera M, et al. p38 maintains E-cadherin expression by modulating TAK1-NF-kappa B during epithelial-to-mesenchymal transition. J Cell Sci 2010;123(Pt 24):4321-4331.

Sun P, Yoshizuka N, New L, Moser BA, Li Y, Liao R, et al. PRAK is essential for ras-induced senescence and tumor suppression. Cell 2007;128(2):295-308.

Sundaresan P, Farndale RW. P38 mitogen-activated protein kinase dephosphorylation is regulated by protein phosphatase 2A in human platelets activated by collagen. FEBS Lett 2002;528(1-3):139-144.

Suzanne M, Irie K, Glise B, Agnes F, Mori E, Matsumoto K, et al. The Drosophila p38 MAPK pathway is required during oogenesis for egg asymmetric development. Genes Dev 1999;13(11):1464-1474.

Svensson C, Part K, Kunnis-Beres K, Kaldmae M, Fernaeus SZ, Land T. Pro-survival effects of JNK and p38 MAPK pathways in LPS-induced activation of BV-2 cells. Biochem Biophys Res Commun 2011;406(3):488-492.

Szasz G, Rosenthal P, Fritzsche W. Gamma glutamyl transpeptidase activity in the serum in hepatobiliary diseases. Dtsch Med Wochenschr 1969;94(38):1911-1917.

Takahashi A, Ohtani N, Hara E. Irreversibility of cellular senescence: dual roles of p16INK4a/Rb-pathway in cell cycle control. Cell Div 2007;2:10.

Takeda R, Suzuki E, Satonaka H, Oba S, Nishimatsu H, Omata M, et al. Blockade of endogenous cytokines mitigates neointimal formation in obese Zucker rats. Circulation 2005;111(11):1398-1406.

Takekawa M, Adachi M, Nakahata A, Nakayama I, Itoh F, Tsukuda H, et al. p53-inducible wip1 phosphatase mediates a negative feedback regulation of p38 MAPK-p53 signaling in response to UV radiation. EMBO J 2000;19(23):6517-6526.

Takekawa M, Maeda T, Saito H. Protein phosphatase 2Calpha inhibits the human stress-responsive p38 and JNK MAPK pathways. EMBO J 1998;17(16):4744-4752.

Takenaka K, Moriguchi T, Nishida E. Activation of the protein kinase p38 in the spindle assembly checkpoint and mitotic arrest. Science 1998;280(5363):599-602.

Tamura K, Sudo T, Senftleben U, Dadak AM, Johnson R, Karin M. Requirement for p38alpha in erythropoietin expression: a role for stress kinases in erythropoiesis. Cell 2000;102(2):221-231.

Tanno M, Bassi R, Gorog DA, Saurin AT, Jiang J, Heads RJ, et al. Diverse mechanisms of myocardial p38 mitogen-activated protein kinase activation: evidence for MKK-independent activation by a TAB1-associated mechanism contributing to injury during myocardial ischemia. Circ Res 2003;93(3):254-261.

Tarla MR, Ramalho F, Ramalho LN, Silva Tde C, Brandao DF, Ferreira J, et al. Cellular aspects of liver regeneration. Acta Cir Bras 2006;21 Suppl 1:63-66.

Taub R. Liver regeneration: from myth to mechanism. Nat Rev Mol Cell Biol 2004; 5(10):836-847.

Theise ND, Saxena R, Portmann BC, Thung SN, Yee H, Chiriboga L, et al. The canals of Hering and hepatic stem cells in humans. Hepatology 1999;30(6):1425-1433.

Thoms HC, Dunlop MG, Stark LA. p38-mediated inactivation of cyclin D1/cyclin-dependent kinase 4 stimulates nucleolar translocation of RelA and apoptosis in colorectal cancer cells. Cancer Res 2007;67(4):1660-1669.

Thomson S, Clayton AL, Hazzalin CA, Rose S, Barratt MJ, Mahadevan LC. The nucleosomal response associated with immediate-early gene induction is mediated via alternative MAP kinase cascades: MSK1 as a potential histone H3/HMG-14 kinase. EMBO J 1999;18(17):4779-4793.

Thorgeirsson SS. Hepatic stem cells in liver regeneration. FASEB J 1996;10(11):1249-1256.

Thorgeirsson SS, Grisham JW. Hematopoietic cells as hepatocyte stem cells: a critical review of the evidence. Hepatology 2006;43(1):2-8.

Thornton TM, Pedraza-Alva G, Deng B, Wood CD, Aronshtam A, Clements JL, et al. Phosphorylation by p38 MAPK as an alternative pathway for GSK3beta inactivation. Science 2008;320(5876):667-670.

Thornton TM, Rincon M. Non-classical p38 map kinase functions: cell cycle checkpoints and survival. Int J Biol Sci 2009;5(1):44-51.

Tietz PS, Larusso NF. Cholangiocyte biology. Curr Opin Gastroenterol 2006; 22(3):279-287.

Trauner M. Molecular alterations of canalicular transport systems in experimental models of cholestasis: possible functional correlations. Yale J Biol Med 1997; 70(4):365-378.

Trauner M. and Boyer J.L. Cholestatic syndromes Curr Opin Gastroenterol. 1999; 15(3):217-28.

Trauner M, Boyer JL. Cholestatic syndromes. Curr Opin Gastroenterol 2003; 19(3):216-231.

Trempolec N, Dave-Coll N, Nebreda AR. SnapShot: p38 MAPK substrates. Cell 2013; (4):924-924.

Tsai LY, Lee KT, Tsai SM, Lee SC, Yu HS. Changes of lipid peroxide levels in blood and liver tissue of patients with obstructive jaundice. Clin Chim Acta 1993;215(1):41-50.

Uhlik MT, Abell AN, Johnson NL, Sun W, Cuevas BD, Lobel-Rice KE, et al. Rac-MEKK3-MKK3 scaffolding for p38 MAPK activation during hyperosmotic shock. Nat Cell Biol 2003;5(12):1104-1110.

Ventura JJ, Tenbaum S, Perdiguero E, Huth M, Guerra C, Barbacid M, et al. p38alpha MAP kinase is essential in lung stem and progenitor cell proliferation and differentiation. Nat Genet 2007;39(6):750-758.

Vermeulen K, Van Bockstaele DR, Berneman ZN. The cell cycle: a review of regulation, deregulation and therapeutic targets in cancer. Cell Prolif 2003; 36(3):131-149.

Vermeulen L, De Wilde G, Van Damme P, Vanden Berghe W, Haegeman G. Transcriptional activation of the NF-kappaB p65 subunit by mitogen- and stress-activated protein kinase-1 (MSK1). EMBO J 2003;22(6):1313-1324.

Vermeulen L, Vanden Berghe W, Beck IM, De Bosscher K, Haegeman G. The versatile role of MSKs in transcriptional regulation. Trends Biochem Sci 2009; 34(6):311-318.

Villares GJ, Zigler M, Dobroff AS, Wang H, Song R, Melnikova VO, et al. Protease activated receptor-1 inhibits the Maspin tumor-suppressor gene to determine the melanoma metastatic phenotype. Proc Natl Acad Sci U S A 2011;108(2):626-631.

Wada T, Stepniak E, Hui L, Leibbrandt A, Katada T, Nishina H, et al. Antagonistic control of cell fates by JNK and p38-MAPK signaling. Cell Death Differ 2008; 15(1):89-93.

Wagner EF, Nebreda AR. Signal integration by JNK and p38 MAPK pathways in cancer development. Nat Rev Cancer 2009;9(8):537-549.

Wang X, Krupczak-Hollis K, Tan Y, Dennewitz MB, Adami GR, Costa RH. Increased hepatic Forkhead Box M1B (FoxM1B) levels in old-aged mice stimulated liver regeneration through diminished p27Kip1 protein levels and increased Cdc25B expression. J Biol Chem 2002;277(46):44310-44316.

Wang X, Liu JZ, Hu JX, Wu H, Li YL, Chen HL, et al. ROS-activated p38 MAPK/ERK-Akt cascade plays a central role in palmitic acid-stimulated hepatocyte proliferation. Free Radic Biol Med 2011;51(2):539-551.

Waseem T, Duxbury M, Ito H, Ashley SW, Robinson MK. Exogenous ghrelin modulates release of pro-inflammatory and anti-inflammatory cytokines in LPS-stimulated macrophages through distinct signaling pathways. Surgery 2008;143(3):334-342.

Webber JL, Tooze SA. New insights into the function of Atg9. FEBS Lett 2010;584(7):1319-1326.

Weier JF, Weier HU, Jung CJ, Gormley M, Zhou Y, Chu LW, et al. Human cytotrophoblasts acquire aneuploidies as they differentiate to an invasive phenotype. Dev Biol 2005;279(2):420-432.

Weier JF, Weier HU, Nureddin A, Pedersen RA, Racowsky C. Aneuploidy involving chromosome 1 in failed-fertilized human oocytes is unrelated to maternal age. J Assist Reprod Genet 2005; 22(7-8):285-293.

Weiss-Schneeweiss H, Emadzade K, Jang TS, Schneeweiss GM. Evolutionary consequences, constraints and potential of polyploidy in plants. Cytogenet Genome Res 2013;140(2-4):137-150.

Westra JW, Peterson SE, Yung YC, Mutoh T, Barral S, Chun J. Aneuploid mosaicism in the developing and adult cerebellar cortex. J Comp Neurol 2008;507(6):1944-1951.

World Health Organisation [Internet]. Health statiscs information systems. Estimates for 2000-2012. [cited May 2014]. Available from: www.who.int/healthinfo/global_burden_disease/estimates/en/index1.html

World Health Organisation [Internet]. World Hepatitis Day [cited 15 July 2013]. Available from: www.who.int/campaigns/hepatitis-day/2013/en

Wiggin GR, Soloaga A, Foster JM, Murray-Tait V, Cohen P, Arthur JS. MSK1 and MSK2 are required for the mitogen- and stress-induced phosphorylation of CREB and ATF1 in fibroblasts. Mol Cell Biol 2002;22(8):2871-2881.

Wisse E, Braet F, Luo D, De Zanger R, Jans D, Crabbe E, et al. Structure and function of sinusoidal lining cells in the liver. Toxicol Pathol 1996 24(1):100-111.

Wood CD, Thornton TM, Sabio G, Davis RA, Rincon M. Nuclear localization of p38 MAPK in response to DNA damage. Int J Biol Sci 2009;5(5):428-437.

Wu X, Zhang W, Font-Burgada J, Palmer T, Hamil AS, Biswas SK, et al. Ubiquitin-conjugating enzyme Ubc13 controls breast cancer metastasis through a TAK1-p38 MAP kinase cascade. Proc Natl Acad Sci U S A 2014;111(38):13870-13875.

Yang HT, Cohen P, Rousseau S. IL-1beta-stimulated activation of ERK1/2 and p38alpha MAPK mediates the transcriptional up-regulation of IL-6, IL-8 and GRO-alpha in HeLa cells. Cell Signal 2008;20(2):375-380.

Zarubin T, Han J. Activation and signaling of the p38 MAP kinase pathway. Cell Res 2005;15(1):11-18.

Zhang S, Han J, Sells MA, Chernoff J, Knaus UG, Ulevitch RJ, et al. Rho family GTPases regulate p38 mitogen-activated protein kinase through the downstream mediator Pak1. J Biol Chem 1995;270(41):23934-23936.

Zhang Y, Gao Y, Zhao L, Han L, Lu Y, Hou P, et al. Mitogen-activated protein kinase p38 and retinoblastoma protein signalling is required for DNA damage-mediated formation of senescence-associated heterochromatic foci in tumour cells. FEBS J 2013;280(18):4625-4639.

Zhang Y, Ren X, Shi M, Jiang Z, Wang H, Su Q, et al. Downregulation of STAT3 and activation of MAPK are involved in the induction of apoptosis by HNK in glioblastoma cell line U87. Oncol Rep 2014;32(5):2038-2046.

Zhang Y, Rivera Rosado LA, Moon SY, Zhang B. Silencing of D4-GDI inhibits growth and invasive behavior in MDA-MB-231 cells by activation of Rac-dependent p38 and JNK signaling. J Biol Chem 2009 8;284(19):12956-12965.

Zheng B, Han M, Bernier M, Wen JK. Nuclear actin and actin-binding proteins in the regulation of transcription and gene expression. FEBS J 2009;276(10):2669-2685.

Zhu AX. Systemic treatment of hepatocellular carcinoma: dawn of a new era? Ann Surg Oncol 2010;17(5):1247-1256.

Zou Y, Bao Q, Kumar S, Hu M, Wang GY, Dai G. Four waves of hepatocyte proliferation linked with three waves of hepatic fat accumulation during partial hepatectomy-induced liver regeneration. PLoS One 2012;7(2).

Zuluaga S, Gutierrez-Uzquiza A, Bragado P, Alvarez-Barrientos A, Benito M, Nebreda AR, et al. p38alpha MAPK can positively or negatively regulate Rac-1 activity depending on the presence of serum. FEBS Lett 2007;581(20):3819-3825.